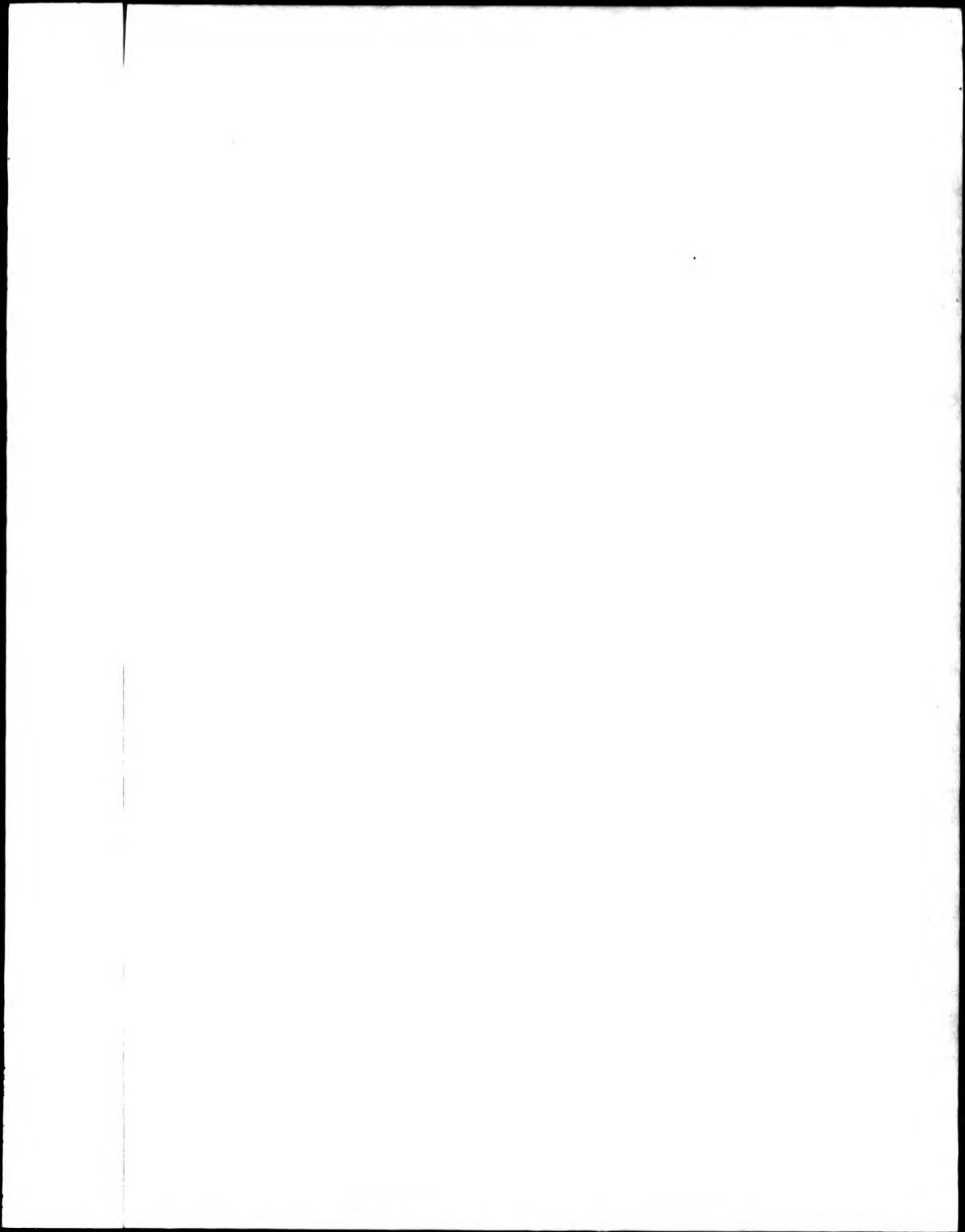
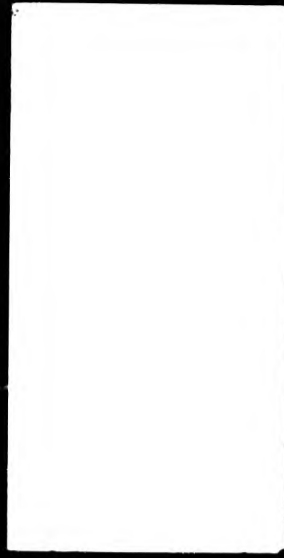
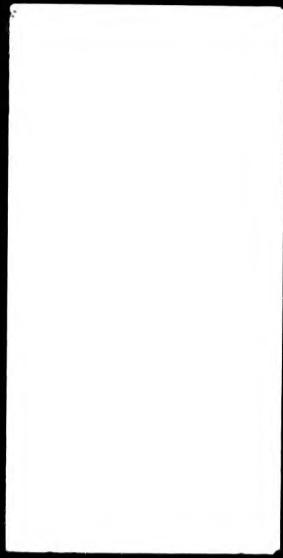


This PDF was created from the British Library's microfilm copy of the original thesis. As such the images are greyscale and no colour was captured.

Due to the scanning process, an area greater than the page area is recorded and extraneous details can be captured.

This is the best available copy

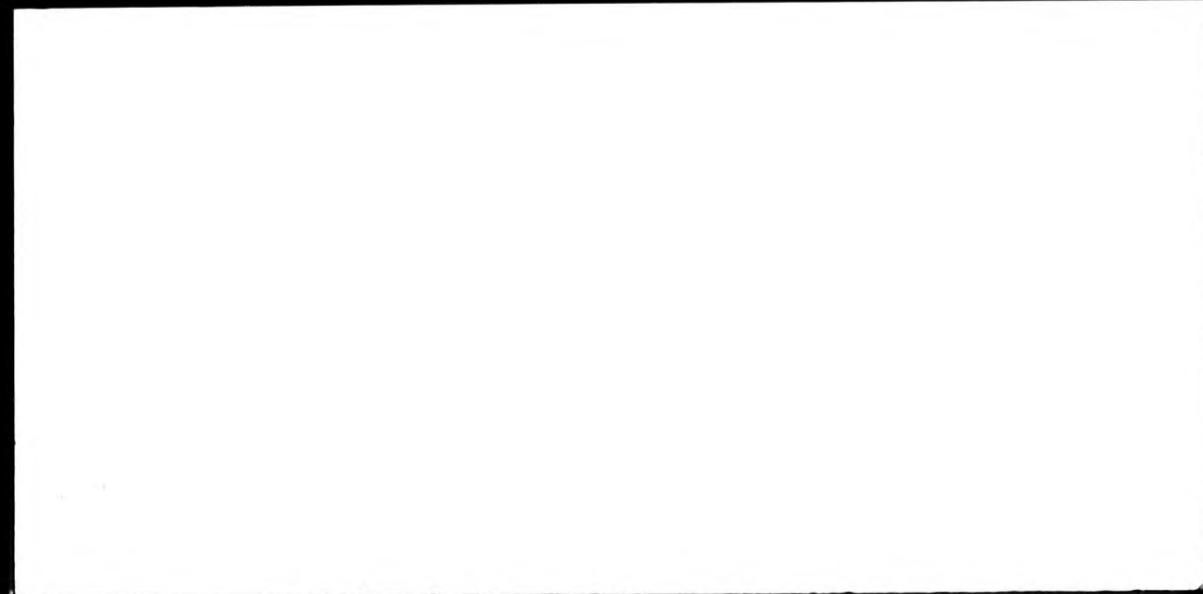


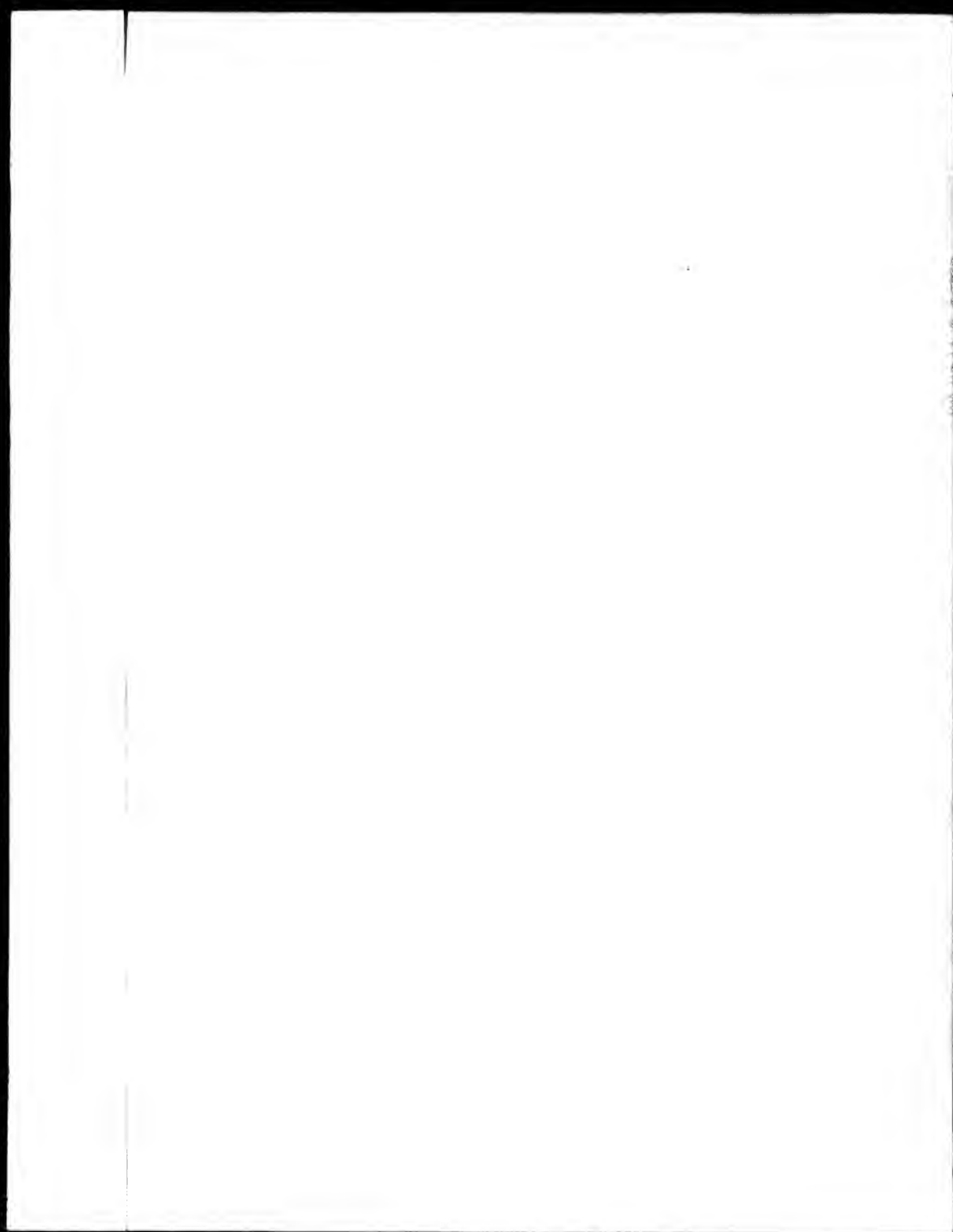
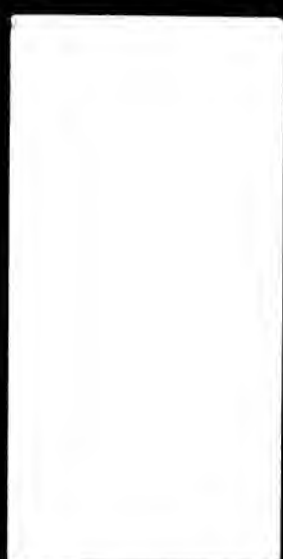


DX



8	4	3	9	2
----------	----------	----------	----------	----------





THE BRITISH LIBRARY DOCUMENT SUPPLY CENTRE

TITLE An Experimental Study of the Magnetic
..... Linear Birefringence and Dichroism of
Liquids, solutions and Dispersions

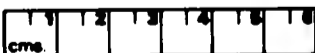
AUTHOR P. J. Batchelor

**INSTITUTION
and DATE** City of London Polytechnic
1982

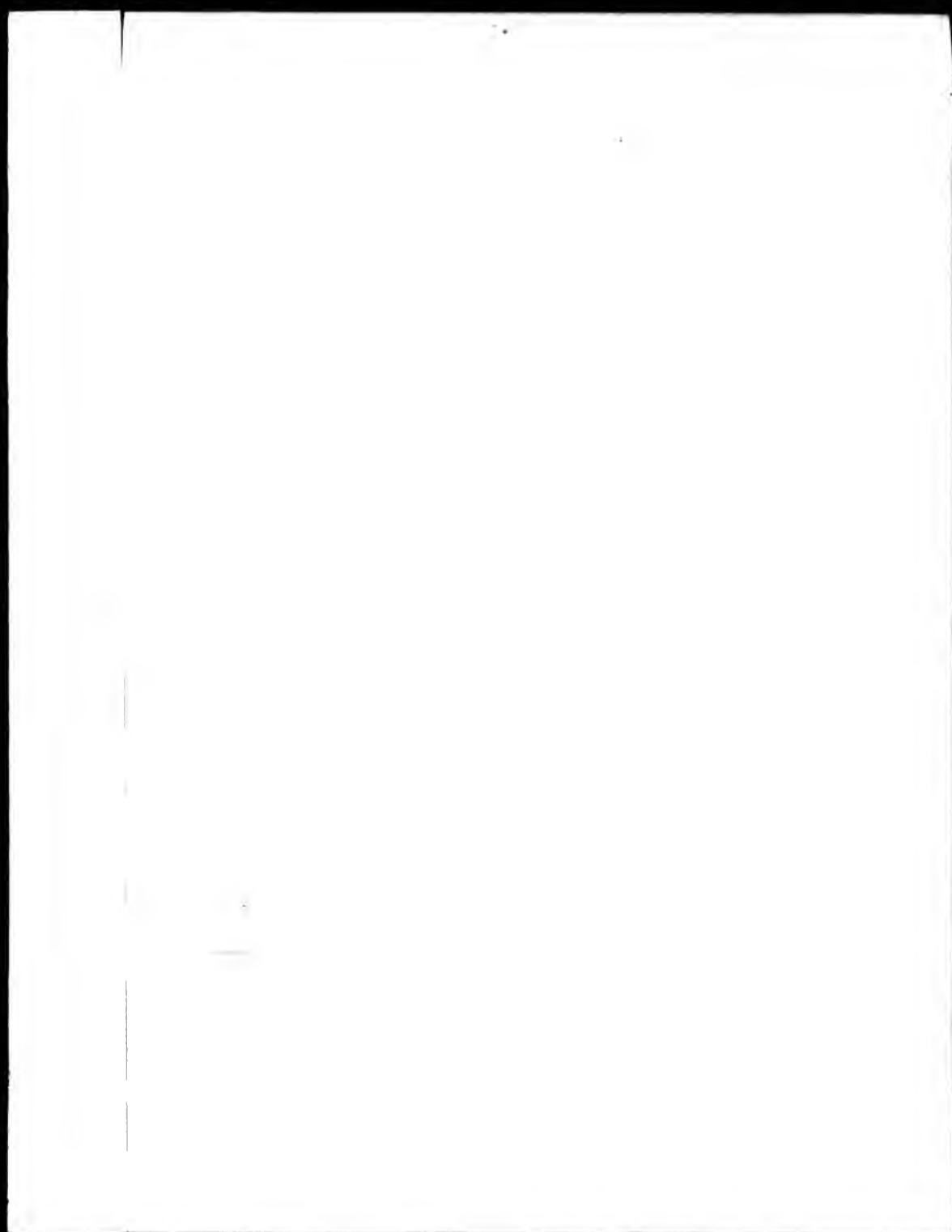
Attention is drawn to the fact that the copyright of
this thesis rests with its author.

This copy of the thesis has been supplied on condition
that anyone who consults it is understood to recognise
that its copyright rests with its author and that no
information derived from it may be published without
the author's prior written consent.

THE BRITISH LIBRARY
DOCUMENT SUPPLY CENTRE
Boston Spa, Wetherby
West Yorkshire
United Kingdom



REDUCTION X 2i



594

**AN EXPERIMENTAL STUDY OF THE MAGNETIC LINEAR
BIREFRINGENCE AND DICHROISM OF LIQUIDS, SOLUTIONS
AND DISPERSIONS**

A thesis submitted for the Degree of Doctor of Philosophy
by

PETER JOHN BATCHELOR

in partial fulfilment of the requirements of the Council for National
Academic Awards

**City of London Polytechnic
Tower Hill Library**

Department of Physics
Sir John Cass School of Science and Technology
City of London Polytechnic
31 Jewry Street
London EC3

December 1982

CONTENTS

	<u>Page</u>
Acknowledgements	i
Abstract	ii
CHAPTER 1 INTRODUCTION	1
CHAPTER 2 THEORIES OF MAGNETIC BIREFRINGENCE AND DICHOISM	3
2.1 Introduction to the Theory of the Cotton-Mouton Effect in Liquids	3
2.2 Classical Theories of Magnetic Birefringence	4
2.3 Modifications to the Langevin-Born Theory	6
2.3.1 Magnetic Hyperpolarizability	6
2.3.2 Collision-Induced Effects	7
2.3.3 Angular Correlations in Liquids	9
2.3.4 Local Field Effects	11
2.4 The Sign of the Cotton-Mouton Constant	14
2.5 Theories on the Magneto-Optical Anisotropy of Chain Molecules	14
2.5.1 The Bond Polarizability Additivity Approximation	14
2.5.2 The Rotational Isomeric Model	17
2.6 Theories on the Magnetic Birefringence and Dichroism of Colloidal Dispersions	18
2.6.1 Derivation of $\Delta n'$	18
2.6.2 Derivation of $\Delta n''$	19
2.6.3 Application of Light Scattering Theories to Colloidal Dispersions	20
CHAPTER 3 THEORY OF THE METHOD AND ERROR ANALYSIS	21
PART A: OCULAR METHOD	21
3.1 Introduction	21
3.2 Theory of the Ocular Method	22
3.3 Systematic Error Analysis - Ocular Method	24
3.3.1 Setting of the Polarizer	25
3.3.2 Setting of the Cell	25
3.3.3 Errors Associated with the Quarter Wave Plate	26
3.3.4 Faraday Rotation in the Cell	27
3.3.5 Combination of Stray Birefringence and Faraday Rotation	27

	<u>Page</u>
PART B: PHOTOMETRIC METHOD	29
3.4 Introduction	29
3.5 Theory of Birefringence Measurements by the Photometric Method	31
3.6 Systematic Error Analysis - Measuring Birefringence	33
3.6.1 Setting of the Polarizer	33
3.6.2 Setting of the Modulator	34
3.6.3 Setting of the Cell	35
3.6.4 Errors Associated with the Quarter Wave Plate	35
3.6.5 Stray Birefringence in Both Cell Windows	37
3.6.6 Faraday Rotation in the Cell	38
3.6.7 Combination of Stray Birefringence and Faraday Rotation	38
3.7 Theory of Dichroism Measurements by Photometric Method	39
3.8 Systematic Error Analysis - Measuring Dichroism	40
3.8.1 Setting of the Polarizer	40
3.8.2 Setting of the Modulator	41
3.8.3 Setting of the Cell	42
3.8.4 Errors Associated with the First Quarter Wave Plate	43
3.8.5 Errors Associated with the Second Quarter Wave Plate	44
3.8.6 Stray Birefringence in a Cell Window	45
3.8.7 Faraday Rotation in the Cell	46
3.9 Mueller Calculus	47
CHAPTER 4 EXPERIMENTAL APPARATUS AND PROCEDURE	52
PART A: OCULAR METHOD	52
4.1 Introduction	52
4.2 Description of the Apparatus	52
4.2.1 The Polariser Bench	52
4.2.2 The Magnet	54
4.2.3 The Sample Cell	55
4.2.4 The Compensator Bench	55
4.3 Alignment of Optical Components	56
4.4 Calibration of Apparatus	57
4.4.1 Calibration of Finely Divided Circle	57
4.4.2 Calibration of Sample Cell	58
4.4.3 Statistical Analysis of Experimental Accuracy	59

	<u>Page</u>
4.4.4 Investigation of the Stray Birefringence in the Cell Windows	59
4.5 Experimental Procedure	61
PART B: PHOTOMETRIC METHOD	62
4.6 Description of the Apparatus	62
4.6.1 Light Source: He-Ne Laser	62
4.6.1 Polarisers and Quarter Wave Plates	67
4.6.3 The Magnet	67
4.6.4 Sample Cells	68
4.6.5 Piezo-Optic Phase Modulator	69
4.6.6 Detection System	71
4.7 Alignment of Optical Components	72
4.7.1 Alignment for Birefringence Measurements	72
4.7.2 Alignment for Dichroism Measurements.	73
4.7.3 Alignment for "Direct" Dichroism Measurements	74
4.8 Cell and Sample Preparation	75
4.8.1 Cell Cleaning	75
4.8.2 Sample Preparation	75
4.9 Calibration of Apparatus	77
4.9.1 Calibration of the Hall Probe	77
4.9.2 Calibration of the Sample Cells	77
4.10 Experimental Procedure	79
4.10.1 Measuring the Magnetic Birefringence of Highly Anisotropic Liquids and Polymers	80
4.10.2 Measuring the Magnetic Birefringence of Weakly Anisotropic Media	81
4.10.3 Measuring the Magnetic Birefringence of Colloidal Dispersions	84
4.10.4 Measuring the Magnetic Dichroism of Colloidal Dispersions	84
CHAPTER 5 EXPERIMENTAL RESULTS AND DISCUSSION	86
5.1 Introduction	86
5.2 Liquids with Large Cotton-Mouton Constants	88
5.3 Liquids of Near-Isotropic Molecules	93
5.3.1 Neat Liquids of Intrinsically Isotropic Molecules	93
5.3.2 Solutions of Intrinsically Isotropic Molecules	96
5.3.3 Neat Liquids of Near-Isotropic Molecules	103

	<u>Page</u>
5.4 Linear, Branched Chain and Cyclo Alkane Neat Liquids and Derivatives	105
5.4.1 n-Alkane Liquids	106
5.4.2 Linear Alkane Derivatives: n-Alcohols, n-Alkenes, Aminoalkanes	119
5.4.3 Branched-Chain Alkane Liquids	127
5.4.4 Liquids of Tetra-alkyl and Tetra-alkoxy Compounds	141
5.4.5 Tri-n-Alkylamine Liquids	147
5.4.6 Cycloalkane Liquids and Derivatives	150
5.5 Polymers of Medium and High Molecular Weight	153
5.4.1 Polyisobutene Neat Liquids	153
5.4.2 Solutions of PBLG	156
5.6 Colloidal Dispersions	161
5.6.1 Fluon Dispersions	161
5.6.2 Other Colloidal Dispersions	176
CHAPTER 6 CONCLUSIONS	179
REFERENCES	184

ACKNOWLEDGEMENTS

I am deeply grateful to my supervisor in this research, Dr. G.H. Maeten. He has given selflessly of his time and energy and has been a constant source of encouragement and guidance.

I am also grateful to Dr. J.V. Champion and Dr. G. Maitland, Imperial College, for their interest and advice on aspects of this work.

Thanks are due to Mr. D.C.L. Wiffen for his expert technical assistance.

I also wish to record my gratitude to my family, who have sustained and encouraged me in this work.

• Finally, I am grateful to the Inner London Education Authority for the award of a Research Assistantship, without which this work could not have been undertaken.

ABSTRACT

This thesis contains an experimental study of the linear birefringence and dichroism induced by magnetic fields in molecular liquids, solutions and colloidal dispersions. The measurements were made using apparatus of greater sensitivity than any previously described; most results were new determinations.

The liquids were mostly linear and branched alkanes, or alkane derivatives, generally being of high molecular flexibility. Results were also obtained for both very low and high anisotropy liquids of rigid molecules. Solutions of low molecular weight liquids and macromolecules (polypeptides) were also studied. An immeasurably small dichroism was found for all the above fluids. The valence-optical scheme, and the existence of intermolecular angular correlations are not sufficient to explain the birefringence results.

Extensive studies were made of the magnetic birefringence and dichroism of crystalline polytetrafluoroethylene of about 0.2 μ m diameter, dispersed in water. These covered a volume fraction range of about 10^{-8} to 0.5, the latter being a highly turbid, concentrated colloidal dispersion. At volume fractions greater than about 0.1, the concentration dependence of the birefringence and dichroism were markedly different, and not explicable on the basis of angular correlation between the colloidal particles.

CHAPTER 1
INTRODUCTION

When a strong uniform magnetic field is applied to an isotropic medium, an anisotropy in the optical properties of that medium is usually induced whereby the refractive index parallel to the field direction differs from that perpendicular to the field. The amount of magnetically induced anisotropy may be determined by passing a beam of linearly polarized light through the medium perpendicular to the magnetic field, and measuring the phase difference induced in the emergent beam. This phenomenon of magnetic double-refraction or birefringence is known as the Cotton-Mouton effect and its character give information concerning the properties and structure of the medium.

Research into this phenomenon dates from the beginning of the twentieth century. It was reported first by Kerr¹ (1901), but the first measurements of organic liquids such as benzene and chloroform were made by Cotton and Mouton² (1907). They noted that the induced birefringence is proportional to the square of the applied magnetic field; the constant of proportionality is known as the Cotton-Mouton constant of the liquid.

Much Cotton-Mouton data exists for organic liquids, some is included in the Landolt-Bornstein tables³ and reviews by Meeten⁴ and Le Fèvre, Murphy and Richie⁵. Recent specialist work has been done by Corfield⁶ and Buckingham et al.⁷ (gases and arenes), Battaglia and Richie⁸ (arenes), Battaglia⁹ (near-isotropic molecular liquids) and Stamm¹⁰ (n-alkanes). There is room for improvement in the accuracy of most of this data because of the limited sensitivity of the apparatus used.

The difficulty in making accurate magnetic birefringence measurements meant that studies such as the effect of branching on the magneto-optical properties of alkanes were not previously practicable. Also, the effect for liquids of symmetric molecules such as tetramethyltin is small enough to be beyond the limit of detection of all but the most sensitive apparatus, hence the lack of data for these interesting liquids.

Madden et al.^{11,12} have shown that in combination with depolarized light scattering results, Cotton-Mouton data can yield the molecular orientational correlation parameter, g_2 of a liquid, giving information

on the liquid structure. Unlike infinite dilution light scattering and electric birefringence studies this method is uncomplicated by local field effects.

Colloidal dispersions are often studied by measuring their electric field induced linear birefringence and dichroism^{13,14}. Linear dichroism is the difference in transmissibilities in light polarized parallel and perpendicular to the field direction; it can be expressed in terms of the anisotropy of the imaginary part of the refractive index. Corresponding magnetic field induced birefringences and dichroism have received far less attention because of their relative smallness. However, magnetic fields have the great advantage of not causing undesirable electric effects such as electrophoresis and Joule heating in electrically conducting dispersions. Previous measurements of magnetically induced linear dichroism have been few and relatively inaccurate because the effect is generally much smaller than, and difficult to separate from, linear birefringence^{15,16}. Results from separate measurement of these two magneto-optical effects give useful information on the optical properties and interactions of colloidal particles in suspension.

CHAPTER 2
 THEORIES OF MAGNETIC BIREFRINGENCE AND DICHROISM

2.1 Introduction to the Theory of the Cotton-Mouton
 Effect in Liquids

If a strong magnetic field is applied to an isotropic medium, the effect is to produce an anisotropy in the medium's optical properties.

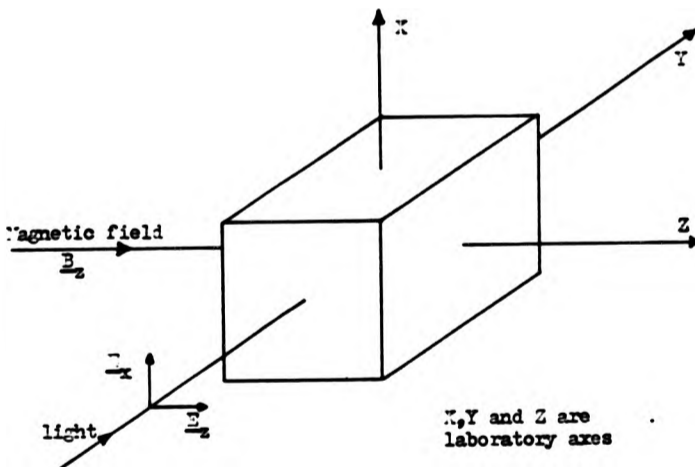


Figure 2.1

When a linearly polarized light beam propagates through the medium perpendicularly to the magnetic field B_z , say along the Y axis as shown in Figure 2.1, the electric vector of the light beam may be resolved into two components along the Z and X axes, E_z and E_x . The anisotropy induced by the magnetic field applied to the medium leads to a phase difference between the components, so that the emergent light is elliptically polarized.

This induced phase difference δ is a direct measure of the induced birefringence such that:

$$\delta = \frac{2\pi l}{\lambda_0} (n_{\parallel} - n_{\perp}) \quad (2.1)$$

where n_{\parallel} and n_{\perp} are the refractive indices parallel and perpendicular

to the applied field, l is the path length of the light through the medium and λ_0 the vacuum wavelength of the light. Cotton and Mouton¹⁷ found that the induced phase difference, δ , was proportional to the square of the applied magnetic flux density, B_z^2 , such that:

$$\delta = 2\pi l C B_z^2 \quad (2.2)$$

where C is the constant of proportionality called the Cotton-Mouton Constant of the medium. In terms of the birefringence, $n_{11} - n_{\perp}$ or Δn , (2.1) and (2.2) give the Cotton-Mouton constant as:

$$C = \frac{\Delta n}{\lambda_0 B_z^2} \quad (2.3)$$

2.2 Classical Theories of Magnetic Birefringence

The Langevin-Born theory may be applied to the magnetic birefringence of liquids although it was originally proposed for the interpretation of the Kerr Effect, the electro-optic analogue of the Cotton-Mouton Effect. This classical theory is based on molecules minimising their interaction energy with a magnetic field by partial orientation. Langevin¹⁸ and Born¹⁹ derived the following expression for the Cotton-Mouton Constant of a gas:

$$C = \frac{N(n^2 + 2)^2}{12nc_0\lambda_0^2} (\theta_1 + \theta_2) \quad (2.4)$$

where N is the number of molecules per m^3
 n is the mean refractive index of the medium
 c_0 is the permittivity of a vacuum

$$\theta_1 = \frac{1}{15kT} \{ \alpha_{\alpha\beta} \chi_{\alpha\beta} - \frac{1}{3} \alpha_{\alpha\alpha} \chi_{\beta\beta} \}$$

$$\text{and } \theta_2 = \frac{1}{15kT^2} \{ \alpha_{\alpha\beta} M_{\alpha} M_{\beta} - \alpha_{\alpha\alpha} M^2 \}$$

where $\alpha_{\alpha\beta}$ are the components of the optical polarizability tensor
 $\alpha_{\alpha\alpha}$ are the principal components, so $\bar{\alpha} = \frac{1}{3} \alpha_{\alpha\alpha}$
 $\chi_{\alpha\beta}$ are the components of the diamagnetic susceptibility tensor
 $\chi_{\beta\beta}$ are the principal components, so $\bar{\chi} = \frac{1}{3} \chi_{\beta\beta}$
 M_{α}, M_{β} are the components of the permanent magnetic moment
 k is the Boltzman Constant
 T is the absolute temperature.

Now, diamagnetic species have no permanent magnetic moment; therefore $M = 0$, and $\theta_2 = 0$.

For an assembly of isolated molecules a magneto-optical anisotropy parameter may be defined by²⁰:

$$\langle \gamma_{mo}^2 \rangle = \frac{1}{2} \langle (a_1 - a_2)(x_1 - x_2) + (a_2 - a_3)(x_2 - x_3) + (a_3 - a_1)(x_3 - x_1) \rangle \quad (2.5)$$

where the angle brackets denote a statistical weighted average of γ_{mo}^2 for different molecular conformations.

$$\begin{aligned} \text{Thus } \langle \gamma_{mo}^2 \rangle &= \frac{3}{2} \langle a_{\alpha\beta} x_{\alpha\beta} - \frac{1}{3} a_{\alpha\alpha} x_{\beta\beta} \rangle \\ &= \frac{45}{2} kT\theta_1 \end{aligned} \quad (2.6)$$

If one introduces a magnetic local field correction $[(\mu_r + 2)/3]^2$, where μ_r is the relative permeability of the medium, and substitutes for $\langle \gamma_{mo}^2 \rangle$ in (2.4) one obtains:

$$C = \frac{L\rho}{30n\lambda_0^2 \epsilon_0 M_m kT} \left(\frac{n^2 + 2}{3} \right)^2 \left(\frac{\mu_r + 2}{3} \right)^2 \langle \gamma_{mo}^2 \rangle \quad (2.7)$$

noting that the molecular number density $N = L\rho/M_m$.

where L is the Avogadro Constant
 ρ is the density of the medium
 M_m is its molar mass.

Therefore knowing the refractive index data etc., and that μ_r is very close to unity for a diamagnetic medium, the Cotton-Mouton constant gives an estimate of the molecular magneto-optical anisotropy, $\langle \gamma_{mo}^2 \rangle$. However, as will be discussed later, this estimate is crude as there are other factors determining C which are not embodied in (2.7).

One may define a Molar Cotton-Mouton Constant, ${}_m C$, analogous to that given by Otterbein²¹ for the Molar Kerr Constant:

$${}_m C = \left[\frac{2nV_m \mu_0^2}{3(n^2 + 2)^3} \right] \lim_{B \rightarrow 0} \left(\frac{\Delta n}{B^2} \right) \quad (2.8)$$

The molar volume $V_m = M_m/\rho$

$$\text{and } C = \lim_{B \rightarrow 0} \left(\frac{\Delta n}{\lambda_0 B^2} \right)$$

$$\text{Therefore } \underline{C} = \frac{2\lambda_o \mu_o^2}{3} \left[\frac{nM \underline{C}}{(n^2+2)^2 \rho} \right] \quad (2.9)$$

2.3 Modifications to the Langevin-Born Theory

The classical theory above is inadequate in a number of respects. Firstly, it does not explain why gases and liquids of highly symmetric, apparently isotropic molecules are weakly birefringent when subjected to a magnetic field. Secondly, it does not account for the variation of C and \underline{C} , depending on state. The possible reasons for these anomalies are discussed in the following subsections.

2.3.1 Magnetic Hyperpolarizability

In order to account for a non-zero magnetic birefringence even in gases of isotropic molecules, Buckingham and Pople²² modified the Langevin-Born equation. The theoretical expression they derived for the molar Cotton-Mouton constant of a system of non-interacting diamagnetic molecules in the limit of zero density ($n \rightarrow 1$) is as follows:

$$\underline{C} = \frac{L\mu_o^2}{270\epsilon_o} \left\{ \eta_{\alpha\delta:\alpha\delta} - \frac{1}{3} \eta_{\alpha\alpha:\beta\beta} + \frac{1}{kT} \left[\alpha_{\alpha\delta} \chi_{\alpha\delta} - \frac{1}{3} \alpha_{\alpha\alpha} \chi_{\beta\beta} \right] \right\} \quad (2.10)$$

The new terms $\eta_{\alpha\delta:\alpha\delta} - \frac{1}{3} \eta_{\alpha\alpha:\beta\beta} = \eta$, the molecular magnetic hyperpolarizability.

Theories of electro-optic hyperpolarizability as applied to the Kerr effect are fairly well developed²³. Magnetic hyperpolarizabilities are much more difficult to measure; recent theoretical developments have been limited to the work of Corfield⁶ and Buckingham et al.⁷ which are briefly discussed as follows.

A basic postulate in physics is that a weak uniform electric field E produces a dipole moment αE in magnitude, where α is the polarizability of the system. This can be modified to accommodate the change in polarizability due to a magnetic field, so the induced electric dipole moment is:

$$\mu_{\text{induced}} = \alpha E + \frac{1}{2} \eta B^2 E \quad (2.11)$$

$\eta_{\alpha\delta:\gamma\delta}$ is a fourth rank tensor representing the modification of the polarizability $\alpha_{\alpha\delta}$ of the molecule by a magnetic field B . η may also be interpreted as the effect of an electric field E on the magnetic

susceptibility $\chi_{\alpha\beta}$ where

$$\chi'_{\alpha\beta} = \chi_{\alpha\beta} + \frac{1}{2} \eta_{\alpha\beta:\gamma\delta} E_{\gamma} E_{\delta} \quad (2.12)$$

The application of the above theories to molecules of various symmetry groups is complex, and depends on the electronic structure of the molecules. Quantum mechanical calculations⁶ show that there will be both diamagnetic and temperature independent paramagnetic contributions to η , $\eta^{(d)}$ and $\eta^{(p)}$ respectively. $\eta^{(d)}$ is negative and depends on the size of the electron cloud whereas $\eta^{(p)}$ is positive, representing the distortion of the cloud. The sign of the Cotton-Mouton constant of intrinsically isotropic molecules will therefore depend on the extent to which excited states are mixed into the ground states by the electric field. Therefore, for molecules with excited state molecular orbitals of low energy and suitable symmetry, one might expect $\eta^{(p)}$ to be dominant yielding a negative value of $\chi_{\alpha\beta}$.

2.3.2 Collision-Induced Effects

Optical polarizability anisotropy can arise in intrinsically isotropic molecules from collisions. Bucaro and Litovitz²⁴ analysed collisional motions in liquids by measurements of the light scattered in the Rayleigh wing from 5 to 500 cm^{-1} . Atoms and molecules become distorted when they interact giving a collision-induced anisotropy. This distortion can be attributed to three types of interaction:

1. Dipole-Induced Dipole (DID). Here a dipole moment is induced in a molecule by the electric field of the incident light. To a first order approximation the total field acting on a molecule is the sum of the external light field and the internal field due to the induced dipoles of neighbouring molecules. Higher order interactions can exist where the induced dipole field acts back on the dipole which induced it etc., but these have not been observed in collision-induced Rayleigh and Raman scattering²⁵. First order effects give an effective pair polarizability varying²⁶ as r^{-3} (r is the distance between atoms or molecules of collision pairs), so it is a long range interaction.
2. Electron Overlap (EO). Here the distortion of electron clouds caused by close collisions leads to an induced pair polarizability. Bucaro and Litovitz²⁴ and Levine and Birnbaum²⁷, using different analyses, proposed that this effect has a r^{-9} dependence.

3. Frame distortion (FD). As the name suggests, this is where the geometry of a polyatomic molecule is distorted by collisions giving a very short range effect suggested²⁴ to vary as r^{-13} .

Thibeau, Oksengorn and Vodar²⁸ assumed only a DID mechanism for interacting argon atoms in a gas from 0 to 150 bars, and extending the work of Buckingham and Stephens²⁹ calculated depolarized scattering intensities which agreed well with those observed. However, experiments on compressed gases, and computer simulations of atomic liquids^{30,31} show that effects due to DID decrease as the density is increased. DID effects are suppressed in liquids because of the symmetrical environment and so EO effects are more important because of their much greater r dependence. Gabelnick and Strauss³² analysed the low frequency depolarized Raman spectrum of CCl_4 and proposed that FD is the most likely cause of induced anisotropy in CCl_4 . Apparently the scattered light intensity observed could be explained by a bending of 9° in the C-Cl bond. However, Tabisz, Wall and Shelton³³ examined collision-induced light scattering spectra from liquid CCl_4 and found the spectra could not be explained by frame distortion alone; in fact there were significant contributions attributable to electron overlap and even long range DID interactions.

Recently Carlson and Flory³⁴ outlined their procedure for the separation of collision-induced from intrinsic molecular DRS, applying it to CCl_4 and four other "isotropic" molecules of T_d symmetry. For a system of independent, non-interacting particles the DRS intensity depends on $\gamma^2 \equiv \frac{3}{2} \text{tr}(\hat{a} \cdot \hat{a})$ where \hat{a} is the anisotropic part of the molecular polarizability tensor \underline{a} . Therefore DRS is quadratic in \hat{a} and will be affected by transient fluctuations in \hat{a} caused by the forementioned collisional mechanisms. However Carlson and Flory assert that since magnetic birefringence is linear in \hat{a} it must be insensitive to transient fluctuations in i.e. $m^C_{\text{collision-induced}} = 0$.

Champion, Dandridge and Meeten²⁰ stated that collisions in liquids that produce fluctuating electro-optic dipoles are likely to also cause magnetic dipoles. This follows from some old work by Gans and Mrowka^{35,36} which relates χ to α and components thereof. Hence Champion et al. postulated that if $\hat{\alpha}$ and $\hat{\chi}$ are the anisotropic parts of $\underline{\alpha}$ and $\underline{\chi}$ then the Cotton-Mouton constant contains terms $[\hat{\alpha} + \delta\hat{\alpha}(t)] \cdot [\hat{\chi} + \delta\hat{\chi}(t)]$ where $\delta\hat{\alpha}$ and $\delta\hat{\chi}$ are time dependent. They expected a collision-induced contri-

bution to magnetic birefringence on the basis that time averaged cross terms $\delta\hat{g}_i \delta\hat{\chi}_i$ are significant. However, their basic assumption that changes in \hat{g} lead to changes in $\hat{\chi}$ is probably incorrect. For example, as explained in Chapter 2, the local environment of a molecule has a great effect on the value of its polarizability anisotropy whilst the molecular diamagnetic susceptibility anisotropy is virtually independent of state.

2.3.3 Angular Correlations in Liquids

The previous theories considered an assembly of isolated, non-interacting molecules. Clearly, modifications must be made due to interactions between molecules in a liquid; these interactions may cause the molecules to be angularly correlated.

Consider, for example, the simple case of a pair-wise interaction in a liquid causing each molecule to be at a definite angle to another, forming a pair over a long time compared to the period of a light wave.

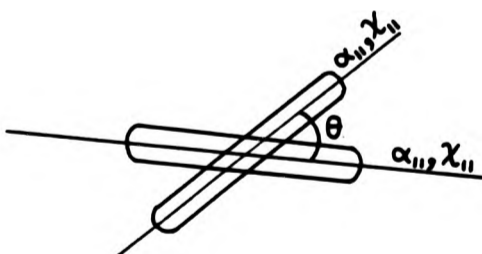


Figure 2.2

Let the pair have an angle θ between major axes of polarizability, and let each molecule have cylindrical symmetry about the $\alpha_{||}, \chi_{||}$ axis as shown in Figure 2.2. If α_{\perp} and χ_{\perp} are the polarizability and susceptibility perpendicular to the symmetry axis then the polarizability and diamagnetic susceptibility tensors are thus

$$\begin{pmatrix} \alpha_{||} & 0 & 0 \\ 0 & \alpha_{\perp} & 0 \\ 0 & 0 & \alpha_{\perp} \end{pmatrix} \text{ and } \begin{pmatrix} \chi_{||} & 0 & 0 \\ 0 & \chi_{\perp} & 0 \\ 0 & 0 & \chi_{\perp} \end{pmatrix}$$

Hence γ_{MO}^2 per molecule is $(\alpha_{||} - \alpha_{\perp})(x_{||} - x_{\perp})$

$$\text{i.e. } \gamma_{MO}^2 = \Delta\alpha\Delta\chi \quad (2.13)$$

Principal axes for the pair are found by symmetry giving:

$$\gamma_{MO}^{2''}(\text{pair}) = \Delta\alpha\Delta\chi(1 + 3 \cos^2 \theta) \quad (2.14)$$

This gives the apparent γ_{MO}^2 per molecule as

$$\gamma_{MO}^{2'}(\text{molecule in pair}) = \Delta\alpha\Delta\chi \frac{(1 + 3 \cos^2 \theta)}{2} \quad (2.15)$$

$$= \gamma_{MO}^2 \left\{ 1 + \frac{1}{2}(3 \cos^2 \theta - 1) \right\} \quad (2.16)$$

So the magneto-optical anisotropy, γ_{MO}^2 , is apparently changed by a factor $1 + \frac{1}{2}(3 \cos^2 \theta - 1)$.

For two parallel molecules $\theta = 0^\circ$ and (2.15) gives $\gamma_{MO}^{2'} = 2\gamma_{MO}^2$. Conversely, for two perpendicular molecules, $\gamma_{MO}^{2'} = \frac{1}{2}\gamma_{MO}^2$. Therefore, angular correlations can increase or diminish the apparent magneto-optical anisotropy of a pair of molecules by a factor of two.

In a liquid, an enormous number of molecules are involved in complex interactions. The orientational correlation parameter, g_2 , is defined as follows^{12,37}:

$$G_2 = 1 + \sum_{j \neq 1}^N \frac{1}{2} \langle 3 \cos^2 \theta_{1j} - 1 \rangle \quad (2.17)$$

for a system of N molecules where θ_{1j} is the angle between the molecular axes of a molecule 1, and another molecule j . Accounting for angular correlations and collision-induced contributions to the molar Cotton-Mouton constant, ${}_m C_{CI}$, (2.10) becomes

$${}_m C = \frac{L\mu_0^2}{270\epsilon_0} \left\{ \eta + \frac{g_2}{kT} [\alpha_{\alpha\beta} x_{\alpha\beta} - \frac{1}{3} \alpha_{\alpha\alpha} x_{\beta\beta}] \right\} + {}_m C_{CI} \quad (2.18)$$

which for symmetric top molecules becomes:

$${}_m C = \frac{L\mu_0^2}{405\epsilon_0} \left\{ \frac{3}{2} \eta + \frac{g_2}{kT} (\Delta\alpha\Delta\chi) \right\} + {}_m C_{CI} \quad (2.19)$$

g_2 can give information on the structure of liquids and may be expressed¹¹

as the radial integral over the average value of the second order Legendre function of $\cos \psi$ (the scalar product of unit vectors along the molecular axis) in each spherical shell around a central molecule:

$$g_2 = 1 + 4\pi\rho \int dr. r^2 g(r) \overline{P_2[\cos\psi](r)} \quad (2.20)$$

where $P_2[\cos\psi](r)$ is the Legendre function, ρ is the density and $g(r)$ is the distribution function of molecular centres. Madden et al.¹¹ calculated that for very small r , $g(r)$ first rises from zero giving a positive integrand since adjacent molecules tend to lie parallel from steric consideration. For r greater than a few molecular diameters the integrand is expected to oscillate about zero.

Therefore the value of g_2 of a simple liquid is determined by the first two or three co-ordination shells, i.e. the first few peaks of $g(r)$, so it depends on whether or not there is cancellation of the first few components in the integrand of (2.20). As mentioned earlier, a value of g_2 significantly greater than unity indicates a tendency to parallel alignment and so can give valuable information concerning the local liquid structure. However, local field effects greatly complicate the measurement of g_2 . These are considered in the following subsection:

2.3.4 Local Field Effects

The electric field acting on a polarizable molecule in a liquid is different in magnitude to that acting on an equivalent molecule in the gas phase. This difference is due to additional fields acting from the induced dipoles of neighbouring molecules in a liquid. This leads to the concept of a local or internal field and one could state that $E_{\text{local}} = E_{\text{incident}} + E_{\text{medium}}$, where E_{incident} is the macroscopic field in the medium and E_{medium} is the field at a molecule due to other induced dipole moments in the system.

Now E_{incident} induces a dipole field $E' = Ea/4\pi\epsilon_0 r^3$ at a distance r from the centre of a bond of polarizability a . Typically $a = 10^{-40} \text{ C}^2 \text{ m}^2 \text{ J}^{-1}$, $r = 10^{-10} \text{ m}$ to give $E' = E$ so contributions to the local electric field from the surrounding medium are not negligible. However, for a magnetic field $H' = H\chi/4\pi r^3$, and for typical diamagnetic substances $\chi = 10^{-34} \text{ m}^3$ giving $H' = 10^{-5} \text{ H}$, and so there is little distortion of the magnetic field at a bond due to magnetic dipoles induced in neighbouring bonds. Therefore molecular diamagnetic susceptibility tensors χ may be

considered as independent of state and local magnetic field corrections are not important. This is reflected in that the relative permeability, μ_r , of diamagnetic substances is very close to unity.

Since the molecular radial and angular distribution functions are not known for liquids, macroscopic models are used to describe the local electric field. The simplest and most often used of these is the spherical Lorentz local field correction:

$$\underline{E}_L/\underline{E} = \frac{1}{3} (n^2 + 2)^2 \quad (2.21)$$

where \underline{E}_L is the local field and \underline{E} the macroscopic field in the medium. This is embodied in the Langevin-Born equation (2.4). The model considers the molecules as residing in a virtual sphere; clearly this is unrealistic.

The Onsager-Böttcher^{38,39} approach considers the polarizable molecule as being surrounded by a cavity and regards the polarizing field \underline{E}_L as being composed of a cavity field, \underline{E}_c , and a reaction field, \underline{E}_r . \underline{E}_c is the field which would exist in the cavity if the molecule was removed, i.e. it is proportional to the macroscopic field in the medium and depends on the shape of the molecule; \underline{E}_r is the field due to the molecule, i.e. it is proportional to the total electric dipole moment and depends on the instantaneous orientation of the molecule. If r is the radius of the molecular cavity and \underline{m} the dipole moment of the molecule in the cavity, it follows that³⁸:

$$\begin{aligned} \underline{E}_L &= \underline{E}_c + \underline{E}_r \\ &= \frac{3n^2}{2n^2 + 1} \underline{E} + \frac{2(n^2 - 1)}{(2n^2 + 1)r^3} \underline{m} \end{aligned} \quad (2.22)$$

Now for non-polar molecules $\underline{m} = \underline{a}\underline{E}_L$, where \underline{a} is the molecular polarizability. Hence it follows that³⁹:

$$\underline{E}_L/\underline{E} = \frac{3n^2}{2n^2 + 1 - 2(n^2 - 1)\underline{a}/r^3} \quad (2.23)$$

Whilst being more realistic than the Lorentz local field, the cavity radius r is ill defined.

The Onsager-Scholte model⁴⁰ considers the cavity as ellipsoidal. From this follows:

$$E_{Li}/E_i = \left[1 - \left(\frac{n^2 - 1}{n^2} \right) \cdot S_i \{ 1 + 3(1 - S_i) \alpha_{ii} / r^3 \} \right]^{-1} \quad (2.24)$$

where E_{Li} and E_i are the components of \underline{E}_L and \underline{E} along the molecular axes i , S_i is a shape factor, α_{ii} are the diagonal values of the molecular polarizability tensor, and $r = (r_1 r_2 r_3)^{1/3}$, where r_1, r_2, r_3 are the radii along the principal axes of the ellipsoid. For a pseudo-spherical molecule $S_i = \frac{1}{3}$ and $\alpha = \alpha_{ii}$ so (2.24) reduces to (2.23). This model was found to be consistent with recent isotropic and anisotropic Rayleigh scattering data⁴¹ of some liquid tetrachloromethane and benzene derivatives.

Local field considerations can be dealt with in another way. Instead of an induced dipole moment $\underline{\mu} = \underline{\alpha} \underline{E}_L$, one can consider $\underline{\mu} = \underline{\alpha}_{eff} \underline{E}$ ⁴², and examine how the effective polarizability α_{eff} is affected by the surrounding medium due to molecules being excluded from a molecule-shaped cavity. Hence the ratio $\Delta\alpha_{eff}/\Delta\alpha$ can be considered as the modification of the Lorentz local field experienced by a molecule due to the local structure of the liquid⁴³. Then equation (2.19) becomes:

$$m^C = \frac{L\omega_o^2}{405\epsilon_o} \left\{ \frac{3}{2}n + \frac{g_2 \Delta\alpha_{eff} \Delta X}{kT} \right\} + m^C_{CI} \quad (2.25)$$

For molecules having a relatively large intrinsic anisotropy such as benzene, n and m^C_{CI} may be considered small relative to the $\frac{g_2 \Delta\alpha_{eff} \Delta X}{kT}$ term³⁷. As indicated earlier ΔX is virtually independent of state but g_2 is difficult to extract since it is combined with $\Delta\alpha_{eff}$, which is another variable property of the medium. The most common method used to separate these variables is to dilute the molecules of interest in a solvent of "isotropic" molecules such as CCl_4 and extrapolate data to infinite dilution⁴⁴⁻⁴⁶, where g_2 should be unity. However, the dielectric permittivity of the solution will change during dilution so $\Delta\alpha_{eff}$ will not generally be constant.

A more satisfying approach is that of Battaglia, Cox and Madden³⁷ who have calculated $\Delta\alpha_{eff}$ and g_2 for some moderately anisotropic liquids of symmetric top molecules using magnetic birefringence, depolarized Rayleigh scattering and diamagnetic anisotropy data. Their method would be difficult to apply to liquids of weakly anisotropic molecules because then magnetic hyperpolarizability and possibly collision-induced contributions will be significant in determining the molar Cotton-Mouton Constant.

2.4 The Sign of the Cotton-Mouton Constant

For diamagnetic molecules possessing even a fairly weak magneto-optical anisotropy the temperature dependent term dominates in (2.25), and can be either positive or negative depending on the relative signs $\Delta\alpha_{\text{eff}}$ and $\Delta\chi$. If the molecule is axially symmetric, a positive value of C or ${}_{\text{m}}C$ indicates that the axis of maximum electro-optic polarizability coincides with that of minimum diamagnetic susceptibility, as defined in (2.4) and (2.5). Coincidence of the two maxima is shown by a negative Cotton-Mouton constant, noting that here since X is always negative for diamagnetic species, numerical and not algebraic values of X are being discussed.

For intrinsically isotropic molecules other terms are responsible for measured values of ${}_{\text{m}}C$, such as magnetic hyperpolarizability or possibly collision-induced contributions. These may be either positive or negative as discussed in the relevant sections.

2.5 Theories of the Magneto-Optical Anisotropy of Chain Molecules

As much of this thesis is concerned with the molar Cotton-Mouton constants of chain molecules such as alkanes, theories on their magneto-optical anisotropies must be considered. An introduction to some of the theories applied follows; they are considered in more detail in the relevant sections of Chapter 5.

2.5.1 The Bond Polarizability Additivity Approximation

The Bond Polarizability Additivity theory (BPA) originally put forward by Wang⁴⁷ and Denbigh⁴⁸ proposes that the polarizability tensor of a molecule can be calculated by summing the individual bond polarizability tensors. Hence, by defining suitable axes theoretical mean molecular polarizabilities ($\bar{\alpha}$) and polarizability anisotropies (γ^2) may be calculated. In the most basic form of BPA it is assumed that bond polarizability tensors are independent of their environment⁴⁹⁻⁵¹ leading to the compilation of tables of experimental bond polarizabilities for various chemical bonds⁵²⁻⁵⁵.

BPA assumes $\alpha_{\text{molecule}} = \sum (\alpha_{\text{bond}})$ where \sum is the sum over all numbers and species of chemical bonds in the molecule. The same assumption is

also applied to the summing of bond diamagnetic susceptibility tensors to obtain χ_{molecule} . Consider a simple axially symmetric molecule having principal axes 1, 2 and 3 as in Figure 2.3.

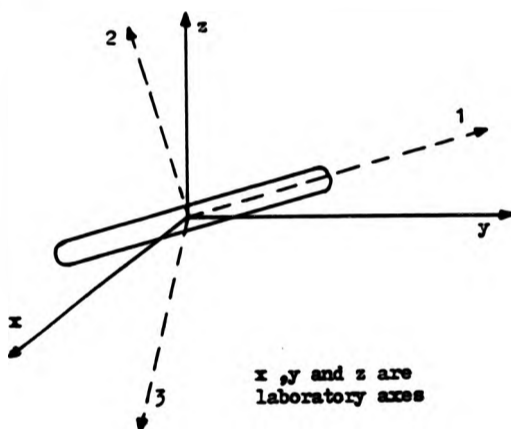


Figure 2.3

Consider an electrical field, E_x applied in the x direction,

$$\left. \begin{aligned} \text{Then } E \text{ along 1 axis} &= E_x \cos(1,x) \\ \text{along 2 axis} &= E_x \cos(2,x) \\ \text{along 3 axis} &= E_x \cos(3,x) \end{aligned} \right\} \quad (2.26)$$

Hence, the induced dipole moments due to the field E_x , for the 1,2,3 principal axes of the molecule are:

$$\left. \begin{aligned} m_1 &= \alpha_{11} E_x \cos(1,x) \\ m_2 &= \alpha_{22} E_x \cos(2,x) \\ m_3 &= \alpha_{33} E_x \cos(3,x) \end{aligned} \right\} \quad (2.27)$$

$$\text{And } m_x = [m_1 \cos(1,x) + m_2 \cos(2,x) + m_3 \cos(3,x)] E_x \quad (2.28)$$

Hence the effective polarizability for a field along the x axis,

$$\alpha_{xx} = m_x / E_x = \alpha_{11} \cos^2(1,x) + \alpha_{22} \cos^2(2,x) + \alpha_{33} \cos^2(3,x) \quad (2.29)$$

The applied field E_x also produces moments m_y and m_z . Hence

$$\alpha_{yy} = \alpha_{11} \cos^2(1,y) + \alpha_{22} \cos^2(2,y) + \alpha_{33} \cos^2(3,y) \text{ etc} \quad (2.30)$$

and for off-diagonal components of α :

$$a_{xy} = a_{11} \cos(1,x) \cos(1,y) + a_{22} \cos(2,x) \cos(2,y) + a_{33} \cos(3,x) \cos(3,y)$$

etc. (2.31)

If suitable axes are chosen \underline{a} can be diagonalized.

Components of \underline{X} may be calculated in a similar fashion and therefore, if one knows the components of \underline{a} and \underline{X} for the constituent bond of a molecule one can calculate γ_{MO}^2 by summing contributions and substituting into (2.5) and (2.6).

As an example, γ_{MO}^2 of the water molecule would be calculated using bond values of \underline{a} and \underline{X} as follows:

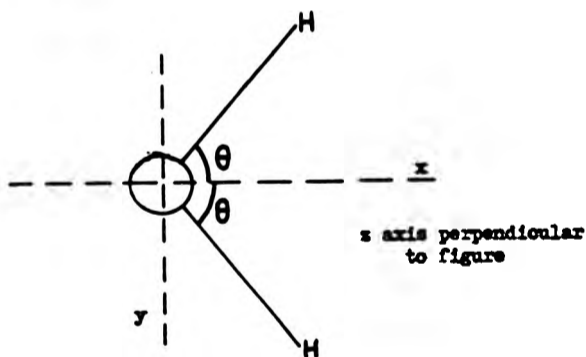


Figure 2.4

For a simple molecule like water the principal axes are obvious, as shown in Fig. 2.4. Assume the OH bonds are cylindrically symmetric.

$$\left. \begin{aligned} \text{Then } a_{11} &= a_{//}^{OH} \\ a_{22} &= a_{33} = a_{\perp}^{OH} \end{aligned} \right\} \quad (2.32)$$

Substituting into (2.32) and (2.33) one gets:

$$\left. \begin{aligned} a_{xx} &= 2a_{//}^{OH} \cos^2 \theta + 2a_{\perp}^{OH} \sin^2 \theta \\ a_{yy} &= 2a_{//}^{OH} \sin^2 \theta + 2a_{\perp}^{OH} \cos^2 \theta \\ a_{zz} &= 2a_{\perp}^{OH} \end{aligned} \right\} \quad (2.33)$$

and similarly for components of \underline{X} . Now, from (2.5),

$$\gamma_{\text{MO}}^2 = \frac{1}{2} \left\{ (\alpha_{\text{XX}} - \alpha_{\text{YY}})(\chi_{\text{XX}} - \chi_{\text{YY}}) + (\alpha_{\text{YY}} - \alpha_{\text{ZZ}})(\chi_{\text{YY}} - \chi_{\text{ZZ}}) + (\alpha_{\text{ZZ}} - \alpha_{\text{XX}})(\chi_{\text{ZZ}} - \chi_{\text{XX}}) \right\} \quad (2.34)$$

Substituting values of $\underline{\alpha}$ and $\underline{\chi}$ as in (2.33) gives:

$$\gamma_{\text{MO}}^2 = (1 + 3\cos^2 2\theta) (\alpha_{\text{H}}^{\text{OH}} - \alpha_{\text{L}}^{\text{OH}}) (\chi_{\text{H}}^{\text{OH}} - \chi_{\text{L}}^{\text{OH}}) \quad (2.35)$$

Hence γ_{MO}^2 is expressed in terms of bond values of polarizability and susceptibility, and only bond anisotropies enter into γ_{MO}^2 .

For the limitation of the BPA approximation, and its application to alkanes, see Section 5.4.

2.5.2 The Rotational Isomeric Model

Polymers such as n-alkanes are non-freely rotating chains by virtue of steric hindrances, due to mutual repulsions between molecular orbitals. Consider the simplest n-alkane chain, ethane (C_2H_6).

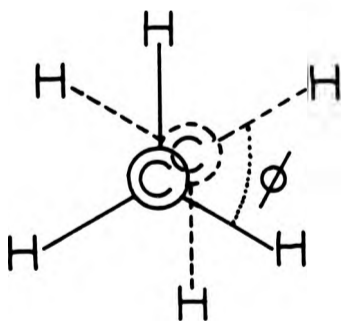


Figure 2.5

An end-on view of the molecule (Fig. 2.5) demonstrates that the internal rotational angle $\phi = 60^\circ$ is preferred to $\phi = 0^\circ$ because the former is the state of least interaction between repulsive molecular orbitals. For chains longer than four carbon atoms (butane) there are real steric hindrances on certain rotations. The following energy level scheme exists for butane⁵⁶.

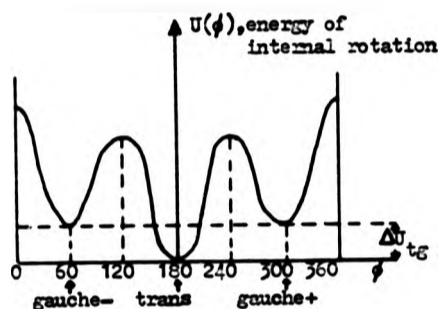


Figure 2.6

The rotational-isomeric state approximation is that molecules exist in the lower energy trans and gauche states only. Then the most important parameter determining the conformation of a molecule for a given temperature is the difference in energy between trans and gauche energy levels, ΔU_{tg} . This is discussed in more detail in Section 5.4.

2.6 Theories of the Magnetic Birefringence and Dichroism of Colloidal Dispersions

The refractive index of colloidal materials is generally complex due to their strong light scattering and extinction, so n should be written as:

$$n = n' - ik'' \quad (2.36)$$

2.6.1 Derivation of $\Delta n'$

The real part of n' of the complex refractive index is related to the phase shift in the wave transmitted in the optical medium. Linear anisotropy of n' gives linear birefringence. Linear birefringence and dichroism result mainly from the preferential orientation of non-spherical molecules in liquid, or colloidal particles in dispersions.

Equation (2.1) gives the linear birefringence $\Delta n'$ in terms of the measured induced phase difference δ as

$$\Delta n' = \frac{\lambda_0}{2\pi l} \delta \quad (2.37)$$

2.6.2 Derivation of $\Delta n''$

The imaginary part, n'' of the complex refractive index is related to the amplitude decrease of the transmitted wave through the medium. Linear anisotropy of n'' gives linear dichroism.

Previous equations within this chapter have related to pure liquids. These have values of dichroism immeasurably small using current equipment, since $|\Delta n''|_{\text{liquid}} \ll |\Delta n'|$. However, colloidal dispersions scatter light much more than liquids and so can have a measurable linear dichroism when subjected to a strong magnetic field.

Consider a ray of light entering a cell of length l containing a turbid medium as shown in Figure 2.7.

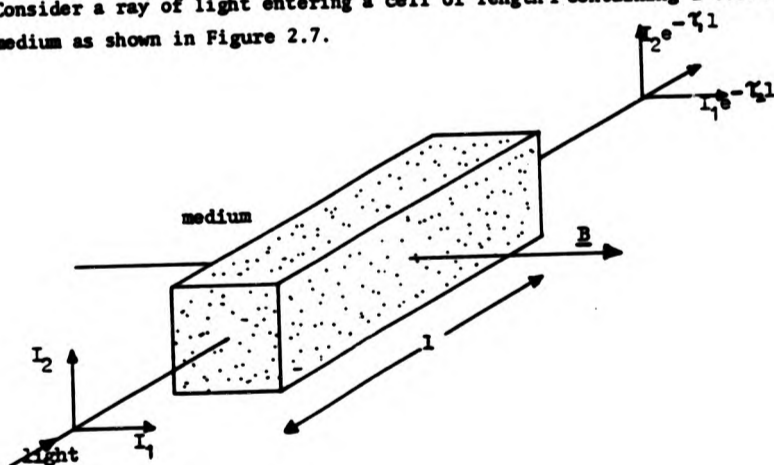


Figure 2.7

When a magnetic field \underline{B} is applied, the preferential orientation of the particle causes an anisotropy of transmissibility of the medium.

For polarized light of intensity I_1 parallel and I_2 perpendicular to the magnetic field, the emergent intensities are $I_1 e^{-\tau_1 l}$ and $I_2 e^{-\tau_2 l}$ respectively⁵⁷, where τ_1 and τ_2 are the respective turbidities. Therefore, for normalised intensities one may define transmissibilities:

$$\begin{aligned} k_1 &= e^{-\tau_1 l} \\ k_2 &= e^{-\tau_2 l} \end{aligned} \quad (2.38)$$

Note that the turbidity or extinction coefficient τ can be related to

the scattering cross-section of a particle, C, as follows⁵⁷:

$$\tau = NC \quad (2.39)$$

where N is the number density of particles. The linear dichroism of a substance may be defined as

$$\frac{\Delta k}{k_a} = 2 \frac{(k_1 - k_2)}{(k_1 + k_2)} \quad (2.40)$$

Substituting (2.38) in the above one gives

$$\frac{\Delta k}{k_a} = 2 \left(\frac{e^{-\tau_1 l} - e^{-\tau_2 l}}{e^{-\tau_1 l} + e^{-\tau_2 l}} \right) \quad (2.41)$$

Now if Δk is small and the transmissibilities are close to unity, $\tau l \ll 1$.

$$\text{Then } \frac{\Delta k}{k_a} = -(\tau_1 - \tau_2)l \quad (2.42)$$

$$= -Nl(C_1 - C_2) \quad (2.43)$$

$$\text{Now } \tau = \frac{4\pi}{\lambda_0} n'' \quad (2.44)$$

$$\text{Therefore } \Delta n'' = n_1'' - n_2'' = \frac{-\lambda_0}{4\pi l} \frac{\Delta k}{k_a} \quad (2.45)$$

giving $\Delta n''$ in terms of the measured dichroism Δk .

2.6.3 Application of Light Scattering Theories to Colloidal Dispersions

For small particles up to $\sim \lambda/20$ in diameter (i.e. 30 nm), phase and amplitude variations over the particle may be neglected. This is defined as the Rayleigh scattering region⁵⁷. Particles of any size that are weak enough scatterers may be each considered as composed of Rayleigh scatterers with phase differences between scattered waves. This is defined as the Rayleigh-Gans-Debye region and is applicable as long as the refractive index difference between particle and medium is small. Larger and more absorbing particles are in the Mie scattering region which is far more complex.

In this thesis, only the Rayleigh theory will be considered in detail, in particular its application to the birefringence and dichroism of Fluon dispersions in Section 5.6.

CHAPTER 3

THEORY OF THE METHOD AND ERROR ANALYSIS


To determine the Cotton-Mouton constants of liquids one needs to measure the magnetically induced phase difference δ given by $\delta = \frac{2\pi l}{\lambda_0} \Delta n$, the origin of which is explained in Chapter 2. Early determinations of δ used ocular methods⁵⁸ and a variety of optical compensators. The accuracy and sensitivity of these quadratic detection methods tended to be low, limiting accurate measurements to substances having fairly large values of C, such as organic liquids with delocalized electron systems. However, it will be shown that much can be achieved by using a simple ocular method.

To achieve greater sensitivity many workers have employed photometric linear detection methods using Faraday modulation^{6,8,10,59,60}, usually with a laser as the light source. The accuracy is limited by stray birefringence in the modulator core, the need for the modulator to be very well shielded from the electromagnet and the tendency to include contributions due to Faraday rotation in the sample as a phase difference. In this thesis a more satisfactory modulator using piezo-optic effect was incorporated in a photometric system yielding more accurate results whilst having few of the drawbacks of a Faraday modulator system. In addition, the piezo-optic modulator enables one to measure linear dichroism, also by linear detection. Therefore it was possible to measure with great accuracy not only the Cotton-Mouton constants of liquids of near-isotropic molecules and mixtures thereof, but also the magnetically induced birefringence and dichroism of colloidal dispersions.

PART A - OCULAR METHOD

3.1 Introduction

A schematic representation of the apparatus is given in the following Chapter (Figure 4.1). Light from a mercury discharge lamp is passed through a system of lens, apertures and filter to produce a monochromatic, near-parallel beam. This beam is passed through a polarizer oriented at 45° to the principal polarization axes of the birefringent medium. In this configuration the phase difference



obtainable is a maximum for a given retardation of the birefringent sample. The elliptically polarized light emergent from the birefringent specimen is incident on a quarter wave plate with its principal axes at 45° to those of the birefringent medium. This resolves the two vibratory components in the ellipse so that a phase difference δ_1 between the two vectors may be simply related to the azimuth of the analyser, β .

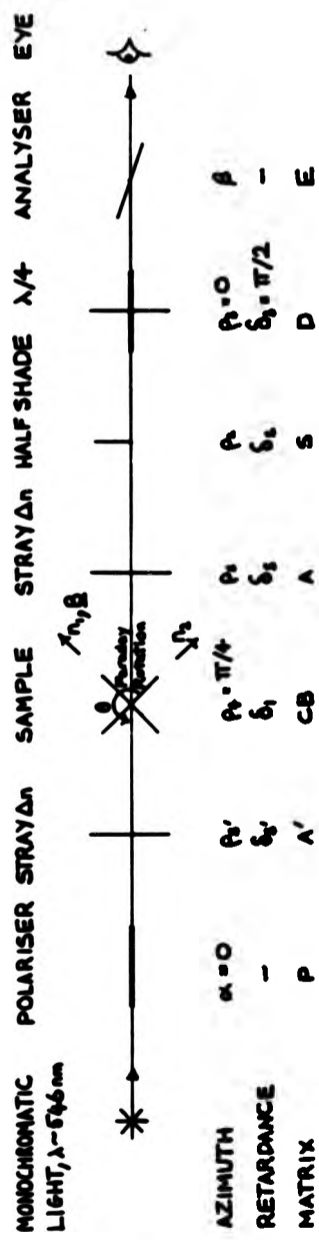
As the intensity of light transmitted by the analyser is a $(\cos\beta)^2$ function, the intensity seen through the telescope near the null point is very insensitive to analyser rotation. Since the null point cannot be accurately determined by eye using this method, an additional phase difference δ_2 is introduced to half the beam by means of a suitably oriented half shade plate interposed between the cell and quarter wave plate as outlined by Jerrard⁶². If the telescope is now focussed on the half shade plate, the analyser may be rotated until the eye matches the intensities of halves of the beam passing and not passing through the retarder. The eye is more efficient at comparing intensities than detecting a null point.

The measurement of phase difference and accompanying errors involved in this Sénarmont method (where a crossed polarizer and analyser are used with a $\lambda/4$ plate) have been previously investigated. Jerrard⁶³ gives a comprehensive coverage of some optical compensators used for the measurement of small phase differences but this involves tedious algebraic analysis and is impractical for more complex systems.

3.2 Theory of the Ocular Method

Mueller calculus employs matrix techniques to describe optical systems enabling one to interpret results and estimate errors quickly and accurately. This method is described in section 3.9 at the end of this Chapter; reference may also be made to Shurcliff⁶⁴. Calculations of results and subsequent error analysis using Mueller calculus are summarized as follows. Schematically the ocular detection method using a half shade plate is illustrated in Figure 3.1, together with a representation of the errors due to Faraday rotation and stray birefringence.

Figure 2.1 Schematic specification of the Secular detection method, including the associated errors



Firstly one should evaluate the balance condition for no errors and consider the effects of the introduction of errors later.

For the half of the beam not traversing the half shade plate the intensity of light emergent from the analyser is derived by performing the matrix multiplication:

$$I_{DC}/I_0 = [E][D][C][P] \quad (3.2)$$

and assuming $\alpha = 0$, $\rho_1 = \pi/4$, $\rho_3 = 0$, $\delta_3 = \pi/2$

Thus, referring to 3.9 for the relevant matrices,

$$2I_{DC}/I_0 = 1 + \cos(2\beta - \delta_1) \quad (3.3)$$

For the light traversing the half shade

$$I_{DSC}/I_0 = [E][D][S][C][P] \quad (3.4)$$

$$\text{Thus } 2I_{DSC}/I_0 = 1 + \cos(2\beta - \delta_1) + \delta_2 \sin 2\rho_2 \sin(2\beta - \delta_1) \quad (3.5)$$

$$\text{For balance } I_{DC} = TI_{DSC} \quad (3.6)$$

where T is the transmittance of the half shade plate.

$$\text{Then } 1 + \cos(2\beta - \delta_1) = T[1 + \cos(2\beta - \delta_1) + \delta_2 \sin 2\rho_2 \sin(2\beta - \delta_1)] \quad (3.7)$$

Rearranging and using the identity $\tan x/2 = \frac{\sin x}{1 + \cos x}$ one obtains

$$\tan\left(\beta - \frac{\delta_1}{2}\right) = \frac{T - 1}{\delta_2 \sin 2\rho_2} \quad (3.8)$$

$$\text{i.e. at the minimum balance } \beta = \frac{\delta_1}{2} + \frac{\pi}{2} - \frac{\delta_2 \sin 2\rho_2}{T - 1} \quad (3.9)$$

Therefore since δ_2 , ρ_2 and T are constant for a given experiment, β is a direct measure of the induced phase difference δ_1 .

3.3 Systematic Error Analysis - Ocular Method

Complete analysis of combinations of errors can lead to very complicated expressions, but it was considered satisfactory to consider each source of error separately plus some logical combinations. Errors have been considered for convenience without the half shade plate in the system. Then the condition for null intensity is that in (3.3): $I_{DC} = 0$ therefore

$$2\beta = \delta_1 + \alpha \quad (3.10)$$

3.3.1 Setting of the Polarizer

The maximum phase difference δ_1 induced by the birefringent medium occurs when the polarizer is inclined at 45° to the magnetic field, i.e. $\rho_1 = \sqrt{A}$ when $\alpha = 0$. To examine the effect of $\alpha \neq 0$ one may again consider the matrix multiplication $I/I_0 = [E][D][C][P]$ as in (3.2) assuming $\rho_1 = \sqrt{A}$, $\rho_3 = 0$, $\delta_3 = \sqrt{2}$ and $\alpha \neq 0$. This gives

$$2I/I_0 = 1 + \cos 2\beta \cos \delta_1 \cos 2\alpha + \sin 2\beta \sin \delta_1 \cos 2\alpha \quad (3.11)$$

$$= 1 + \cos 2\alpha \cos(2\beta - \delta_1) \quad (3.12)$$

$$\therefore \text{null at } \cos(2\beta - \delta_1) = \frac{-1}{\cos 2\alpha} \quad (3.13)$$

For very small α , $\cos 2\alpha \approx 1$ and $2\beta = \delta_1 + \alpha$ as before. So for small phase differences, small errors in setting the polarizer have a negligible effect on the position of the null. One can see from (3.13) that a larger error will shift the null point but as this is constant it will not affect the accuracy of the experiment.

3.3.2 Setting of the Cell

The error referred to here is the error of setting all the other components relative to the magnet, which determines the principal axes of the birefringent medium.

The required intensity is given by the matrix multiplication:

$$I/I_0 = [E][D][C][P] \text{ with } \rho_1 = \sqrt{A} \text{ in } [C]$$

This gives

$$2I/I_0 = 1 + \cos 2\beta [\cos \delta_1 + \cos^2 2\rho_1 (1 - \cos \delta_1)] + \sin 2\beta \sin 2\rho_1 \sin \delta_1 \quad (3.14)$$

If $\rho_1 = \sqrt{A} - \Delta_1$ where Δ_1 is the error in setting the cell

$$\left. \begin{aligned} \text{then } \cos 2\rho_1 &= \sin 2\Delta_1 = 2\Delta_1 \\ \text{and } \sin 2\rho_1 &= \cos 2\Delta_1 = 1 - \Delta_1^2 \text{ if } \Delta_1 \text{ small} \end{aligned} \right\} \quad (3.15)$$

Then, if δ_1 is small and ignoring third order terms:

$$2I/I_0 = 1 + \cos 2\beta \cos \delta_1 + \sin 2\beta \sin \delta_1$$

i.e. at null $2\theta = \delta_1 + \pi$ as before

So, as long as the cell is set reasonably accurately, the null position is unchanged.

3.3.3 Errors Associated with the Quarter Wave Plate

(a) Error in Retardance of $\lambda/4$ Plate

Consider $I/I_0 = [E][D][C][P]$ with $\delta_3 \neq \pi/2$ in [D]. This gives

$$2I/I_0 = 1 + \cos 2\theta \cos \delta_1 + \sin 2\theta \sin \delta_1 \sin \delta_3 \quad (3.16)$$

If $\delta_3 = \pi/2 - \Delta_3$ where Δ_3 is the error in the retardance of the $\pi/4$ plate.

Then $\sin \delta_3 = \cos \Delta_3 = 1 - \frac{1}{2} \Delta_3^2$ if Δ_3 small

$$\text{Then } 2I/I_0 = 1 + \cos(2\theta - \delta_1) - \frac{1}{2} \Delta_3^2 \sin 2\theta \sin \delta_1 \quad (3.17)$$

If δ_1 small, last term is a third order correction and can be ignored and at null $2\theta = \delta_1 + \pi$ as before.

Therefore null errors in the $\lambda/4$ plate retardation do not affect the experimental accuracy.

(b) Setting of $\lambda/4$ Plate

Consider $I/I_0 = [E][D][C][P]$ with $\rho_3 \neq 0$ in [D]

$$\begin{aligned} \text{This gives } 2I/I_0 = 1 + \cos 2\theta (\cos^2 2\rho_3 \cos \delta_1 - \sin 2\rho_3 \sin \delta_1) \\ + \sin 2\theta (\cos 2\rho_3 \sin 2\rho_3 \cos \delta_1 + \cos 2\rho_3 \sin \delta_1) \end{aligned} \quad (3.18)$$

Using small angle approximations for ρ_3 as in (3.15) and ignoring third order terms we get:

$$2I/I_0 = 1 + \cos(2\theta - \delta_1) + 2\rho_3 \sin(2\theta - \delta_1) + 2\rho_3^2$$

At the null point making a small angle approximation

$$\tan(2\theta - \delta_1) = 2\rho_3 \quad (3.19)$$

$$\text{i.e. } 2\theta = \pi + \delta_1 + 2\rho_3$$

which gives a constant error ρ_3 shifting the null point but not actually affecting the accuracy of the experiment.

3.3.4 Faraday Rotation of the Cell

If there is a component of the magnetic field parallel to the light beam, the plane of polarization will be rotated by an angle $\theta = VB/\mu_0$, where V is the Verdet constant dependent on the material. Faraday rotation has long been thought to be a troublesome feature in the determination of small Cotton-Mouton constants since the rotation induced can be large compared to small induced phase differences.

For simple calculations it may be possible to consider the rotation as a separate operation to birefringence but it is fundamentally more correct to consider a matrix⁶⁵ (matrix [CB]) containing both these effects simultaneously.

Then the required intensity is given by $I/I_0 = [E][D][CB][P]$. Then

$$2I/I_0 = 1 + \cos 2\beta \cos D + \frac{\delta_1}{D} \sin 2\beta \sin D \quad (3.20)$$

where $D = (4\theta^2 + \delta_1^2)^{1/2}$

Then at the null if D is small:

$$0 = -\sin 2\beta (1 - \frac{1}{2}D^2) + \delta_1 \cos 2\beta$$

i.e. $\tan 2\beta = \delta_1 (1 + \frac{1}{2}D^2)$

So if δ_1 and β are small:

$$2\beta = \delta_1 (1 + 2\theta^2) + \pi \quad (3.21)$$

Since the error due to θ depends on the square of the magnetic field, it cannot be detected by field reversal. Faraday rotations can be large and do not vary much for organic liquids, for example CCl_4 in the 20 cm cell at the highest magnetic field ($\sim 2T$) would cause a 3° rotation for a 1° misalignment of the magnet. Substituted into (3.21) this gives an error of about 0.5% in the measurement of δ_1 . The magnet was aligned more accurately than this and typical errors due to Faraday rotation alone are estimated at about 0.1% which is not serious.

3.3.5 Combination of Stray Birefringence and Faraday Rotation

It is simple to show that stray birefringence due to the cell windows will be simply additive to the birefringence induced in the medium and as long as any drift in the stray birefringence can be compensated for,

it will not affect the results. However previous workers^{6,7} have found that a combination of stray birefringence and Faraday rotation affects the accuracy of measurements of small phase differences.

So error calculations should consider a combination of Faraday rotation and birefringence in the cell (θ and δ_1 in the matrix [CB] together with stray birefringence in a cell window (δ_s at azimuth ρ_s in the matrix [A]). The required intensity is given by the matrix multiplication:

$$I/I_0 = [E][D][A][CB][P]$$

$$\therefore 2I/I_0 = 1 + \cos 2\theta \left[\cos D - \delta_1 \delta_s \sin 2\rho_s \frac{\sin D}{D} \right] + \sin 2\theta \left[\delta_s \sin 2\rho_s \cos D + (2\theta \delta_s \cos 2\rho_s + \delta_1) \frac{\sin D}{D} \right] \quad (3.22)$$

Then at null for small D and ignoring third order terms:

$$0 = -\sin 2\theta \left[1 - \frac{1}{2} D^2 \right] + \cos 2\theta \left[\delta_s \sin 2\rho_s + 2\theta \delta_s \cos 2\rho_s + \delta_1 \right]$$

$$\text{i.e. } \tan 2\theta = \frac{\delta_1 + \delta_s \sin 2\rho_s + 2\theta \delta_s \cos 2\rho_s}{1 - \frac{1}{2} D^2}$$

$$\text{i.e. } 2\theta = \pi + \left(1 + \frac{1}{2} D^2 \right) \left[\delta_1 + \delta_s (\sin 2\rho_s + 2\theta \cos 2\rho_s) \right]$$

$$\text{i.e. } 2\theta = \pi + \delta_1 (1 + 2\theta^2) + \delta_s (\sin 2\rho_s + 2\theta \cos 2\rho_s) \quad (3.23)$$

which is the same null condition as in (3.21) with the addition of a $\delta_s (\sin 2\rho_s + 2\theta \cos 2\rho_s)$ term. Of this the $\delta_s \sin 2\rho_s$ term is independent of magnetic field and can be compensated for but the $2\theta \delta_s \cos 2\rho_s$ term is significant as it demonstrates how the null point can depend linearly on the magnetic field. In principle errors arising from this can be detected by field reversal but δ_s and ρ_s will tend to change with time. Inserting a value of 50 mrad for θ and 100 μ rad for δ_s gives a maximum error of 10 μ rad in the null position which is small compared to the overall experimental error of this method.

PART B - PHOTOMETRIC METHOD

3.4 Introduction

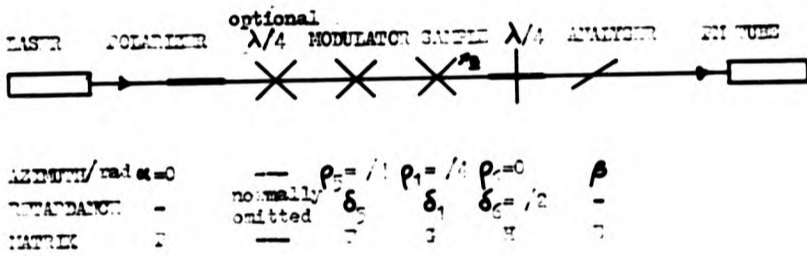
Described below are linear detection methods for measuring both birefringence and dichroism. Apparatus was constructed in order to make measurements to a very high degree of accuracy ranging from the magnetic birefringence of near-isotropic molecules to the magnetic dichroism of colloidal dispersions. Schematically the apparatus is represented in Figures 4.3 and 3.2.

The first method for measuring birefringence only is in principle a simple modification of the ocular method described in Part A. Briefly, linearly polarized monochromatic light from a Helium-Neon Laser is modulated by a piezo-optic modulator and is then incident on the birefringent medium. If the modulator and medium have their principal axes at 45° to the plane of polarization of the laser beam then the degree of ellipticity of the emergent light is a maximum. The emergent modulated elliptically polarized light is then incident on a quarter wave plate whose principal axes are at 45° to those of the birefringent medium, resolving the modulated components of the ellipse and effectively rotating the original plane of polarization so that the phase difference δ_1 induced in the medium can be related to β , the azimuth of the analyser. The signal received at the detector (a photomultiplier) is demodulated using a phase sensitive detector and the analyser rotated to give a null in the modulated intensity.

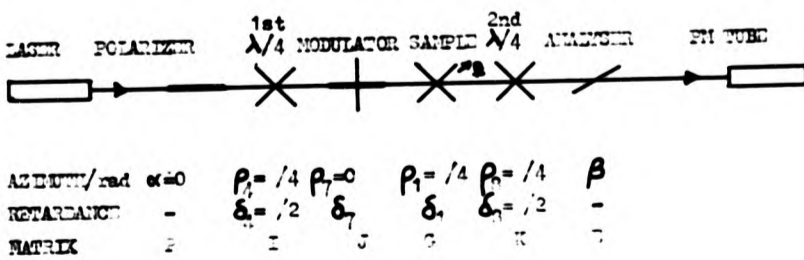
The second method for measuring birefringence and dichroism employs an extra quarter wave plate. Monochromatic linearly polarized light is incident on the first $\lambda/4$ plate set at 45° to the plane of polarization, causing emergent light to be circularly polarized. This is modified by the magnetically induced birefringence and dichroism of the sample and emerges as elliptically polarized light. The piezo-optic modulator will modulate birefringent or dichroic components if it is oriented at 45° or 0° respectively. The appropriate modulated component at the fundamental frequency w of the modulator is converted into linearly polarized light by the second $\lambda/4$ plate oriented at 0° or 45° for birefringence and dichroism respectively and the azimuth of the analyser changed for a null in the demodulated intensity.

Figure 3.2 Schematic specifications of Photometric method

a) Measuring birefringence Δn



b) Measuring dichroism $\Delta k/k_0$



As can be seen, two similar methods for measuring birefringence have been outlined above. The first employs fewer components (only one $\lambda/4$ plate) and so should be slightly more accurate. The advantage of the second method is that since only the azimuths of the modulator and second $\lambda/4$ plate have both to be altered by 45° when making successive measurements of dichroism and birefringence these components could be mechanically linked with bump stops 45° apart so the change can be made quickly and precisely.

As many more birefringence than dichroism measurements were made, the simpler method was used almost exclusively because of the extra accuracy attainable.

3.5 Theory of Birefringence Measurements by Photometric Method

Once more the application of Mueller calculus greatly simplifies calculations concerning trains of optical devices.

If the principal transmission axes are k_1 and k_2 we define

$$k_a = \frac{1}{2}(k_1 + k_2), \quad k_g = (k_1 k_2)^{1/2}, \quad \Delta k = k_1 - k_2 \quad (3.24)$$

Then the required intensity is given by performing the matrix multiplication-

$$I/I_0 = [E][H][G][F][P]$$

Then making the assumptions contained in Figure 3.2a i.e. that all components are perfectly aligned:

$$2I/I_0 = k_a + k_g \cos 2\delta (\cos \delta_1 \cos \delta_5 - \sin \delta_1 \sin \delta_5) \\ + k_g \sin 2\delta (\sin \delta_1 \cos \delta_5 + \cos \delta_1 \sin \delta_5) \quad (3.25)$$

$$= k_a + k_g \cos(2\delta - \delta_1 - \delta_5) \quad (3.25a)$$

Now the phase difference induced in the piezo-optic modulator, $\delta_5 = \Delta_5 \sin \omega t$ where Δ_5 is the maximum phase difference and ω is the frequency of oscillation. Therefore if δ_5 is small, to a second order approximation:

$$\cos\delta_5 = 1 - \frac{1}{2}\Delta_5^2 = 1 - \frac{1}{2}\Delta_5^2 \sin^2 \omega t = 1 - \frac{1}{4}\Delta_5^2 (1 - \cos 2\omega t) \quad (3.26)$$

$$\text{and } \sin\delta_5 = \delta_5 = \Delta_5 \sin \omega t$$

Substituting (3.26) in (3.25) and rearranging gives:

$$2I/I_0 = k_a + k_g \left[\left(1 - \frac{1}{4}\Delta_5^2 + \frac{1}{4}\Delta_5^2 \cos 2\omega t \right) \cos(2\theta - \delta_1) + \Delta_5 \sin \omega t \sin(2\theta - \delta_1) \right] \quad (3.27)$$

Now one can examine terms in I at various frequencies:

Zero frequency: I_z

$$2I_z = k_a + k_g \left(1 - \frac{1}{4}\Delta_5^2 \right) \cos(2\theta - \delta_1) \quad (3.28)$$

$$\text{Gives a null at } k_a = \left(\frac{1}{4}\Delta_5^2 - 1 \right) k_g \cos(2\theta - \delta_1)$$

$$\text{i.e. when } \cos(2\theta - \delta_1) = \frac{k_a}{k_g \left(\frac{1}{4}\Delta_5^2 - 1 \right)}$$

Now Δ_5^2 is very small ($\sim 10^{-6}$) and for small dichroisms $k_a = k_g$.

$$\text{Therefore } \cos(2\theta - \delta_1) = -1$$

$$\text{Then } 2\theta = \delta_1 + \pi \quad \text{at null} \quad (3.29)$$

Fundamental frequency: I_w

$$2I_w = k_g \Delta_5 \sin \omega t \sin(2\theta - \delta_1) \quad (3.30)$$

$$\text{Gives a null at } \sin(2\theta - \delta_1) = 0$$

$$\text{i.e. } 2\theta = \delta_1 + n\pi \quad \text{at null where } n \text{ is an integer} \quad (3.31)$$

Double frequency: I_{2w}

$$2I_{2w} = \frac{1}{4} k_g \Delta_5^2 \cos 2\omega t \cos(2\theta - \delta_1) \quad (3.32)$$

$$\text{Gives a null at } \cos(2\theta - \delta_1) = 0$$

$$\text{i.e. } 2\theta = \delta_1 \pm \pi/2 \quad \text{at null} \quad (3.33)$$

Note that since Δ_5 is small (typically 10^{-3} radians), Δ_5^2 is very small so the I_{2w} signal will generally be very much smaller than the I_w one. This means that measurements of I_w could be made without needing a twin-T filter to reject I_{2w} .

For null of I_w , $\sin(2\theta - \delta_1) = 0$ so $\cos(2\theta - \delta_1) = \pm 1$

For smallest I_z choose $\cos(2\theta - \delta_1) = -1$

Then at I_w null point:

$$I_z = \frac{1}{2}(k_e - k_g) \quad - \text{very small if dichroism low}$$

$$I_{2w} = -\frac{1}{8}k_g\Delta_5^2 \cos 2\omega t \quad - \text{very small}$$

Note that since $I_w \propto \Delta_5$ in (3.30), this is a linear detection method for δ_1 and hence $\Delta\alpha$.

3.6 Systematic Error Analysis - Measuring Birefringence

As before it was considered satisfactory to reckon each source of error separately plus some logical combinations. (3.31) gives the null condition of I_w as $2\theta = \delta_1 + \pi$.

3.6.1 Setting of the Polarizer

As for the ocular method, the maximum phase difference δ_1 induced by the birefringent medium occurs when the polarizer is inclined at 45° to the magnetic field i.e. $\rho_1 = \pi/4$ when $\alpha = 0$.

To examine the effect of $\alpha \neq 0$, one may again consider the matrix multiplication $I/I_0 = [S][H][G][F][P]$ but with $\alpha \neq 0$. Then

$$2I/I_0 = k_g + \frac{1}{2}\Delta k \sin 2\alpha + k_g \cos 2\alpha [\cos 2\theta (\cos \delta_1 \cos \delta_5 - \sin \delta_1 \sin \delta_5) + \sin 2\theta (\sin \delta_1 \cos \delta_5 + \cos \delta_1 \sin \delta_5)] \quad (3.34)$$

Rearranging and using the second order approximation for δ_5 in (3.26) one gets the fundamental frequency component:

$$2I_w = k_g \cos 2\alpha (\Delta_5 \sin \omega t \sin(2\theta - \delta_1)) \quad (3.35)$$

with a null at $\sin(2\theta - \delta_1) = 0$ as before.

Therefore an error in setting the polarizer will not affect the position of the null, only the "depth" of null is altered leading to reduced sensitivity.

3.6.2 Setting of the Modulator

For measuring birefringence the azimuth of the modulator should be $\rho_5 = \pi/4$. To examine the effect of a setting error consider $I/I_0 = [E][H][G][F][P]$ with $\rho_5 \neq \pi/4$.

$$\begin{aligned} \text{Then } 2I/I_0 &= k_g + \frac{1}{2} \Delta k \cos 2\rho_5 \sin 2\rho_5 (1 - \cos \delta_5) \\ &+ k_g \cos 2\theta \cos \delta_1 [\cos^2 2\rho_5 (1 - \cos \delta_5) + \cos \delta_5] - k_g \cos 2\theta \sin \delta_1 \sin 2\rho_5 \sin \delta_5 \\ &+ k_g \sin 2\theta \sin \delta_1 [\cos^2 2\rho_5 (1 - \cos \delta_5) + \cos \delta_5] + k_g \sin 2\theta \cos \delta_1 \sin 2\rho_5 \sin \delta_5 \end{aligned} \quad (3.36)$$

Rearranging and using the second order approximation for δ_5 from (3.26) one gets the fundamental frequency component:

$$2I_w = \Delta_5 \sin \omega t \sin 2\rho_5 (k_g \sin 2\theta - \delta_1) \quad (3.37)$$

Now if $\rho_5 = \pi/4 - \Delta'$ where Δ' is the modulator setting error, then $\sin 2\rho_5 = \cos 2\Delta' = 1 - 2\Delta'^2$ if Δ' small.

Substitute in (3.37) to get

$$2I_w = (1 - 2\Delta'^2) k_g \Delta_5 \sin \omega t \sin(2\theta - \delta_1) \quad (3.38)$$

Giving a null at $\sin(2\theta - \delta_1) = 0$ as before.

So again the "depth" of null is altered.

3.6.3 Setting of the Cell

Ideally the azimuth of the "cell" (i.e. the direction of the magnetic field) should be $\rho_1 = \pi/4$. To examine an error in this consider

$$I/I_0 = [E][H][H][F][P] \text{ with } \rho_1 \neq \pi/4.$$

$$\begin{aligned} \text{Then } 2I/I_0 = & k_a + k_g \cos 2\beta \left[\cos \delta_5 \{ \cos^2 2\rho_1 (1 - \cos \delta_1) + \cos \delta_1 \} - \sin \delta_5 \sin 2\rho_1 \sin \delta_1 \right] \\ & + k_g \sin 2\beta \left[\cos \delta_5 \sin 2\rho_1 \sin \delta_1 + \sin \delta_5 \cos \delta_1 \right] \end{aligned} \quad (3.39)$$

Rearranging and approximating for δ_5 as in (3.26) one gets:

$$2I_w = k_g \Delta_5 \sin \alpha t (-\cos 2\beta \sin 2\rho_1 \sin \delta_1 + \sin 2\beta \cos \delta_1) \quad (3.40)$$

Now if $\rho_1 = \pi/4 - \Delta_1$, where Δ_1 is the setting error

then $\sin 2\rho_1 = \cos 2\Delta_1 = 1 - 2\Delta_1^2$ if Δ_1 small.

Substitute in (3.40) to get

$$2I_w = \Delta_5 k_g \sin \alpha t (\sin(2\beta - \delta_1) + 2\Delta_1^2) \quad (3.41)$$

$$\text{Gives null at } \sin(2\beta - \delta_1) = -2\Delta_1^2 \quad (3.42)$$

So the position of the null is shifted by a constant amount not affecting the accuracy of the experiment.

3.6.4 Errors Associated with the Quarter Wave Plate

(a) Setting of the $\pi/4$ Plate

Ideally the azimuth of the first axis of the $\pi/4$ plate should $\rho_6 = 0$.

To examine an error in this setting consider

$$I/I_0 = [E][H][G][F][P] \text{ with } \rho_6 \neq 0, \delta_6 = \pi/2$$

$$\begin{aligned}
\text{Then } \frac{2I}{I_0} &= k_a + \frac{1}{2} \Delta k [\cos 2\beta \cos 2\rho_6 \sin 2\rho_6 + \sin 2\beta (1 - \cos 2\rho_6)] \\
&+ k_g \cos 2\beta [\cos^2 2\rho_6 (\cos \delta_1 \cos \delta_5 - \sin \delta_1 \sin \delta_5) - \sin 2\rho_6 (\sin \delta_1 \cos \delta_5 + \cos \delta_1 \sin \delta_5)] \\
&+ k_g \sin 2\beta [\cos 2\rho_6 \sin 2\rho_6 (\cos \delta_1 \cos \delta_5 - \sin \delta_1 \sin \delta_5) + \cos 2\rho_6 (\sin \delta_1 \cos \delta_5 \\
&\quad + \cos \delta_1 \sin \delta_5)] \quad (3.43)
\end{aligned}$$

Rearranging and approximating for δ_5 as in (3.26) one gets:

$$\begin{aligned}
2I_w &= -k_g \Delta_5 \sin \omega t (\cos^2 2\rho_6 \cos 2\beta \sin \delta_1 + \sin 2\rho_6 \cos 2\beta \cos \delta_1 + \\
&\quad \cos 2\rho_6 \sin 2\rho_6 \sin 2\beta \sin \delta_1 - \cos 2\rho_6 \sin 2\beta \cos \delta_1) \quad (3.44)
\end{aligned}$$

Now if $\rho_6 = \Delta_6$, a small setting error

$$\text{then } \cos 2\rho_6 = 1 - 2\Delta_6^2, \quad \cos^2 2\rho_6 = 1 - 4\Delta_6^2$$

Substituting in (3.43), for small δ_1 and ignoring third order terms:

$$2I_w = k_g \Delta_5 \sin \omega t [\sin(2\beta - \delta_1) - 2\Delta_6 \cos(2\beta - \delta_1)] \quad (3.45)$$

Giving a constant offset of the null, $2\Delta_6$ which does not affect the accuracy of the experiment.

(b) Error in Retardance of the $\lambda/4$ Plate

Previously the retardance of the $\lambda/4$ plate has been assumed to be exactly 90° . Now consider the matrix multiplication

$$I/I_0 = [E][M][G][F][P] \text{ with } \delta_6 \neq \pi/2.$$

$$\begin{aligned}
\text{Then } 2I/I_0 &= k_a + k_g \cos 2\beta (\cos \delta_1 \cos \delta_5 - \sin \delta_1 \sin \delta_5) + \frac{1}{2} \Delta k \sin 2\beta \cos \delta_6 \\
&+ k_g \sin 2\beta \sin \delta_6 (\sin \delta_1 \cos \delta_5 + \cos \delta_1 \sin \delta_5) \quad (3.47)
\end{aligned}$$

Rearranging and approximating for δ_5 as in (3.26) one gets:

$$2I_w = k_g \Delta_5 \sin \omega t (\sin \delta_6 \sin 2\beta \cos \delta_1 - \cos 2\beta \sin \delta_1) \quad (3.48)$$

Now if $\delta_6 = \pi/2 - \delta'$ where δ' is a small retardance error

$$\sin\delta_6 = \cos\delta' = 1 - \frac{1}{2}\delta'^2; \text{ and if } \delta_1 \text{ is small}$$

$$\text{Then } 2I_w = k_g \Delta_s \sin\omega t \left(\sin(2\theta - \delta_1) - \frac{\delta'^2 \delta_1}{2} \right) \quad (3.49)$$

$$\text{Giving a null at } \sin(2\theta - \delta_1) = \frac{\delta'^2 \delta_1}{2}$$

$$\text{i.e. } 2\theta = n\pi + \delta_1 \left(1 + \frac{\delta'^2}{2} \right) \quad (3.50)$$

So if δ' is typically 10^{-2} rad, the relative error in measuring δ_1 is $\sim 0.01\%$. This error is insignificant and will only affect the accuracy of measuring absolute values of C since all measurements using the same $\lambda/4$ plate will contain the same relative error. Even if $\delta' = 10^{-1}$ rad ($\sim 6^\circ$) the relative error will only be $\sim 1\%$.

3.6.5 Stray Birefringence in Both Cell Windows

To test the effect on accuracy of stray birefringence consider $I/I_0 = [E][H][A][G][A'][F][P]$ where [A] and [A'] are Mueller matrices representing the stray birefringence of the cell windows. Then the fundamental frequency component is given as

$$\begin{aligned} \frac{2I_w}{\Delta_s \sin\omega t} = & \frac{1}{2} \Delta k \delta_s \cos 2\theta_s + \cos 2\theta \left[(-\delta_s \sin 2\theta_s \cos \delta_1 - \sin \delta_1) \right. \\ & - \delta_s \sin 2\theta_s (-\delta_s \sin 2\theta_s \sin \delta_1 + \cos \delta_1) \left. \right] + \sin 2\theta \left[\delta_s \sin 2\theta_s (-\delta_s \sin 2\theta_s \cos \delta_1 \right. \\ & \left. - \sin \delta_1) + (-\delta_s \sin 2\theta_s \sin \delta_1 + \cos \delta_1) - \delta_s \delta_s \cos 2\theta_s \cos 2\theta_s \right] \quad (3.51) \end{aligned}$$

assuming that the stray phase differences δ_s and δ'_s are small and that $k_s = k'_s = 1$, i.e. dichroism is small.

Then ignoring third order terms and assuming δ_1 is small

$$\frac{2I_w}{\Delta_s \sin\omega t} = \sin(2\theta - \delta_1) - (\delta_s \sin 2\theta_s + \delta'_s \sin 2\theta'_s) \cos(2\theta - \delta_1) \quad (3.52)$$

$$\text{Giving a null when } \tan(2\theta - \delta_1) = \delta_s \sin 2\theta_s + \delta'_s \sin 2\theta'_s \quad (3.53)$$

So small stray birefringences are purely additive to the birefringence of the medium and as long as any drifts can be compensated for, they will not affect the results.

3.6.6 Faraday Rotation in the Cell

As described in 3.3.4, Faraday rotation can be a worrying feature when measuring small magnetically induced phase differences. Consider the matrix multiplication $I/I_0 = [E][H][GB][F][P]$ where $[GB]$ is a Mueller matrix containing simultaneous birefringence and Faraday rotation. For simplicity the sample will be considered to be non-dichroic; then the fundamental frequency component is given as

$$\frac{2I_w}{\Delta_s \sin \omega t} = \frac{-\delta_1}{D} \sin D \cos 2\theta + \left[1 - \left(\frac{\delta_1}{D} \right)^2 (1 - \cos D) \right] \sin 2\theta \quad (3.54)$$

where $D = (4\theta^2 + \delta_1^2)^{1/2}$ as before.

Then if D and δ_1 are small, ignoring third order terms

$$\tan 2\theta = \delta_1 \quad (3.55)$$

i.e. for small δ_1 , $2\theta = \pi + \delta_1$ as before.

3.6.7 Combination of Stray Birefringence and Faraday Rotation

In the ocular method it was found that this combination could lead to small errors in the measurement of birefringence. Consider $I/I_0 = [E][H][A][GB][F][P]$ where $[GB]$ is a matrix representing birefringence and Faraday rotation in the cell, and $[A]$ represents stray birefringence in a cell window. Then the fundamental frequency component is given as:

$$\begin{aligned} \frac{2I_w}{\Delta_s \sin \omega t} = & \left(-\frac{\delta_1}{D} \sin D \right) (\cos 2\theta + \delta_s \sin 2\theta_s \sin 2\theta) \\ & + \left[\frac{2\theta\delta_1}{D} (1 - \cos D) \right] (\delta_s \cos 2\theta_s \sin 2\theta) \\ & + \left[1 - \frac{\delta_1^2}{D^2} (1 - \cos D) \right] \left[-\delta_s \sin 2\theta_s \cos 2\theta + \sin 2\theta \right] \end{aligned} \quad (3.56)$$

if the stray birefringence δ_s is very small.

Then for D small and ignoring third order terms:

$$\frac{2I_w}{\Delta_s \sin \omega t} = -\delta_1 \cos 2\theta + \sin 2\theta - \delta_s \sin 2\theta_s \quad (3.57)$$

$$\text{giving a null at } \tan 2\theta = \delta_s \sin 2\theta_s + \delta_1 \quad (3.58)$$

Which is similar to (3.53) in that the stray birefringence is purely additive to a second order approximation and thus can be compensated for.

3.7 Theory of Dichroism Measurements by Photometric Method

Consider now the matrix multiplication

$$I/I_0 = [E][K][G][J][I][P]$$

Then making the assumptions contained in Figure 3.2b, i.e. that all components are perfectly aligned for dichroism measurements:

$$2I/I_0 = k_a + \frac{1}{2}\Delta k \sin\delta_7 + \sin 2\theta \left(\frac{1}{2}\Delta k + k_a \sin\delta_7 \right) - \cos 2\theta (k_g \cos\delta_1 \cos\delta_7) \quad (3.59)$$

Now the phase difference induced in the piezo-optic modulator, $\delta_7 = \Delta_5 \sin \omega t$ where Δ_5 is the maximum phase difference and ω the frequency of oscillation as before. Therefore if δ_7 is small, to a second order approximation as in (3.26)

$$\left. \begin{aligned} \cos\delta_7 &= 1 - \frac{1}{4}\Delta_5^2 (1 - \cos 2\omega t) \\ \sin\delta_7 &= \Delta_5 \sin \omega t \end{aligned} \right\} \quad (3.60)$$

Substituting (3.60) in (3.59) and rearranging gives:

$$2I/I_0 = k_a + \Delta_5 \sin \omega t \left(\frac{1}{2}\Delta k + k_a \sin 2\theta \right) - \left(1 + \frac{1}{4}\Delta_5^2 \cos 2\omega t \right) k_g \cos 2\theta \cos\delta_1 + \frac{1}{2}\Delta k \sin 2\theta \quad (3.61)$$

Again one can examine terms in I at various frequencies.

Zero frequency I

$$2I_z = k_a - k_g \cos 2\theta \cos\delta_1 + \frac{1}{2}\Delta k \sin 2\theta \quad (3.62)$$

$$\text{Gives null at } k_a = k_g \cos 2\theta \cos\delta_1 - \frac{1}{2}\Delta k \sin 2\theta \quad (3.63)$$

Fundamental frequency I

$$2I_w = \Delta_5 \sin \omega t \left(\frac{1}{2}\Delta k + k_a \sin 2\theta \right) \quad (3.64)$$

$$\text{Gives null at } k_a \sin 2\theta = -\frac{1}{2}\Delta k \quad (3.65)$$

$$\text{i.e. when } \sin 2\theta = -\frac{1}{2} \left(\frac{\Delta k}{k_a} \right) \quad (3.66)$$

$$\text{and using s.a.s. } 2\theta = -\frac{1}{2} \frac{\Delta k}{k_a} \quad (3.67)$$

Double frequency I_{2w}

$$2I_{2w} = -\frac{1}{4}\Delta_5^2 k_g \cos 2wt \cos 2\theta \cos \delta_1 \quad (3.68)$$

Again note that the I_{2w} term will be very small so that measurements of I_w can be made satisfactorily without filtering out I_{2w} .

Then at the I_w null point, if δ_1 is small:

$$I_z = \frac{1}{2}(k_a - k_g) \quad \text{- very small for small dichroism}$$

$$I_{2w} = -\frac{1}{8}\Delta_5^2 k_g \cos 2wt \quad \text{- very small as } \Delta_5 \text{ is small}$$

Noting again that since $I_w \propto \Delta_5$ in (3.64), this is a linear detection method for Δk and so potentially can give values of dichroism orders of magnitude more accurately than previously obtained.

3.8 Systematic Error Analysis - Measuring Dichroism

As previously it was considered satisfactory to evaluate each source of error separately.

(3.67) gives the null condition of I_w as $2\theta = -\frac{1}{2}\left(\frac{\Delta k}{k_a}\right)$

3.8.1 Setting of the Polarizer

For measuring dichroism the relative azimuths of the polarizer and first $\lambda/4$ plate are adjusted to give circularly polarized light and ideal relative positions are given in Figure 3.26. To examine the effect of a polarizer misalignment consider the matrix multiplication $I/I_0 = [E][K][C][J][I][P]$ but with $\alpha \neq 0$. This gives:

$$\begin{aligned} 2I/I_w = & k_a + \frac{1}{2}\Delta k(\sin 2\alpha \cos \delta_7 + \cos 2\alpha \sin \delta_7) + \frac{1}{2}\Delta k \sin 2\theta \\ & + k_a \sin 2\theta (\sin 2\alpha \cos \delta_7 + \cos 2\alpha \sin \delta_7) \\ & - k_g \cos 2\theta \cos \delta_1 (\cos 2\alpha \cos \delta_7 - \sin 2\alpha \sin \delta_7) \end{aligned} \quad (3.69)$$

Rearranging and approximating for δ_7 as in (3.60) one gets the fundamental frequency component when α is small as follows:

$$\frac{2I_w}{\Delta_s \sin \omega t} = (1 - 2\alpha^2) \left(\frac{1}{2} \Delta k + k_a \sin 2\theta \right) + 2\alpha k_g \cos 2\theta \cos \delta_1 \quad (3.70)$$

So assuming δ_1 and θ are small and ignoring third order terms:

$$\frac{2I_w}{\Delta_s \sin \omega t} = \frac{1}{2} \Delta k + k_a \sin 2\theta + 2\alpha k_g \quad (3.71)$$

Giving a null at $\frac{1}{2} \Delta k + 2\alpha k_g = -k_a \sin 2\theta$

$$\text{i.e. } 2\theta = -\frac{1}{2} \left(\frac{\Delta k}{k_a} \right) - 2\alpha \quad (3.72)$$

Since for small Δk , $k_g = k_a$

Therefore for small dichroism and birefringence, the null is offset by a constant angle α , so accuracy need not be affected.

3.8.2 Setting of the Modulator

For measuring dichroism the azimuth of the modulator should be $\rho_7 = 0$. To examine the effect of a setting error consider $I/I_0 = [E][K][G][J][I][P]$ with $\rho_7 \neq 0$.

This gives

$$\begin{aligned} 2I/I_0 = & k_a + \frac{1}{2} \Delta k \cos 2\rho_7 \sin \delta_7 + \sin 2\theta \left(\frac{1}{2} \Delta k + k_a \cos 2\rho_7 \sin \delta_7 \right) \\ & + k_g \cos 2\theta (\sin \delta_1 \sin 2\rho_7 \sin \delta_7 - \cos \delta_1 \cos \delta_7) \end{aligned} \quad (3.73)$$

Rearranging and approximating for δ_7 one gets the fundamental frequency component:

$$\frac{2I_w}{\Delta_s \sin \omega t} = \left(\frac{1}{2} \Delta k + k_a \sin 2\theta \right) \cos 2\rho_7 + k_g \cos 2\theta \sin \delta_1 \sin 2\rho_7 \quad (3.74)$$

Now if $\rho_7 = \Delta'$, the modulator setting error, then if Δ' is small:

$$\frac{2I_w}{\Delta_s \sin \omega t} = (1 - 2\Delta'^2) \left(\frac{1}{2} \Delta k + k_a \sin 2\theta \right) + 2\Delta' k_g \cos 2\theta \sin \delta_1$$

and for small δ_1 , $\sin \delta_1 = \delta_1$ and for small Δk , $k_g = 1$.

Then ignoring third order terms:

$$\frac{2I_w}{\Delta_s \sin \omega t} = \frac{1}{2} \Delta k + k_a \sin 2\theta + 2\Delta' \delta_1 \quad (3.75)$$

$$\text{So } 2\delta = -\frac{1}{k_a} \left(\frac{\Delta k}{2} + 2\Delta'\delta_1 \right) \quad \text{at null} \quad (3.76)$$

So a simultaneous birefringence δ_1 will effectively introduce a relative error in the dichroism measurement of $\frac{4\Delta'\delta_1}{\Delta k}$. Usually phase differences induced in colloidal dispersions are much larger than linear dichroism under the same conditions. For example for a 0.45 volume fraction of GPI dispersion in a 0.1 mm pathlength cell and $0.34T^2$ squared magnetic field, $\delta_1 = 2 \times 10^{-2}$, $\Delta k/k_a = 1.1 \times 10^{-3}$ and if the setting error Δ' is say 10^{-2} rad ($\sim 0.5^\circ$), the relative error in measuring Δk is over 0.7 i.e. the measured Δk is over 70% higher than the real value. This is disturbing and means that to reduce errors in the measurement of Δk to below 1% using these values, Δ' must not exceed 10^{-4} radians, i.e. the modulator must be set to within half a minute of arc. The achievement of this will be discussed in the next chapter.

3.8.3 Setting of the Cell

The azimuth of the "cell" (i.e. the direction of the magnetic field should be $\rho_1 = \pi/4$. To examine an error in this consider $I/I_0 = [E][K][G][J][I][P]$ with $\rho_1 = \pi/4$. Then

$$\begin{aligned} 2I/I_0 = & k_a + \frac{1}{2}\Delta k \sin\delta_7 + \sin 2\delta \left[\frac{1}{2}\Delta k + k_a \sin\delta_7 \{1 - \cos^2 2\rho_1 (1 - \cos\delta_1)\} \right. \\ & \left. + \cos\delta_7 \cos 2\rho_1 \sin\delta_1 \right] + \cos 2\delta \left[\sin\delta_7 \cos 2\rho_1 \sin\delta_1 - k_a \cos\delta_7 \cos\delta_1 \right] \end{aligned} \quad (3.77)$$

Rearranging an approximation for δ_7 as in (3.60) one gets:

$$\frac{2I_w}{\Delta_3 \sin w t} = \frac{1}{2}\Delta k + k_a \sin 2\delta [1 - \cos 2\rho_1 (1 - \cos\delta_1)] + \cos 2\delta \cos 2\rho_1 \sin\delta_1$$

Now $\rho_1 = \pi/4 - \Delta_1$ where Δ_1 is the setting error.

Then $\cos 2\rho_1 = \sin 2\Delta_1 \approx 2\Delta_1$ for small error.

Then substituting in (3.77), and for δ_1 small:

$$\frac{2I_w}{\Delta_3 \sin w t} = \frac{1}{2}\Delta k + k_a \sin 2\delta + 2\Delta_1 \delta_1 \quad (3.78)$$

$$\text{So } 2\delta = -\frac{1}{k_a} \left(\frac{\Delta k}{2} + 2\Delta_1 \delta_1 \right) \quad \text{at null} \quad (3.79)$$

yielding the same serious error as discussed in the previous section.

From this it appears that the relative modulator/cell setting is extremely important.

3.8.4 Errors Associated with the First Quarter Wave Plate
(between Polarizer and Modulator)

(a) Setting of the First $\lambda/4$ Plate

This quarter wave plate should be aligned such that the azimuth of its last axis is $\rho_4 = \pi/4$. To examine an error in this setting consider $I/I_0 = [E][K][G][J][I][P]$ with $\rho_4 \neq \pi/4$, $\delta_4 = \pi/2$. Then

$$\begin{aligned} 2I/I_0 = & k_a + \frac{1}{2}\Delta k(\cos\delta_7 \cos 2\rho_4 \sin 2\rho_4 + \sin\delta_7 \sin 2\rho_4) + \frac{1}{2}\Delta k \sin 2\theta \\ & + k_a \sin 2\theta (\cos\delta_7 \cos 2\rho_4 \sin 2\rho_4 + \sin\delta_7 \sin 2\rho_4) \\ & - k_g \cos 2\theta \sin\delta_1 \cos^2 2\rho_4 - k_g \cos 2\theta \cos\delta_1 (-\sin\delta_7 \cos 2\rho_4 \sin 2\rho_4 \\ & + \cos\delta_7 \sin 2\rho_4) \end{aligned} \quad (3.80)$$

Rearranging and approximating for δ_7 as in (3.60) one gets:

$$\frac{2I_w}{\Delta_5 \sin \omega t} = \frac{1}{2}\Delta k \sin 2\rho_4 + k_a \sin 2\theta \sin 2\rho_4 + k_g \cos 2\theta \cos\delta_1 \cos 2\rho_4 \sin 2\rho_4 \quad (3.81)$$

Now if $\rho_4 = \pi/4 - \Delta_4$ where Δ_4 is a small setting error

$$\sin 2\rho_4 = \cos 2\Delta_4 = 1 - 2\Delta_4^2$$

$$\text{and } \cos 2\rho_4 = \sin 2\Delta_4 = 2\Delta_4$$

Substituting into (3.81) and ignoring third order terms one gets:

$$\frac{2I_w}{\Delta_5 \sin \omega t} = (1 - 2\Delta_4^2) \left(\frac{1}{2}\Delta k + k_a \sin 2\theta \right) + 2\Delta_4 k_g \cos 2\theta \cos\delta_1 \quad (3.82)$$

which is essentially the same expression as (3.70), and so at the null point

$$2\theta = -\frac{1}{2} \left(\frac{\Delta k}{k_a} \right) - 2\Delta_4 \quad (3.83)$$

So the null is effectively shifted by a constant Δ_4 . Comparison with (3.81) shows that an error in relative alignment of the first $\lambda/4$ plate and polarizer produces this offset which does not affect the accuracy of the measurements.

(b) Error in Retardance of the First $\lambda/4$ Plate

Quarter wave plates are made to give a retardance very close to $\pi/2$ at the specified wavelength. To investigate the effects of an error in this retardance consider $I/I_0 = [E][K][G][J][I][P]$ with $\rho_4 = 0$, $\delta_4 = \pi/2$.

Then

$$2I/I_0 = k_a + \frac{1}{2}\Delta k \sin\delta_7 \sin\delta_4 + \sin 2\beta \left(\frac{1}{2}\Delta k + k_a \sin\delta_7 \sin\delta_4 \right) - k_g \cos 2\beta (\sin\delta_1 \cos\delta_4 + \cos\delta_1 \cos\delta_7 \sin\delta_4) \quad (3.84)$$

Rearranging and approximating for δ_7 as in (3.60) one gets:

$$\frac{2I_w}{\Delta_5 \sin \omega t} = \sin\delta_4 \left(\frac{1}{2}\Delta k + k_a \sin 2\beta \right) \quad (3.85)$$

Now if $\delta_4 = 90 - \delta'$ where δ' is a small retardance error

$$\therefore \sin\delta_4 = \cos\delta' = 1 - \frac{1}{2}\delta'^2$$

$$\text{Then } \frac{2I_w}{\Delta_5 \sin \omega t} = \left(1 - \frac{1}{2}\delta'^2 \right) \left(\frac{1}{2}\Delta k + k_a \sin 2\beta \right) \quad (3.86)$$

with a null as before if $2\beta = -\frac{1}{2}\left(\frac{\Delta k}{k_a}\right)$

So a retardance error only reduces the "depth" of the null.

3.8.5 Errors Associated with the Second Quarter Wave Plate (Between Cell and Analyser)

(a) Setting of the Second $\lambda/4$ Plate

Ideally the azimuth of the fast axis of the second $\lambda/4$ plate should be $\rho_8 = \pi/4$. To examine an error in this setting consider $I/I_0 = [E][K][G][J][I][P]$ with $\rho_8 \neq \pi/4$, $\delta_8 = \pi/2$. Then

$$2I/I_0 = k_a + \frac{1}{2}\Delta k \sin\delta_7 + \cos 2\beta \left[-k_g \cos^2 2\rho_8 \sin\delta_1 \cos\delta_7 + \left(\frac{1}{2}\Delta k + k_a \sin\delta_7 \right) \cos 2\rho_8 \sin 2\rho_8 - k_g \sin 2\rho_8 \cos\delta_1 \cos\delta_7 \right] + \sin 2\beta \left[-k_g \cos 2\rho_8 \sin 2\rho_8 \sin\delta_1 \cos\delta_7 + \left(\frac{1}{2}\Delta k + k_a \sin\delta_7 \right) (1 - \cos^2 2\rho_8) + k_g \cos 2\rho_8 \cos\delta_1 \cos\delta_7 \right] \quad (3.87)$$

Rearranging and approximating for δ_7 as in (3.60) one gets:

$$\frac{2I_w}{\Delta_5 \sin \omega t} = \frac{1}{2}\Delta k + k_a \sin 2\beta (1 - \cos^2 2\rho_8) + k_a \cos 2\beta \cos 2\rho_8 \sin 2\rho_8 \quad (3.88)$$

Now $\rho_8 = \pi/4 - \Delta_8$ where Δ_8 is a small setting error

$$\begin{aligned} \therefore \cos 2\rho_8 &= \sin 2\Delta_8 = 2\Delta_8 \\ \sin 2\rho_8 &= \cos 2\Delta_8 = 1 - 2\Delta_8^2 \end{aligned}$$

Substituting in (3.38) and ignoring third order terms one gets

$$\frac{2I_w}{\Delta_8 \sin \omega t} = \frac{1}{2} \Delta k + (1 - 4\Delta_8^2) k_a \sin 2\delta + 2\Delta_8 k_a \cos 2\delta \quad (3.89)$$

So at null point, a small angle approximation for δ gives:

$$2\delta = - \frac{(1 + 4\Delta_8^2)}{2} \left(\frac{\Delta k}{k_a} \right) - 2\Delta_8 \quad (3.90)$$

The Δ_8 term is merely a null offset but note the multiplying factor if $1 + 4\Delta_8^2$. If Δ_8 is typically 10^{-2} rad ($\sim 0.6^\circ$) the relative error in measuring Δk is 0.04% which can be safely ignored.

(b) Error in Retardance of the Second $\lambda/4$ Plate

The retardance of the second $\lambda/4$ plate has been assumed to be exactly 90° . Now consider the matrix multiplication $I/I_0 = [E][K][G][J][I][P]$ with $\rho_8 = \pi/4$, $\delta_8 \neq \pi/2$. Then

$$\begin{aligned} 2I/I_0 &= k_a + \frac{1}{2} \Delta k \sin \delta_7 + \sin 2\delta \left(\frac{1}{2} \Delta k + k_a \sin \delta_7 \right) \\ &\quad - k_a \cos 2\delta (\cos \delta_8 \sin \delta_1 \cos \delta_7 + \sin \delta_8 \cos \delta_1 \cos \delta_7) \end{aligned} \quad (3.91)$$

Rearranging and approximating for δ_7 as in (3.60) one gets:

$$\frac{2I_w}{\Delta_8 \sin \omega t} = \frac{1}{2} \Delta k + k_a \sin 2\delta$$

Giving a null at $2\delta = - \frac{1}{2} \left(\frac{\Delta k}{k_a} \right)$ as before.

3.8.6 Stray Birefringence in a Cell Window

Consider $I/I_0 = [E][K][A][G][J][I][P]$ where $[A]$ is a Mueller matrix representing stray birefringence in a cell window.

Approximating for δ_7 as in (3.60) and considering the fundamental frequency component only one gets:

$$\frac{2I_w}{\Delta_8 \sin \omega t} = \frac{1}{2} \Delta k + k_a \sin 2\delta + \delta_8 \cos 2\rho_8 \quad (3.92)$$

$$\text{This gives a null at } 2\theta = -\frac{1}{2}\left(\frac{\Delta k}{k_a}\right) - \theta_1 \cos 2\theta_a \quad (3.93)$$

So stray birefringence is purely additive and may thus be compensated for.

3.8.7 Faraday Rotation in the Cell

Consider $I/I_0 = [E][K][GB'][J][I][P]$ where $[GB']$ is a Mueller matrix containing simultaneous dichroism, birefringence and Faraday rotation. Unfortunately, to the author's knowledge, no such matrix has been derived that contains these three effects simultaneously. The best approximation to $[GB']$ is the simultaneous birefringence/Faraday rotation matrix $[GB]$ followed by the appropriate dichroism matrix $[M_{\text{dichroic}}^{45^\circ}]$.

Making the normal small angle approximations and considering the fundamental frequency component only, one gets:

$$\frac{2I_w}{\Delta_s \sin \omega t} = \frac{1}{2}\Delta k + k_a \sin 2\theta (1 - 2\theta^2) - \theta \theta_1 \cos 2\theta \quad (3.94)$$

where θ is the Faraday rotation.

$$\text{This gives a null at } 2\theta = -\frac{(1 + 2\theta^2)}{2}\left(\frac{\Delta k}{k_a}\right) + \theta \theta_1 \quad (3.95)$$

which introduces a relative error of $\sim \frac{2\theta \theta_1}{\Delta k} + 2\theta^2$ in dichroism measurements.

Consider the example quoted in 3.8.2 where $\theta_1 = 2 \times 10^{-2}$ and $\Delta k/k_a = 1.1 \times 10^{-3}$. Also say that $\theta = 10^{-2}$ ($\sim 0.6^\circ$). Then relative error = 0.2 i.e. the measured dichroism is nearly 20% higher than the real value. This is a worrying error and means that to reduce errors in $\Delta k/k_a$ to less than 1% in the above example, θ must be less than 5×10^{-4} rad (~ 2 minutes). However, because the $\theta \theta_1$ term in (3.95) is linear in θ , errors arising from this can fortunately be detected by field reversal.

3.9 Mueller Calculus

The use of Mueller calculus enables one to calculate the effect of a series of polarizers, retarders and even scatterers on a beam of light with great simplicity as follows.⁶⁴ The incident light beam is characterized by the Stokes vector which is a four parameter column vector:

$$\begin{bmatrix} I \\ M \\ C \\ S \end{bmatrix} \quad \begin{array}{l} \text{where } I \text{ is the intensity} \\ M \text{ is the horizontal preference} \\ C \text{ is the } +45^\circ \text{ preference} \\ S \text{ is the right circular preference} \end{array}$$

Each has dimensions of intensity as the vector is normalized, often only the relative values are required.

Any polarizer or retarder is described by a 4×4 matrix called the Mueller matrix so naturally there are matrices describing any birefringent element or optical devices. These matrices have contained in them the phase difference introduced, the differential absorbance and the azimuth of the device.

By simple matrix algebra the result of a chain of devices may be computed. The Stokes vector of the incident beam is written on the right with successive matrices arranged in order from right to left. The result of the computation will be the Stokes vector of the emergent light, a four parameter column vector simplified by the fact that in this application only the emergent intensity, i.e. the top element, is required.

The relevant Stokes vectors and Mueller matrices used in preceding sections are as follows. Note that they are empirically derived i.e. they are not the result of electromagnetic theory.

(a) Stokes vector for linearly polarized light.

$$\begin{bmatrix} 1 \\ \cos 2\alpha \\ \sin 2\alpha \\ 0 \end{bmatrix} \quad \text{where } \alpha \text{ is the azimuth}$$

(i) A special case is when $\alpha = 0$ i.e. horizontally polarized light.

$$\begin{bmatrix} 1 \\ 1 \\ 0 \\ 0 \end{bmatrix} = \{P\}$$

(b) Mueller matrix for an ideal homogeneous linear analyser, where θ is the azimuth of the transmission axis.

$$\begin{bmatrix} 1 & \cos 2\theta & \sin 2\theta & 0 \\ \cos 2\theta & \cos^2 2\theta & \cos 2\theta \sin 2\theta & 0 \\ \sin 2\theta & \cos 2\theta \sin 2\theta & \sin^2 2\theta & 0 \\ 0 & 0 & 0 & 0 \end{bmatrix} = \{E\}$$

(c) Mueller matrix for an ideal homogeneous linear retarder where ρ_i = any azimuth i of the fast axis and δ_i = any retardance

$$\begin{bmatrix} 1 & 0 & 0 & 0 \\ 0 & \cos^2 2\rho_i (1 - \cos \delta_i) + \cos \delta_i & \cos 2\rho_i \sin 2\rho_i (1 - \cos \delta_i) & -\sin 2\rho_i \sin \delta_i \\ 0 & \cos 2\rho_i \sin 2\rho_i (1 - \cos \delta_i) & 1 - \cos^2 2\rho_i (1 - \cos \delta_i) & \cos 2\rho_i \sin \delta_i \\ 0 & \sin 2\rho_i \sin \delta_i & -\cos 2\rho_i \sin \delta_i & \cos \delta_i \end{bmatrix}$$

where $i = 1, 2, 3, 4, 5, 6, 7, 8$, s or s' representing matrices [C] and [G], [S], [D], [I], [F], [H], [J], [K], [A], and [A'] respectively.

Four special cases may appropriately be mentioned here:

(i) When $i = 1$ or 5 , $\rho_i = \pi/4$, any δ_i i.e. for a birefringent medium with its principal axes at 45° to the polarizer, [C], [G], and [F] reduce to:

$$\begin{bmatrix} 1 & 0 & 0 & 0 \\ 0 & \cos \delta_i & 0 & -\sin \delta_i \\ 0 & 0 & 1 & 0 \\ 0 & \sin \delta_i & 0 & \cos \delta_i \end{bmatrix}$$

(ii) When $i = 7$, $\rho_i = 0$, any δ_i i.e. for a birefringent medium with its principal axes at 0° to the polarizer, [J] reduces to:

$$\begin{bmatrix} 1 & 0 & 0 & 0 \\ 0 & 1 & 0 & 0 \\ 0 & 0 & \cos\delta_7 & \sin\delta_7 \\ 0 & 0 & -\sin\delta_7 & \cos\delta_7 \end{bmatrix}$$

(iii) When $i = 3$ or 6 , $\rho_3 = 0$, $\delta_i = \pi/2$ i.e. a $\lambda/4$ plate with principal axes at 90° to the polarizer. [D] and [H] reduce to

$$\begin{bmatrix} 0 & 0 & 0 & 0 \\ 0 & 1 & 0 & 0 \\ 0 & 0 & 0 & 1 \\ 0 & 0 & -1 & 0 \end{bmatrix}$$

(iv) When $i = 4$ or 8 , $\rho_i = \pi/4$, $\delta_i = \pi/2$ i.e. a $\lambda/4$ plate with principal axes at 45° to the polarizer. [I] and [K] reduce to

$$\begin{bmatrix} 0 & 0 & 0 & 0 \\ 0 & 0 & 0 & -1 \\ 0 & 0 & 1 & 0 \\ 0 & 1 & 0 & 0 \end{bmatrix}$$

(d) Dichroism is represented by a homogeneous non-scattering, non-depolarizing, non-birefringent polarizer with principal transmission axes k_1 and k_2 . With the maximum transmission axis horizontal the matrix of a purely dichroic material is given by:

$$\frac{1}{2} \begin{bmatrix} (k_1+k_2) & (k_1-k_2) & 0 & 0 \\ (k_1-k_2) & (k_1+k_2) & 0 & 0 \\ 0 & 0 & 2\sqrt{k_1 k_2} & 0 \\ 0 & 0 & 0 & 2\sqrt{k_1 k_2} \end{bmatrix} = M_{\text{dichroic}}^{0^\circ}$$

However, in this report the maximum transmission axis is 45° to the horizontal.

$$\text{Now } M^{0^\circ} = T(-2\theta)M^{0^\circ}T(+2\theta)$$

where $T(-2\theta)$ and $T(+2\theta)$ are the rotator and counter-rotator matrices²⁷.

$$T(+2\theta) = \begin{bmatrix} 1 & 0 & 0 & 0 \\ 0 & \cos 2\theta & \sin 2\theta & 0 \\ 0 & -\sin 2\theta & \cos 2\theta & 0 \\ 0 & 0 & 0 & 1 \end{bmatrix}$$

Similarly for $T(-2\theta)$ which is actually the same as the Faraday notation matrix. From this

$$M_{\text{dichroic}}^{45^\circ} = \frac{1}{2} \begin{bmatrix} (k_1+k_2) & 0 & (k_1-k_2) & 0 \\ 0 & 2\sqrt{k_1 k_2} & 0 & 2\sqrt{k_1 k_2} \\ (k_1-k_2) & 0 & (k_1+k_2) & 0 \\ 0 & 2\sqrt{k_1 k_2} & 0 & 2\sqrt{k_1 k_2} \end{bmatrix}$$

For a medium which is both birefringent and dichroic with its principal axes at 45° to the horizontal, the above matrix is combined with matrices [C] and [G] in section (c)(i) to give:

$$\frac{1}{2} \begin{bmatrix} (k_1+k_2) & 0 & (k_1-k_2) & 0 \\ 0 & 2\sqrt{k_1 k_2} \cos \delta_1 & 0 & -2\sqrt{k_1 k_2} \sin \delta_1 \\ (k_1-k_2) & 0 & (k_1+k_2) & 0 \\ 0 & 2\sqrt{k_1 k_2} \sin \delta_1 & 0 & 2\sqrt{k_1 k_2} \cos \delta_1 \end{bmatrix} = [G]$$

(e) Faraday rotation is represented by the Mueller matrix for an ideal homogeneous non-linear retarder. For left circular polarized light $\delta_i = 2\theta$ where θ is the rotation and matrix is:

$$\begin{bmatrix} 1 & 0 & 0 & 0 \\ 0 & \cos 2\theta & -2\sin 2\theta & 0 \\ 0 & \sin 2\theta & \cos 2\theta & 0 \\ 0 & 0 & 0 & 0 \end{bmatrix}$$

But Faraday rotation and birefringence should be included in the same matrix since both occur simultaneously in the cell. This was formulated⁶⁵ as follows for an azimuth $\rho_i = 45^\circ$, retardance δ_i and optical rotation θ .

$$\begin{bmatrix} 1 & 0 & 0 & 0 \\ 0 & \cos D & \frac{2\theta}{D} \sin D & \frac{-\delta_i}{D} \sin D \\ 0 & \frac{-2\theta}{D} \sin D & 1 - \frac{4\theta^2}{D^2} (1 - \cos D) & \frac{2\theta\delta_i}{D} (1 - \cos D) \\ 0 & \frac{\delta_i}{D} \sin D & \frac{2\theta\delta_i}{D^2} (1 - \cos D) & 1 - \frac{\delta_i^2}{D^2} (1 - \cos D) \end{bmatrix} = \begin{matrix} \text{[CB] and} \\ \text{[CB]} \end{matrix}$$

where $D = (4\theta^2 + \delta_i^2)^{\frac{1}{2}}$

CHAPTER 4

EXPERIMENTAL APPARATUS AND PROCEDURE

4.1 Introduction

This chapter is in two parts, Part A being a description of the experimental apparatus and procedure adopted for the ocular detection of the linear birefringence magnetically induced in diamagnetic liquids. As previously mentioned, the apparatus²⁵ is not novel, rather tiring to use and is of limited accuracy although repeated measurements enabled one to measure phase differences, δ_1 to within 40 μ rad so that birefringences, Δn as low as 4×10^{-11} could be measured.

Part B is an account of the photometric detection apparatus and method designed to greatly improve this sensitivity to the point where phase differences could be measured within an error of about ± 1 μ rad given the lower limits of measurable birefringence and linear dichroism as $\Delta n = 10^{-12}$ and $\Delta k/k_a = 10^{-5}$ respectively. This may be compared to previously described systems using Faraday modulation^{6-8,10} which can only measure phase differences to ± 5 -10 μ rad and cannot measure linear dichroism accurately.

PART A: OCULAR METHOD

4.2 Description of the Apparatus

Figure 4.1 represents schematically the main features of the experimental arrangement. The basis of the apparatus consisted of two optical benches each one metre long, separated by a large electro-magnet, the pole pieces of which were parallel to the optical benches. A stainless steel sample cell was supported between the pole pieces by a duralumin cradle which was rigidly clamped to the bench ends.

4.2.1 The Polarizer Bench

The instruments to the left of the magnet in Figure 4.1 produced a monochromatic linearly polarized collimated light beam and they were as follows:

A high intensity mercury arc lamp source, A.

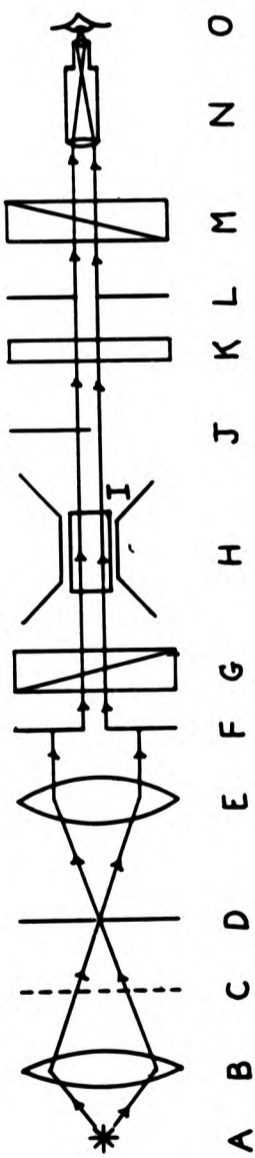
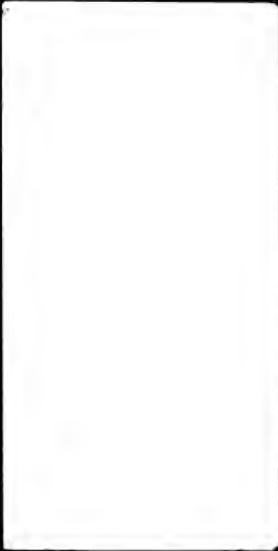


Figure 4.1 Schematic diagram of the Ocular detection system



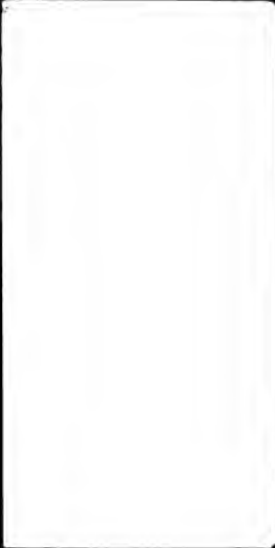
A green interference filter peaking at 546 nm, C.
A system to produce a narrow beam of parallel light consisting of a lens B focusing light from A onto a pinhole D in the focal plane of a lens E. The parallel light beam emerging from E, after being further collimated by an adjustable aperture F, was linearly polarized at 45° to the horizontal by a Glans-Thompson prism G mounted on a PTI divided circle.

4.2.2 The Magnet

The magnet, H in Figure 4.1, was a Newport Instruments type E large watercooled 7-inch electromagnet of a conventional shortened turn design. It was fitted with highly polished 45° conical tips which had a 4.5 inch (11.4 cm) face diameter and were clamped to the yoke to give a uniform air gap of 13 mm. Each coil was wound with 1550 turns of copper strip with a cold resistance of 4Ω rising to a maximum allowable hot resistance of 5.5Ω.

The magnet was designed for ESR, NMR etc. work and so had a very high field homogeneity (better than 1 part in 10^5) using the appropriate shims. The current passed through these coils was supplied by a Maudsley 6.5 kW critically excited motor/generator and controlled by a Newport power supply control box type C225. This arrangement was capable of supplying the magnet with 22 amps at 200 volts dc with a stability of 1 part in 10^5 . Magnetic fields between 0 and 2.2 Teslas were accurately controlled by adjusting a three digit potentiometer combined with an ammeter to measure coil current, on the front of the control console.

The flux density B in the magnet air gap was measured using a Bell Gaussmeter type 620 (fsd 10^{-5} to 3T) and a Bell transverse Hall probe type STB-0402 1X (1X linear up to 1T). Using the above meter and probe, checks had previously been made⁶⁶ on the homogeneity of the magnetic field which was found to be satisfactory within the experimental error. The Hall probe was mounted in a clamp enabling it to be swung into the air gap with the cell installed so B could be measured in situ.



4.2.3 The Sample Cell

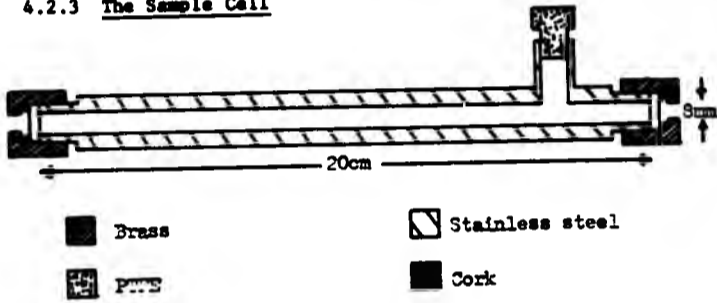
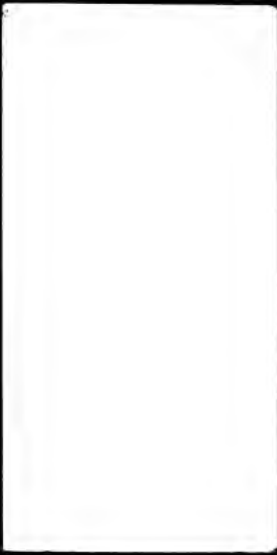


Figure 4.2 Sectional view of sample cell

The sample cell (I in Figure 4.1) was made from a 20 cm long, $\frac{1}{8}$ inch diameter rod of non-magnetic stainless steel, type 316 (formerly EN58J). This had flats machined on the sides 12 mm apart in order to fit loosely between the magnet pole pieces. It had an 8 mm hole drilled through it to give a volume of about 10 cm³. Threaded brass end caps and cork washers held the 15 mm diameter spectroil special quartz windows onto the ends of the cell which had been ground optically flat. The cell was filled through the side arm using a syringe attached to a Millipore stainless steel filter holder and then sealed with a PTFE stopper to prevent evaporation and the ingress of dust. The cell was designed so that its windows were outside the high magnetic field and so were not affected by it.

4.2.4 The Compensator Bench

The instruments to the right of the magnet in Figure 4.1 were designed to measure the induced phase difference of the polarized light emerging from the sample cell. They consisted of a half shade plate J which induced a small phase difference to half the light beam, a quarter-wave plate K to convert the elliptically polarized light emergent from the cell to linearly polarized light, an adjustable aperture L to prevent stray light entering the analyser, an analyser M to measure the azimuth θ of the linearly polarized light and a telescope N which could be focused on the edge of the half shade plate.



The half shade plate was mounted on a PTI divided circle and consisted simply of a thin glass rectangular coverslip with aluminium holders glued on each end, one end being fixed to the divided circle and the other to a micrometer and spring arrangement designed to stretch the glass, so making it birefringent.

The quarter wave plate was also mounted on a PTI divided circle and the analyser was of the high quality dichroic type mounted on a very finely divided circle (made by the Precision Tool Company) which was controlled by a large micrometer, such that individual readings could be measured accurate to 10^{-5} radians.

For convenience of operation the telescope was mounted perpendicular to the optical benches and a mirror used to enable one to focus on the half shade plate.

4.3 Alignment of Optical Components

The optical benches were firmly secured to a wooden topped concrete bench and then had to be accurately aligned. They were made exactly horizontal by the use of a spirit level and shims, and then made parallel using a length of cotton stretched between two optical stands. By eye it was confirmed that the cotton went through the centre of the air gap between the magnet pole pieces.

The components were adjusted so that a collimated horizontal light beam from the polarizer bench travelled diametrically through the air gap of the electromagnet. The magnet had to be adjusted so that the direction of magnetic flux was perpendicular to the beam in order to avoid Faraday rotation and other effects. To achieve this the cell was filled with filtered deionized water (which has a very low Cotton-Mouton constant but a high Verdet constant) and placed in its cradle between the pole pieces. The quarter wave and half shade plates were removed from the bench and the polarizer and analyser crossed for minimum intensity as viewed through the telescope. As shown in the previous chapter, small amounts of Faraday rotation should not affect the position of the null point much, but misalignment of the magnet may make the null point brighter or broader and hence reduce the sensitivity. About 2 Teslas was applied to the cell and the whole magnet assembly rotated about its

vertical axis until a minimum intensity was again attained, and then locked in position. This ensures that the magnetic field is perpendicular to the light beam to within a fraction of a degree.

Now the optical elements were aligned as follows: The polarizer and analyser were crossed and the cell filled with "Analar" quality benzene (which has a large Cotton-Mouton constant, about $6 \times 10^{-3} \text{ T}^{-2} \text{ m}^{-1}$) and placed between the magnet pole pieces. Then, while applying about 2T to the cell, the crossed polarizer and analyser were rotated together to the lowest transmitted intensity position as viewed through the telescope. The principal refractive indices of the birefringent liquid were then aligned with the azimuths of polarizer and analyser and one principal axis was also aligned with the direction of magnetic flux.

After switching off the magnet, the analyser was then rotated 45° and the polarizer rotated to the lowest intensity position. The $\lambda/4$ plate was replaced on the compensator bench and rotated for extinction and after the half shade plate had been installed at a suitable azimuth the analyser was rotated to the balanced intensity position. The components of the system were now set at the azimuths indicated in Figure 3.1 and the apparatus was ready to be used.

4.4 Calibration of Apparatus

This involved calibration of the finely divided circle and the sample cell. Also, statistical investigations were made of the experimental accuracy and troublesome errors due to stray birefringence in the cell windows.

4.4.1 Calibration of the Finely Divided Circle

The micrometer used to rotate the divided circle carrying the analyser had to be calibrated to determine the number of microradians rotated per micrometer scale division and it was found that a micrometer movement of $1 \mu\text{m}$ corresponded to an analyser rotation of $10.52 \pm 0.01 \mu\text{rad}$.

The Cotton-Mouton constant of a medium is calculated using equation
(2.3) $C = \frac{\delta_1}{2\pi B^2}$. At balance the analyser reading $\theta = \frac{\delta_1}{2} + \frac{\pi}{2}$ so a

change of δ_1 corresponds to a change of 28. Combining the above equation:

$$C = \frac{\delta}{\pi l B^2} \quad (4.1)$$

and since the analyser reading $\delta \text{ } \mu\text{rad} = 10.52 \times \text{micrometer reading } M \text{ } \mu\text{m}$

$$\text{then } C = \frac{10.52M}{\pi l B^2} \quad (4.2)$$

Now the effective cell length, l_{eff} , was found to be 12.43 cm (see below) so when the 20 cm cell is being used:

$$C = 24.35 \times 10^{-6} \text{ M/B}^2 \quad (4.3)$$

Therefore the Cotton-Mouton constant of a medium may be found using this apparatus by plotting a graph of M versus B^2 and substituting the gradient in (4.3).

4.4.2 Calibration of 20 cm Stainless-Steel Sample Cell

When the 20 cm stainless-steel cell was used, its ends were outside of the 11.4 cm diameter pole pieces. Hence the magnetic field varied along the length of the cell and the value of $\int B^2 dl$ must be used instead of simply $B^2 l$ in the expression for deriving the Cotton-Mouton constant (equation (2.2)). l is the length of the sample in a magnetic field B and the positions of the cell windows define the limits of the integral.

One method of finding $\int B^2 dl$ is to measure B at convenient intervals along the cell using a gaussmeter, then calculating $\int B^2 dl$ graphically. This procedure may be repeated for a range of currents applied to the magnet, but it is very tedious. For the sample pole piece configuration employed here, $\int B^2 dl$ rises commensurately with B_m , the magnetic induction measured at the centre of the pole-piece gap⁶⁶.

A much simpler way to calibrate the cell was to use a "standard" liquid such as nitrobenzene in the cell. Rearranging equation (2.2) one obtains the effective cell length, $l_{\text{eff}} = \frac{1}{2\pi C} \cdot \frac{\delta}{B_m^2}$. Hence if one plots the phase difference induced, δ , against the magnet induction measured in the middle of the pole-piece gap and C is known, then l_{eff} can be measured. The Cotton-Mouton constant of nitrobenzene is very large and hence has often been measured to a high degree of accuracy. The Landolt-Bornstein tables³ set the standard for nitrobenzene, at room temperature and $\lambda = 546 \text{ nm}$, to $(26.2 \pm 0.2) \times 10^{-3} \text{ T}^{-2} \text{ m}^{-1}$ and although

these tables give a spread of results, all but two lie in the range 25.7 to $27.2 \times 10^{-3} \text{ T}^{-2} \text{ m}^{-1}$ (corrected to 546 nm). Some other values obtained at 546 nm are 26.4×10^{-3} by Meeten⁶⁷ and $26.2 \times 10^{-3} \text{ T}^{-2} \text{ m}^{-1}$ by Goldet⁶⁸ so the standard appears reasonable and consistent.

Another method was used to calibrate the cell which was more absolute and concise. The Cotton-Mouton constant of a liquid having a large value of C , such as nitrobenzene, was measured using a cell of short pathlength which was accurately known (1 cm). Here one could use known values of B_m^2 to calculate C since the magnetic field was constant along the 1 cm pathlength. Then one could define an effective cell length,

$$l_{\text{eff}} = \frac{1}{B_m^2} \int_{-1/2}^{1/2} B^2 dl.$$

The 20 cm pathlength cell was filled with nitrobenzene and the induced phase difference, δ , measured for different values of B_m .

$$\text{Then } l_{\text{eff}} = \frac{(\delta/B_m^2)}{(\delta/B_m^2)_{l=1 \text{ cm}}} l_{\text{eff}} \times 1 \text{ cm}$$

Hence l_{eff} was found to be 12.43 cm .

4.4.3 Statistical Analysis of Experimental Accuracy

The cell was removed from the magnet and twenty simultaneous independent measurements made of δ to test the accuracy obtainable using a number of readings.

In fact four groups of twenty measurements were made, each group having a typical spread of about $12 \mu\text{m}$ corresponding to about $240 \mu\text{rad}$ spread in the measurement of phase difference δ_1 . Standard deviations S in these samples varied from 60 to $100 \mu\text{rad}$ yielding a standard error of the mean σ_m of 12 to $22 \mu\text{rad}$ using the relationship⁶⁹ $\sigma_m = \frac{S}{\sqrt{N}}$. 95% confidence in the mean is about $2\sigma_m$ so with a sample of $N=20$ a typical reliable error of the mean will be $\pm 30 \mu\text{rad}$. It was found later that the 10 readings taken gave a typical random error of $\pm 40 \mu\text{rad}$.

4.4.4 Investigation of the Stray Birefringence of the Cell Windows

By virtue of the light pressure which must be exerted on the quartz windows by their retainers and washers these windows will exhibit some

stray strain birefringence. As shown in Chapter 3 this will not be troublesome unless it varies significantly within the time of an experiment. To see if and how it varies with time an exhaustive survey was made using three pairs of windows and in each case filling the cell with deionized water. For each pair of windows ten measurements of δ were made at fifteen-minute intervals.

The results are tabled below:

Table 4.1 The Variation of Stray Birefringence with Cell Window Type

Cell Window Type	Variation of stray birefringence $\mu\text{rad/hr.}$
Fused quartz pair number 1	$+80 \pm 5$
Zero stress optical number A	-70 ± 3
"Spectrosil" special quartz number 2	0 ± 10
No cell	$+5 \pm 5$

As a series of readings at different magnetic fields would take up to one hour to complete per sample, the window drift recorded for the first two sets of windows could seriously affect the accuracy of measurements of small Cotton-Mouton constants. It should be noted that measurements were also made without a cell (see Table 4.1) to confirm that the drift was due to the windows alone. Fortunately all the time dependent studies showed that any window drift was approximately linear over the time scale considered, so if measurements were taken at fixed time intervals for incrementally rising magnetic fields and then for falling fields, the errors due to drifting stray birefringence largely cancelled.

After testing for stray birefringence variation the spectrosil special quartz windows were used although it does not necessarily mean that because no significant variation was recorded in Table 4.1 they are perfect in this respect. In fact subsequent tests showed that the way the windows were handled was very important and the time variation may be interpreted as a gradual relaxation of the stress imposed on the windows when their retainers were screwed on. Some "zero stress optical" windows were tried but they were not totally transparent and were easily etched by water, so they were not used.

4.5 Experimental Procedure

Before each run the cell was prepared and filled with the desired liquid as follows:

The stainless steel cell was firstly thoroughly washed out with an appropriate volatile solvent, such as propanol or acetone, to dissolve any residue of the previous sample. It was left in a hot ($\sim 70^{\circ}\text{C}$) oven for an hour to fully evaporate the solvent and then blown through with filtered compressed air to disperse any dust particles remaining in the cell. The cell windows were also washed in a solvent and carefully cleaned with lens tissue before finally blowing off the remaining specks of dust. These windows were held on the ends of the cell with the screw-on brass retainers and cork washers taking great care to exert only the gentlest of forces on them in order to minimise time-varying strain birefringence.

The cell was filled via its sidearm (see Figure 4.2) with the desired sample using a 20 cm³ hypodermic syringe attached to a Millipore stainless steel filter holder. Depending on the chemical properties of the sample and its viscosity, either Millipore or PTFE filters were used with pore sizes ranging from 0.05 to 0.22 μm in order to filter out dust particles. The cell had to be filled quickly, to reduce the possibility of contamination by airborne dust, and carefully to exclude air bubbles. In order to fill the cell at a reasonable rate, the polyisobutene sample filling had to be performed in the oven using a filter press. After the cell was satisfactorily filled, the PTFE bung was inserted in the side arm to prevent the ingress of dust and evaporation of the sample.

After the filled cell had been inspected for air bubbles and dust on the windows it was installed in its cradle between the magnet pole pieces. The mercury arc lamp source was switched on, the Hall probe swung into place and a mercury-in-glass thermometer inserted next to the cell. Owing to the temperature variation of refractive index the beam through the cell was usually strongly deviated by the sample until it equilibrated with the temperature of the magnet pole tips.

The apparatus demanded the use of the observer's eyes, judgement and concentration in comparing intensities so ten minutes were allowed for dark adaption. After focusing the telescope on the edge of the half shade plate, the plate's azimuth was altered for maximum sensitivity

and a balance point in the field of view found for no magnetic field applied to the cell. During observation a very dim light provided illumination of the analyser micrometer and a set routine for observations was established so that each reading was of the same duration. The three digit control potentiometer on the magnet power supply was adjusted to a number of predetermined positions, six in all, from 0 to 550 corresponding to flux densities of 0 to 2T. At each of these positions the magnetic flux density was measured and the system balanced ten times, noting the analyser rotation. This was repeated, this time decreasing the magnetic field at the same rate as it was increased so that analyser readings at the same field could be averaged, in order to offset the effects of time-varying stray birefringence in the cell windows.

To investigate the non-quadratic effect of Faraday rotation in the cell, for some liquids with very low Cotton-Mouton constants, C was measured with the magnetic field reversed and the value compared with that obtained for the magnetic field in the normal direction. The approximate temperature of the cell as indicated by the thermometer was noted at the beginning and end of each run.

PART B - PHOTOMETRIC METHOD

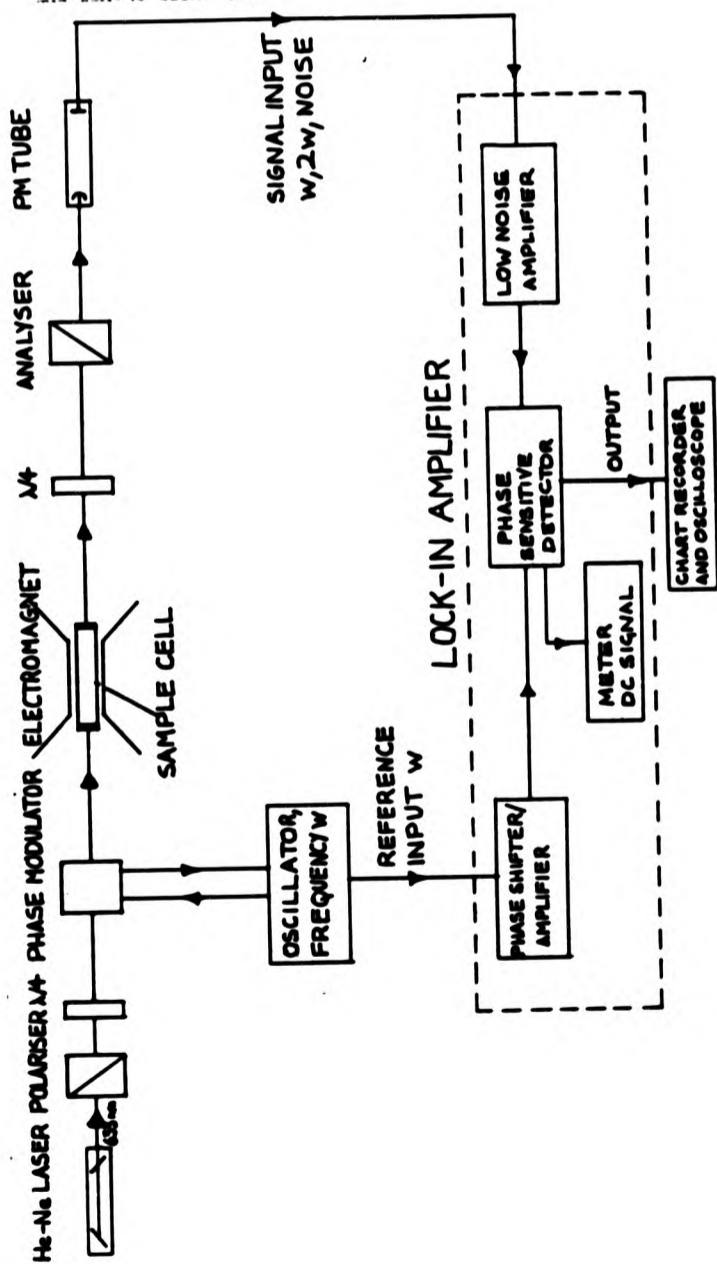
4.6 Description of the Apparatus

The complete photometric system is represented schematically in Figure 4.3. As in the ocular method, its basis is two optical benches separated by a large electromagnet having a cradle to support simple cells of various path lengths. As photometric systems are much more vulnerable to magnetic interference of the components (namely the modulator and photomultiplier tube), extra optical benches were used to space the components further from the magnet, and the resulting distance between the laser and PM tube was over 5 metres. Figures 4.4, 4.5 and 4.6 are photographs of the apparatus used.

4.6.1 Light Source - He-Ne Laser

A Spectra-Physics model 136P continuous-working He-Ne laser gave a monochromatic source of light of wavelength 632.8 nm and power output

Figure 4.7 Photovoltaic system for measuring magnetic birefringence and linear dichroism



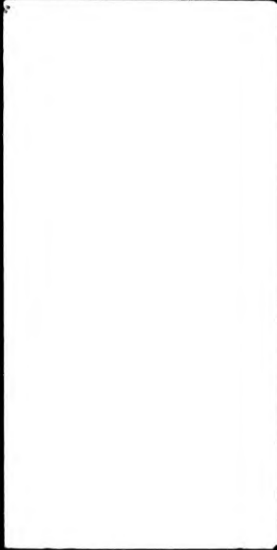


Figure 4.4 Laser, polarizer and modulator



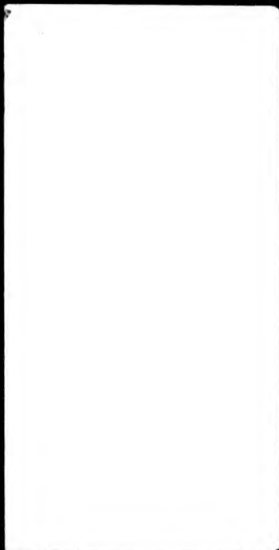


Figure 4.5 Instrumentation



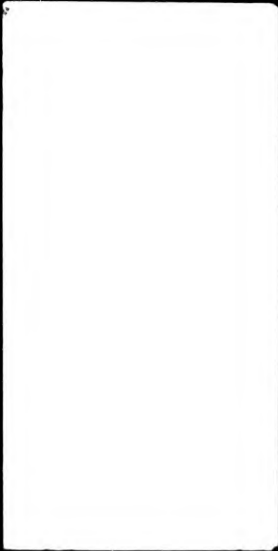
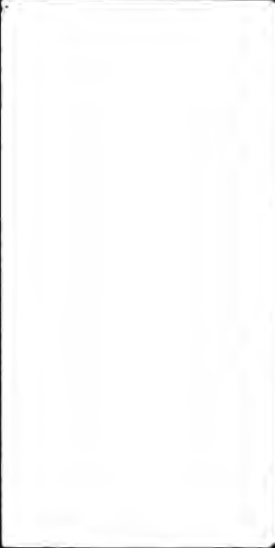


Figure 4.6 Detector bench and magnet





of over 2 mW. The beam was polarised with a diameter of 0.5 mm and full angle divergence of <1.6 mrad, so the beam diameter was less than 8 mm on reaching the PM tube over 5 m away and a focusing lens was not needed. Angular drift of <0.02 mrad (temperature stable) was insignificant over a 5 m range.

This highly directional nature of the beam makes the laser incomparable when operating over relatively long ranges and very suitable for this application. A disadvantage compared to a tungsten bulb as a source is the laser's amplitude stability. A $<1\%$ rms short term (ripple + noise) and $<5\%$ long-term drift was confirmed but procedures adopted to compensate for this (see Section 4.9) minimised the problem.

4.6.2 Polarisers and Quarter Wave Plates

The laser was polarized with a 200:1 polarization ratio which was improved by using a Glane-Thompson prism (having an extinction ratio of 10^6) mounted on a PTI divided circle. Combinations of prism and good quality dichroic polarizers were assessed and it was found that a Glane-Thompson polarizer in combination with a dichroic analyser gave the best extinction. A selected dichroic analyser was mounted in the micrometer controlled very finely divided circle as used in the ocular method.

Quarter wave plates were mounted on PTI divided circles and consisted of mica sheet between glass covers, as supplied by F. Wiggins & Sons Ltd. who stated the phase retardation to be $90 \pm 1^\circ$ at a wavelength of 632.8 nm. Small errors in retardation have been shown (in Chapter 3) to have a negligible effect on the accuracy of the experiment.

To prevent the quarter wave plates being affected by draughts, expanded polystyrene boxes were fabricated with small holes for the light to pass through. Ideally, quartz quarter wave plates would be used for their thermal and mechanical stability, but these of course are much more expensive than the conventional mica ones.

4.6.3 The Magnet

The main features of the magnet have been described in 4.2.2. Wedge-shaped pole tips were designed for use with the Newport magnet but unfortunately they were not produced in time for the work described

in this thesis. They effectively concentrate the magnetic flux in half the area of the conical tips described previously and apply the flux over virtually the whole length of the 20 cm cell, increasing the effective cell length by over 50%. Conservative estimates indicate this would reduce the error in the measurement of small birefringences by approximately 2.5 times.

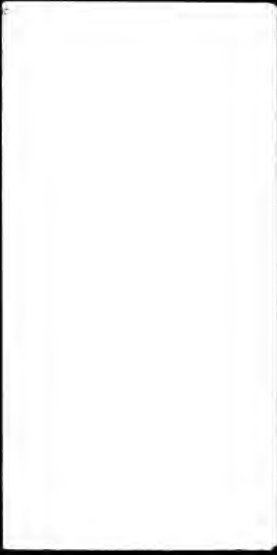
For examining the magnetic birefringence and dichroism of highly magneto-optically anisotropic media, in this case the more concentrated PTFE dispersions, much lower magnetic fields (0 to 0.5 T) were required to be accurately reproduced in much smaller increments. For this a Farnell L30D stabilized power supply was used capable of supplying 0 to 2 Amps at 0 to 30 volts. For this application the Bell Gaussmeter previously described was connected to a 3½ digit Farnell digital multi-meter which displayed the magnetic field to an error of less than 0.5%.

4.6.4 Sample Cells

For the measurement of the magnetic birefringence of neat liquids, mixtures and polymers the 20 cm pathlength cell described in 4.2.3 was used. For the measurement of the Cotton-Mouton constant of expensive liquids the effective volume of the cell was reduced from 10 cm³ to about 4 cm³ by using a stainless steel sleeve of inside diameter $\frac{3}{16}$ " (~5 mm) and where necessary to about 2 cm³ using a brass sleeve (stainless not available in this size) of ID $\frac{1}{8}$ " (~3 mm). These bore reductions presented no problems except that the laser beam had to be collimated slightly to ensure that light did not touch the sides of the cell.

Because of the laser's narrow beam it would have been advantageous to use a thin walled narrow bore cell enabling a reduction in the magnet pole tip separation (increasing the magnetic field) or alternatively maintain the existing separation (13 mm) and build a water jacket around a slimmer cell to allow temperature dependent work to be done. Unfortunately there was insufficient time and resources to achieve these objectives.

For work involving concentrated colloidal dispersions having a large magnetic birefringence or dichroism shorter path lengths were used to reduce the effective induced phase differences to a reasonable value and reduce multiple scattering to a minimum. 13 mm wide Helma "Blue"



and Optiglass "Spectrosil" quartz cells were used in path lengths 10, 1, 0.2 and 0.1 mm, the last two being demountable. Also used for "direct" dichroism measurements were the lower quality Helma "Yellow" glass cells in 5, 2 and 1 mm path lengths.

4.6.5 Piezo-optic Phase Modulator

The design of the phase modulator is shown in Figure 4.7 and is of the same principle as that used by Koeman and Janeschitz-Kriegl⁷⁰. Its purpose is to provide modulation of the linearly polarized beam before the light enters the cell. In effect an alternating phase difference is induced which acts as a carrier signal for the phase difference or dichroism introduced by the medium in the cell. A piece of glass or quartz becomes birefringent when stretched by virtue of its stress-optical coefficient, but when it is simply bent the effect due to stretching on the outside of the bend is cancelled by that due to the compression of the inside. However, because the window is effectively offset from the centre of the bending axis, it can easily be seen that arrangements as per Figure 4.7 will make the window birefringent on bending because the face of the window next to the plate will not be strained so much as that furthest from the plate.

Adjustable bump-stops about 45° apart were attached to a divided circle as shown. Bolted onto this was the vibrating plate which was essentially a 100 × 20 × 2 mm mild steel strip with a 10 mm hole drilled in the middle over which was Araldited a glass window of 22 mm diameter and 5 mm thickness. This plate was driven at its fundamental resonant frequency (~190 Hz) using a small polarized electromagnet close enough to it to maintain a sufficient amplitude of vibration. The electromagnet was powered by a Farnell sine-square oscillator type LPM2, and normally only a 0.2V RMS sine wave was used in order not to overload the electromagnet. The chosen plate gave typically 2 minutes (0.6 m rad) which was found to be sufficient.

To eliminate the effects of strong magnetic fields on the modulator it was enclosed in a mumetal magnetic shield and positioned 2 m away from the large electromagnet. Also a polystyrene box was fabricated so that the modulator would not be subject to sudden temperature changes.

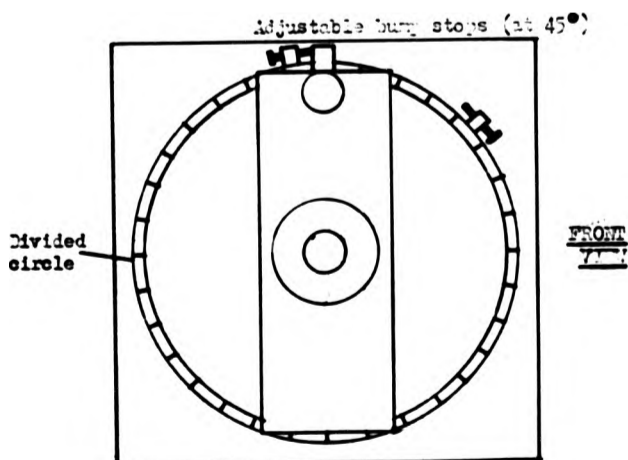
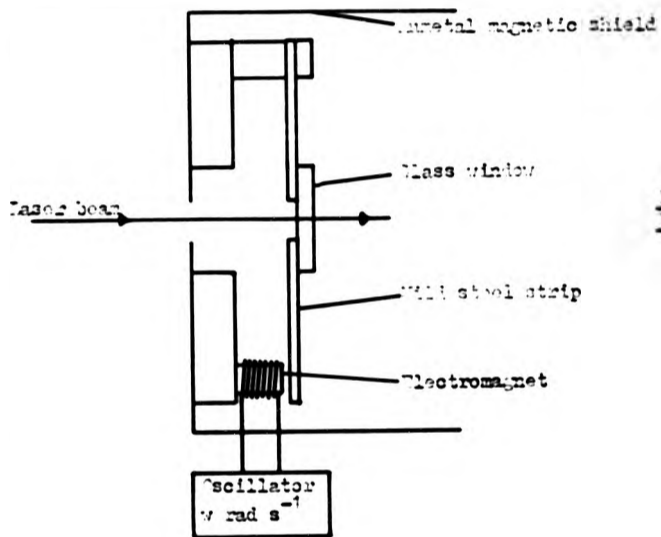


Figure 1. Design of piezo-optic phase modulator

4.6.6 Detection System

The detection system consists of basically three elements designed to detect, demodulate and display the signal due to the birefringence or dichroism induced in the medium under examination.

(a) Photomultiplier


An EMI type 9658C 2 inch tube proved suitable ("C" indicates it was below the maker's usual specification). It had an S20 prismatic cathode with optically increased red response for laser applications (quantum efficiency typically 10% at 633 nm). A mumetal shield was wrapped round the tube and held at cathode potential to act as an electrostatic and magnetic shield. These were housed in a Products For Research Inc. PMT housing complete with potted dynode chain assembly. Also used was an EMI PMT magnetic focussing assembly designed to reduce the effective cathode area and hence the dark current. Finally a second mumetal shield was fabricated to enclose the complete housing ensuring protection from stray magnetic fields.

Power was supplied by a Brandenburg photomultiplier power supply type 472R capable of supplying 0 to 2 kV although it was operated typically in the 500-700 V region.

The dynode chain was designed so that the PMT gave a linear response with a high gain. Now if linearity is a critical factor (as is the case for the measurement of small birefringences and dichroism), the dynode current I_d should be chosen such that the anode current $I_a < 100 I_d^{.71}$. So if operating at 650 V for example, if the dynode chain resistance $R_d = 2.5 \text{ M}\Omega$ and includes a 150 V Zener diode then $I_d = 0.2 \text{ mA}$ so I_a should be less than $2 \mu\text{A}$ for linearity. Therefore with an oscilloscope input impedance of $\sim 1 \text{ M}\Omega$, the voltage displayed on the 'scope under these conditions must be $< 2 \text{ V}$. In fact voltages observed were typically much less than 1 V so the criterion for linearity was satisfied.

(b) Lock-In Amplifier

Once detected accurately, the signal was demodulated using an Ortec-Brookdeal 9501 Lock-In Amplifier incorporating phase sensitive detection, the essential components of which are illustrated in Figure 4.3. A reference signal was obtained from the oscillator which drove the modulator so that the amplifier only responded to signals in phase



with the reference signal. In this way a DC voltage is output which represents the small birefringence or dichroism induced in the medium under investigation. This is an established method of recovering small signals from noise.

(c) X-Y Recorder

For a permanent, easily analysable record of experimental results the output of the Lock-In amplifier was applied to a Bryans 26000 XY recorder operating as an Xt recorder. This gave linearity and repeatability of better than 0.1% FSD.

4.7 Alignment of Optical Components

Components were aligned similarly as described for the ocular method in Section 4.3, such that the laser beam passed diametrically through and parallel to the magnet pole pieces. Also essentially as before, with just the laser, analyser and PM tube on the optical benches, the analyser was crossed with the polarization of the laser for a minimum intensity at the PM tube. Then the 20^o cm cell was filled with benzene (having a large Cotton-Mouton constant) and placed between the magnet pole pieces in its cradle. Maximum field was applied and the "crossed" analyser and laser rotated together to the lowest transmitted intensity position whereby the principal axes of the birefringent liquid, analyser and laser polarization were coincident. Then after reducing the magnetic field to zero, the analyser was rotated by 45° as was the laser to the lowest intensity position. This procedure ensures that the plane of polarization of the light incident on the birefringent medium is at 45° to the principal axes of the refractive index of the medium for maximum sensitivity of birefringence measurements.

A Glan-Thompson prism polarizer was then installed. To sharpen the polarization of the laser it was rotated to the lowest intensity position so that it was crossed with the analyser.

4.7.1 Alignment for Birefringence Measurements

The quarter wave plate was installed between the magnet and analyser and rotated for extinction after carrying out the above procedure.

The modulator was then placed between polarizer and cell as in Figure

3.2 as far from the magnet and as near to the laser as possible. The oscillator was adjusted to drive the modulator at its resonant frequency at a suitable voltage and then the azimuth of the modulator was changed until a maximum modulated intensity was received by the PM tube and viewed on the oscilloscope. The modulator was then set with its principal axes at 45° to those of the birefringent liquid and the apparatus was set up for the exclusive measurement of birefringence.

4.7.2 Alignment for Dichroism Measurements

After proceeding as in 4.7 so that just the analyser, polariser, laser and PM tube were installed in the optical benches, firstly a quarter wave plate was placed between the magnet and analyser and polariser crossed. It was then removed, put aside and a second identical quarter wave plate installed in its place and the procedure repeated. Both quarter wave plates were then rotated by 45° such that their principal axes coincided with those of the dichroic medium. Then the first $\lambda/4$ plate was installed between the polariser and cell such that circularly polarized light was incident on the medium and the second quarter wave plate placed between the cell and analyser as in Figures 3.2 and 4.2 to resolve the components of the light emergent from the medium, elliptically polarized due to the medium being dichroic.

After the components were finely adjusted for the best null in intensity as displayed on the oscilloscope it was found that two rays were emergent from the second $\lambda/4$ plate with a very narrow angle between them and a difference in polarization. These apparently corresponded to an O and e ray and presumably arose from $\lambda/4$ plate imperfection. This phenomenon was a problem since at a null of the e ray the almost superposed O ray was quite bright and reduced greatly the sharpness of the null. This problem was solved by collimating the laser beam so it was less than 3 mm diameter at the PM tube, and increasing the distance between the second $\lambda/4$ plate and PM tube to a reasonable maximum (~ 70 cm). Then near a null two distinct circular images separated by ~ 1 mm could be seen on a screen placed over the PM tube and it was a simple matter to use a collimator such that it passed only the e ray.

Section 3.8 shows that the setting of the modulator is very critical in the measurement of the linear dichroism of a medium which exhibits

linear birefringence under the same conditions. Normally phase differences induced in colloidal dispersions are much larger than simultaneous linear dichroism so, for example in order to reduce the contribution due to birefringence to below 1% for the PTFE "GP1" dispersions, it was calculated that the modulator had to be set within half a minute of arc.

The modulator was first rotated 45° from the position used for measuring birefringence so it was within a degree of the azimuth desired for exclusive dichroism measurements. Then the 20 cm cell was filled with benzene which had been double filtered to remove as much dust as possible so that the magnetic dichroism of the sample was negligible. Organic liquids have an immeasurably small linear magnetic dichroism, whilst dust can be highly dichroic. The full magnetic field was then applied which resulted in a change in the output of the lock-in amplifier indicating that some birefringence was being measured due to the modulator not being set perfectly. The azimuth of the modulator was then finely adjusted using the screw adjuster on the bump-stop (see Figure 4.7) until there was no change in the output of the lock-in amplifier on applying full field. The apparatus was then set up for the exclusive measurement of linear dichroism.

4.7.3 Alignment for "Direct" Dichroism Measurements

In order to check the magnetic dichroism results obtained for the more concentrated of the PTFE "GP1" dispersions, which exhibited a large dichroism, the transmittivities k_1 and k_2 were measured directly. The quarter wave plates and modulator were removed from the optical benches and the polarizer rotated by 45° so that the light incident on the sample was polarized either parallel or perpendicular to the direction of the magnetic field. A reference piece of polaroid was used to determine the plane of polarization which then could be arranged to be parallel to the field i.e. so that horizontally polarized light was incident on the sample. The analyser was crossed with this and then rotated by 90° to the uncrossed position. The apparatus was now set up to measure the transmittivity parallel to the field k_1 . To measure k_2 (perpendicular to the field) both polarizer and analyser were rotated by 90° to pass only vertically polarized light.

4.8 Cell and Sample Preparation

Preparation and filling of the 20 cm cell has been described in section 4.5. The measurement of the magnetic birefringence and dichroism of concentrated colloidal dispersions necessitated the use of short pathlength quartz cells as described in 4.6.4.

4.8.1 Cell Cleaning

In most cases the quartz cells were cleaned with acetone or propanol followed by filtered carbon tetrachloride. After containing a colloidal dispersion they sometimes benefited from ultrasonic treatment in the "Soniclean" to remove all particles adhering to the cell walls. The exteriors of the quartz cells were cleaned using a pad of lens tissue moistened with acetone.

4.8.2 Sample Preparation

(a) Neat Liquids and Mixtures

These were used without additional purification as most were of at least 99% purity from new bottles. Mixtures were made using pipettes and volumetric flasks thoroughly cleaned several times with filtered CCl_4 and dried. A check on the composition of these mixtures was made using a Paar DMA40 Digital Density Meter (see later).

The 20 cm cell was used almost exclusively and filled with filtered samples as previously described. As the photometric detection method is so much more sensitive than the ocular method the liquids had to be filtered with the utmost care since small particles of dust could give an effect quadratically dependent on magnetic field and hence inseparable to the effect due to the liquid.

(b) Polymers and Polymer Solutions

The neat polyisobutene samples were filtered using Millipore filters of pore size ranging from 0.05 to 0.45 μm depending on the degree of polymerization and hence the viscosity of the sample. The most viscous (Byvis 5, $M_n = 780$) had to be filtered in the oven at about 60°C using a filter press and the sample cell, once filled, had to be left in the oven for some time in order that all air bubbles were removed.

The solid poly- α -amino acid poly- γ -benzyl-L-glutamate (PBLG, $M_n = 215,000$) was studied in two solvents, N,N-dimethylformamide (DMF) and dichloroacetic acid (DCA) which had been cleaned of dust using 0.2 μm pore size Milipore PTFE filters. Stock solutions of 30 kg m^{-3} PBLG/DMF and 14 kg m^{-3} PBLG/DCA were prepared using a chemical balance and volumetric flasks. Concentrations ranging from 0.1 to 30 kg m^{-3} PBLG/DMF were prepared from the stock solution using pipettes and volumetric flasks. Unfortunately, because the polymer solid included some dust, the more concentrated of the samples tended to be dirty. However in time the dust settled even in the most concentrated of the PBLG/DMF samples but in the 14 kg m^{-3} PBLG/DCA solution dust remained suspended due to the highly polar nature of DCA and so the solution scattered light strongly. Because of this and the corrosive nature of DCA a 10 mm pathlength quartz cell was used for this sample, whereas all the PBLG/DMF samples were used in the 20 cm stainless steel cell.

(c) Colloidal Dispersions

The "Fluon GP1" PTFE dispersion has a nominal weight fraction of 0.6 in water (manufacturer's stated bottle concentration). Weight fractions ranging from 10^{-8} to 0.6 PTFE/water were prepared using pipettes and volumetric flasks. The water used was double distilled, deionized and filtered twice using a Millipore filter of 0.05 μm pore size. Cells of pathlengths 0.1 to 10 mm were used, the lower pathlengths generally being used for the higher concentrations to ensure sufficient light transmission, reduce the possibility of multiple scattering and to reduce the magnetic birefringence/dichroism to a manageable level.

The sample of human erythrocytes studied was diluted to $\sim 5 \times 10^{-3}$ weight fraction in water, adding ethan-1,2-diol for density matching ~~and~~ to increase the viscosity, so reducing the sedimentation rate of the particles. Because of the high turbidity of these particles in suspension this was the highest weight fraction that could effectively be used in a 1 mm pathlength cell.

The sample of "Ravacryl 344" acrylic co-polymer was diluted to $\sim 10^{-3}$ weight fraction in water. Because of turbidity this was about the maximum concentration usable in a 10 mm cell.

4.9 Calibration of Apparatus

The calibration of the finely divided circle holding the analyser has been discussed in 4.4.1. The Hall probe was calibrated more accurately and the sample cell recalibrated as follows.

4.9.1 Calibration of the Hall Probe

The 20 cm sample cell was filled with double filtered "Analar" benzene for calibration purposes and then installed in its cradle between the magnet pole pieces. The Hall probe was swung into position and a mercury-in-glass thermometer inserted next to the cell. Until the temperature of the cell and contents equilibrated with that of their surroundings the beam through the cell was strongly deviated by virtue of the temperature variation of refractive index of the sample.

As the Hall probe was stated to be linear to within 1% only up to 1 Tesla it needed to be calibrated above this field. For diamagnetic liquids such as benzene there is only a weak interaction of the molecules with the magnetic field B therefore the induced birefringence Δn is proportional to B^2 . So knowing accurately the actual value of the magnetic field up to 1 Tesla it was possible to calculate the constant of proportionality (and therefore the Cotton-Mouton constant) between Δn and B^2 and hence calculate the actual value of B over the range 1 to 2.2 Teslas from the measured birefringence. This could be compared to the value of magnetic field indicated by the Hall probe and Gaussmeter as shown in Figure 4.8.

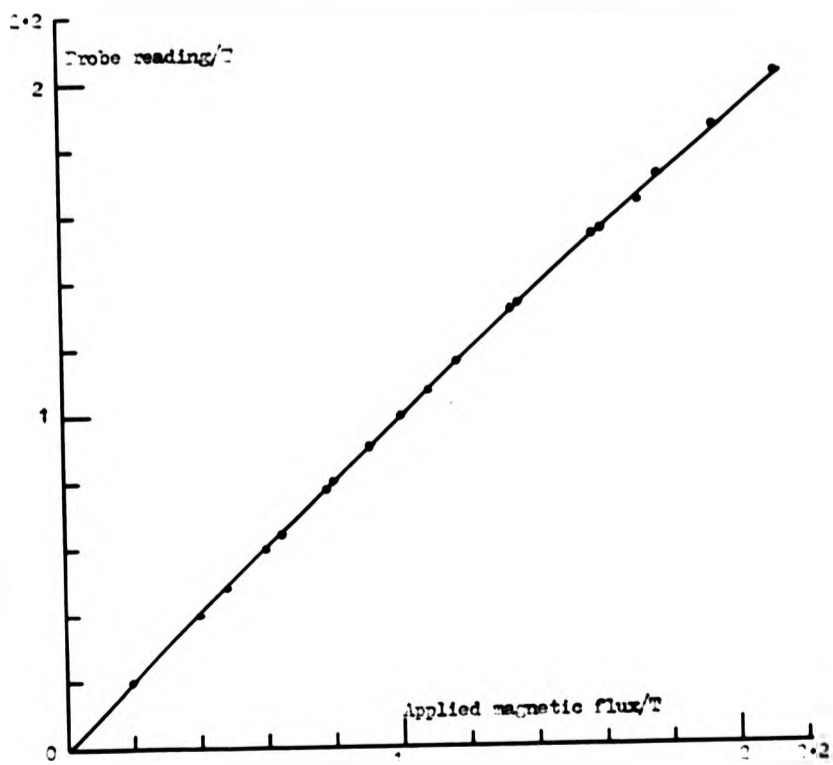
4.9.2 Calibration of the Sample Cells

(a) 20 cm Stainless-Steel Cell

The effective path length of the 20 cm cell has been measured previously in 4.4.2 and due to the increased accuracy of the photometric method a check was made of this calibration. Again using nitrobenzene as a standard (microanalytical quality) the experimental Cotton-Mouton constant of $21.4 \times 10^{-3} \text{ T}^{-2} \text{ m}^{-1}$ agreed well with 21.9×10^{-3} derived for 633 nm from the Landolt-Bornstein tables³.

The 10 mm quartz cell enabled a more reliable calibration to be made because the whole of the cell was in the uniform magnetic field between the pole pieces. The Cotton-Mouton constant of nitrobenzene measured in this way was $21.5 \times 10^{-3} \text{ T}^{-2} \text{ m}^{-1}$, in good agreement with experimental

Figure 4.3 Calibration of the Hall probe



error of the value previously obtained. Similarly a value for benzene $(6.55 \pm 0.03) \times 10^{-3} \text{ T}^{-2} \text{ m}^{-1}$ for the case of the 20 cm cell (assuming a 12.43 cm pathlength) compared with that of $(6.58 \pm 0.07) \times 10^{-3} \text{ T}^{-2} \text{ m}^{-1}$ obtained in the 10 mm cell.

(b) The Quartz Cells

These cells had the advantage of a well defined pathlength but because of this the windows were in the full magnetic field and therefore likely to be affected by it. They were found to give no detectable magnetic birefringence and yet they exhibited small magnetic dichroism, typically $\frac{2(k_{\parallel} - k_{\perp})}{(k_{\parallel} + k_{\perp})} = 7 \times 10^{-5}$ at 2 Teslas. There is an absorption peak in silica even of UV grade⁷² near $\lambda = 600 \text{ nm}$. Typically the Zeeman effect can give splittings of $3 \times 10^{11} \text{ Hz}$ (20 cm^{-1}) at fields of 2T giving a splitting of nearly 1 nm at the laser wavelength of 633 nm. Therefore if the absorption changes by 10^{-2} (1%) in 100 nm, in 1 nm it would change by 10^{-4} , the same order of magnitude of the measured magnetic dichroism. Fortunately this is small and could be subtracted from the value obtained when the cell contained a sample.

4.10 Experimental Procedure

Optical components were scrupulously cleaned and aligned as previously described. Collimators were used at various points to eliminate stray light and to enable the system to be operated without the need for total darkness. All electrical components in the detection system used coaxial cable and BNC plugs to reduce noise and pick-up in the leads to a minimum. Care was taken in routing the cables and avoiding earth loops.

All equipment was switched on and left to warm up for an hour or until the intensity drift of the laser was reduced to a minimum (<1% short-term). The frequency of the oscillator was finely adjusted for resonance of the modulator plate, indicated by the maximum sinusoidal signal from the FM tube as displayed on the oscilloscope. The applied voltage was adjusted to give a reasonable phase difference (0.2 V RMS yielded ~ 2 minutes of phase).

The FM tube was set to a suitable operating voltage, normally 600 V unless the sample was highly turbid such as the "Kavacryl" acrylic co-

polymer dispersion when 800 V was used or when the induced birefringence was particularly large such as for the more concentrated of the "Fluon GP1" PTFE dispersions when ~500 V was used.

The lock-in amplifier was set to detect components modulated at the fundamental frequency and filters to reject frequencies below 100 Hz and above 1000 Hz were switched in. It was set at a reasonable time constant (1 or 3 seconds) and appropriate sensitivity (~20 mV). Then with the analyser set slightly off the null position so that a reasonable signal was output from the lock-in amplifier, the phase shifter control was adjusted to null the output and then changed by 90° to maximise the output i.e. the signal and reference were in phase.

The XY plotter was set to an appropriate sensitivity on the Y axis whereas the X axis was set to a slow time base, normally 25 or 50 sec/cm.

The water supply to the electromagnet was switched on and the magnet power supply set to give maximum field (~2.2 T). The DC level of the PM tube signal was noted as was any significant change in the signal output from the lock-in amplifier as displayed on the oscilloscope and the XY plotter. Any change was due either to the interaction of the magnetic field with the apparatus or electrical pickup in the leads and had to be systematically eliminated because of the accuracy of measurements to be performed. The field was also increased and decreased with its direction reversed until all pickup had been reduced to an immeasurable value.

4.10.1 Measuring the Magnetic Birefringence of Highly Anisotropic Liquids and Polymers

In general because the induced phase differences were not too large the 20 cm stainless steel cell was used, excepting some measurements when a 10 mm quartz cell was used. The cell was installed in its cradle between the magnet pole pieces and allowed over an hour to reach thermal equilibrium. The Hall probe was swung into place and the analyser adjusted for a zero output from the lock-in amplifier.

For the measurement of the magnetic birefringence of very magneto-optically anisotropic molecules having a Cotton-Mouton constant greater than about $0.3 \times 10^{-3} \text{ T}^{-2} \text{ m}^{-1}$ e.g. benzene, acetone, the following

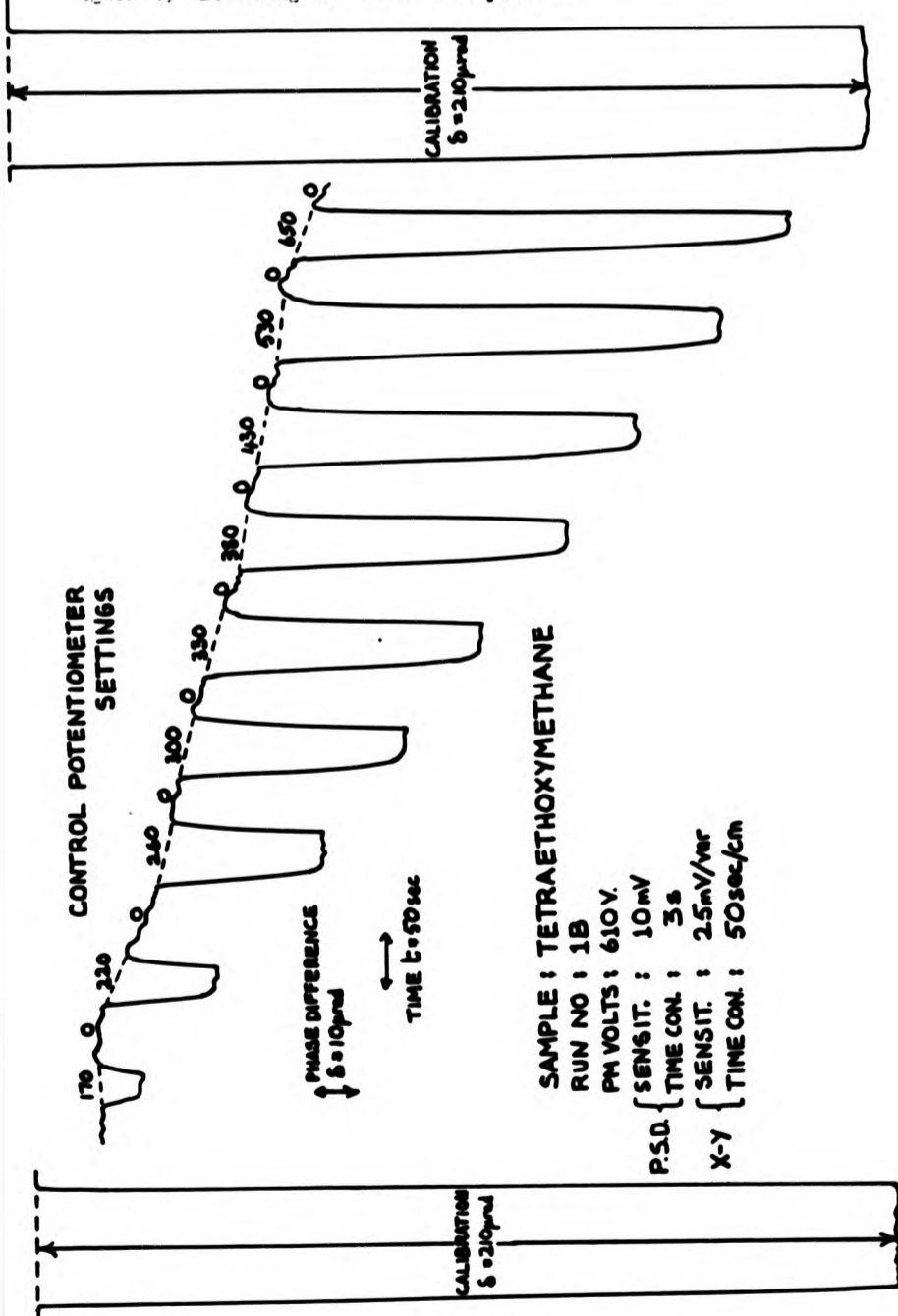
procedure was adopted. The three digit control potentiometer on the magnet power supply was adjusted to a number of predetermined positions, ten in all, from 0 to 650 corresponding to accurately known flux densities between 0 and 2.2 T. At each of these positions the analyser was rotated for zero output of the lock-in amplifier, noting the amount of rotation. All this was performed swiftly to minimize the effect of the time varying stray birefringence in the cell windows and as a check, the analyser position at zero field was remeasured at the end of the run. Checks for any non-quadratic effect such as Faraday rotation were made by repeating the run with the field direction reversed.

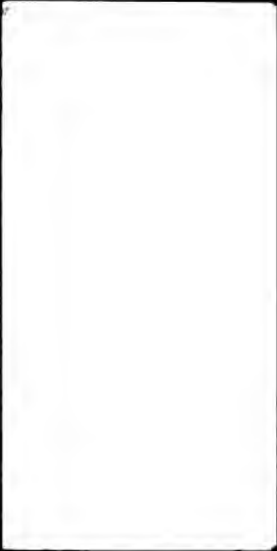
4.10.2 Measuring the Magnetic Birefringence of Weakly Anisotropic Media

If the above technique was applied to weakly anisotropic media the analyser rotation required for a null would be too small to accurately measure directly. This was because the minimum resolvable analyser rotation using the large micrometer was equivalent to an induced phase difference of ~ 20 μ rad, also the micrometer had a backlash of about this amount. Clearly a resolution more than an order of magnitude better than this was desirable for the accurate measurement of the magneto-optical anisotropy of neatly isotropic molecules. Now because the intensity input to the PM tube at the modulation frequency I_w is proportional to the modulation depth Δ_s , this is a linear detection method for Δn as outlined in 3.5. So providing the emergent light from on the media is of constant flux and the output of the PM tube is directly proportional to the input of photons as discussed in 4.6.6, the output of the lock-in amplifier (LIA) is proportional to the birefringence of the medium and could be recorded on the XY plotter. With the analyser adjusted for zero output at zero field, the maximum magnetic field was applied and the sensitivity of the LIA adjusted to give a reading near FSD on its internal scale. The XY plotter was also adjusted in sensitivity to give about three-quarters of FSD at full field.

Because the analyser rotation for FSD was normally too small to be measured accurately using the micrometer, in order to calibrate the scale the sensitivity of the LIA was suitably decreased (typically 10X) so that the analyser rotation could be increased by the same factor to give the same FSD on the XY plotter. Figure 4.9 shows the

Figure 1.9. Birefringence measurement procedure





typical procedure. The time base was set at 50 sec/cm and the analyser rotated by an amount equivalent to an induced phase difference here of 2.1 μ rad (0.1 mm on the micrometer) with the sensitivity of the LIA reduced by a factor of 10 so that the calibration was 210 μ rad (of phase) = 164 mm on the graph. To get an accurate calibration this was left for \sim 100 seconds and then the analyser was rotated back to its previous position. The sensitivity of the LIA was increased to its original value, the magnet water supply and generator switched on. The control potentiometer was left at zero for 50 seconds, increased to a predetermined position for 50 seconds and then set to zero for another 50 seconds. This procedure was repeated for ten predetermined positions from 0 to 650 again corresponding to accurately known flux densities between 0 and 2.2 T. After this the water and generator were switched off and the calibration procedure repeated.

The reason the field was zeroed between each setting can be seen from Figure 4.9. The base line drifts fortunately in a fairly linear fashion due mainly to stray birefringence in the cell windows and temperature variations. Measurements could then be made of the peak heights from the base line and converted into phase differences or birefringences using the calibration. As can be seen induced phase differences of \sim 1 μ rad can be resolved making this an extremely sensitive method. However, its accuracy depends on the amplitude stability of the laser beam which varied typically by 1% over the course of the experiment and contributed a maximum error of about 1% to results obtained which is small compared to the experimental error for quasi-isotropic media. As a check at least two runs were performed for each sample, the results from which almost invariably agreed within experimental error.

For media with larger magneto-optical anisotropies e.g. benzene, acetone, where the Cotton-Mouton constant is desired to be known to within less than 1% the standard method of rotating the analyser as described in 4.10.1 was used. This was much less sensitive but was independent of the amplitude stability of the laser.

4.10.3 Measuring the Magnetic Birefringence
of Colloidal Dispersions

Depending on the magnitude of the induced birefringence the methods described in 4.10.1 and 4.10.2 were used with amendments as follows. The cell pathlength was selected firstly so that sufficient light was transmitted to enable accurate measurements to be made on the sample. It had to be long enough to give a reasonable effect, but short enough in the case of the "Fluon GP1" PTFE dispersions so that the effect was not too large and so that the possibility of multiple scattering could be eliminated. To reduce the induced birefringence of these samples further, a range of much smaller magnetic fields (0 to 0.5 T) were accurately obtained using the Farnell L30D 2 Amp power supply.

Because of the danger of sedimentation affecting the results, each cell was positioned such that the laser beam passed as near as possible through the centre of the sample. Then providing sedimentation was not too rapid the number of particles entering the scattering volume = the number leaving, so the density of particles remains approximately constant. To confirm this, birefringence measurements were made on a range of concentrations of the PTFE dispersions. There was no significant change in the magnetic birefringence of these samples after they had been left for 100 minutes.


4.10.4 Measuring the Magnetic Dichroism
of Colloidal Dispersions

(a) Measurements Using Phase Modulation

These measurements were performed as for birefringence, since it is also a linear detection method, except that the system was set up for the exclusive measurement of dichroism as previously described in 4.7.2.

(b) Direct Dichroism Measurements

This method involved measuring the transmittivities k_{\parallel} and k_{\perp} separately and the apparatus was aligned as described in 4.7.2(a). The PM tube signal was output direct to the XY plotter as the magnet power supply was adjusted to give a range of predetermined magnetic fields with firstly horizontal and then vertically polarized light incident on the sample.



This was a very insensitive method so only the more concentrated of the PTFE dispersions could be examined in this way. Nevertheless it was a useful check on results obtained using the phase modulator.

CHAPTER 5

EXPERIMENTAL RESULTS AND DISCUSSION

5.1 Introduction

As explained in Chapter 2, current theory shows that the molar Cotton-Mouton constant (${}_{\text{m}}C$) of molar liquids depends on a number of parameters, some of which are difficult to separate. The relative importance of these depends on the molecular species.

Molecular liquids with large Cotton-Mouton constants have large magneto-optical anisotropies (γ_{MO}^2), so magnetic hyperpolarizability (η) and collision-induced contributions (${}_{\text{m}}C_{\text{CI}}$) may be regarded as relatively insignificant. By virtue of their delocalized molecular orbitals, benzene derivatives yield large values of ${}_{\text{m}}C$. A short study of some of these was made in order to assess the relative importance of the orientational correlation parameter (g_2) and the effect of local fields.

In contrast, liquids of near-isotropic molecules have near-zero values of γ_{MO}^2 and so any η or ${}_{\text{m}}C_{\text{CI}}$ contributions to ${}_{\text{m}}C$ will be relatively significant. The sensitivity of the apparatus allowed a study of mixtures of isotropic tetramethyltin and carbon tetrachloride in order to see if any intermolecular contributions to ${}_{\text{m}}C$ could be detected.

Homologous series of linear alkanes and derivatives, branched alkanes, cycloalkanes and alkanes containing a tri- or tetra-functional branch, were studied extensively. It was of interest to consider the relative importance of contributions to ${}_{\text{m}}C$ in these weakly anisotropic molecular liquids and compare the results, where possible, with light scattering results for the same series. ${}_{\text{m}}C$ was examined as a function of chain length with reference to established valence-optical and conformational theories, and as a function of molecular shape to establish the importance of molecular angular correlations.

A range of low to medium molecular weight polyisobutenes was measured; these are of interest since bond additive theories predict them to be magneto-optically isotropic apart from their end groups. The Cotton-Mouton constant, C , of high molecular weight PBLG was measured at a range of concentrations in two solvents. This was to study the effect

on the macromolecular conformation of the solvents, and to examine how polymer-polymer interactions affected C as the concentration of PBLG was increased.

The magnetic birefringence and dichroism of a very wide range of concentration of the colloidal dispersion, ICI 'Fluon' were measured. Fluon consists of roughly ellipsoidal, highly crystalline PTFE particles. It was of interest to calculate the principal refractive indices of the particles from measurements of the dilute dispersions, using O'Koncki's theory¹⁷⁷. A study of how the magnetic birefringence and dichroism varied with concentration for the concentrated dispersions enabled an examination of particle-particle interactions, and the applicability of the O'Koncki theory to dispersions containing particles larger than dipole scatterers.

5.2 Liquids with Large Cotton-Mouton Constants

By definition, diamagnetic liquids having a relatively large Cotton-Mouton constant must be highly anisotropic magnetically or optically. This can apply to liquids consisting of small molecules with π -electron systems, especially arenes which have ring systems where delocalized electrons can flow much more easily round than across the ring thereby having high diamagnetic susceptibility anisotropies. When the molar Cotton-Mouton constant, ${}_{\text{m}}C$ is negative, the directions of maximum optical polarisability and maximum (negative) diamagnetic susceptibility are coincident, or nearly so, but when groups such as $\text{C}=\text{C}$, $\text{C}=\text{O}$ or NO_2 are present these quantities are more nearly at right angles to each other and ${}_{\text{m}}C$ is positive.

Using both photometric and ocular methods ${}_{\text{m}}C$ was measured for nitrobenzene, benzene and propanone (acetone) in order to check the apparatus and to compare results with those obtained by other workers. ${}_{\text{m}}C$ was also measured for three other arenes - methylbenzene (toluene), hexafluorobenzene and 1,3,5-trifluorobenzene, using the photometric method only. These liquids were obtained from a variety of suppliers and had purities stated in excess of 99%; any impurities would be expected to have similar Cotton-Mouton constants. The photometric apparatus was calibrated as described in 4.9, using a 10 mm pathlength quartz cell containing benzene. Some workers have used nitrobenzene as a standard by virtue of its very large value of C and this procedure was adopted for the ocular method. In the Landolt-Bornstein tables³ (1955) its standard value at 20°C and $\lambda = 546 \text{ nm}$ is $(26.6 \pm 0.2) \times 10^{-3} \text{ T}^{-2} \text{ m}^{-1}$. The quoted variation with wavelength is quite large (from 0.0362 at 436 nm to 0.0214 $\text{T}^{-2} \text{ m}^{-1}$ at 656 nm). Goldet⁶⁸ (1938) showed that at 20°C the rate of decrease of C with increasing temperature was small (less than 0.5% per Kelvin for arenes) so that the precise temperature at which the measurements were made was not very important whereas the precise wavelength of the light should be known.

Readings of the analyser micrometer (M) at balance for set values of magnetic induction (B) were noted as described in 4.10.1 and C calculated following the procedure outlined in 4.4.1. The gradient of B^2 versus M was obtained both graphically and using a standard least-squares line-fit computer program which also gave standard error estimates. ${}_{\text{m}}C$ was calculated using equation (2.9) and refractive index and density data from the literature^{73,74}.

Table 5.1 Liquids with large Cotton-Mouton constants

Worker	Conditions		$10^3 C$	$10^{27} \frac{mC}{m^3 A^{-2} mol^{-1}}$	Reference
	T/°C	λ/nm	$/T^{-2} m^{-1}$		(date)
NITROBENZENE					
Present work	20±1	546	26.6 ± 0.2	124 ± 1	- (1978)
Present work	20±1	633	21.4 ± 0.1	116 ± 0.5	- (1979)
Battaglia & Richie	25	633	21.0	114	8 (1977)
Cotton & Mouton	16.3	578	25.3	125	3,75 (1910)
Grodde	20	546	24.6	115	3,76 (1938)
Snellman	18.3	546	30.9	144	3,77 (1944)
Goldet	21.5	546	26.2	122	3,68 (1938)
BENZENE					
Present work	20±1	546	6.23 ± 0.04	26.5 ± 0.2	- (1978)
Present work	20±1	633	5.04 ± 0.01	24.9 ± 0.1	- (1979)
Corfield	23	633	4.99 ± 0.19	24.6 ± 1.0	(1969)
Battaglia & Richie	25	633	5.01 ± 0.15	24.8 ± 0.8	8 (1977)
Stamm	20	633	5.89	29.1	10 (1979)
Champion et al.	25	546	6.86	29.2	16 (1977)
Cotton & Mouton	18.3	578	5.90	26.6	3,78 (1913)
Grodde	20	546	6.80	29.0	3,76 (1938)
Snellman	18	546	7.12	30.3	3,77 (1944)
Goldet	21	546	6.35	27.1	3,68 (1938)
Konig	20	546	6.80	29.0	79 (1938)
PROPANONE (ACETONE)					
Present work	20±1	546	0.437 ± 0.01	1.69 ± 0.03	- (1978)
Present work	20±1	633	0.392 ± 0.001	1.76 ± 0.01	- (1979)
Battaglia & Richie	25	633	0.26	1.01	8 (1977)
Snellman	18.8	546	0.49	1.90	3,77 (1944)
METHYLBENZENE (TOLUENE)					
Present work	20±1	633	5.44 ± 0.02	32.1 ± 0.1	- (1979)
Corfield	23	633	5.11 ± 0.11	30.0 ± 0.6	6 (1969)
Battaglia & Richie	25	633	5.29 ± 0.16	31.2 ± 0.9	8 (1977)
Cotton & Mouton	17.5	578	6.20	33.4	3,78 (1913)
Snellman	18.5	546	7.30	37.2	3,77 (1944)
HEXAFLUOROBENZENE					
Present work	20±1	633	4.71 ± 0.03	32.9 ± 0.2	- (1980)
Corfield	23	633	4.77 ± 0.18	33.3 ± 1.3	6 (1969)
Battaglia & Richie	25	633	4.91 ± 0.15	34.3 ± 1.0	8 (1977)
1,3,5- TRIFLUOROBENZENE					
Present work	20±1	633	6.85 ± 0.03	41.7 ± 0.2	- (1980)
Corfield	23	633		42.6 ± 1.1	6 (1969)

Results are shown in Table 5.1 together with those of some other workers. Results at different wavelengths cannot be strictly compared. From the table it can be seen that comparative results obtained are mostly in good agreement with published values. The photometric results ($\lambda = 633 \text{ nm}$) are generally in excellent agreement with those obtained by some recent workers^{6,8} at the same wavelength, the main exception being Stamm's¹⁰ (1979) value of C for benzene which is about 17% higher than that of Corfield⁶ (1969), Battaglia and Richie⁸ (1977) and the present value, which agree to within 1%.

It was observed that for the liquids of more anisotropic molecules the DC intensity at the balance point increased with the applied magnetic field thereby decreasing the accuracy. This was thought to be due to partial depolarization of the light beam and was not noticeable at all in the study of weakly anisotropic media. Despite this it can be seen from Table 5.1 that the photometric method used here reduced experimental error by nearly an order of magnitude compared to recent results using systems based on Faraday modulation, even though these systems employed more specialized magnets producing much higher magnetic fields.

As can be seen from Table 5.1 the calculated value of \bar{C} for benzene at 20°C and $\lambda = 633 \text{ nm}$ was $(24.9 \pm 0.1) \times 10^{-27} \text{ m}^5 \text{ A}^{-2} \text{ mol}^{-1}$. Plainly the largest contribution to this must be due to the large intrinsic molecular anisotropy but it is instructive to consider a theoretical value calculated from independent gas phase measurements of optical and diamagnetic susceptibility anisotropies. Alms, Burnham and Flygare⁸⁰ (1975) measured optical polarizabilities by depolarized Rayleigh scattering (DRS) and obtained the following results for benzene:

$$\begin{aligned} \bar{\alpha} &= 1.179 \times 10^{-39} \\ \alpha_{\parallel} &= 0.745 \times 10^{-39} \\ \alpha_{\perp} &= 1.397 \times 10^{-39} \text{ C}^2 \text{ m}^2 \text{ J}^{-1} \end{aligned}$$

where \parallel is the C₆ rotational symmetry axis.

Flygare and Shoemaker⁸¹ (1970) quoted measurements of molecular susceptibility anisotropies obtained from pure rotational spectra in high magnetic fields as follows:⁸²

$$\begin{aligned} \chi_{xx} - \chi_{yy} &= 0 \\ \chi_{zz} - \frac{1}{2}(\chi_{xx} + \chi_{yy}) &= -1.235 \times 10^{-27} \text{ m}^3 \end{aligned}$$

where z is the C₆ axis.

From these, neglecting hyperpolarizability, a value of $\underline{m}C$ may be calculated as being nearly $50 \times 10^{-27} \text{ m}^5 \text{ A}^{-2} \text{ mol}^{-1}$ for benzene which is almost double that obtained experimentally in the liquid phase. König⁷⁹ (1938) compared gas and liquid values of $\underline{m}C$ for benzene measured at $\lambda = 546 \text{ nm}$. His value for the gas (extrapolated to atmospheric pressure and 20°C) was 58.7×10^{-27} , virtually twice that of his liquid value of $29.0 \times 10^{-27} \text{ m}^5 \text{ A}^{-2} \text{ mol}^{-1}$. Also Corfield's⁶ vapour phase value of 37.7×10^{-27} is much larger than the $24.6 \times 10^{-27} \text{ m}^5 \text{ A}^{-2} \text{ mol}^{-1}$ obtained for liquid benzene. Therefore there must either be significant negative contributions to $\underline{m}C$ in the liquid phase or a mechanism reducing the intrinsic anisotropy of benzene molecules.

Since the π -electron cloud is relatively easily distorted there will be some contribution due to magnetic hyperpolarizability; estimates vary from 8% by Corfield⁶ (from analysis of the temperature dependence of $\underline{m}C$ of benzene vapour) down to less than 2% by Battaglia and Richie⁸ (1977) so the discrepancy is not yet accounted for. It is often proposed⁶ that for benzene angular and radial correlations in the liquid state tend to decrease the orienting effect of the magnetic field and some recent calculations of the orientational correlation factor, g_2 , for benzene finding it to be significantly less than unity^{83,84} reinforce this view and lead to the postulation of some kind of diatropic edge to face configuration⁸⁵ reducing the apparent molecular anisotropy. However Battaglia, Cox and Madden³⁷ (1979) have shown from DRS and magnetic birefringence results and making some justifiable assumptions (see Section 2.3.4) that g_2 for benzene is in fact greater than unity (1.16 ± 0.1). They showed that there is a reduction in the intrinsic polarizability anisotropy, $\alpha_{\parallel} - \alpha_{\perp}$ or $\Delta\alpha$ of a molecule to an effective anisotropy $\Delta\alpha_{\text{eff}}$ in a liquid, limiting the extraction of truly molecular properties. They calculated that the ratio $\Delta\alpha_{\text{eff}}/\Delta\alpha$ (633 nm) = 0.54 for benzene. Buckingham, Stiles and Richie⁸⁶ (1971) and Keyes and Ladanyi⁸⁷ (1977) analysed interaction-induced scattering, finding that the dominant contributions causing the reduction in $\Delta\alpha$ were due to the exclusion of molecules from a molecule-shaped cavity as outlined in Section 2.3.4. Therefore, since $\Delta\chi$ is virtually independent of state because of the weakness of diamagnetic interactions, the reduction of $\Delta\alpha$ to $\Delta\alpha_{\text{eff}}$ is responsible for the large reduction in $\underline{m}C$ of benzene in going from the gas to liquid state.

In the vapour phase Corfield⁶ (1969) found that the trend in \bar{C} for some fluorobenzenes was $C_6H_6 > C_6H_3F_3 > C_6F_6$. This was attributed to the decrease in ΔX caused by the decreased mobility of the π -electron ring system on the introduction of highly electronegative fluorine atoms. As one can see from Table 5.1 the pattern is completely different in the liquid phase where $C_6H_3F_3 > C_6F_6 > C_6H_6$. Contrary to that found for benzene, \bar{C} of tri- and hexafluorobenzene was approximately 50% higher in the liquid phase⁶. Corfield attributed this to a tendency to parallel alignment of C_6F_6 molecules which is greater in $C_6H_3F_3$ possibly because of intermolecular H-F bonding. Madden et al.⁸⁸ (1982) found that the ratios $\Delta\alpha_{eff}/\Delta\alpha$ for C_6F_6 and $C_6H_3F_3$ were very similar to that of C_6H_6 reinforcing the theory that this value is determined primarily by shaped cavity effects. They obtained a value of 2.7 for g_2 of C_6F_6 and $C_6H_3F_3$. For non-polar liquids it has been thought that g_2 must be close to unity but this was based on the assumption that g_2 arises from a weak angular correlation with its nearest neighbours.

Madden et al.⁸⁸ observed that the value of g_2 of arenes appears to correlate with how closely the molecules are packed. They expressed g_2 in terms of a radial integral over the average value of the second order Legendre function of $\cos\psi$ (the scalar product of unit vectors along the molecular axis), in each spherical shell ground in central molecule.

As discussed in Section 2.3.3:

the Legendre function = $P_2[\cos\psi](r)$

where r is the radius of the shell.

$$g_2 = 1 + 4\pi\rho/drr^2 g(r) \overline{P_2[\cos\psi](r)}$$

where ρ is the density and $g(r)$ the distribution function of molecular centres.

For close packing, the nearest neighbours should be more parallel than antiparallel so for a very small radius, $g(r)$ first rises from zero and the integrand is positive. For the second co-ordination shell, i.e. the second peak of $g(r)$, it is postulated that the integrand is negative and for larger r the integrand is expected to oscillate about zero. Hence a non-unity value of g_2 arises mainly from an imperfect

cancellation of the positive and negative integrands for the first and second co-ordination shells. Hence S_2 reflects a near cancellation of angular correlations of a central molecule with the first two co-ordination shells of neighbouring molecules, and a value of ~ 1 for S_2 indicates a cancellation rather than an absence of correlations.

Corfield⁶ has compared her values of ρ_C for arenes in the vapour and liquid states with those obtained by Le Fevre and Murthy⁸⁹ (1966) at infinite dilution in CCl_4 . However, measurements of solutes in solvents are not comparable with gas phase data because solute molecules will exclude the solvent molecules from a shaped cavity, thus modifying $\Delta\epsilon_{\text{eff}}$ as previously outlined. There will also be DID interactions and complex solute-solute and solute-solvent angular and radial correlations between molecules to consider.

5.3 Liquids of Near-Isotropic Molecules*

5.3.1 Neat Liquids of Intrinsically Isotropic Molecules

Because carbon tetrachloride (CCl_4) and tetramethyl tin ($Sn(CH_3)_4$) molecules are tetrahedrally symmetric, they are intrinsically magneto-optically isotropic and liquids of these molecules have very small Cotton-Mouton constants. Both samples had a purity exceeding 99% (the CCl_4 was of spectroscopic quality) and they were obtained from Koch-Light and Aldrich Ltd. Refractive index and density data were obtained from the literature⁷⁴ and the density data checked using a Paar DMA 40 digital density meter. Any measurable linear dichroism was always attributable to colloidal-sized dust particles which became apparent by producing mostly a non-quadratic dependence of Δn on E and could be reduced to a very low value by liquid filtration using 50 nm Millipore filters. The ability to measure linear dichroism accurately was a useful check for the presence of dust in liquids used for birefringence measurements in particular as the birefringence caused by the smallest dust particles had a quadratic dependence on the field and so was indistinguishable from that of the liquid.

* Some of the results obtained in this section have been published by - P.J. Batchelor, J.V. Champion and G.H. Maeten - JCS Faraday II (1980), 76, 1610.

The experimental procedure was performed four times for each liquid in order to verify the accuracy of the results. For half of these the magnetic field direction was reversed; all results obtained agreed to within the experimental errors quoted in Table 5.2. The table shows that there is some variation in recent results for ϵ_C and ϵ_C of CCl_4 . Corfield's⁶ (1969) value of ϵ_C $((-166 \pm 6) \times 10^{-30} \text{ m}^5 \text{ A}^{-2} \text{ mol}^{-1})$ obtained using a 70 cm pathlength cell in a specially built magnet, agrees with that obtained here $((-165 \pm 3) \times 10^{-30})$ at $\lambda = 633 \text{ nm}$. Other literature values are of much lower accuracy. Also of note is that the values of ϵ_C obtained here using the ocular method ($\lambda = 546 \text{ nm}$) and photometric method agree to within experimental error although the photometric method reduces the error by at least an order of magnitude.

It is interesting to compare the value of ϵ_C obtained for CCl_4 $(-165 \times 10^{-30} \text{ m}^5 \text{ A}^{-2} \text{ mol}^{-1})$ with that of chloroform, CHCl_3 (-2990×10^{-30}) in Table 5.2. It demonstrates that even for molecules such as chloroform which are not very anisotropic, the intrinsic anisotropy overwhelms other effects.

Single, isolated CCl_4 , $\text{Sn}(\text{CH}_3)_4$ and $\text{Si}(\text{CH}_3)_4$ molecules have tetrahedral symmetry for which symmetry considerations dictate that the magneto-optical anisotropy, $\gamma_{\text{MO}}^2 = 0$. Any radical correlations which may exist in the liquid state do not contribute to γ_{MO}^2 because of the negligible intermolecular magnetic DID interactions. According to equation (2.10) the molar Cotton-Mouton constant now becomes

$$\epsilon_C = L \mu_0^2 \epsilon_0^{-1} \eta / 270 \quad (5.1)$$

and values of the magnetic hyperpolarizability η have been so derived^{6,8} assuming that no other mechanism contributes to ϵ_C in liquids. Dimers and structure in "isotropic" liquids such as CCl_4 have been suggested and this is fully discussed in the next section on liquid mixtures.

For $\text{Sn}(\text{CH}_3)_4$ ϵ_C was found to be $(95 \pm 6) \times 10^{-30} \text{ m}^5 \text{ A}^{-2} \text{ mol}^{-1}$, smaller and of opposite sign to that of CCl_4 . This agrees to within experimental error with $(0 \pm 200) \times 10^{-30}$ obtained for the highly volatile (boiling point 27°C) $\text{Si}(\text{CH}_3)_4$ by Battaglia⁹ (1978). He concluded that his null result indicated that collision-induced and

Table 5.2 Neat liquids of near-isotropic molecules

Liquid	Wavelength λ/nm	10^6 C $/\text{T}^{-2} \text{ m}^{-1}$	10^{30} mC $/\text{m}^5 \text{ A}^{-2} \text{ mol}^{-1}$	Reference (date)
CCl_4	633	-30 ± 0.5	-165 ± 3	Present work
	546	-37 ± 5	-180 ± 30	Present work
	633	-43		10 (1979)
	633	-53 ± 12	-300 ± 70	8 (1977)
	633		-166 ± 6	6 (1969)
	578		-150	58 (1949)
$\text{Sn}(\text{CH}_3)_4$	633	11.9 ± 0.7	95 ± 6	Present work
$\text{Si}(\text{CH}_3)_4$	633		0 ± 200	9 (1978)
CBrCl_3	633	-650 ± 2	-2990 ± 10	Present work
	633	-680	-3130	10 (1979)
	578	-690	-2900	3,78 (1913)
	546	-770	-3060	3,90 (1934)
H_2O	633	-9 ± 0.6	-10.1 ± 0.7	Present work
	546	-39		3,91 (1930)

hyperpolarizability contributions to χ_C were comparable in magnitude and opposite in sign.

Buckingham, Prichard and Whiffen⁷ (1967) studied the magnetic birefringence of some diamagnetic gases including isotropic methane and sulphur hexafluoride. The molar Cotton-Mouton constant of CH_4 was found to be $(84 \pm 50) \times 10^{-30} \text{ m}^5 \text{ A}^{-2} \text{ mol}^{-1}$, and that of SF_6 was $(-220 \pm 130) \times 10^{-30}$. This difference in sign is most interesting, showing that there are probably at least two effects operating even in the gas phase which is relatively free from collisions and correlations. These results were interpreted in terms of the magnetic hyperpolarizability, a fourth rank tensor η describing the effect of a magnetic field on the usual optical polarizability tensor:

$$\text{Polarizability } \Pi_{\alpha\beta} = \alpha_{\alpha\beta} + i\eta_{\alpha\beta,\gamma\delta} \frac{H_\gamma H_\delta}{\gamma} \quad (5.2)$$

which is similar to the expression for magnetic susceptibility (2.12). A magnetic field will affect the polarizability Π by firstly distortion of the electronic structure through η which is a temperature independent process, and secondly partial orientation of the molecule, i.e. changing α , which depends on reciprocal temperature. As stated

in Chapter 2, n contains both diamagnetic and paramagnetic terms $n^{(d)}$ and $n^{(p)}$ of opposite signs whose magnitudes depend on the size of electron cloud and the availability of appropriate excited states respectively. Therefore Buckingham et al. explained that $n^{(d)}$ dominates in gases such as CH_4 so ${}_m C$ is positive whereas in systems such as SF_6 , because appropriate molecular orbital energy levels are closer, $n^{(p)}$ dominates leading to a negative ${}_m C$. Using similar arguments it may well be that in $\text{Sn}(\text{CH}_3)_4$ $n^{(d)}$ dominates whereas in CCl_4 $n^{(p)}$ dominates. However in the liquid phase there is the possibility of significant intermolecular contributions to ${}_m C$ as previously discussed so it would be instructive to compare liquid and gas phase values of ${}_m C$ for the same intrinsically isotropic substance.

5.3.2 Solutions of Intrinsically Isotropic Molecules

A series of CCl_4 and $\text{Sn}(\text{CH}_3)_4$ solutions (eight in all including the neat liquids) were made up covering the entire concentration range. Densities were measured very accurately at $20 \pm 0.05^\circ\text{C}$ using the Paar DMA 40 digital density meter and results are displayed on Figure 5.1. This shows a linear dependence of density on concentration within a density error of $\pm 0.1\%$ i.e. volumes were additive within this error. It also demonstrates that solutions had been constituted to a reasonable accuracy. To check for differential evaporation of the two components during cell filling, densities were checked before and after each run and found to agree within experimental error. This was to be expected since CCl_4 and $\text{Sn}(\text{CH}_3)_4$ have very similar boiling points. Figure 5.2 shows the molar Cotton-Mouton constants of these mixtures plotted versus mole fraction.

If, as is usually assumed, magnetic hyperpolarizability is the only contribution to the magnetic birefringence in CCl_4 and $\text{Sn}(\text{CH}_3)_4$ then from equation (2.10) we may write for the neat liquids the following:

$${}_m C_1^o = \frac{L \mu_o^2 n_1}{270 \epsilon_o} \quad (5.3)$$

$$\text{and } {}_m C_2^o = \frac{L \mu_o^2 n_2}{270 \epsilon_o} \quad (5.4)$$

where subscripts 1 and 2 refer to $\text{Sn}(\text{CH}_3)_4$ and CCl_4 respectively. Since magnetic DID interactions are negligible, radial correlations in liquid or solution will provide no contribution to the magnetic

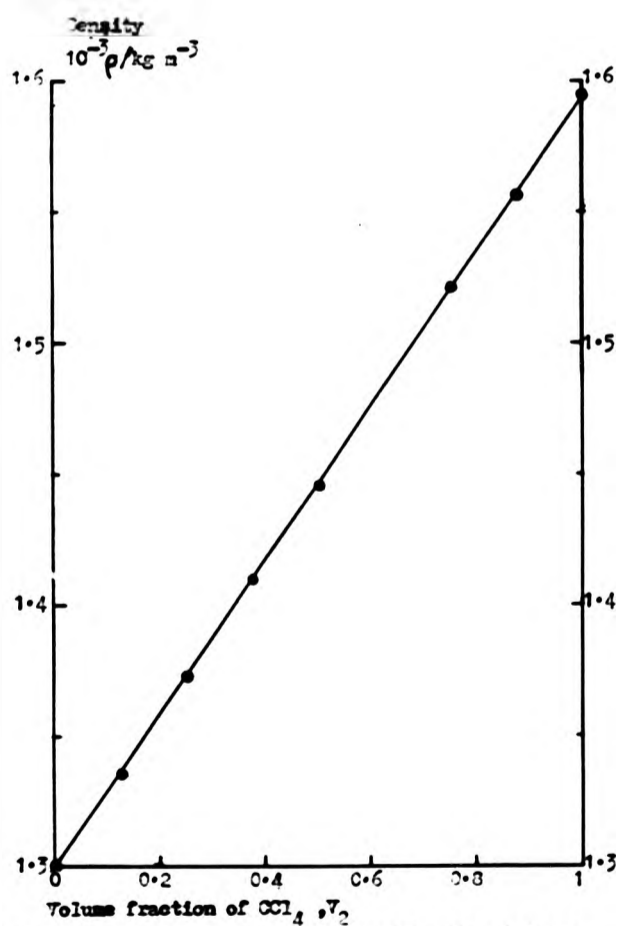


Figure 5.1 Density vs. volume fraction for mixtures of CCl_4 and $\text{Sn}(\text{CH}_3)_4$ at 20°C

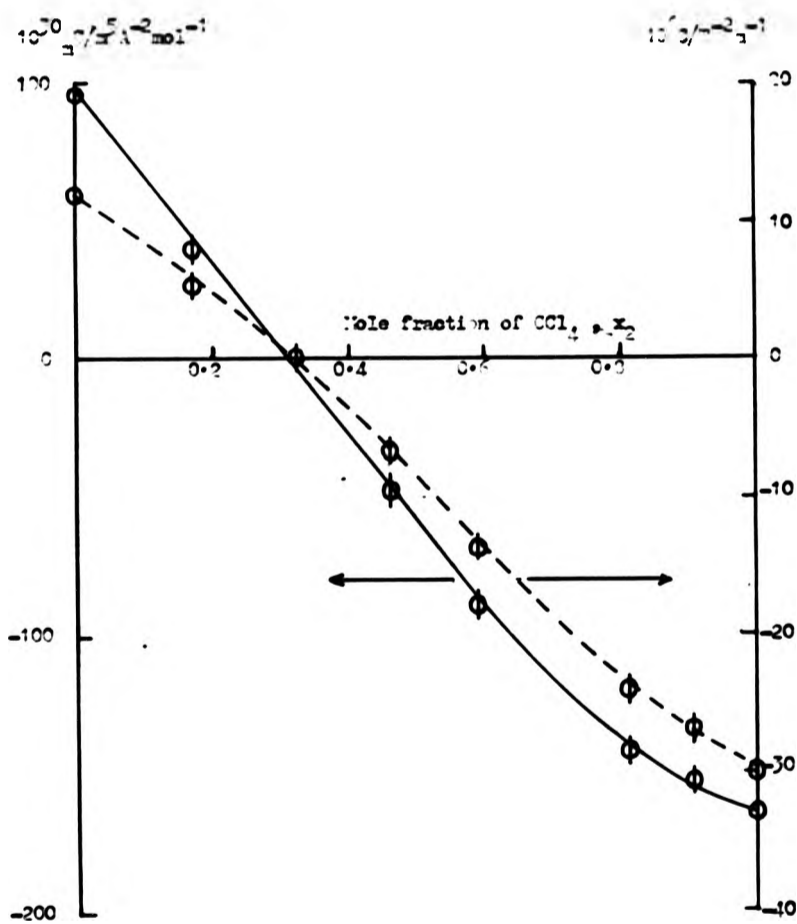


Figure 5.2 Molar and bulk Cotton-Mouton constants of $\text{CCl}_4/\text{Sn}(\text{CH}_3)_4$ solutions vs. mole fraction of CCl_4

birefringence. If each molecule is isotropic orientations correlations should be absent and we may put:

$${}_{\text{m}}C_1^{\circ} = {}_{\text{m}}C_1 = {}_{\text{m}}C_1^{\infty} \quad (5.5)$$

where superscripts \circ and ∞ refer to neat liquid and infinite dilution values respectively.

$$\text{Also } {}_{\text{m}}C_2^{\circ} = {}_{\text{m}}C_2 = {}_{\text{m}}C_2^{\infty} \quad (5.6)$$

where ${}_{\text{m}}C_1$ and ${}_{\text{m}}C_2$ are partial molar Cotton-Mouton constants at arbitrary dilutions. Hence the molar Cotton-Mouton constant of the solution,

$${}_{\text{m}}C = X_1 \cdot {}_{\text{m}}C_1^{\circ} + X_2 \cdot {}_{\text{m}}C_2^{\circ} \quad (5.7)$$

So the measured ${}_{\text{m}}C$ should vary linearly with mole fraction from one neat liquid to the other. Figure 5.2 shows this not to be the case.

Partial molar Cotton-Mouton constants may be defined like other partial molar quantities²⁸ as follows:

$${}_{\text{m}}C_1 = \left(\frac{\partial {}_{\text{m}}C}{\partial n_1} \right)_{n_2} \quad \text{and} \quad {}_{\text{m}}C_2 = \left(\frac{\partial {}_{\text{m}}C}{\partial n_2} \right)_{n_1} \quad (5.8)$$

where n_1 is the number of moles of $\text{Sn}(\text{CH}_3)_4$ and n_2 the number of moles of CCl_4 . They are intensive quantities so may be derived by the standard method of intercepts^{92,93} applied to graph 5.2. In this method a tangent to the curve intersects the $X_2 = 0$ axis at ${}_{\text{m}}C_1$ and the $X_2 = 1$ axis at ${}_{\text{m}}C_2$. Therefore the quantities ${}_{\text{m}}C_1$ and ${}_{\text{m}}C_2$ are in this case variables dependent on composition being ${}_{\text{m}}C_1^{\infty}$ and ${}_{\text{m}}C_2^{\infty}$ at $X_2 = 1$ and 0 respectively. This approach contrasts with the usual Le Fèvre method^{8,89,94} of obtaining infinite dilution molar Cotton-Mouton (or Kerr) constants where the molar Cotton-Mouton constant of the solvent (usually CCl_4) is assumed to be independent of its concentration in the solution. There CCl_4 is treated as an isotropic solvent and because of the insensitivity of the equipment used, it is often assumed to have a zero Cotton-Mouton constant.

Figures 5.3 and 5.4 show that ${}_{\text{m}}C_1$ and ${}_{\text{m}}C_2$ change quite rapidly when the mole fraction of CCl_4 , X_2 , is greater than about 0.5. Thereby CCl_4 and $\text{Sn}(\text{CH}_3)_4$ yield anomalous contributions when surrounded by CCl_4 molecules so $\text{Sn}(\text{CH}_3)_4$ behaves as an inert solvent for CCl_4 but not vice versa. Hence CCl_4 as a neat liquid has an intermolecular

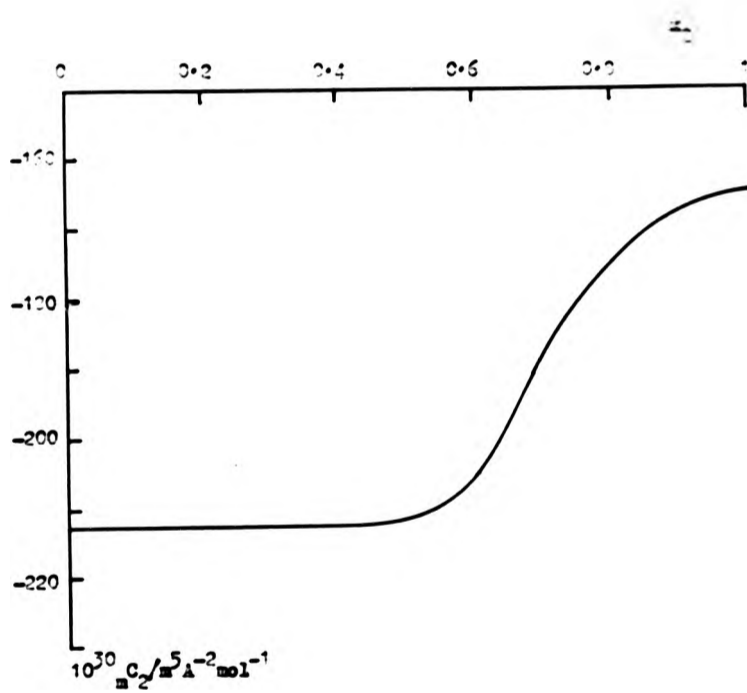


Figure 5.3 The partial molar Cotton-Mouton constant of CCl_4 in solution with $\text{Sn}(\text{CH}_3)_4$ vs. mole fraction of CCl_4

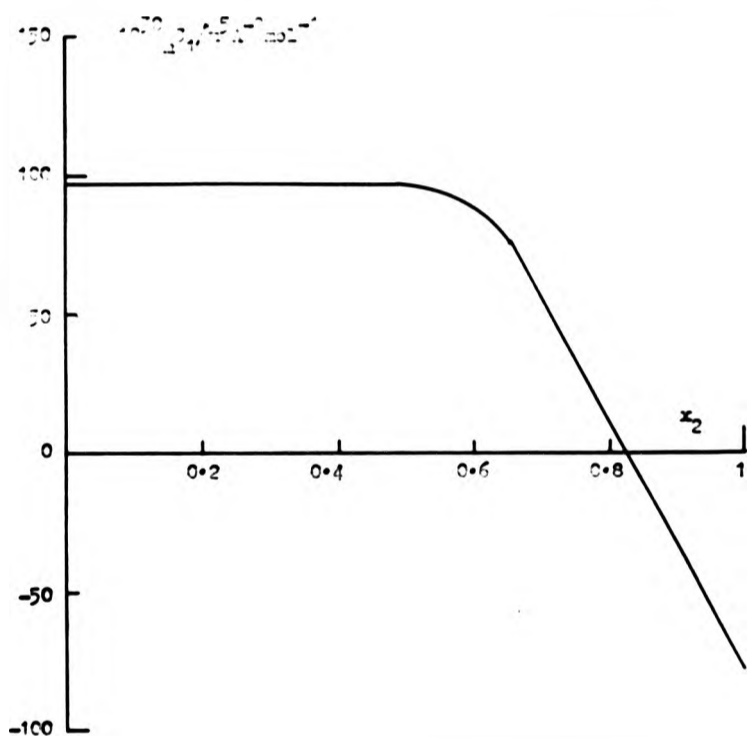


Figure 5.4 The partial molar Cotton-Mouton constant of $\text{Sn}(\text{CH}_3)_4$ in solution with CCl_4 vs. mole fraction of CCl_4

mechanism which contributes to the magnetic birefringence and being intermolecular it ceases when the CCl_4 molecules are sufficiently widely separated in dilute solution with $\text{Sn}(\text{CH}_3)_4$.

The fact that this intermolecular contribution to the birefringence changes rapidly as CCl_4 is diluted shows that CCl_4 is not a truly isotropic solvent and thus is not entirely suitable for infinite dilution Cotton-Mouton constant studies. The difference in ${}_{\text{m}}C_2^0$ and ${}_{\text{m}}C_2^{\infty}$ is only about 0.05×10^{-27} SI (see Figure 5.3) which is about three orders of magnitude smaller than ${}_{\text{m}}C$ for arena liquids, in which case CCl_4 can be treated as an inert solvent. However when the solute species is only weakly anisotropic such as an n-alkane molecule, magnetic birefringence studies of molecular orientational correlation ^{10,95} using CCl_4 as a solvent must be viewed with caution. Figure 5.4 shows that using CCl_4 as a solvent changes the molar Cotton-Mouton constant of $\text{Sn}(\text{CH}_3)_4$ from a positive value in the neat liquid to an apparently negative value at infinite dilution. It follows that attempts to derive directly molecular magnetic hyperpolarizabilities from Cotton-Mouton constant measurements on neat liquids of isotropic molecules are incorrect unless any other contributions to the magnetic birefringence can be subtracted.

There are several possible origins of the intermolecular contribution to the magnetic birefringence in neat CCl_4 . As stated earlier, magnetic DID interactions are too small to affect the magnetic birefringence via a distortion of the radial distribution function. It is possible that the magnetic hyperpolarizabilities of molecules are significantly affected by intermolecular interactions but like magnetic susceptibility anisotropies they would be expected to be virtually independent of state. As discussed in Chapter 2 a collisional contribution to magnetic birefringence has been suggested²⁰ but, for reasons discussed in Chapter 2, this is unlikely to be significant.

Prengel and Gornall⁹⁶ (1976) studied the Raman spectra of low pressure gaseous methane and found a rotational band attributable to $\text{CH}_4 \cdot \text{CH}_4$ dimers. If these intermolecular bound states exist in the gas phase they could lead to some specific orientational correlations in the liquid. From X-ray diffraction studies Greubel and Clayton⁹⁷ (1967) and Marten, Danford and Levy⁹⁸ (1967) found evidence for structure in

liquid CCl_4 . However, the evidence is difficult to translate into a meaningful model. Reichelt, Weidner and Zimmerman⁹⁹ (1974) and Zimmerman¹⁰⁰ (1978) obtained a good fit to their X-ray data by considering only parallel and antiparallel pairs of CCl_4 molecules. The optimum distance between molecules in a pair was found to be only slightly more than if the Cl atoms touched each other at their Van der Waals radii, therefore any liquid structure in CCl_4 seems to be determined by the maximum space filling efficiency.

It is clear that if the intermolecular interactions or environment affect the properties of one Cl atom or C-Cl bond as described above, the Td symmetry and hence isotropy will be destroyed. Also any structure would be changed with the addition of, and dilution by, molecules of a different sort.

5.3.3 Neat Liquids of Near-Isotropic Molecules

Two different liquids are considered here: trichloromethane (chloroform) and water.

(a) Chloroform

Spectroscopic grade chloroform was obtained from Koch-Light and was filtered with a 50 nm Millipore filter before use. Reference to Table 5.2 shows that the molar Cotton-Mouton constant of $-2.99 \times 10^{-27} \text{ m}^5 \text{ A}^{-2} \text{ mol}^{-1}$ is in very good agreement with those obtained previously. It is interesting to compare this value with the -0.165×10^{-27} obtained for CCl_4 which demonstrates that the magnetic birefringence of CHCl_3 is almost entirely due to its intrinsic anisotropy, other contributions such as magnetic hyperpolarizability probably accounting for only 5% of this value. If this is true for a liquid of molecules which are not highly anisotropic it means that hyperpolarizability and other contributions to liquids with large Cotton-Mouton constants might account for less than 1% of the measured value of \underline{C} .

(b) Water

Water is interesting in that reported values of \underline{C} and \underline{C} are very small (see Table 5.2), even though H_2O possesses C_{2v} symmetry and so is intrinsically anisotropic. Double distilled deionized water was obtained of a very high purity. Because water is a polar liquid, it

tends to suspend dust particles so it was filtered four times using a 50 nm Millipore filter. A check that the measured dichroism was negligibly small confirmed that virtually all the dust particles had been removed.

The value of $(-10.1 \pm 0.7) \times 10^{-30} \text{ m}^5 \text{ A}^{-2} \text{ mol}^{-1}$ obtained for $\underline{\underline{C}}$ is much lower than the available literature values, which agree closely with each other³. However being about 50 years old these values are likely to be of low accuracy, possibly due to dust or other impurities.

It is interesting to compare the experimental liquid phase value of $\underline{\underline{C}}$ with a theoretical value calculated from independent gas phase measurements of optical and diamagnetic susceptibility anisotropies. Murphy¹⁰ (1977) combined results from rotational Raman spectra and DRS with mean polarizability data in order to evaluate the molecular polarizability tensor for water vapour. He found the principal components of this at $\lambda = 514.5 \text{ nm}$ to be:

$$\begin{aligned} \alpha_{xx} &= (163.3 \pm 0.3) \times 10^{-42} \\ \alpha_{yy} &= (170.0 \pm 1.5) \times 10^{-42} \\ \alpha_{zz} &= (137.4 \pm 1.5) \times 10^{-42} \text{ C}^2 \text{ m}^2 \text{ J}^{-1} \end{aligned}$$

where the x axis is in the molecular plane along the C2 axis and the z axis is that perpendicular to the plane. Flygare and Shoemaker⁸¹ (1970) quoted measurements of diamagnetic susceptibility anisotropies made by Kukolich and Flygare¹⁰²⁻³ (1969) from pure rotational spectra in high magnetic fields as follows:

$$\begin{aligned} \chi_{xx} - \chi_{yy} &= (-23 \pm 13) \times 10^{-30} \\ \chi_{zz} - \frac{1}{2}(\chi_{xx} + \chi_{yy}) &= (-13 \pm 13) \times 10^{-30} \text{ m}^3 \end{aligned}$$

Although these results involve large errors, a study made of MO energy levels confirmed them to be essentially correct giving a theoretical $\langle \gamma_{\text{MO}}^2 \rangle$ of $(0.22 \pm 0.2) \times 10^{-75} \text{ C}^2 \text{ m}^5 \text{ J}^{-1}$ leading to an $\underline{\underline{C}}$ of $(+10 \pm 9) \times 10^{-30} \text{ m}^5 \text{ A}^{-2} \text{ mol}^{-1}$ of equal magnitude but opposite sign to that obtained by experiment. A value of $\langle \gamma_{\text{MO}}^2 \rangle$ may also be obtained by using the above principal components of $\underline{\underline{g}}$ to find those of $\underline{\underline{X}}$ as in the Gans-Mrowka equations^{99,100}. These give a smaller positive value of $\langle \gamma_{\text{MO}}^2 \rangle$ but as stated by Bothner-By and Pople¹⁰⁴ (1965), the G-M equations imply that the largest negative diamagnetic susceptibility is invariably at right angles to the largest optical polarizability

component. We know that this cannot always be true since negative Cotton-Mouton constants imply these components are parallel, so there is much doubt about the validity of the G-M approach.

The apparent change in the sign of m_C going from the gas to liquid phase cannot be caused by the orientational correlation parameter S_2 as this is simply a multiplying factor, although one might expect S_2 to be greater than unity due to extensive hydrogen bonding in water. The indicated negative value of m_C^{liquid} could be due to a dominant $\eta^{(p)}$ contribution from the mixing of ground state MOs with excited states as described in Sections 2.3.1 and 5.3.1.

5.4 Linear, Branched-chain and Cyclo Alkane Heat Liquids and Derivatives*

A systematic study of some short chain molecules was carried out in order to probe further the inter- and intramolecular interactions affecting the Cotton-Mouton constants of liquids. Results were analysed with reference to valence-optical theories (bond polarizability additivity), bond and atomic interaction theories, the rotational isomeric model, local field theories and molecular orientational correlations in liquids.

The study commenced with the simplest linear saturated hydrocarbon chains, n-alkanes, and progressed to linear derivatives such as n-alcohols. Both light and heavily branched alkanes were then considered leading to a study of alkanes with a tri- or tetra-functional branch point (tri- and tetra-alkyl compounds). Then some cycloalkanes were considered leading finally to a comparison of results of all the above to see what overall trends were evident.

* Some of the results contained in this section, those for n-alkanes and n-alcohols obtained by the ocular method at $\lambda = 546 \text{ nm}$, have been published by:

J.V. Champion, A. Dandridge, G.H. Maeten - Faraday Disc. C.S. (1978), 66, 266.

5.4.1 n-Alkane Liquids

n-alkanes are about the simplest short chain polymer molecules, having the general formula $C_n H_{2n+2}$. An examination of how the magneto-optical anisotropy per backbone atom ($\langle \gamma_{MD}^2 \rangle / n_A$) varies with the number of backbone atoms can lead to a greater understanding of inter- and intramolecular interactions.

The Cotton-Mouton constant, C, of most of the liquid n-alkanes was measured by the photometric method at $\lambda = 633$ nm and some by the less accurate ocular method at $\lambda = 546$ nm. The room-temperature liquids in this series range from pentane (boiling point 36°C) to pentadecane (melting point 10°C). Samples used were obtained from Aldrich and Koch-Light Ltd. and had stated purities in excess of 99%.

Any impurities were likely to be related compounds so resultant errors in C would be small. All samples were filtered as previously described in Section 4.5.

Table 5.3 shows the measured bulk value of C in order to make a comparison with values obtained by other workers. From dispersion considerations¹⁰⁵ the Cotton-Mouton constant is wavelength dependent so strictly, comparisons should be made with results of very similar wavelengths. Consequently the only results found in the literature which could be compared with those obtained by the photometric method ($\lambda = 633$ nm) were those of Fischer et al.¹⁰⁶ (1979) which were in good agreement. Agreement between results obtained by the ocular method and those from the literature³ at 546 nm was variable, being good for the higher alkanes but progressively worsening for the shorter chains. However, most of the literature results are some thirty or forty years old, when the apparatus was generally less accurate and the liquids less pure.

C for each liquid was calculated using equation (2.9); appropriate refractive index and density data was mainly obtained from the literature⁷⁴.

Figure 5.5 shows \bar{C} as a function of the number of carbon atoms, n_A , for the n-alkanes measured at $\lambda = 546$ and 633 nm. Immediately one can see that the dependence of \bar{C} on n_A is not linear even for high n_A . Also interesting is that $\bar{C}_{546\text{nm}}$ is higher than \bar{C}_{633} by an

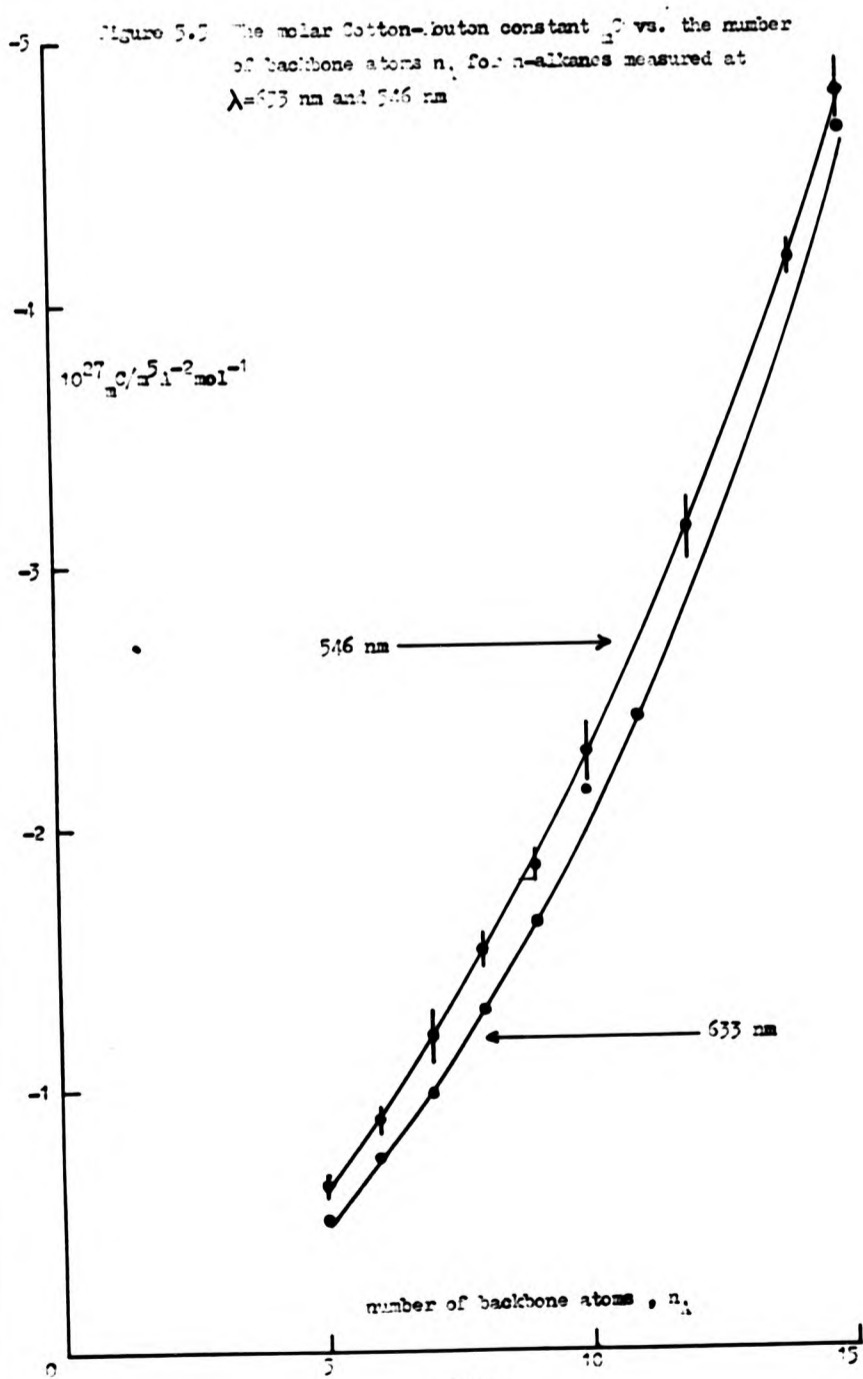


Table 5.3 Bulk Cotton-Mouton constants of n-alkanes at (20 ± 1)°C

Liquid	Wavelength λ/mm	10 ⁶ C/T ⁻² m ⁻²		Reference
		This work	Literature	
Pentane	633	-71 ± 1	-65	106 (1979)
	546	-103 ± 7	-63	3,58 (1949)
Hexane	633	-94 ± 1	-	
	546	-129 ± 10	-76	3,58 (1949)
Heptane	633	-112 ± 1	-	
	546	-158 ± 15	-105	3,58 (1949)
	578	-	-116	3,107 (1934)
Octane	633	-134 ± 1	-132	106 (1979)
	546	-182 ± 10	-	
	578	-	-150	3,108 (1931)
Nonane	633	-154 ± 1	-	
	546	-202 ± 8	-188	66 (1978)
	578	-	-160	3,108 (1931)
Decane	633	-185 ± 1	-	
	546	-230 ± 12	-226	66 (1978)
	578	-	-209	3,108 (1931)
Undecane	633	-194 ± 1	-	
	578	-	-234	3,108 (1931)
Dodecane	633	-	-220	106 (1979)
	546	-273 ± 11	-290	66 (1978)
			-281	3,58 (1949)
			-250	3,76 (1938)
Tetradecane	546	-325 ± 4	-	
	578	-	-271	3,108 (1931)
Pentadecane	633	-290 ± 2	-	
	546	-346 ± 10	-	
Hexadecane	633	-	-310	106 (1979)

almost constant amount irrespective of n_A . This indicates a possible systematic error in the measurement of C by the less accurate ocular method. Perhaps Faraday rotation, which is virtually independent of n_A , is contributing significantly to C_{546} but not to the more accurate C_{633} .

Figure 5.6 shows $|C|^{\frac{1}{2}}$ plotted versus n_A for $\lambda = 633$ nm. This shows that for the liquid n-alkanes $C \propto n_A^2$ for $n_A = 5$ to 15 with the extrapolated graph intercepting almost exactly at the origin.

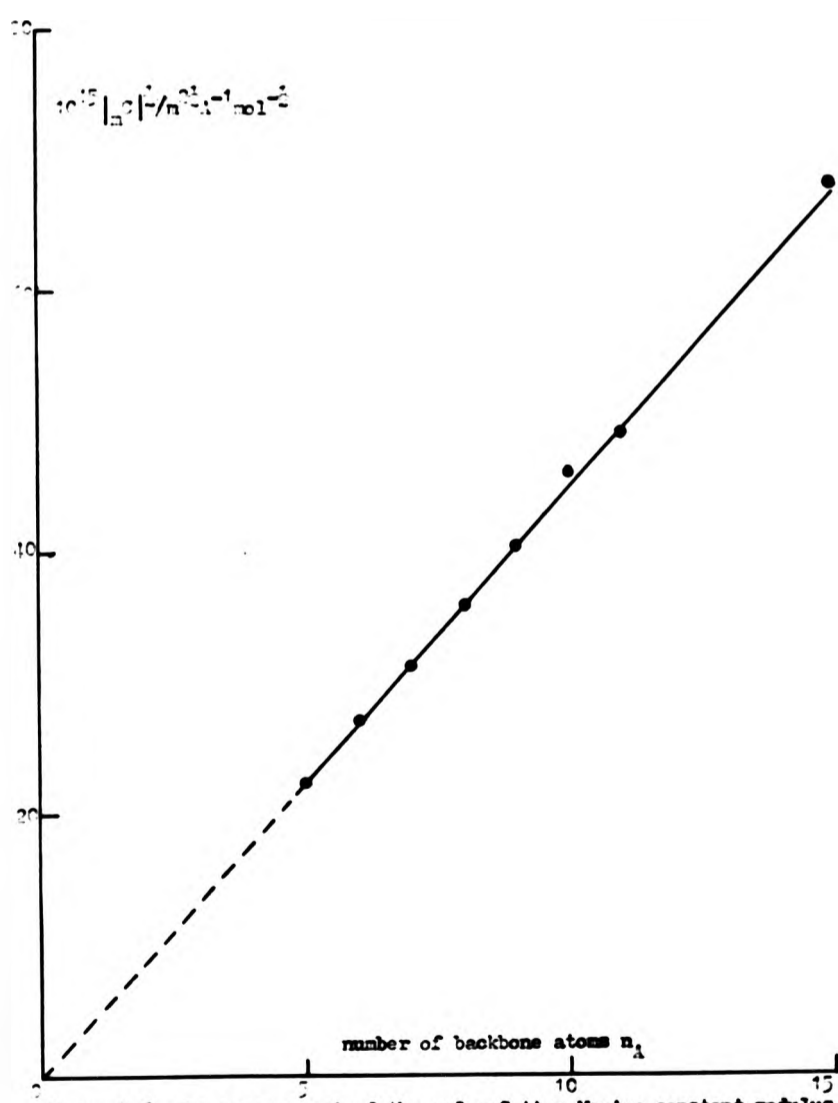


Figure 5.6 The square root of the molar Cotton-Kiuton constant modulus vs. the number of backbone atoms n_1 for n-alkanes measured at $\lambda = 633 \text{ nm}$

Analysis of results with respect to valence-optical theory and the rotational isomeric model

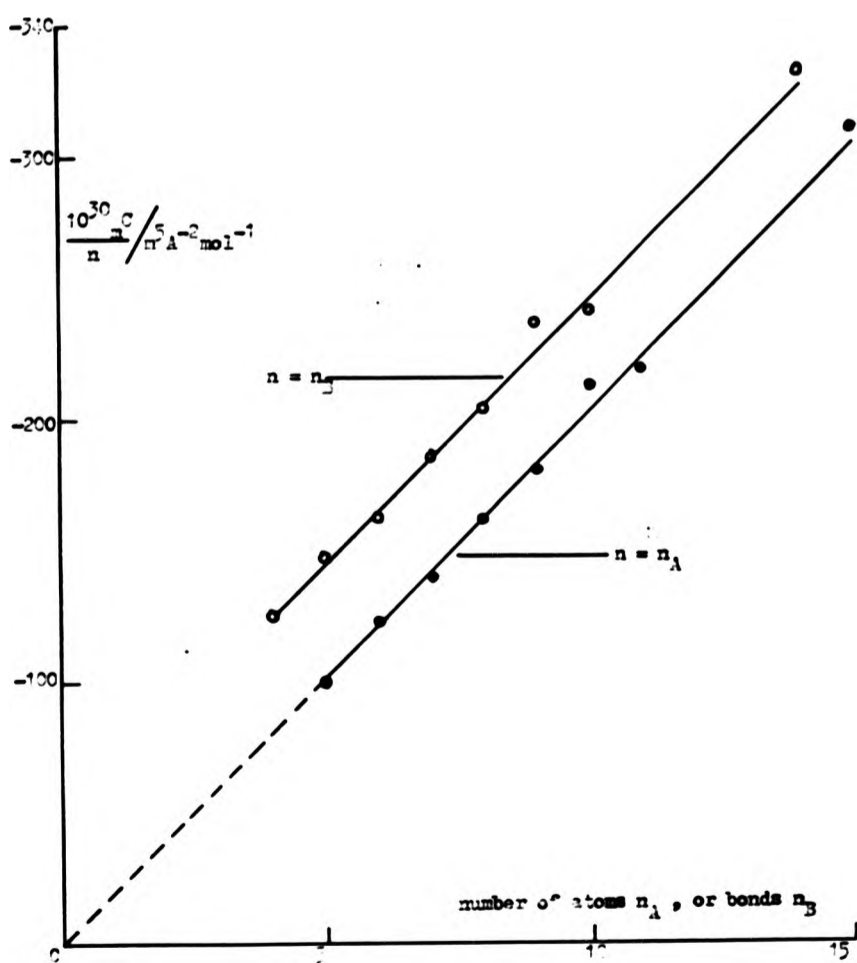
Figure 5.7 shows γ_{MO}^2/n plotted versus n where n is the number of atoms n_A , or bonds n_B . Most authors consider measured optical anisotropies in terms of the bond polarizability additivity scheme (BPA). As discussed in 2.5.1, the BPA theory can be used to obtain theoretical values of molecular polarizability anisotropies (γ^2) and magneto-optical anisotropies (γ_{MO}^2) using bond polarizability and susceptibility tensors. Figure 5.7 shows an intercept at the origin when n is the number of atoms but not when it is the number of bonds. This appears to favour a theory based on atomic properties. However, the non-zero value of γ_{MO}^2/n at $n_B = 0$ is normally explained in terms of hyperpolarizability.

In combination with the rotational isomeric model (RIM) theoretical calculations⁴⁴ give $\langle \gamma^2 \rangle = \Gamma_o^2 \langle \Lambda^2 \rangle$ for the n -alkanes, where the angled brackets denote a statistically weighted average over all conformations. $\Gamma_o^2 = \Delta\alpha_{\text{CC}} - 2\Delta\alpha_{\text{CH}}$ if the C-C backbone angle is tetrahedral (109.5°), or $\Delta\alpha_{\text{CC}} - 1.95\Delta\alpha_{\text{CH}}$ if it is 112°⁴⁵. Here $\Delta\alpha_{\text{CC}}$ and $\Delta\alpha_{\text{CH}}$ are the optical anisotropies of C-C and C-H bonds respectively. $\Lambda(\Delta U, n_B)$ is a parameter which is a function of the number of bonds n_B , the trans-gauche potential energy difference ΔU_{tg} and the gauche + gauche - potential energy difference $\Delta U_{\text{g+g-}}$.

If one assigns diamagnetic anisotropies $\Delta\chi_{\text{CC}}$ and $\Delta\chi_{\text{CH}}$ to these bonds then an analogous diamagnetic quantity $\Gamma_m = \Delta\chi_{\text{CC}} - 2\Delta\chi_{\text{CH}}$ may be defined^{4,8} representing the diamagnetic anisotropy of ethane. Hence in an analogous expression to that given above for $\langle \gamma^2 \rangle$, the magneto-optical anisotropy $\langle \gamma_{\text{MO}}^2 \rangle = \Gamma_o \Gamma_m \langle \Lambda^2 \rangle$.

Assuming Γ_o and Γ_m are constants, then $\langle \gamma_{\text{MO}}^2 \rangle / n_B$ theoretically lies between two limits depending on the C-C bond intramolecular potential energy. If $\Delta U = 0$ as in the freely jointed chain model then $\langle \gamma_{\text{MO}}^2 \rangle / n_B$ is virtually constant¹⁰⁹. At the other extreme if $\Delta U = \infty$, giving a fully extended all-trans chain, $\langle \gamma_{\text{MO}}^2 \rangle / n_B$ is virtually proportional to n_B^{-20} . However, substituting reasonable values of 2.1 to 2.5 kJ mole⁻¹ for ΔU_{tg} and 8 to 10.5 kJ mole⁻¹ for $\Delta U_{\text{g+g-}}$ in the rotational isomeric model gives $\langle \gamma_{\text{MO}}^2 \rangle / n_B$ virtually constant above $n_B = 10^{44,109}$. This applies even if the bond angles are not quite tetrahedral⁴⁵.

Figure 5.7 The molar Cotton-Deuton constant per backbone bond/atom vs. the number of backbone bonds/atoms for n-alkanes measured at $\lambda = 633 \text{ nm}$



As outlined in Chapter 2, the molar Cotton-Mouton constant of a neat liquid is:

$${}^m C = \frac{L\mu_0^2}{405\epsilon_0} \left\{ \frac{1}{kT} g_2 \langle \gamma_{mo}^2 \rangle + \frac{3}{2} \eta_{eff} \right\} + {}^m C_{CI}$$

i.e. for a given temperature ${}^m C$ is a function of $\langle \gamma_{mo}^2 \rangle$, the orientational correlation parameter g_2 , the magnetic hyperpolarisability η_{eff} and any collision-induced contribution ${}^m C_{CI}$. If it is assumed that the intrinsic anisotropy $\langle \gamma_{mo}^2 \rangle$ is the dominant contribution to ${}^m C$, then the dependence of ${}^m C$ on n_D shown in Figure 5.7 implies that $\langle \gamma_{mo}^2 \rangle / n_D$ is proportional to n_D (plus a small constant) for $n_D = 4$ to 14.

Clearly this experimental result conflicts with the combination of BPA and RIM as applied above to n-alkanes. There are several possible explanations for this disagreement which preserve the principles of bond polarisability additivity:

(a) Alkane molecules fully extended (all-trans)

It has been suggested¹¹⁰ that the type of disagreement discussed above could be due to n-alkane molecules being more extended than indicated by statistical theory i.e. favouring the all-trans confirmation in the liquid phase. There is no evidence to support this despite the fact that n-alkanes naturally crystallise in the all-trans conformation in order to achieve close-packing in the solid.

Estimates of ΔU_{tg} have been made using a number of different techniques in gas, liquid and solution states. Bothorel⁵⁶ compiled data from a number of independent sources, using spectrometry, calorimetry, Raman scattering, electron diffraction in the gas phase, viscosity measurements and infrared spectroscopy in the liquid phase to show that ΔU_{tg} probably lies in the region 2 to 3.4 kJ mole⁻¹. More recently this has been confirmed by small angle neutron scattering¹¹¹ of long chain n-alkanes (C16 and C36) in neat liquid solution states showing that the conformation of n-alkane molecules is not greatly different in the molten state from that suggested by the RIM model. It has been suggested that n-alkane molecules might be more globular¹¹² in the liquid than in the gas phase and studies of the longitudinal acoustic mode in their infrared spectra¹¹³ have shown that the percentage of molecules in the all-trans conformation in a liquid actually decreases with increasing pressure.

(b) Magnetic hyperpolarizability

The magnetic birefringence of liquids of near-anisotropic molecules is often thought to arise wholly from the molecular magnetic hyperpolarizability, η ^{6,8}. However, as discussed earlier in section 5.3, even in these liquids there may be other contributions to ${}_{\text{m}}C$ such as a collision-induced one.

The contribution of η to the molar Cotton-Mouton constant, ${}_{\text{m}}C$ of magneto-optically anisotropic molecules is normally considered to be small^{7,8,114-6} but one might expect a reasonable η contribution in liquids of weakly anisotropic molecules²⁰.

A bond additivity model analogous to that used for molecular polarizabilities has been suggested for electric hyperpolarizabilities²³. Electric mean hyperpolarizabilities of n-alkanes as obtained from electric birefringence measurements¹¹⁷ have been shown to be approximately bond additive, as have those obtained from third harmonic measurements¹¹⁸. The latter results showed hyperpolarizabilities to be virtually independent of molecular geometry, since for the same number of carbon atoms there was little difference in the results between cyclo and n-alkanes.

If magnetic hyperpolarizabilities follow the same trends they should be scalar bond additive as are mean bond polarizabilities. Then one would expect the contribution from the effective magnetic hyperpolarizability, η_{eff} to ${}_{\text{m}}C$ of n-alkanes to be proportional to n_{B} which does not explain the observed n_{B}^2 dependence. Hence η_{eff} is probably small in liquid n-alkanes.

(c) Collision-induced contributions

Collision-induced effects have been dealt with at length in 2.3.2 and collisional contributions to the molar Cotton-Mouton constant, ${}_{\text{m}}C_{\text{CI}}$, were considered with reference to liquids of near-isotropic molecules in 5.3.

Recent depolarized light scattering measurements²⁰ show that the collision-induced contribution to $\langle \gamma^2 \rangle$ in liquid n-alkanes is a less than linear function of n_{B} and accounts for a decreasing proportion of the total integrated depolarized scattered intensity as n_{B} is increased. Therefore even if there is an equivalent contribution ${}_{\text{m}}C_{\text{CI}}$ to ${}_{\text{m}}C$ of



n-alkanes, it is likely to be small and will not be proportional to n_B^2 .

(d) CH₃ end-group effects

The CH₃ end-groups are not as anisotropic as the CH₂ group in n-alkanes¹¹⁹ and so will reduce $\langle \gamma_{\text{MO}}^2 \rangle$. This effect might be observable for short chains but one would expect it to be progressively diluted and level off as the chainlength increases. Hence it cannot explain the observed trend of \bar{m}_C versus n_B .

(e) Local field effects

Local field theories have been discussed in detail in section 2.3.4. It has been shown that cavity field effects reduce markedly ($\sim 5X$) the depolarized scattering in liquids of small, non-spherical molecules⁸⁷. If one defines $\Delta\alpha$ as $\alpha_{\parallel} - \alpha_{\perp}$ for an isolated molecule then molecules having the major polarizability along the long axis, i.e. $\Delta\alpha$ positive, are effectively less anisotropic in an ellipsoidal cavity¹²⁰. This is because the local field is greatest along the short axis, increasing relatively the short axis polarizability. Some recent work starting from the measured birefringence of paraffin crystals and using a part dipole lattice model of alkanes in the crystalline state¹²¹ has concluded that Γ_0 is negative. Other workers do not support this claim. Values of Γ_0 and $\Delta\alpha_{\text{eff}}$ calculated from light scattering data vary greatly with state^{119,122-3} and are much greater in the gas phase. This is consistent with a positive value of $\Delta\alpha$ since a cavity field would increase $\Delta\alpha_{\text{eff}}$ if the major polarizability was along the short axis. Could molecular-shaped cavity field corrections explain the observed quadratic dependence of \bar{m}_C on n_B for liquid n-alkanes? As the length of chain increases the molecule tends to become more globular as the proportion of gauche configurations increases. Thus if $\Delta\alpha$ is positive, $\Delta\alpha_{\text{eff}}/\Delta\alpha$ should increase with chain length and could be a factor in the observed trend of \bar{m}_C . This will be considered more later.

(f) Molecular orientational correlations

As indicated earlier in the chapter the value of \bar{m}_C depends to some extent on the orientational correlation parameter g_2 which is a multiplying factor of $\langle \gamma_{\text{MO}}^2 \rangle$. The second rank orientational parameter is

$$g_2 = 1 + \sum_{j \neq i} \frac{1}{2} \langle 3 \cos^2 \theta_{ij} - 1 \rangle$$

where θ_{ij} is the relative orientation of two molecules. g_2 can be



interpreted as a measure of order in a substance and is clearly defined as above but is elusive to measurement since it is normally combined with other factors such as $\Delta\alpha_{\text{eff}}^{37}$.

There are two models for chain conformation and order in amorphous polymers:

(i) The coil model¹²⁴ considers the amorphous phase as homogeneous and random in structure. The constituent molecules are unperturbed and have a theta-solvent conformation.

(ii) The bundle model¹²⁵ proposes that there are small domains with nematic liquid crystalline order i.e. chains are packed into bundles.

The first contention that amorphous and liquid polymers have not significant order above their chain diameter is supported by small^{106,111,126} and medium¹²⁶ angle neutron scattering, small¹²⁶⁻⁷ and wide^{106,127} angle X-ray scattering, recent electron micrographs¹²⁶, Raman scattering⁴² and rubber elasticity studies¹²⁶. Only specific heat and light scattering studies^{106,126,128-30} indicate some short range order in polymers such as amorphous polyethylene and liquid n-alkanes. Light scattering (especially depolarized Raleigh scattering) evidence will be discussed later in this section. It suggests a very weak local segmental correlation^{106,129-30} largely independent on chain length with a range only of order ~ 1 nm. This would enhance χ_C^{131} but this effect should level off above a fairly short chain length, and so would not alone explain the observed quadratic dependence of χ_C on chain length.

It therefore seems that either neutron, X-ray etc. techniques are relatively insensitive to molecular orientational correlations or that optical theories used to interpret light scattering results of polymers, such as the bond polarizability additivity approximation are erroneous.

Modifications to the Bond Polarizability Additivity Scheme

As discussed earlier, the molecular diamagnetic susceptibility tensor χ_{dia} can be considered as independent of state and so Γ_{dia} is constant for a particular localized bond. However it has been shown that for the same bond, bond polarizability anisotropies and hence Γ_{dia} vary

according to their chemical environment⁵³. Mean polarizabilities can be considered independent of their environment to a good approximation¹²², hence it appears that components of $\underline{\alpha}$ may change whilst preserving the value of $\bar{\alpha}$ ¹³².

Therefore the assumptions of the bond polarizability additivity (BPA) approximations should be examined. These are:

- (i) Electron flow between bonds is negligible. This might be reasonable for a σ -bond.
- (ii) Molecular polarizability properties originate solely from bonding electron orbitals.
- (iii) Bonds can be considered as independent polarizable units.

If (i) and to a lesser extent (ii) are seriously in error the whole concept of bond additivity breaks down. This will be discussed later. A number of workers have questioned assumption (iii) and modified the theory to allow interaction between bonds. Using the Silberstein¹³³ model describing a bond as two induced dipoles having a separation r , Fitzer¹³⁴ showed that $\Delta\alpha_{\text{bond}}$ varied strongly with r whereas $\bar{\alpha}_{\text{bond}}$ was virtually independent of r .

A field polarizing a particular bond, $E_{\text{local}} = E_{\text{incident}} + E_{\text{medium}}$ as before, where E_{medium} is due to induced dipole moments of surrounding bonds. Intermolecular contributions from E_{medium} cause Γ_{O} to vary greatly with state as discussed earlier. Γ_{O} also increases with chain length^{119,123,135} so intramolecular contributions due to interaction between bonds must be considered¹³⁶.

Rovell and Stein¹²² considered induced dipole interactions between bonds in ethane and found that CC and CH bond anisotropies vary much more with interactions than mean bond polarizabilities. This approach has been generalized¹⁴² to show that if quadrupole and higher order interactions are neglected, then the molecular polarizability tensor may be regarded as the sum of bond polarizability tensors if the latter are locality dependent. However these intramolecular internal field effects depend on r^{-3} and so should level off as the chain length is increased¹¹⁹. Therefore this modification to BPA will not alone explain the observed dependence of α_{C} on chain length although the evidence so far suggests

that a combination of shaped cavity field effects and dipole-induced interactions along the chain could explain these results. To consider this further it may be instructive to compare the Cotton-Mouton results with other published light-scattering data of n-alkanes.

Comparison with other light-scattering data

Many workers have measured $\langle \gamma^2 \rangle$ of the n-alkanes in neat liquid, solution and in the gas phase. Most of these results were obtained by depolarized light scattering and it is instructive to compare the variation of $\langle \gamma^2 \rangle$ with chain length with that observed for C_m .

Most work has been done in comparing neat liquid $\langle \gamma^2 \rangle$ values with those obtained at infinite solution in a suitable solvent, normally "isotropic" CCl_4 . $\langle \gamma^2 \rangle$ liquid is greater than $\langle \gamma^2 \rangle$ solution^{56,126,137-9} and the ratio $\langle \gamma^2 \rangle_{\text{liquid}} / \langle \gamma^2 \rangle_{\text{solution}}$ tends to decrease with increasing asymmetry of solvent molecules^{45,139-40}. The difference between liquid and solution values has often been attributed to molecular orientational correlation (MOC) of the solute molecules^{46,56,138-9,141}. Solution values are often taken as a validation of BPA since $\langle \gamma^2 \rangle / n$ appears to be levelling off at high n^{56,137,139,143}. However, some of the extrapolations to infinite dilution are of questionable accuracy^{45,140} because it is claimed¹⁴³⁻⁴ that the solute concentrations used were not low enough. Different equipment and equations can give a factor of 2.5X difference in calculated values of $\langle \gamma^2 \rangle_{\text{solution}}$ ^{45,143}. Also as shown in 5.3, CCl_4 should not be regarded as an inert solvent for infinite dilution studies of the molecular anisotropy of weakly anisotropic molecules. Also internal field problems arise since each C-C bond is surrounded partly by other C-C bonds and partly by C-Cl bonds which have a much greater polarizability anisotropy²⁰. Therefore the difference between $\langle \gamma^2 \rangle_{\text{liquid}}$ and $\langle \gamma^2 \rangle_{\text{solution}}$ is unlikely to be due to molecular orientational correlations alone.

For neat liquid n-alkanes, $\langle \gamma^2 \rangle$ follows the same trend as C_m i.e. $\langle \gamma^2 \rangle \propto n^2$ ^{20,44,56,136-7}. Recall that $\langle \gamma^2 \rangle = \Gamma_o^2 \langle \Lambda^2 \rangle$ and $\langle \gamma^2 \rangle = \Gamma_o \Gamma_m \langle \Lambda^2 \rangle$ from BPA, if one assumes C_m for n-alkanes depends mainly on $\langle \gamma^2_{\text{MD}} \rangle$. Therefore, if both $\langle \gamma^2 \rangle$ and $\langle \gamma^2_{\text{MD}} \rangle$ have the same chain length dependence then Γ_m should increase with n at the same rate as Γ_o . As discussed previously Γ_o should increase with n up to a point due to intramolecular internal field effects but Γ_m should be virtually independent of n. This shows the assumptions on which BPA is based to be incorrect.

Collated gas phase measurements of $\langle \gamma^2 \rangle$ of n-alkanes up to decane^{20, 136, 145} show that $\langle \gamma^2 \rangle_{\text{gas}}$ is approximately $3X \langle \gamma^2 \rangle_{\text{liquid}}$ due to intermolecular local field effects, but more importantly $\langle \gamma^2 \rangle_{\text{gas}}$ is also approximately proportional to n^2 . Intramolecular local field effects mean that BPA is not strictly applicable even to isolated molecules^{123, 146} but as described before these effects should level off above a short chain length. Obviously the effect of molecular orientational correlations will be small and cannot be used to justify BPA in the gas phase. Therefore it is probable that the use of MOC to justify BPA in the liquid phase is incorrect and that BPA is not a reasonable scheme to use in the theoretical calculation of molecular optical anisotropies.

Breakdown of bond polarizability additivity:
the interacting atom model

The assumptions forming the basis of BPA theory as outlined earlier are highly questionable. Not all C-C bonds can be considered as equivalent¹⁴⁷⁻⁸ but this can be accounted for.

Teixeira-Dias and Murrell¹⁴⁹ used molecular orbital theory to calculate the polarizability tensors of methane, ethane and propane. They showed that whilst mean polarizabilities are bond additive, anisotropies are not, due to large intramolecular internal fields and electron flow between bonds. So the concept of electrons being localized in bonds may be unrealistic even for σ -bonds. Longitudinal and transverse bond polarizabilities may be largely determined by an electronic transition which involves an orbital extending over the whole of the molecule, e.g. in CS_2 ⁸⁰, in which case bonds cannot be considered as separate entities. Also there may be significant interaction between non-bonded atoms¹⁵⁰.

Applequist, Carl and Fung¹⁵¹ applied the Silberstein¹³³ model for molecular polarizability to some simple polyatomic molecules. Atoms were considered as isotropically polarizable units located at their nuclei and interacting via their induced dipole fields. This interacting atom model (IAM) is at fault in the same way as the interacting bond theory used by Rowell and Stein¹²² in that it approximates a continuous electronic charge distribution as a collection of point induced dipoles. Ladanyi and Keyes¹⁵² extended the IAM to include n-alkane gases. By virtue of the model's simplicity there are only

two adjustable parameters α_C and α_H and results were interpreted as predicting $\langle \gamma^2 \rangle \propto n_B^2$ for $n_B = 6$ to 10. This is in agreement with experiment, contrary to the BPA approximation.

Unfortunately even a model having the IAM's simplicity is difficult to apply to neat liquids and solutions where the solvent modifies interactions such that BPA might be emulated¹⁵³.

5.4.2 Linear Alkane Derivatives -

n-Alcohols, n-Alkenes, Aminoalkanes

Initially three ranges of hydrocarbon chain were studied, namely the n-alkanes (dealt with in 5.4.1), n-alcohols and n-alkenes. These were chosen because they are short chain polymers readily available in a range of molecular weights and of high purity, and they have been much studied by other techniques. The n-alkanes are the simplest having the general formula $C_n H_{2n+2}$, n-alcohols having an OH group at one end of the chain are $C_n H_{2n+1} OH$, and n-alkenes have one C=C double bond at the end of the chain so are $C_n H_{2n}$. Since all these chains are based on methylene CH_2 building blocks (apart from the end groups), an examination of how the molar Cotton-Mouton constant per backbone atom, $\frac{C}{n_A}$, varies with n_A for each series might lead to a greater understanding of the factors determining $\frac{C}{n_A}$. In addition a limited number of n-alkylamines, possessing an NH_2 end group, and di-n-alkylamines, with an NH in the middle of the chain, were chosen to examine the effect on $\frac{C}{n_A}$ of changing the position of the substituted group.

The Cotton-Mouton constant of all except the n-alkenes was measured by the photometric method at $\lambda = 633$ nm. Also the ocular method at $\lambda = 546$ nm was used for all except the aminoalkanes. The n-alcohols and n-alkenes available which are liquid at room temperature are methanol to undecanol (melting point $11^\circ C$) and hexene (boiling point $63^\circ C$) to octadecene (mp $16^\circ C$) respectively. Samples used were obtained from Fluka, Aldrich, Hopkins and Williams, and Koch-Light Ltd. The alcohols had stated purities in excess of 99% except nonanol (96%) and undecanol (98%), the alkenes had purities in excess of 95% except octadecene (90%), and the aminoalkanes had purities in excess of 99% except n-octylamine (96%). All samples were filtered as described



in 4.5; PTFE filters had to be used for the lower alcohols (up to hexanol) and the aminoalkanes, since these dissolve the standard Millipore filters.

Appropriate refractive index and density data was mainly obtained from the literature⁷⁴, and n_D for each liquid calculated using equation (2.9).

Figure 5.8 shows n_D measured at $\lambda = 546$ nm as a function of the number of backbone atoms (C or O), for the liquid n-alcohols, n-alkenes and n-alkanes. The n-alkane results were analysed in the previous section and are illustrated here for comparison purposes. The relation between the curves is interesting. The tendency towards linearity for high n_D as predicted by basic bond polarizability additivity theory (BPA) is not observed for any of the series.

The C=C end group of the n-alkenes contains a σ and a π bond. Since for a π bond the directions of maximum optical polarizability and ~~maximum~~ (negative) susceptibility are at right angles, the shorter chain alkenes ($n_A < 9$) have a positive value of n_D . Because the π bond is much more anisotropic than a C-C σ bond it is not until nonene, where the end group is well diluted, that the anisotropy of the saturated chain becomes dominant. As BPA would predict, n_D of an n-alkene is greater than that of an equivalent alkane by a constant amount within experimental error, giving an effective n_D value of $(1.22 \pm 0.05) \times 10^{-27} \text{ m}^5 \text{ A}^{-2} \text{ mol}^{-1}$ for $-\text{CH}_2$ replacing $-\text{CH}_3$ on the end of an alkane chain. However, n_D of the n-alcohols varies from being $0.2 \times 10^{-27} \text{ m}^5 \text{ A}^{-2} \text{ mol}^{-1}$ greater than the equivalent alkane for butanol to nearly 0.5×10^{-27} less for undecanol.

Figure 5.9 shows n_D measured at $\lambda = 633$ nm as a function of the number of backbone atoms for the liquid n-alkanes and n-alcohols. Also included for interest are water, ethan-1,2-diol (ethylene glycol) plus some linear monoaminoalkanes. These results are of much greater accuracy than those displayed in Figure 5.8 yet one can see that the difference in n_D between the n-alcohols and alkanes is very similar to that described above. Note that water seems to fit quite neatly on the graph for the n-alcohols, and that the substitution of an OH group at each end of an alkane molecule such as ethylene glycol seems to have twice the effect on n_D as substituting only one. The molar



Figure 5.3 The Molar Cotton-Mouton constant vs. the number of backbone atoms for n-alkanes, n-alcohols and n-alkenes measured at $\lambda = 546 \text{ nm}$

- n-alkanes
- n-alcohols
- + n-alkenes

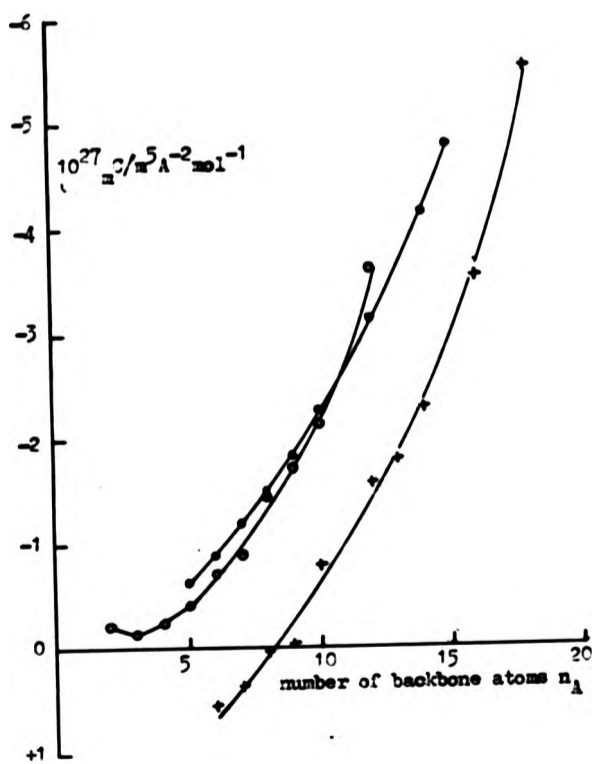
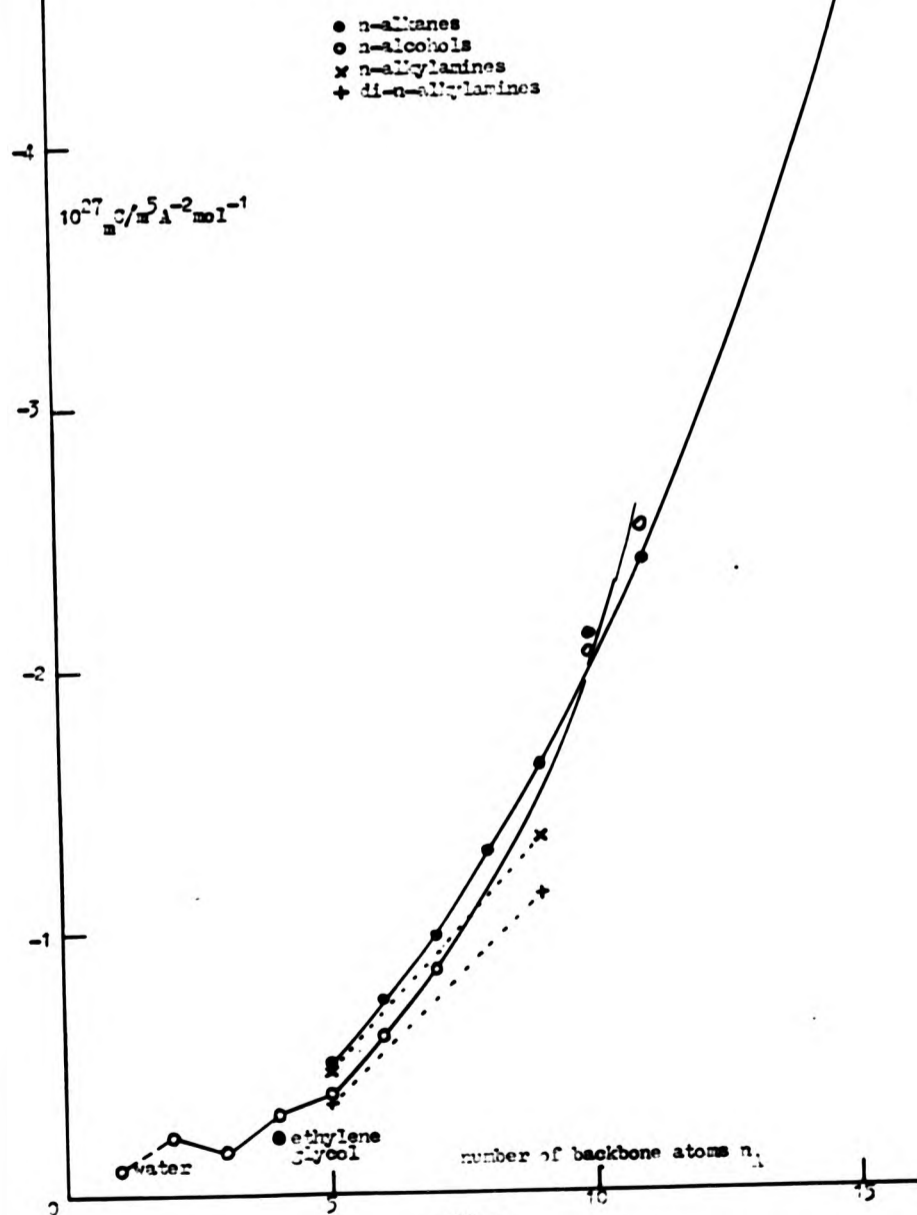


Figure 5.9 The molar Cotton-Kouton constant ϵ_m vs. the number of backbone atoms n , for n-alkanes, n-alcohols and related compounds, and monoaminoalkanes measured at $\lambda = 633 \text{ nm}$



Cotton-Mouton constants of the aminoalkanes follow a similar trend to the n-alkanes with an apparent slightly lower dependence on n_A . Putting the N in the middle of the chain (di-n-alkylamines) seems to raise μ_C by a small constant amount. This is not certain because only two of each species were measured.

Figures 5.10 and 5.11 show μ_C/n_A plotted versus n_A for the liquids measured at $\lambda = 546$ and 633 nm respectively. Figure 5.10 shows how the effect of the $-\text{CH}_2$ end group in the n-alkanes is diminished as it is diluted by increasing the saturated chain length. Figure 5.11 shows that μ_C/n_A is lowered slightly by moving an amine group from the end to the middle of an alkane chain. This is possibly due to a change in molecular conformation or it could be because with the amine group at the end there is one C-N bond whereas there are two when it is situated in the middle of the chain.

The more accurate n-alkane results (at $\lambda = 633$ nm) give $\mu_C/n_A = K_0 n_A$ where K_0 is a constant, as discussed in the previous section. For the n-alcohols, $\mu_C/n_A = K_1(n_A + K_2)$ for $n_A = 5$ to 11, where K_1 and K_2 are constants. The erratic behaviour of the graph at $n_A < 5$ is predicted by BPA theory²⁰. The observation that for $n_A < 10$, μ_C for an n-alcohol is somewhat less than the equivalent alkane value would be explained conventionally (using the BPA theory) by saying that Γ_{CO} is lower than Γ_{CC} ¹⁵⁴. (Γ_{CC} equals the previously defined Γ_O , Γ_{CO} is its analogue for a C-O bond). From depolarized light scattering measurements of polyoxyethylene oligomers, Patterson and Flory¹⁵⁵ deduced that $\Delta\alpha_{CO}$ was about 0.6 $\Delta\alpha_{CC}$. Therefore one would expect μ_C/n_A to be lower for the n-alcohols than the n-alkanes, but the difference should decrease steadily with increasing n_A as the OH group is progressively diluted by the CH_2 groups. Figures 5.10 and 5.11 show that whilst $\mu_C/n_A \propto (n_A + \text{constant})$ for both alkanes and alcohols above $n_A = 5$, the constant of proportionality is greater for the n-alcohols so that for $n_A > 10$, μ_C is greater for alcohols. This is worthy of further examination.

The average conformation of n-alkanes will be slightly different to that of n-alcohols of the same chain length and under the same conditions. However, since the OH group is at the end of the chain it will not have much effect on the conformation and any perturbation should become unimportant at high n_A . Likewise, additional

Figure 5.10 The molar Cotton-Kouton constant per backbone atom $\frac{3/n_1}$ vs. the number of backbone atoms n_1 for n-alkanes, n-alcohols, n-alkenes measured at $\lambda = 210 \text{ nm}$

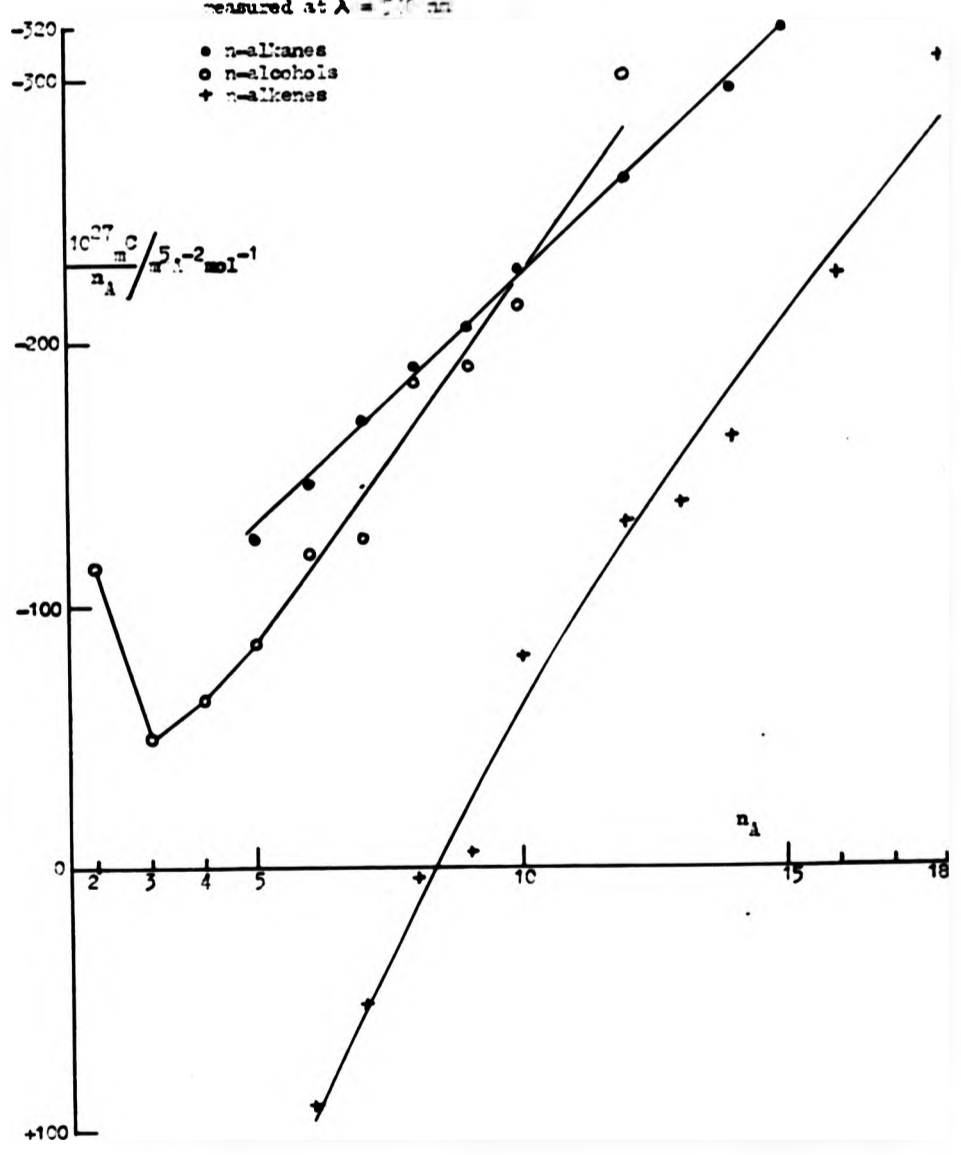
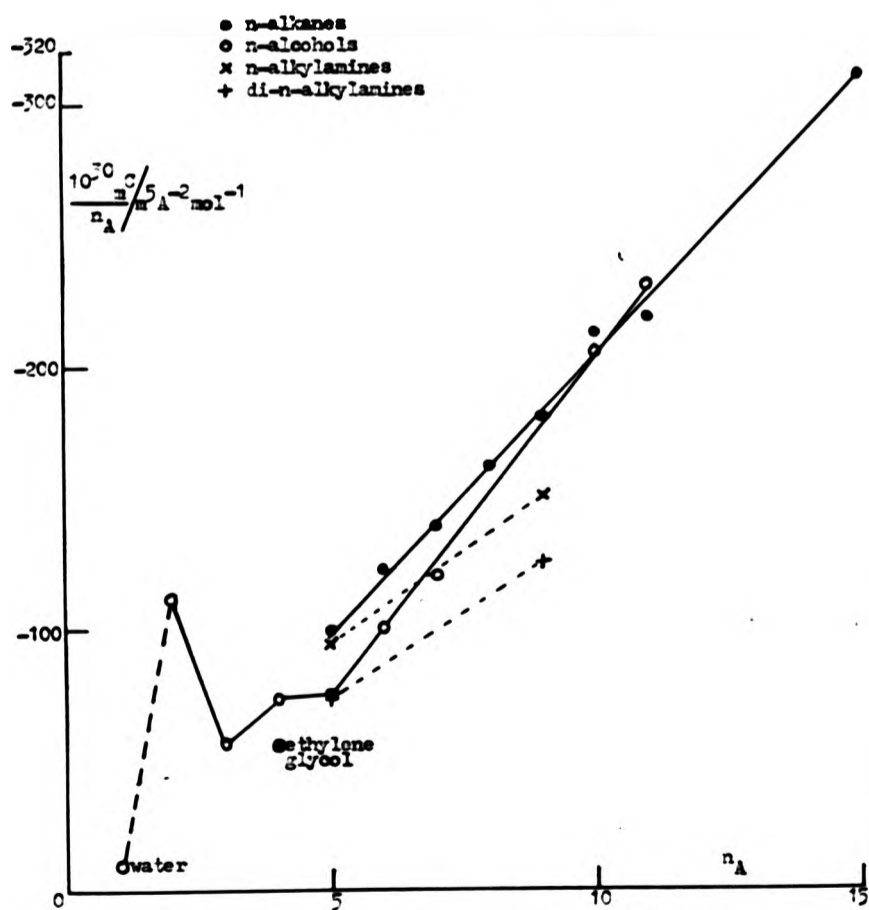


Figure 5.11 The molar Cotton-Kiuton constant per backbone atom $\frac{[\theta]_D}{n_A}$ vs. the number of backbone atoms n_A for n-alkanes, n-alcohols and related compounds, and monoaminoalkanes measured at $\lambda = 633$ nm



contributions from hyperpolarizability, collision-induced and shaped cavity effects because of the OH group should be insignificant at high n_A . Hydrogen bonding may cause the molecular orientational correlation parameter, S_2 , to be significantly different in the alcohols. This could explain the difference in gradient between the alkane and alcohol graphs but cannot account alone for the observed crossing at $n_A = 10$.

Champion, Dandridge and Maeten²⁰ determined $\langle \gamma^2 \rangle$ for the liquid n-alkanes and alcohols by depolarized light scattering. They separated $\langle \gamma^2 \rangle$ into low frequency $\langle \gamma^2 \rangle_l$ and high frequency $\langle \gamma^2 \rangle_h$ contributions and plotted $\langle \gamma^2 \rangle_l / n_B$ and $\langle \gamma^2 \rangle_h / n_B$ versus n_B for both species. They state that with the exception of methanol, alcohol and alkane $\langle \gamma^2 \rangle$ data lie on the same straight line, within their typical $\pm 5\%$ error. However, more detailed analysis shows that in fact the gradients are distinctly different for the different species, with $\langle \gamma^2 \rangle_h / n_B$ and $\langle \gamma^2 \rangle_l / n_B$ increasing more with n_B for the n-alcohols and overtaking the equivalent alkane value at n_B between 7 and 9 (i.e. n_A between 8 and 10). This agrees very well with the trends in $\frac{C}{n_A}$, where $\frac{C}{n_A}$ was greater for the n-alcohols over $n_A = 10$. Hence the effect is probably not magnetic in origin and even if the optical local field correction factor had been $[(n^2+2)/3]^4$ the difference remains.

Both depolarized Rayleigh scattering intensities¹⁴¹ and the magnetic birefringence¹⁰⁶ of n-alkane liquids decrease more with increasing temperature near the melting point than expected from elementary orientational theory, i.e. they deviate from a $(kT)^{-1}$ dependence. It has been postulated that this is due to Frenkel's heterophase fluctuations¹⁴¹ whereby tiny short-lived crystallites are progressively formed in the liquid as the freezing point is closely approached. Since n-alcohols have much higher melting points and viscosities one would expect such an effect to be greater than in the equivalent alkanes but it would not explain the observed crossing at $n_A = 10$. Using accepted theories, this behaviour can only be explained by a combination of two effects - one proportional to n^2 and which determines the gradient of $\frac{C}{n_A}$ versus n_A , the other proportional to n and thus determining the intercept. As outlined earlier, the origin of the first effect is highly debatable. It has been shown²⁰ that $\langle \gamma^2 \rangle_l / n_B$ is slightly higher for the higher n-alcohols than the equivalent n-alkanes. If there is a corresponding collision-induced contribution

to μ_C this would lead to a vertical shift in the graph and explain the second effect.

5.4.3 Branched Chain Alkane Liquids

The branched chain alkane molecules considered here consist, with one exception (3-ethylheptane), of n-alkanes where one or more of the hydrogen atoms has been substituted by a methyl group (CH_3). Since these additions to an alkane chain change its shape and conformation, an examination of how the molar Cotton-Mouton constant, μ_C , varies with the extent of branching, methyl group position and the length of chain might lead to a greater insight into the factors determining μ_C .

The Cotton-Mouton constants of most of the liquid branched chain alkanes available at reasonable prices were measured by the photometric method at $\lambda = 633 \text{ nm}$. Samples used were obtained from Aldrich, Koch-Light and Fluka Ltd. The majority had stated purities in excess of 99% and were filtered carefully before use as described in 4.5. Because a good proportion of the samples were expensive (≈ 10 per 5g), a stainless steel sleeve was inserted in the sample cell to reduce its effective volume as described in 4.6.4. If the liquid was carefully filtered then only about 3 to 4 cm^3 of liquid was required, the only penalty being that the amount of light entering the cell was reduced by the sleeve.

The Cotton-Mouton constants of 31 branched chain alkanes were measured, probably for the first time since they are rather small and no literature values could be found. μ_C for each liquid was calculated using equation (2.9). Where possible, appropriate refractive index and density data was obtained from the literature^{73-4,156}, otherwise the Paar digital density meter and Abbé refractometer were employed.

Table 5.4 shows the bulk and molar Cotton-Mouton constants of the lightly branched monomethylalkanes measured and Table 5.5 shows the results obtained for the medium and heavily branched alkanes.

Lightly branched chain alkanes

Figure 5.12 gives the molar Cotton-Mouton constant plotted versus methyl group position for four series of monomethylalkanes including 1-methyl alkanes (i.e. the n-alkane isomer). The first observation

Table 5.4 Bulk and molar cotton-Mouton constants of monomethylalkanes at $(20 \pm 1)^\circ\text{C}$ and $\lambda = 633 \text{ nm}$

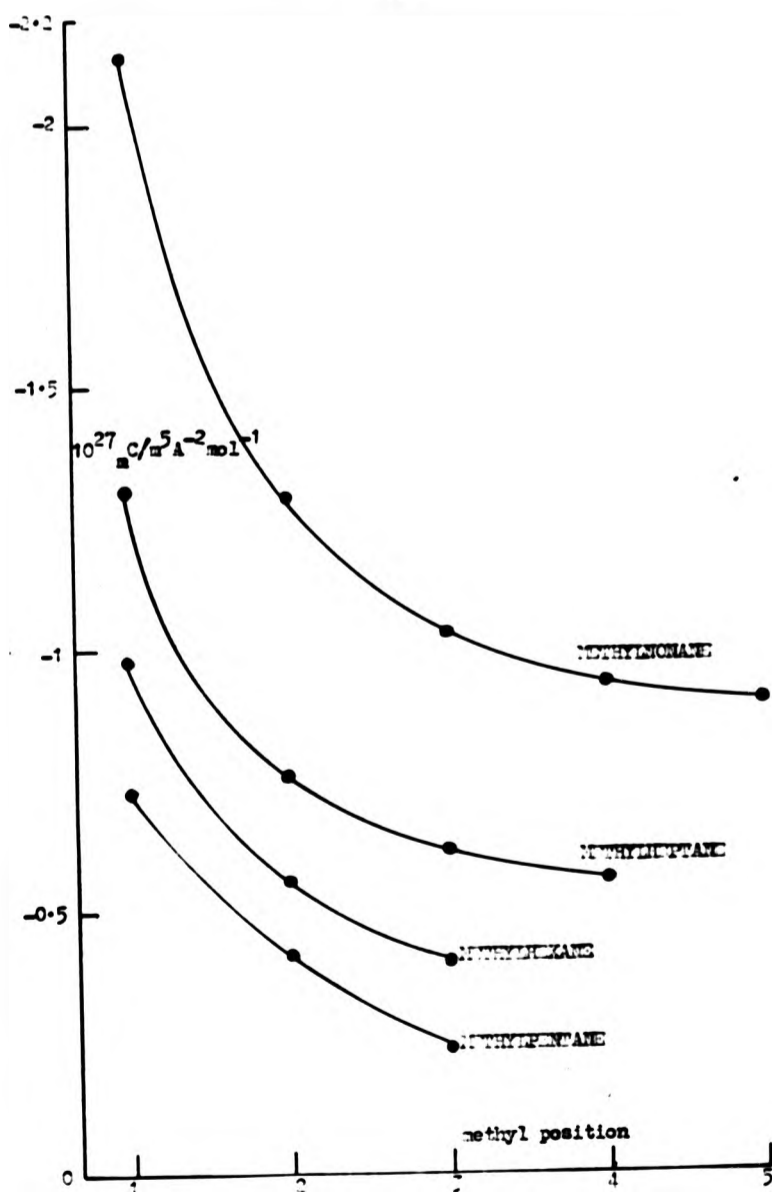
Number	Liquid	$10^6 \frac{C}{T^{-2} \text{ m}^{-1}}$	$10^{27} \frac{\text{m}^3 \text{ C}}{\text{m}^5 \text{ A}^{-2} \text{ mol}^{-1}}$
5	2-methylbutane	-30	-0.21
6	2-methylpentane	-52	-0.42
7	2-methylhexane	-63	-0.56
8	2-methylheptane	-78	-0.76
9	2-methylnonane	-112	-1.29
10	3-methylpentane	-31	-0.24
11	3-methylhexane	-46	-0.40
12	3-methylheptane	-64	-0.62
13	3-methylnonane	-90	-1.03
14	4-methylheptane	-58	-0.56
15	4-methylnonane	-82	-0.94
16	5-methylnonane	-79	-0.90

Note: results accurate to last figure (both tables)

Table 5.5 Bulk and molar Cotton-Mouton constants of medium and heavily branched alkanes at $(20 \pm 1)^\circ\text{C}$ and $\lambda = 633 \text{ nm}$

Number	Liquid	$10^6 \frac{C}{T^{-2} \text{ m}^{-1}}$	$10^{27} \frac{\text{m}^3 \text{ C}}{\text{m}^5 \text{ A}^{-2} \text{ mol}^{-1}}$
17	3-ethylheptane	-50	-0.52
26	2,2-dimethylbutane	-1	-0.01
27	2,2-dimethylpentane	-3	-0.03
28	2,2-dimethylhexane	-15	-0.15
29	2,2-dimethylheptane	-31	-0.33
18	2,3-dimethylbutane	-10	-0.08
19	2,3-dimethylpentane	-15	-0.13
20	2,4-dimethylpentane	-15	-0.13
21	2,4-dimethylhexane	-20	-0.19
22	2,5-dimethylhexane	-32	-0.31
23	2,6-dimethyloctane	-48	-0.55
30	3,3-dimethylpentane	-8	-0.03
31	2,2,3-trimethylbutane	-1	-0.01
32	2,2,4-trimethylpentane	-23	-0.23
24	2,3,4-trimethylpentane	+10	+0.09
33	2,2,5-trimethylhexane	+1	+0.01
25	2,6,10,14-tetramethylpentadecane	-60	-1.19
34	2,2,4,6,6-pentamethylheptane	-26	-0.34
35	2,2,4,4,6,8,8-heptamethylnonane	-29	-0.48

Figure 3.10 The molar Cotton-Deuton constant θ vs. methyl group position for methylalkanes measured at $\lambda = 500 \text{ nm}$





is that the methylalkanes have a much smaller value of $\bar{\mu}_C$ than the appropriate n-alkane isomer (typically 40-60%). The Bond Polarizability Additivity scheme, as discussed in previous sections, would go some way towards predicting this, since a chain would be less anisotropic when branched. Dipole-induced dipole interactions along the chain which enhance $\bar{\mu}_C$ will also be effectively reduced by the branch. Shaped-cavity effects will tend to increase $\bar{\mu}_C$ of the more globular branched alkanes as discussed in 5.4.1 but in this case they are probably marginal compared to the reduction in molecular anisotropy due to branching.

The most interesting feature of Figure 5.12 is the way $\bar{\mu}_C$ decreases as the methyl group is moved towards the centre of the chain. The Bond Polarizability Additivity theory predicts (see later) that $\langle \gamma_{MO}^2 \rangle$ is constant for any methyl group position (except the inappropriate 1-methyl) provided that the chain information remains the same.

Champion, Meeten and Tench¹⁵⁷⁻⁸ measured the flow birefringence of structural isomers of octanol, nonanol and decanol. These isomers, based on linear hydrocarbon chains with the OH group moved to different points on the chain, are analogous to the monomethylalkanes where the methyl group is replaced by an OH. The stress-optical coefficient, \bar{V} , (analogous to $\bar{\mu}_C$) of these alcohols was found to show a very similar dependence to the position of the substituted group as that shown in Figure 5.12 with \bar{V} decreasing as the OH group is shifted towards the middle of the chain. It was suggested that this trend was due to the differing molecular orientational correlations of the isomers. However, theoretical calculations of \bar{V} assumed bond polarizability additivity and an all-trans chain conformation. As discussed in 5.4.1, bond polarizability additivity is not valid for n-alkane liquids and conformation changes of the isomers must be considered.

An all-trans model is completely unrealistic since a study of molecular models indicates that the bonds on either side of the branch point are energetically much more likely to be in a gauche than the trans configuration i.e. ΔU_{tg} is negative. Thus the nearer the branch is to the centre of the molecule, the more crumpled and less anisotropic the molecule should be, as observed experimentally. Flory¹²⁶ showed that the optical anisotropy of n-alkane chains could be



regarded as the sum of the anisotropies of trans sequences. If so, since it has been shown (at least for $n_A > 4$) that ${}_m C \propto n_A^2$ for a linear chain, then a gauche configuration at the branch point will result in a lowering of the optical anisotropy the nearer the branch is to the middle. Then ${}_m C$ of a linear chain should be approximately double that with a methyl group in the middle (providing ${}_m C \propto n_A^2$ even for short chains) since the latter is effectively two half chains. Figure 5.12 shows this to be true and a segment theory for calculating ${}_m C$ will be discussed later in this section.

Figure 5.13 shows the molar Cotton-Mouton constant of some lightly and medium branched alkane series plotted versus n_A . These follow the same type of trend as the n-alkanes, which is also shown on the graph. The effect of moving the methyl group along the chain is illustrated as discussed above.

Medium and heavily branched chain alkanes

Also shown in Figure 5.13 is the effect of having two methyl groups on a chain. These reduce the molecular anisotropy further but if they are attached to the same carbon atom in the skeletal chain, as in 2,2-dimethylalkanes, $|{}_m C|$ is reduced further than if the methyl groups are bonded to separate parts of the chain as in 2, n_B -dimethylalkanes. If molecular orientational correlations were important one might predict the opposite since the former species leave a larger proportion of the chain unperturbed and so should lead to less steric restraint and a greater degree of correlation between molecules.

Partly because of the tendency to form gauche configurations at branch points, end-to-end distances vary less with molecular weight for branched than linear chain molecules¹⁵⁹. Therefore the shape of the molecule will vary less with molecular weight and any effects on ${}_m C$ due to molecular-shaped cavity field corrections will be lessened. Figure 5.14 possibly reflects this in that whilst ${}_m C = K_3(n_A + K_4)$ where K_3 and K_4 are constants, even for light and medium branched alkanes, the constant of proportionality, K_3 , is significantly smaller for the branched species.

Depolarized light scattering results show that the molecular optical anisotropy $\langle \gamma^2 \rangle$ is also sensitive to branching for alkane liquids¹⁶⁰. Rowell and Stein's interactive bond polarizability additivity model¹²²

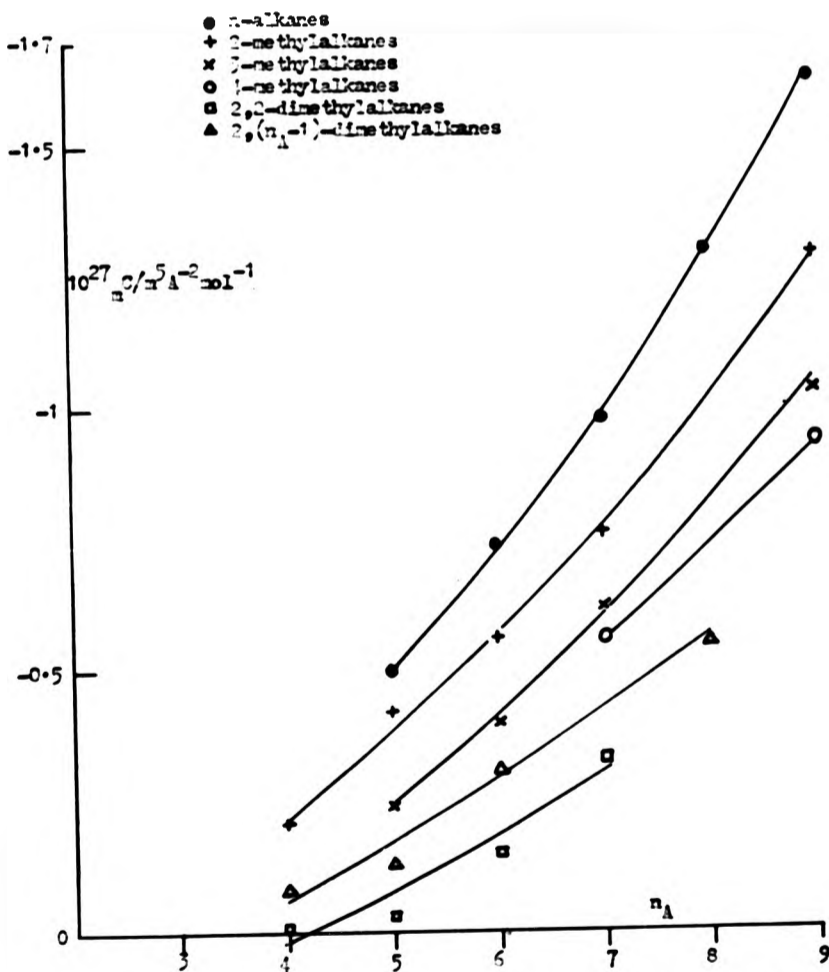
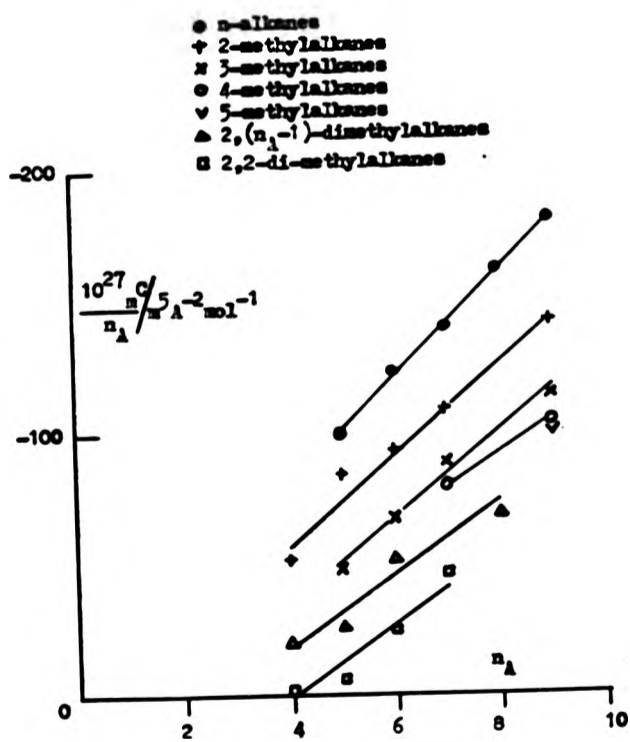


Figure 5.13 The molar Cotton-Kubon constant C vs. the number of backbone atoms n_A for lightly and medium branched alkanes measured at $\lambda = 633 \text{ nm}$



Figure 5.14 The molar Cotton-Kretschmann constant per backbone atom $\frac{c}{n_A}$ vs. the number of backbone atoms n_A for some lightly and medium branched alkanes measured at $\lambda = 633$ nm



has been used in an effort to predict $\langle \gamma^2 \rangle$ for some lowmolecular weight branched alkanes¹⁶¹. Agreement between theory and experiment was particularly poor for the heavily branched alkanes. This could partly be because the theory considers only dipole-induced dipole interactions between bonds, neglecting interactions between close non-bonded atoms¹⁵⁰. Table 5.5 shows that a couple of the heavily branched alkanes have positive molar Cotton-Mouton constants (2,3,4-trimethylpentane and 2,2,5-trimethylhexane). This is surprising since positive values of μ_C are normally associated with delocalized electrons yet the valence electrons in alkanes are usually considered as being localized in C-C σ -bonds. However, a stable delocalized state has been predicted in 2,2-dimethylpropane¹⁶² and this could also be the case for some other branched alkanes with possibly an excited state molecular orbital extending over the whole of a molecule.

Graph theoretical method to derive the effective μ_C of substructures within a molecule

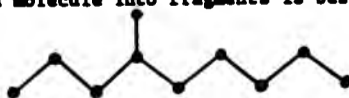
Since bond polarizability additivity does not appear to be valid for normal or branched alkane molecules in the pure liquid state, a graph theoretical method is used here to determine a scheme of segment additivity. In graph theoretical approaches¹⁶³, substructures of a molecule are considered and one searches for the numerical values of these fragments which give acceptable results for the property under investigation of the molecule as a whole.

Many schemes were tried. The following, scheme A, was the most successful of realistic schemes involving unbranched fragments and used a minimum number of adjustable parameters. It is based on the carbon atoms only and is such that any carbon atom belongs to one fragment only.

Each fragment is unbranched and labelled according to its number of carbon atoms so for example, pentane $\equiv e$ (5 carbon atoms) and octane $\equiv h$ (8 carbon atoms).

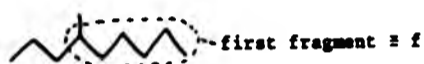
The method of breaking a molecule into fragments is best illustrated by example:

4-methylnonane \equiv

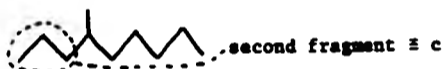


Consider the longest unbranched section of the molecule first. This

first fragment contains up to and including the carbon atom at the branch like so:



It includes 6 carbon atoms so is labelled f . Next consider the second largest unbranched segment:



It continues up to the branch but does not include the carbon atom at the branch since this has already been included in the first fragment.

Lastly consider the remaining segment:



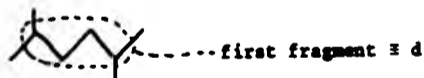
It contains only one carbon atom so is labelled a .

Now all the carbon atoms have been accounted for, so



Next consider 2,5-dimethylhexane,

The longest unbranched segment is now in the middle of the molecule and terminates at two branch points. It contains 4 carbon atoms so is labelled d .



All that remain are 4 unlinked carbon atoms



So 2,5-dimethylhexane, $= d + 4a$.

This process was executed for a total of 35 branched and linear (pentane to octane) chain alkanes. In order to predict the eight adjustable parameters (a to h) least squares calculations were made using a microcomputer, which also gave the rms error.

Initially two sets of calculations were made, the first set (scheme A1) using the light and medium branched alkane data (numbers 5 to 25) in Tables 5.4 and 5.5) and the second set (scheme A2) using all branched chain alkane data (numbers 5 to 35). The heavily branched alkanes (numbers 26 to 35) included in the second set were defined as those having more than one methyl group on any one carbon atom in the chain. Table 5.6 shows the values of the fragments (a to h) for schemes A1 and A2. Table 5.7 shows the calculated theoretical molar Cotton-Mouton constants using these values for the 35 alkanes.

Also included in Table 5.7 is the difference between theoretical and experimental values, or the "error" in μ_C for each alkane. As can be seen, scheme A1 predicts μ_C for the n-alkanes from pentane to octane (nos. 1 to 4) to within a very small error ($<0.03 \times 10^{-27} \text{ m}^5 \text{ A}^{-2} \text{ mol}^{-1}$) and all but one of the light and medium branched alkanes to within $0.08 \times 10^{-27} \text{ m}^5 \text{ A}^{-2} \text{ mol}^{-1}$ with an rms error average for the scheme of $\sim 0.04 \times 10^{-27}$, typically 5%. Scheme A2 includes the highly branched alkanes and predictions are generally more erroneous with an average error of $\sim 0.14 \times 10^{-27}$. Therefore, while the scheme works very well for the light and medium branched alkanes, its predictions are very poor for heavily branched alkanes. This indicates the possibility of molecular anisotropies being affected by interactions between close non-bonded atoms, which has been cited as one of the reasons for the breakdown of the bond polarizability additivity scheme¹⁵⁰⁻².

In an attempt to predict μ_C for the heavily branched alkanes the scheme was modified. In scheme B, one starts with a new fragment, x, which includes a dimethyl group. So for example:

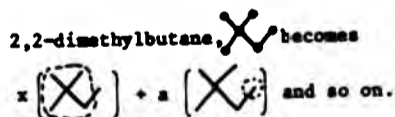


Table 5.6 gives the value of x as very close to zero which is probably due to the near-isotropic nature of the fragment. Since the light and medium branched alkanes do not include x, their values predicted by scheme B are very similar to those predicted by scheme A1 as listed in Table 5.7. Table 5.8 gives the molar Cotton-Mouton constants predicted by scheme B for the heavily branched alkanes. One can readily see that excepting three alkanes (nos. 32, 34, 35) the difference

Table 5.6 Calculated molar Cotton-Mouton constants of alkane substructures from graph-theoretical analysis of light and medium branched alkanes (numbers 5-25, Tables 5.4, 5.5) and all branched alkanes (numbers 5-35).

Substructure	Fragment	$10^{27} \frac{C \text{ theory}}{m^5} \text{ A}^{-2} \text{ mol}^{-1}$	
		Scheme A1 (Nos. 5-25)	Scheme A2 (Nos. 5-35)
•	a	+0.007	+0.013
/	b	-0.028	-0.068
∩	c	-0.195	-0.227
∩∩	d	-0.365	-0.327
∩∩∩	e	-0.535	-0.492
∩∩∩∩	f	-0.763	-0.627
∩∩∩∩∩	g	-1.009	-0.975
∩∩∩∩∩∩	h	-1.304	-1.314
		Scheme B (Nos 5-35) is scheme A1 with minor adjustments plus:	
X	x	+0.002	
		Scheme C (Nos 5-35) is scheme B plus:	
X∩	y	-0.26	

Table 5.7 Calculated theoretical molar Cotton-Mouton constants of linear and branched chain alkanes using results from graph theoretical analysis as shown in Table 5.6 (schemes A1 and A2)























Number (see Tables 5.4 & 5.5)	Structure	Fragments	$10^{27} \text{ } m^C \text{ theory} / \text{m}^5 \text{ } A^{-2} \text{ mol}^{-1}$	
			($ m^C_{\text{theory}} - m^C_{\text{expt}} $ in brackets) SCHEME A1	SCHEME A2
1		e	-0.53(0.03)	-0.49(0.01)
2		f	-0.76(0.02)	-0.63(0.11)
3		g	-1.01(0.03)	-0.98(0)
4		h	-1.30(0)	-1.31(0.01)
5		c + 2a	-0.17(0.04)	-0.20(0.01)
6		d + 2a	-0.35(0.07)	-0.30(0.12)
7		e + 2a	-0.52(0.04)	-0.47(0.09)
8		f + 2a	-0.75(0.01)	-0.60(0.16)
9		h + 2a	-1.29(0)	-1.29(0)
10		c + b + a	-0.22(0.02)	-0.27(0.03)
11		d + b + a	-0.39(0.01)	-0.38(0.02)
12		e + b + a	-0.56(0.06)	-0.55(0.07)
13		g + b + a	-1.03(0)	-1.03(0)
14		d + c + a	-0.56(0)	-0.54(0.02)
15		f + c + a	-0.95(0.01)	-0.84(0.10)
16		e + d + a	-0.90(0)	-0.81(0.09)
17		e + 2b	-0.59(0.07)	-0.63(0.11)
18		b + 4a	0 (0.08)	-0.02(0.06)
19		c + b + 2a	-0.21(0.08)	-0.27(0.14)
20		c + 4a	-0.16(0.03)	-0.17(0.04)
21		c + b + 3a	-0.20(0.01)	-0.25(0.06)
22		d + 4a	-0.34(0.03)	-0.28(0.03)

Table 5.7 continued













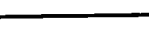
Number (see Tables 5.4 & 5.5)	Structure	Fragments	$10^{27} \mu\text{C theory}/\text{m}^5 \text{A}^{-2} \text{mol}^{-1}$	
			$(\mu\text{C}_{\text{theory}} - \mu\text{C}_{\text{expt}} $ in brackets) SCHEME A1	SCHEME A2
23		e + b + 3a	-0.55(0)	-0.52(0.03)
24		2b + 4a	-0.02(0.11)	-0.08(0.17)
25		e + 2d + 6a	-1.22(0.03)	-1.07(0.12)
26		c + 3a	-	-0.19(0.18)
27		d + 3a	-	-0.29(0.26)
28		e + 3a	-	-0.46(0.31)
29		f + 3a	-	-0.59(0.26)
30		c + b + 2a	-	-0.27(0.24)
31		b + 5a	-	0 (0.01)
32		c + 5a	-	-0.16(0.07)
33		d + 5a	-	-0.26(0.27)
34		c + b + 7a	-	-0.20(0.14)
35		c + 2b + 9a	-	-0.25(0.23)

Table 5.8 Calculated theoretical molar Cotton-Mouton constants of heavily branched chain alkanes from graph theoretical analysis (as shown in Table 5.6) by three schemes - Schemes A2, B and C

Number	Structure	Fragments		
		SCHEME A2	SCHEME B	SCHEME C
26		$c + 3a$	$x + a$	as Scheme B
27		$d + 3a$	$x + b$	"
28		$e + 3a$	$x + c$	"
29		$f + 3a$	$x + d$	"
30		$c + b + 2a$	$x + 2a$	"
31		$b + 5a$	$x + 2a$	"
32		$c + 5a$	$x + b + a$	y
33		$d + 5a$	$x + b + 2a$	as Scheme B
34		$c + b + 7a$	$2x + b$	$y + b + a$
35		$c + 2b + 9a$	$2x + c + 4a$	$y + x + c$

Number	$10^{27} \frac{m^3}{A^2} \text{mol}^{-1} (m^3 C_{\text{theory}} - m^3 C_{\text{expt}} \text{ in brackets})$		
	SCHEME A2	SCHEME B	SCHEME C
26	-0.19(0.18)	+0.01(0.02)	As Scheme B
27	-0.29(0.26)	-0.03(0)	"
28	-0.46(0.31)	-0.18(0.03)	"
29	-0.59(0.26)	-0.36(0.04)	"
30	-0.27(0.24)	+0.01(0.04)	"
31	0 (0.01)	+0.01(0.02)	"
32	-0.16(0.07)	-0.02(0.21)	-0.26(0.03)
33	-0.26(0.27)	-0.01(0.02)	As Scheme B
34	-0.20(0.14)	-0.02(0.32)	-0.30(0.04)
35	-0.25(0.23)	-0.16(0.32)	-0.45(0.03)

between theoretical and experimental values of μ_C has been reduced to a very low level ($\leq 0.04 \times 10^{-27}$).

The three alkanes still showing a large error uniquely contain the group XX . Therefore it is a natural progression to scheme C whereby one starts with this near fragment, y . So for example:

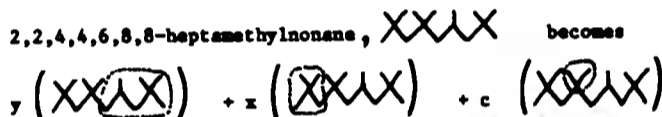


Table 5.6 gives the value of y as $-0.26 \times 10^{-27} \text{ m}^3 \text{ A}^{-2} \text{ mol}^{-1}$. Using this, scheme C reduces the error for all heavily branched alkanes to $\leq 0.04 \times 10^{-27}$ as shown in Table 5.8. In the empirical schemes discussed above it should be stressed that in all cases the number of adjustable parameters is considerably less than the number of molecules for which accurate μ_C values can be predicted. For example, scheme C predicts μ_C accurately for at least 35 liquids using only 10 adjustable parameters.

Thus it has been shown that the molar Cotton-Mouton constant of alkane liquids can be predicted by summing appropriate substructural values although more complex substructural units must be considered for heavily branched alkanes. This implies that molecular-shaped cavity field effects and molecular orientational correlations are not very important in determining molar Cotton-Mouton constants of alkane liquids since it appears that μ_C is mainly dependent on the constituents of the molecules and not on molecular shape. However, it may be that in some way effects such as cavity shape are taken into account in the empirical scheme.

5.4.4 Liquids of Tetra-alkyl and Tetra-alkoxy Compounds

The examination of the molar Cotton-Mouton constants of tetra-alkyl and tetra-alkoxy compounds was an extension of the work on the branched chain alkanes of the previous section. The compounds studied consisted of molecules with a tetravalent central atom namely carbon, silicon, tin and titanium. Tetrahedrally attached to the central atom are four linear (excepting one sample) alkane or alkoxy chains of equal length. Their general formula is $\text{M}(\text{Me}_n)_4$ and $\text{M}(\text{OMe}_{n-1})_4$ respectively where M is the central metal or semi-metal atom and Me is a CH_3 or CH_2 methyl group.

The Cotton-Mouton constants, C, of 13 tetra-alkyl and tetra-alkoxy compounds were measured by the photometric method at $\lambda = 633$ nm. To the author's knowledge this is the first time C has been measured for these compounds. These 13 were virtually all such compounds commercially available at reasonable prices, and were obtained from Aldrich, Koch Light and Fluka Ltd. All had stated purities in excess of 95%; the majority were greater than 97% pure.

The compounds measured could be categorized according to their physical states as follows:

(a) High molecular weight compounds

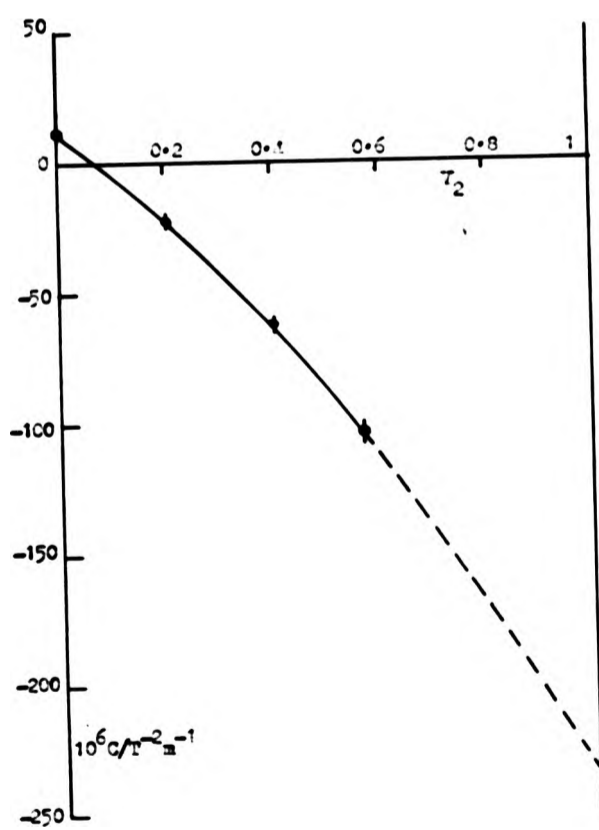
These, namely tetraoctyltin and tetradodecyltin were of sufficiently high molecular weight to be virtually solid at room temperature. Hence magnetic birefringence measurements were made with them in solution with a suitable "isotropic" (see 5.4.2) solvent, tetramethyltin.

Four different strength solutions were made up for each compound, the volume fraction V_2 of the solute varying from 0 to 0.6. C was measured for each volume fraction and an extrapolation made to $V_2 = 1$ to obtain an estimate of the pure liquid value. The results and extrapolation for tetradodecyltin are shown in Figure 5.15. The extrapolation seems reasonable as C is a bulk quantity but obviously there is a fairly large error in extrapolating to this extent. A similar, virtually linear, dependence of C on V_2 was noted for tetraoctyltin in tetramethyltin except that the measurements were less accurate due to tetraoctyltin strangely being less soluble than tetradodecyltin.

(b) Tetraalkoxytitanium compounds

Three compounds of this type were obtained of low molecular weight ($n_A = 3$ to 5). They were of relatively low purity and consequently had a yellowish tint. Because of their polymeric nature¹⁶⁴, unlike other tetraalkyl or tetraalkoxy compounds in this molecular weight range, they were very viscous. They also reacted slowly with the water vapour in the air to form insoluble solid crystals, presumably of titanium oxide. Because of this, filtering had to be done quickly necessitating the use of relatively large pore size (0.22 μ m) Millipore filters.

Figure 5.15 The bulk Cotton-Mouton constant C vs. volume fraction T_2 of tetradodecyltin in solution with tetramethyltin



(c) Low molecular weight simple liquids

These remaining compounds were of sufficiently low molecular weight to be completely liquid at room temperature. They formed the bulk of this section being 8 out of the 3 studied here. Only one of the 8, tetraisopropylmethane, did not consist of linear chains. 3 had n-alkoxy and 4, n-alkyl chains with central atoms being carbon, silicon or tin. All were carefully filtered before use as previously described.

The molar Cotton-Mouton constant for each compound was calculated using equation (2.9) and appropriate literature⁷³⁻⁴ or measured values of refractive index and densities. Table 5.9 shows the bulk and molar Cotton-Mouton constants of all these compounds.

Figure 5.16 shows the molar Cotton-Mouton constant per skeletal atom (i.e. neglecting hydrogen atoms), $\frac{C}{n_D}$ plotted versus the number of backbone atoms in each of the four arms, n_A . A line has been drawn through the points, neglecting for now the tetraalkoxytitanium compounds.

Firstly it may be seen that the values for tetraethoxy-methane and silane are very similar showing that the central atom probably has little effect on the value of $\frac{C}{n_D}$. Secondly, values of tetraethylsilane and its alkoxy equivalent, tetramethoxysilane, differ significantly but not substantially. This can be explained by conformational differences since there is a different trans-gauche potential energy barrier for a C-C to a C-O bond. Also the oxygen atoms themselves may contribute differently to $\frac{C}{n_D}$.

The line drawn in Figure 5.16 is a reasonable fit to the data with the exception of tetra-n-pentoxysilane at $n_A = 6$. The reason for this discrepancy is not known, it could be a contaminated sample.

Figure 5.16 shows that for $n_A > 4$, $\frac{C}{n_D} \propto n_A$. The graph bears a striking resemblance to Figure 5.11 which displayed similarly the n-alkane and n-alcohol data. Even the discontinuities at $n_A < 5$ are similar, but more interestingly the graphs have an almost identical gradient. The bond polarizability additivity theory predicts that for the non-polymeric compounds studied in this section their magneto-optical anisotropy will be zero if the chains are in the fully extended all-trans conformation, i.e. the effect of each chain would effectively be cancelled by the others. As discussed in 5.4.1 these chains will

Table 5.9 Bulk and molar Cotton-Mouton constants of tetraalkyl and tetraalkoxy compounds at $(20 \pm 1)^\circ\text{C}$ and $\lambda = 633 \text{ nm}$

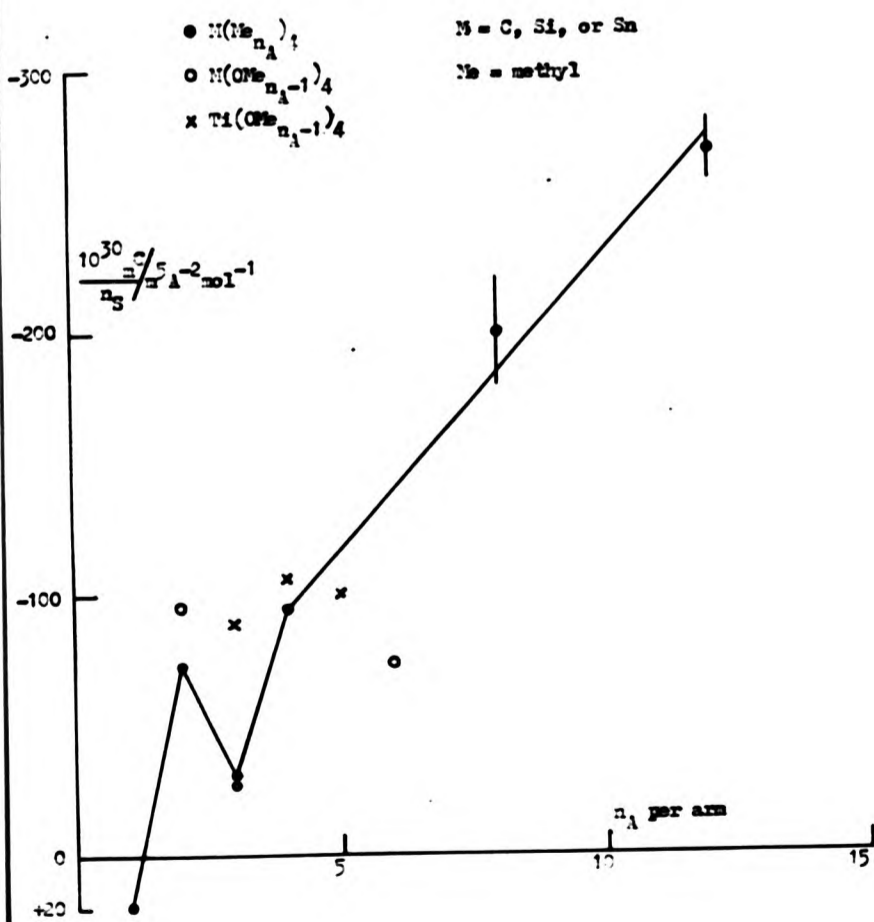
Compound	Formula	Measured state	$10^6 C/T^{-2} \text{ m}^{-1}$	$10^{27} \frac{C}{\text{m}^5 \text{ A}^{-2} \text{ mol}^{-1}}$
Tetramethyltin	$\text{Sn}(\text{Me})_4$	Liquid	$+11.9 \pm 0.7$	$+0.095 \pm 0.006$
Tetraethylsilane	$\text{Si}(\text{Me}_2)_4$	Liquid	-60	-0.66
Tetramethoxysilane	$\text{Si}(\text{OMe})_4$	Liquid	-96	-0.86
Tetraethoxysilane	$\text{Si}(\text{OEt})_4$	Liquid	-27	-0.36
Tetraethoxymethane	$\text{C}(\text{OEt})_4$	Liquid	-33	-0.41
Tetraisopropylmethane	$\text{C}(\text{Me}(\text{Me})_2)_4$	Liquid	-48	-0.82
Tetra-n-butyltin	$\text{Sn}(\text{Me}_4)_4$	Liquid	-87	-1.61
Tetra-n-pentoxysilane	$\text{Si}(\text{OMe}_5)_4$	Liquid	-77	-1.84
Tetra-n-octyltin	$\text{Sn}(\text{Me}_8)_4$	*Solution	-180 ± 20	-6.4 ± 0.7
Tetra-n-dodecyltin	$\text{Sn}(\text{Me}_{12})_4$	*Solution	-233 ± 10	-13.2 ± 0.6
Tetraethoxytitanane	$\text{Ti}(\text{OEt})_4$	Viscous Liquid	-92 ± 14	-1.14 ± 0.05
Tetra-n-propoxytitanane	$\text{Ti}(\text{OMe}_3)_4$	Viscous Liquid	-118 ± 2	-1.80 ± 0.05
Tetra-n-butoxytitanane	$\text{Ti}(\text{OMe}_4)_4$	Viscous Liquid	-110 ± 2	-2.09 ± 0.05

Notes:

All results accurate to last figure unless stated.

* Neat liquid results extrapolated from solution measurements (see text)

Figure 5.16 The molar Cotton-Kubon constant per skeletal atom $\frac{[\alpha]_D}{n_A}$ vs. the number of backbone atoms, n_A , per arm for tetra-*n*-alkyl and tetra-*n*-alkoxy compounds





not generally be all trans so one would predict a non-zero value of $[\eta]_C$. However, bond polarizability additivity theory would still predict a great deal of cancellation to give much smaller molar Cotton-Mouton constants than those observed.

The similarity in the gradients of the graphs in Figures 5.16 and 5.11 shows that optically the arms of these compounds behave as separate chains. Reinforcing this view is that the points corresponding to the polymeric tetra-*n*-alkoxytitanium compounds also lie reasonably on the graph. Thus by far the most important factor determining $[\eta]_C$ is the molecular constituents, not the shape. This conclusion supports that reached in the previous section on branched chain alkanes and shows in particular that molecular orientational correlations are not important in determining molar Cotton-Mouton constants of alkane-based liquids since one would expect such correlations to vary greatly on going from a linear to a jointed chain molecule.

5.4.5 Tri-*n*-alkylamine Liquids

The interesting results of the previous sections prompted a further study of molecules containing alkane chains. Tri-*n*-alkylamine liquids consist of molecules with three equal length *n*-alkane chains attached to a central nitrogen atom. The ends of these chains are tetrahedrally bonded to the nitrogen in the same way as those in the previous section, the fourth chain being replaced here by the nitrogen's lone pair of electrons. The general formula of these liquids is $N(\text{Me}_{n_A})_3$ where Me represents a CH_3 or CH_2 methyl group and n_A is the number of backbone carbon atoms in each alkane chain.

The Cotton-Mouton constant of six of these liquids was measured by the photometric method at $\lambda = 633 \text{ nm}$ with n_A ranging from 2 to 10. In addition tri-*n*-butoxyborane was measured, it being of interest because the three oxygens are bonded to the boron in a planar rather than tetrahedral configuration. Samples used were obtained from Aldrich, Koch-Light and Fluka Ltd. All were carefully filtered using Millipore PTFE filters before use as described previously and all had purities stated to be in excess of 95%. Appropriate refractive index and density data were obtained from the literature⁷³⁻⁴.

Table 5.10 shows the bulk and molar Cotton-Mouton constants of these

Table 5.10 Bulk and molar Cotton-Mouton constants of neat liquid tri-n-alkylamines (and tributoxyborane) at $(20 \pm 1)^\circ\text{C}$ and $\lambda = 633 \text{ nm}$

Liquid	Formula	$10^6 \text{C/T}^{-2} \text{ m}^{-1}$	$10^{27} \text{C/m}^3 \text{ A}^{-2} \text{ mol}^{-1}$
Triethylamine	$\text{N}(\text{Me}_2)_3$	-24	-0.20
Tripopylamine	$\text{N}(\text{Me}_3)_3$	-33	-0.37
Tributylamine	$\text{N}(\text{Me}_4)_3$	-55	-0.76
Trihexylamine	$\text{N}(\text{Me}_6)_3$	-81	-1.58
Trioctylamine	$\text{N}(\text{Me}_8)_3$	-127	-3.19
Tridecylamine	$\text{N}(\text{Me}_{10})_3$	-160	-4.92
Tributoxyborane	$\text{B}(\text{OMe}_4)_3$	-35	-0.56

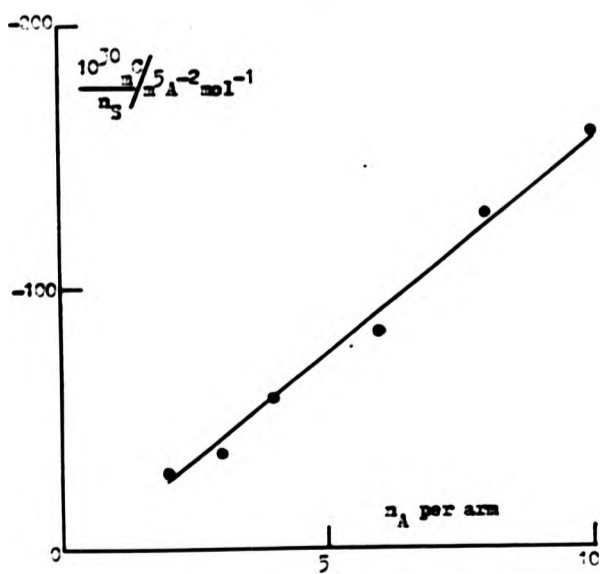
All results accurate to last figure.

liquids. Figure 5.17 shows the molar Cotton-Mouton constant per skeletal atom, C/n_s plotted against the number of backbone carbon atoms, n_A , in each alkane arm for the tri-n-alkylamines.

As was found for the n-alkanes, C/n_s is proportional to n_A whereas a combination of bond polarizability additivity theory and the rotational isomeric model predicts that a similar quantity, $\langle \gamma^2 \rangle / n_s$ tends to a constant at high n_s for similar molecules containing a tri-functional branch point¹⁶⁰.

The gradient of the graph in Figure 5.17 is very similar to the equivalent for the linear aminoalkanes as displayed in Figure 5.11. The only puzzling factor is that for low n_A (<5) there is no evidence for the discontinuities as recorded in Figure 5.11 for the n-alcohols, and Figure 5.16 for tetra-n-alkyl and alkoxy compounds. This apart, the same conclusion must be drawn as in the previous two sections, that the alkane chains are behaving as though they are independent. The value of C for tetrabutoxyborane was rather low but because this was the only measurement on this type of molecule it could not be ascertained whether this was due to the symmetry change or the change in the central atom.

Figure 5.17 The molar Cotton-Mouton constant per skeletal atom $\frac{C/n_3}{n_3}$ vs. the number of backbone atoms, n_A , per arm for tri-*n*-alkylamines



5.4.6 Cycloalkane Liquids and Derivatives

Magnetic birefringence measurements on cycloalkanes and their derivatives are of some interest since these molecules are generally more rigid with better defined conformations than their linear isomers, being based on saturated hydrocarbon rings.

The Cotton-Mouton constant of 13 of these liquids was measured by the photometric method at $\lambda = 633$ nm. Five of these were normal unsubstituted cycloalkanes with the number of skeletal carbon atoms ranging from 5 to 10. Two were monomethyl- and three were dimethylcycloalkanes. Finally, three liquids of molecules with two rings, bicycloalkanes, were measured.

Samples used were obtained from Aldrich, Koch-Light and Fluka Ltd. and were filtered before use as previously described. All had purities stated to be in excess of 97% and the majority were more than 99% pure. Appropriate refractive index and density data was obtained from the literature⁷³⁻⁴.

Table 5.11 shows the bulk and molar Cotton-Mouton constants of these liquids. The only known published values are for cyclohexane, a commonly used solvent. Corfield's⁵ value of m_C for this liquid under the same conditions is $(-0.90 \pm 0.03) \times 10^{-27} \text{ m}^5 \text{ A}^{-2} \text{ mol}^{-1}$ which is over 30% higher than that recorded here. This discrepancy cannot be explained here since samples used were of high purity and previous comparable results have agreed very well, even for near isotropic carbon tetrachloride. Since Battaglia and Richie's⁸ recorded value of m_C $((-0.70 \pm 0.07) \times 10^{-27} \text{ m}^5 \text{ A}^{-2} \text{ mol}^{-1})$ agrees with the present value within experimental error, it is probable that Corfield's value is in error.

The most remarkable result of the unbranched monocycloalkanes is that of cyclopentane. This has a positive molar Cotton-Mouton constant which in hydrocarbons is normally associated with delocalized electrons. Delocalized stable states have been predicted for some heavily branched alkanes¹⁶² and may exist in some cycloalkanes. Unlike cyclohexane, the angles between C-C bonds in cyclopentane cannot be tetrahedral so the molecules are strained. The most stable conformation is puckered with one carbon atom out of the plane of the other four¹⁶⁵. The change in CCC angles means that the hybrid orbitals will not be sp^3 ,¹⁴⁷

Table 5.11 Bulk and molar Cotton-Mouton constants of cycloalkanes at $(20 \pm 1)^\circ\text{C}$ and $\lambda = 633 \text{ nm}$

Liquid	$10^6 C/T \text{ m}^{-1}$	$10^{27} \frac{C}{m^3} \text{ A}^{-2} \text{ mol}^{-1}$
Cyclopentane	+23	+0.12
Cyclohexane	-106	-0.67
Cycloheptane	-86	-0.60
Cyclooctane	-90	-0.69
Cyclodecane	-139	-1.28
Methylcyclopentane	+5	+0.03
Methylcyclohexane	-108	-0.81
cis-1,2-Dimethylcyclohexane	-72	-0.59
trans-1,2-Dimethylcyclohexane	-102	-0.86
cis/trans-1,4-Dimethylcyclohexane	-106	-0.90
Bicyclo[4.3.0]Nonane	+98	+0.79
cis-Decalin(Bicyclo[4.4.0]Decane)	-131	-1.13
trans-Decalin(Bicyclo[4.4.0]Decane)	-216	-1.94

All results accurate to last figure.

possibly leading to an accessible delocalized molecular orbital in cyclopentane.

The molar Cotton-Mouton constants of cyclohexane, cycloheptane and cyclooctane are very similar, despite the higher molecular weight molecules appearing to be more anisotropic¹⁶⁵. This suggests the presence of a positive contribution to their molar Cotton-Mouton constants. The strain energy per molecule increases from cyclohexane to cyclooctane so it may be surmised that there might be some correlation between strain energy and the amount of electron delocalisation.

To investigate this, the molar Cotton-Mouton constants of cyclo- and normal-alkane isomers were compared in Table 5.12. It shows a good agreement between the measured excess $\frac{C}{m}$ for the cycloalkanes (compared to their n-alkane isomers) and the strain energy per carbon atom. This is a crude comparison since cyclo- and n-alkane isomers

Table 5.12 Comparison of difference in molar Cotton-Mouton constants of equivalent cyclo- and normal-alkanes with the strain energy per carbon atom for cycloalkanes

Number of carbon atoms n_A	$10^{27} \frac{mC}{m^3} A^{-2} mol^{-1}$		Excess mC $10^{27} (mC_c - mC_n)$	Strain energy per carbon atom ^a $E_S/n_A \text{ kJ mol}^{-1}$
	n-alkanes $10^{27} mC_n$	cycloalkanes $10^{27} mC_c$		
5	-0.50	+0.12	0.62	5.4
6	-0.74	-0.67	0.07	0.3
7	-0.90	-0.60	0.30	3.8
8	-1.30	-0.69	0.61	5.1
10	-2.13	-1.28	0.85	5.1

* reference 165.

do not have the same conformation but it does indicate that there may be some relation between the amount of distortion of bond angles and the extent of electron delocalization in saturated hydrocarbons.

The monomethylcycloalkanes have values of mC slightly more negative than their parent cycloalkanes, therefore the additional methyl group on average makes these molecules more anisotropic.

The results for the dimethylcyclohexanes show that the positions and relative configurations of methyl groups are important, enhancing or diminishing the molecular anisotropy accordingly as was observed for the n-alkanes.

The last group, bicycloalkanes, consists of molecules where two cycloalkanes have been joined such that they share two carbon atoms. Bicyclo[4.3.0]nonane consists of cyclohexane joined to cyclopentane. It has a relatively large positive molar Cotton-Mouton constant, much larger than that of cyclopentane alone. This result is difficult to explain since one would expect any positive contribution arising from electron delocalization in the cyclopentane ring to be more than offset by the molecular anisotropy. Bicyclo[4.4.0]decane (decalin) consists of two cyclohexane rings and has two isomeric forms. The two rings joined through two equatorial-type bonds give the trans form whilst an

axial and equatorial union gives the cis isomer. The trans form is elongated and fairly rigid whilst cis-decalin is more crumpled and fairly flexible. Therefore the much larger negative value of μ_C for the trans isomer was expected.

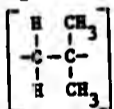
In conclusion, cycloalkanes based on cyclohexane have predictable molar Cotton-Mouton constants whilst the others studied have values of μ_C which can largely be explained by electron delocalization arising from strains in the rings.

5.5 Polymers of Medium and High Molecular Weight

Two completely different types of polymers were studied here. Firstly a range of medium molecular weight neat liquid polyisobutenes which are very heavily branched chain alkanes, and secondly, a high molecular weight sample of the poly- α -amino acid PELG at a range of concentrations in two different solvents.

5.5.1 Polyisobutene Neat Liquids

Polyisobutenes consist of heavily branched hydrocarbon chain molecules having the repeat group



and a C=C double bond at, or adjacent to, one end of the molecule.

It is interesting to examine the variation of the molar Cotton-Mouton constant, μ_C , with molecular weight and in particular to probe further the effects of intramolecular internal fields in such molecules, since it has been shown that these effects enhance the magneto-optical anisotropy of the unbranched n-alkane species.

The Cotton-Mouton constant of five low to medium molecular weight polyisobutenes was measured by the photometric method at $\lambda = 633 \text{ nm}$ and room temperature. The dimer (2,4,4-trimethylpent-1-ene) and the trimer were high purity (>99%) samples obtained from Aldrich Ltd. The other three were commercial samples donated by BP Chemicals Ltd. Since polyisobutene can only be obtained monodisperse for very low

molecular weights¹⁶⁶ these three "Hyvis" samples were polydisperse with $M_w/M_n = 2$. In number average terms, Hyvis 04, 07 and 5 correspond approximately to the hexamer, octamer and tetradecamer respectively¹⁶⁷.

All samples were filtered as previously described. To facilitate filtering the higher molecular weight Hyvis samples were warmed in an oven to $\sim 60^\circ\text{C}$.

Table 5.13 shows the measured bulk and molar Cotton-Mouton constants. Appropriate refractive index, density and number average molecular weight data was obtained from the literature^{74,167}. A literature value¹⁶⁸ for the Cotton-Mouton constant of Hyvis 5 of $(0 \pm 20) \times 10^{-6} \text{ T}^{-2} \text{ m}^{-1}$ is in reasonable agreement with the value of $(26 \pm 1) \times 10^{-6} \text{ T}^{-2} \text{ m}^{-1}$ recorded here.

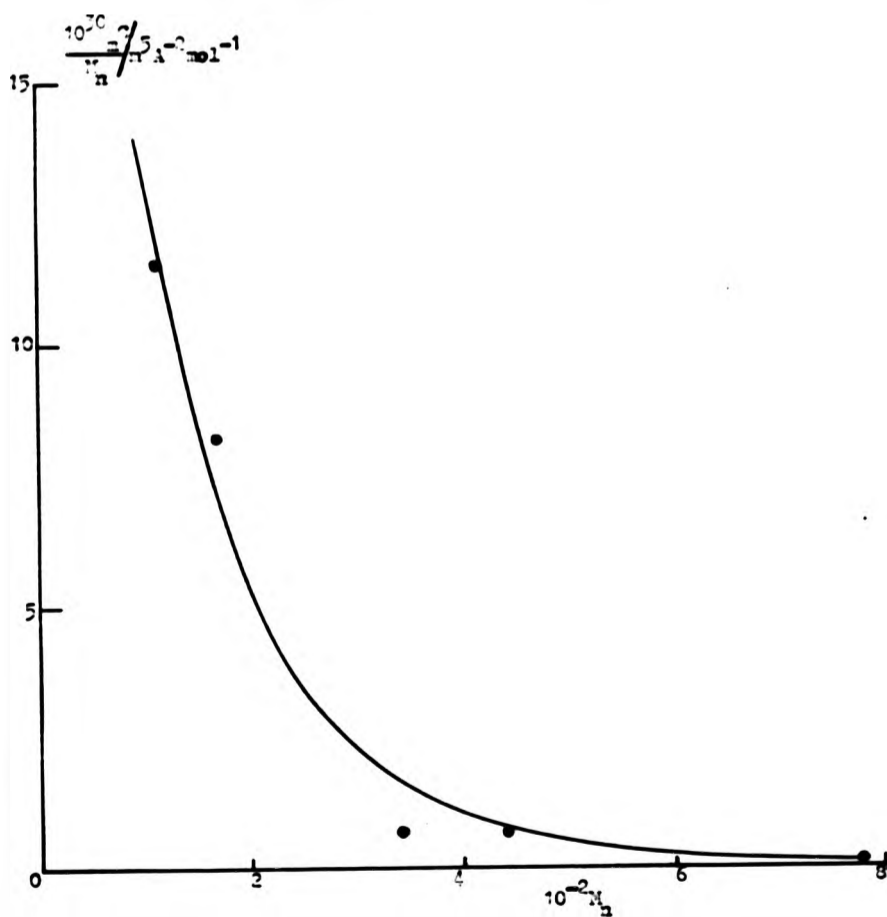
Table 5.13 Bulk and Molar Cotton-Mouton constants of polyisobutenes at $(20 \pm 1)^\circ\text{C}$ and $\lambda = 633 \text{ nm}$

Polymer Name	M_n	$\frac{10^6 C}{T^{-2} \text{ m}^{-1}}$	$\frac{10^{27} \text{ m}^3 C}{\text{m}^5 \text{ A}^{-2} \text{ mol}^{-1}}$
Diisobutylene	112.2	139 ± 1	1.30 ± 0.01
Triisobutylene	116.3	110 ± 2	1.37 ± 0.02
Hyvis 04	340	103 ± 1	2.36 ± 0.02
Hyvis 07	440	100 ± 2	2.92 ± 0.06
Hyvis 5	780	26 ± 1	1.26 ± 0.05

Figure 5.18 gives the molar Cotton-Mouton constant per unit number average molecular weight, $\text{m}^3 C/M_n$, plotted versus M_n . At low M_n the C-C end group dominates and $\text{m}^3 C/M_n$ is relatively large as seen for the lower n-alkenes in 5.4.2. As M_n is increased, $\text{m}^3 C/M_n$ becomes smaller as the polymer chain becomes longer and the C-C end group is progressively diluted. It can be seen that $\text{m}^3 C/M_n \rightarrow 0$ as $M_n \rightarrow \infty$, so the main polymer chains are magneto-optically isotropic.

If all the bond angles in a polyisobutene chain are tetrahedral then the bond polarizability additivity scheme predicts it is optically isotropic

Figure 5.18 The ratio Cotton-Mouton constant per unit molecular weight $\frac{10^{20} \gamma_{CM}}{M_n}$ vs. molecular weight M_n of polyisobutenes

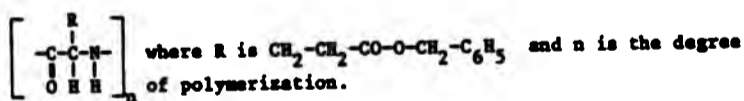


irrespective of conformation¹⁶⁹. Steric repulsions strain the skeletal bonds opening up the C-CH₂-C bond angles by ~12° and this causes the chain to be slightly optically anisotropic. However, results from strain birefringence¹⁶⁹, flow and electro-optical birefringence and depolarized light scattering¹⁶⁸ yield experimental optical anisotropies an order of magnitude higher than predicted and comparable with that of n-decane²⁰. This has been explained by dipole-induced dipole interactions along the chain¹⁶⁸ which partially accounted for the enhancement in anisotropy of the n-alkanes as discussed earlier in this Chapter.

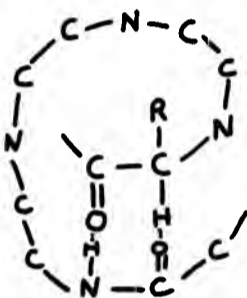
As the magneto-optical anisotropy is negligible for polyisobutene chains if the effect of the C=C end group is accounted for, a near-zero diamagnetic anisotropy is implied. This demonstrates that unlike their optical counterparts, the effect of interactions between magnetic dipoles is very small as discussed earlier. Therefore diamagnetic bond tensors are almost locality independent allowing the application of the bond polarizability additivity scheme.

5.5.2 Solutions of PBLG

Poly-γ-benzyl-L-glutamate (PBLG) is a synthetic poly-α-amino acid commercially available in the molecular weight range 15,000 to 500,000. These high molecular weight polymers are obtained as neat solids in the form of white flexible fibrous sheets. The chemical structure of PBLG is



For investigating the solution properties of macromolecules, poly-α-amino acids are in many respects suitable since they have a fairly well defined structure in solution. Dissolved in suitable solvents such as dimethylformamide (DMF), PBLG molecules approximate to fairly rigid rods¹⁷⁰. This arises from the formation of an alpha-helix due to intramolecular hydrogen bonding as shown below.



The pitch of the helix is $\sim 0.5 \text{ nm}^{171}$. The molecular weight per mer is 219 and since one turn contains $3\frac{2}{3}$ mers, the molecular weight per turn is 803.7.

Some highly polar organic acid solvents such as dichloroacetic acid (DCA) break up the intramolecular hydrogen bonding, so the helical rod gives way to a random coil conformation¹⁷⁰.

A sample of PBLG was obtained from Sigma Ltd. and had a number average molecular weight, $M_n = 215,000$. High purity (>99%) samples of the DMF and DCA solvents were obtained from Koch-Light Ltd. Suitable quantities of each were filtered into dust-free flasks as previously described using Millipore PTFE filters. DCA was particularly difficult to get clean since its highly polar nature meant it was viscous, corrosive and retained dust. However, most of the dust was removed by quadruple filtering using a $0.2 \mu\text{m}$ filter.

A stock solution of weight fraction 30 kg m^{-3} PBLG in DMF was prepared as described earlier without additional purification of the PBLG. This corresponds to a volume fraction of ~ 0.0227 (since the density of PBLG is $\sim 1320 \text{ kg m}^{-3}$ ¹⁷⁰). It was further diluted to produce a range of concentrations from 0.1 to 30 kg m^{-3} . A solution containing 14 kg m^{-3} of PBLG in DCA was also prepared. The more concentrated DMF solutions were of high viscosity and turbid. The implications of this will be discussed later.

The magnetically induced birefringence, $\Delta n'$ was found to be proportional to B^2 for all PBLG/DMF solutions up to the maximum

attainable magnetic induction of 2.2T. Maret et al.¹⁷² found that $\Delta n' \propto B^2$ up to $B = 14T$ for a variety of nucleic acids. If one assumes that $\alpha_{11} > \alpha_{12}$, i.e. Δn is positive, then the observed positive sign of $\Delta n'/B^2$ indicates that the magnetic susceptibility $\Delta \chi$ is positive. Hence PBLG orients perpendicularly to the magnetic field as was found for DNA¹⁷². $\Delta \chi$ originates mainly from the magnetically anisotropic phenyl groups and the π -electrons of CONH groups¹⁷³.

Table 5.14 shows the experimental Cotton-Mouton constants of PBLG/DMF and PBLG/DCA solutions. The larger errors for PBLG/DCA reflect the greater amount of dust in solution and the use of a shorter pathlength cell. In addition a specific Cotton-Mouton constant, C_{sp} is shown in the table for each concentration. Having subtracted the solvent contribution to C , C_{sp} is the Cotton-Mouton constant per unit concentration of PBLG. The first point of note is that C_{sp} is many times larger for DMF than DCA as a solvent. This reflects that the magnetic birefringence of macromolecular solutions depends on the degree of order between themers of chains, i.e. the conformation of the macromolecule. In this case it is intrachain order, i.e. PBLG molecules approximate to rigid rods in DMF but are random coils in DCA, as discussed earlier.

Table 5.14 Bulk and Specific Cotton-Mouton constants of solutions of PBLG in DMF and DCA at $20 \pm 1^\circ C$ and $\lambda = 633 \text{ nm}$

Concentration of PBLG kg m^{-3}	Solvent	Cotton-Mouton constant $10^6 C/T^{-2} \text{ m}^{-1}$	Specific CMC $C_{sp} = \frac{10^6 (C - C_{\text{solvent}})}{\text{concentration}} / T^{-2} \text{ m}^2 \text{ kg}^{-1}$
0	DMF	571 ± 2	-
0.1	DMF	581 ± 2	100 ± 30
0.2	DMF	586 ± 3	60 ± 15
0.3	DMF	585 ± 2	47 ± 10
1	DMF	628 ± 2	57 ± 3
3	DMF	749 ± 2	60 ± 1
10	DMF	1175 ± 12	61 ± 1.2
30	DMF	2480 ± 10	64.3 ± 0.4
0	DCA	-15 ± 3	-
14	DCA	50 ± 80	4 ± 6

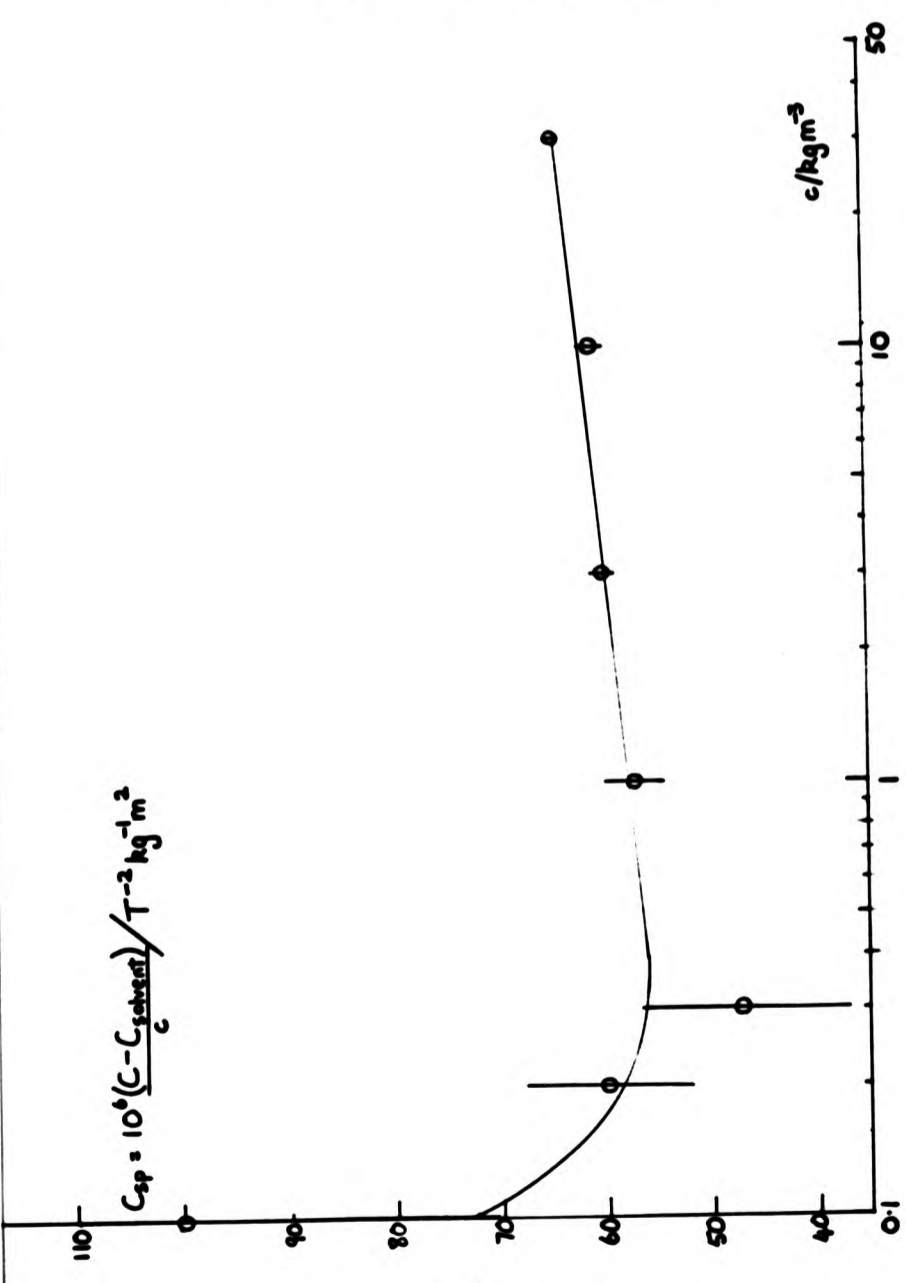
Figure 5.19 shows C_{sp} plotted versus the concentration of PBLG in DMF. C_{sp} appears to drop between 0.1 and 0.3 kg m⁻³ of PBLG (although the errors are large for these low concentrations) and then increases slowly and linearly by ~15% between 0.3 and 30 kg m⁻³ PBLG. A consideration of polymer size alone can indicate the severity of polymer-polymer interactions in solution¹⁷³. For $M_n = 215,000$ the PBLG α -helix has a length of ~134 nm which would sweep out a spherical volume in space of 1.26×10^{-21} m³. If this is taken to be a collision-free volume then polymer-polymer interactions should occur above ~0.3 kg m⁻³. This approximation neglects long range (e.g. dipolar or electrostatic) forces between molecules and also that translational diffusion would reduce the volume available to each macromolecule, but demonstrates that in relatively dilute deaggregated systems considerable intermolecular polymer interactions are likely to be present.

An increase of C_{sp} of only 15% between 0.3 and 30 kg m⁻³ does not indicate parallel association of PBLG molecules. However the viscosity of these solutions greatly increased over this range. The high viscosity of PBLG in certain solvents has been taken to indicate the formation of large molecular aggregates even in dilute solution¹⁷⁴. Other evidence for intermolecular associations was that the turbidity of PBLG/DMF solutions increased with concentration, which indicates that aggregates exist in the solutions studied.

Maret et al.^{172,176} showed that C_{sp} of rod-like high molecular weight DMA in buffered aqueous solution was almost constant up to a concentration of 10 kg m⁻³. They assumed this meant there were no angular correlations or interactions between molecules even though these DMA solutions gell at ~4 kg m⁻³. O'Konski et al.¹⁷⁷ made saturation electric birefringence measurements on high molecular weight PBLG in dichloroethane (a rod promoting solvent) and found that the optical anisotropy dropped between 0 and 10 kg m⁻³. This trend was explained as being due to head to tail anti-parallel association of the permanent dipoles of each chain. Between 10 and 60 kg m⁻³ the optical anisotropy per chain increased slowly and gradually suggesting that the antiparallel proportion was decreasing.

In a study of a number of solutions of rigid and semi-flexible macromolecules in high magnetic fields, Maret et al.¹⁷⁸ found that C_{sp} was

Figure 3.10 The specific Cotton-Mouton constant C_{sp} of IBIG vs. concentration c of IBIG in dimethylformamide



virtually constant up to a pronounced critical concentration when C_{sp} increased suddenly, indicating the formation of parallel aligned domains of molecules, i.e. liquid crystals. This concentration depends on ionic strength and rod length. This point obviously has not been reached in the present work indicating that clusters of parallel molecules have not been formed in the solutions studied here. However, the viscosity and turbidity evidence cited earlier indicates that even at low concentrations aggregates of molecules are being formed and so it is only above the critical concentration that these align in parallel side by side rather than end to end.

5.6 Colloidal Dispersions

This section is mainly concerned with studies of aqueous dispersions of highly crystalline polytetrafluoroethylene (PTFE) particles known commercially as ICI 'Fluon'. In addition the magnetic birefringence and dichroism of a dispersion of acrylic co-polymer lattices and suspensions containing human erythrocyte particles were measured.

5.6.1 Fluon Dispersions

These water-based commercial dispersions consist of non-spherical PTFE particles which are greater than 95% crystalline¹⁷⁹. The sample used, 'Fluon' GP1 was donated by ICI Plastics Division. In its concentrated form (stated by the manufacturers to be a weight fraction of 0.6 PTFE), Fluon is white and turbid. To fully disperse the PTFE particles the sample bottle was gently rolled; shaking caused foaming.

A small quantity ($\sim 2 \text{ cm}^3$) was weighed, carefully dried in an oven and then reweighed. The weight fraction of PTFE was found to be 0.637. Using a 25 cm^3 specific gravity bottle the density of the concentrated dispersion was found to be 1553 kg m^{-3} . A simple calculation gives the particle density as 2170 kg m^{-3} compared to 2302 kg m^{-3} ¹⁸⁰ for the 100% crystalline material and $(2170 \pm 30) \text{ kg m}^{-3}$ for commercial PTFE.¹⁸¹

The shape and size of the PTFE particles was determined by electron microscopy¹⁸². This showed most particles to be prolate spheroids having a major:minor axis ratio of about 2:1 and a major diameter of $\sim 250 \text{ nm}$. With the exception of a small percentage of longer, thinner

rod-like particles the dispersion appeared fairly monodisperse. The character of this dispersion is typical of dispersions of highly crystalline PTFE particles; the spheroidal particles consist of folded polymer chains and the rods consist of PTFE molecules with their major axes parallel to the axis of the rod¹⁷⁹.

A range of concentrations of Fluon was prepared and appropriate sample cells filled as described in Chapter 4. The magnetic birefringence and dichroism of these dispersions was then measured using the phase modulator as described in 4.10.3 - 4. The magnetically induced dichroism of concentrated Fluon in cells of pathlength 0.1 to 5 mm was also measured directly as described in 4.10.4.

(a) Birefringence and dichroism results

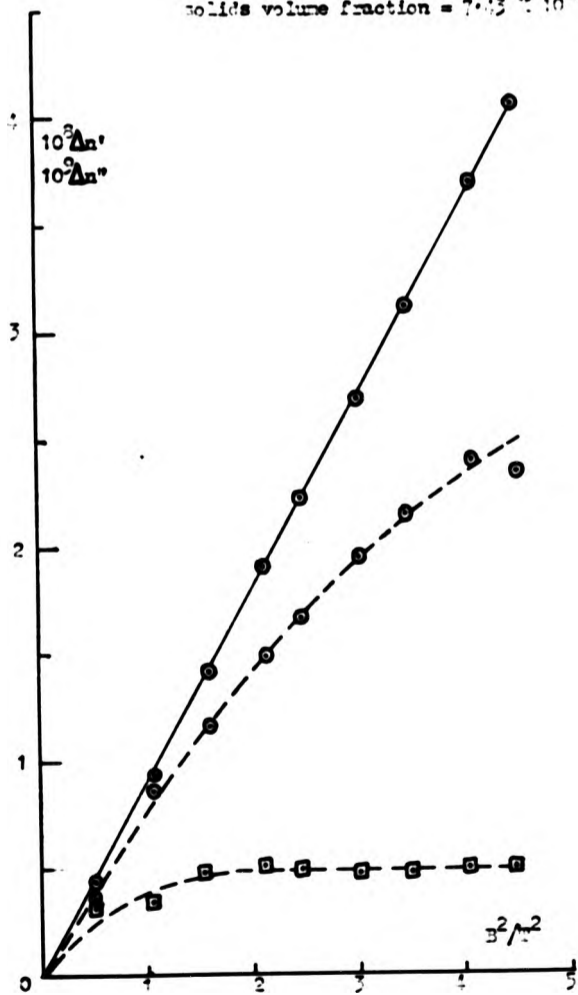
The real and imaginary refractive index anisotropies, $\Delta n'$ and $\Delta n''$, were calculated from the measured induced phase difference and dichroism using equations (2.37) and (2.45).

For samples of bottle concentration ($V_2 = 0.446$) down to a low volume fraction ($V_2 = 10^{-4}$), both $\Delta n'$ and $\Delta n''$ were observed to depend quadratically on the magnetic induction B . As in molecular liquids this indicates that the energy of interaction between the magnetic field and the magnetic dipole induced in the particle is very small compared to the thermal energy kT at room temperature, i.e. the particles have a small diamagnetic susceptibility anisotropy, $\Delta\chi$.

Figure 5.20 shows $\Delta n'$ and $\Delta n''$ plotted against B^2 for some very dilute Fluon dispersions. For a volume fraction $V_2 = 7.43 \times 10^{-6}$, $\Delta n'$ is proportional to B^2 whereas $\Delta n''$ is not. Assuming that real and imaginary birefringences both originate solely from the preferential orientation of the PTFE particles by the magnetic field and that they are small particles with a weak diamagnetic anisotropy, then $\Delta n''$ should also depend quadratically on B . An explanation for it not doing so is that the dispersion contained significant amounts of dust, i.e. particles much larger than Fluon and possessing relatively large magnetic dipole moments. In the plot of $\Delta n''$ versus B^2 for $V_2 = 7.43 \times 10^{-7}$, $\Delta n''$ is virtually constant for $B^2 > 1.5T^2$. This is because the concentration of PTFE particles is so low that the dichroism due to the dust dominates that due to the Fluon. This saturation at $B^2 = 1.5T^2$ is probably due to the virtually complete orientation of the dust particles in the

Figure 5.20 The real (continuous line, $\Delta n'$) and Imaginary (broken line, $\Delta n''$) parts of the complex birefringence of TiO₂ dispersions, plotted against the square of the applied magnetic induction B^2 .

solids volume fraction = 7.45×10^{-3}
 solids volume fraction = 7.45×10^{-3}



direction of the applied magnetic field.

As discussed in earlier sections concerning magnetic birefringence measurements on pure liquids, large dust particles contribute significantly to $\Delta n''$ but negligibly to $\Delta n'$. Hence, although $\Delta n''$ of Fluon could be accurately measured down to $V_2 = 7.43 \times 10^{-6}$, $\Delta n'$ could be measured down to $V_2 = 7.43 \times 10^{-9}$, a concentration of PTFE lower than 1 part in 100 million. The smallest measurable value of $\Delta n'$ was $\sim 10^{-12}$, that of $\Delta n''$ was $\sim 10^{-10}$.

Figure 5.21 shows both $\Delta n'/V_2 B^2$ and $\Delta n''/V_2 B^2$ plotted versus volume fraction of PTFE, V_2 . As can be seen, the range of concentration measured is very large (8 decades for $\Delta n'$) yet both $\Delta n'$ and $\Delta n''$ are proportional to V_2 up to relatively large volume fractions, ~ 0.2 for $\Delta n'$ and $\sim 10^{-2}$ for $\Delta n''$.

(b) Direct dichroism results

$\Delta n''$ for concentrated Fluon was also calculated from turbidity (transmission) measurements using light polarized parallel and perpendicular to the magnetic field. Four different pathlengths were used. The measurements were made by placing the sample cell between polarizers set first parallel and then perpendicular to B .

Figure 5.22 shows $\Delta n''_{\text{apparent}}/V_2 B^2$ plotted versus pathlength. This shows that $\Delta n''$ appears to decrease virtually linearly with increasing pathlength. With the longer pathlength, intense scattering was evident; very little coherent light was transmitted through the sample. Under these conditions the effects of multiple scattering are likely to be important. A simple explanation for the decrease of the measured $\Delta n''$ shown in Figure 5.21 is that the strongly multiple-scattered light was depolarized in the forward direction, thus reducing the turbidity change on applying the magnetic field for light of both parallel and perpendicular polarization within the sample cell. This would decrease the observed intensity change and the calculated value of $\Delta n''$ as shown in Figure 5.21. For a very long cell the depolarization would be complete and no dichroism would be measurable. Figure 5.22 shows that reliable $\Delta n''$ values were obtainable for pathlengths of about 0.5 mm or less for concentrated Fluon.

Using the polarized light transmission method of measuring $\Delta n''$ described

Figure 3.21 $\Delta n'$ and $\frac{10^5 \Delta n'}{V_2 B^2}$ plotted against the solids volume fraction V_2 of Pluron dispersions

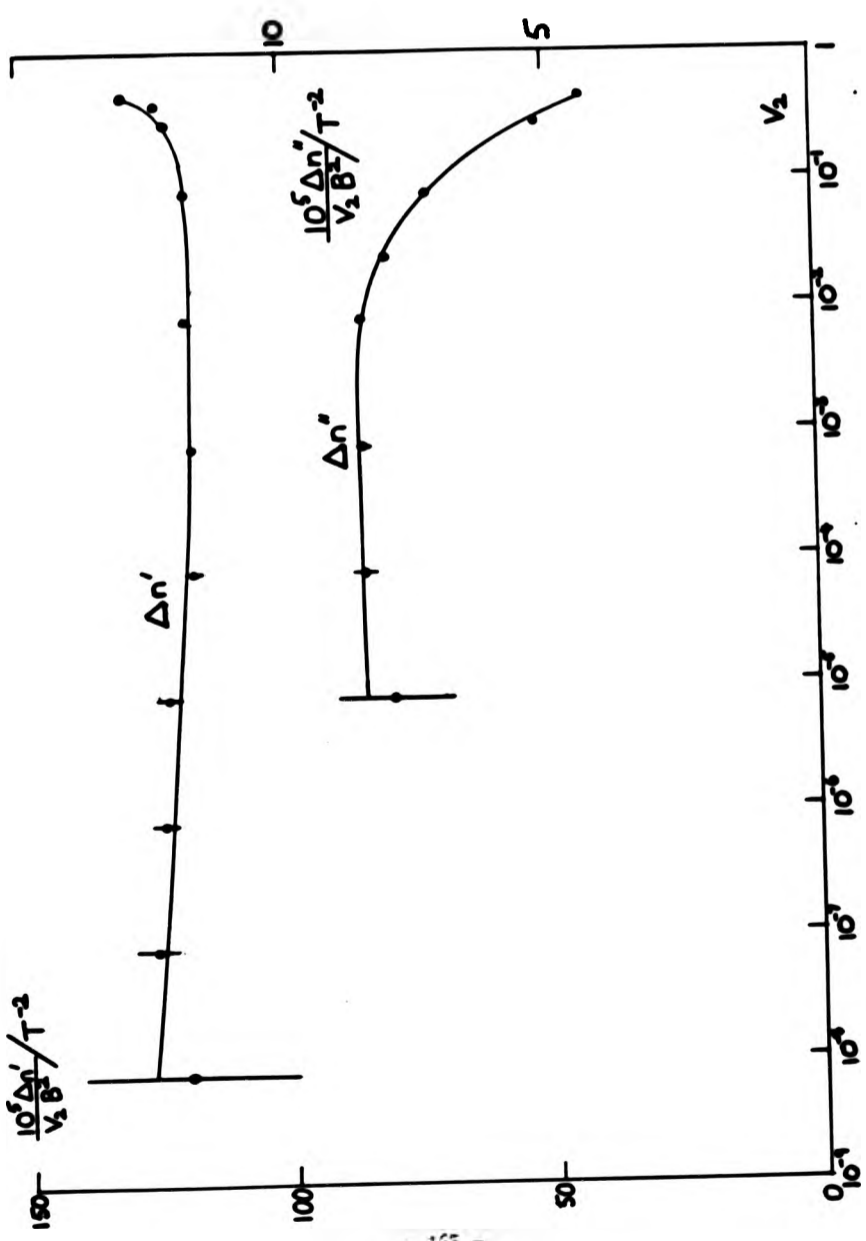
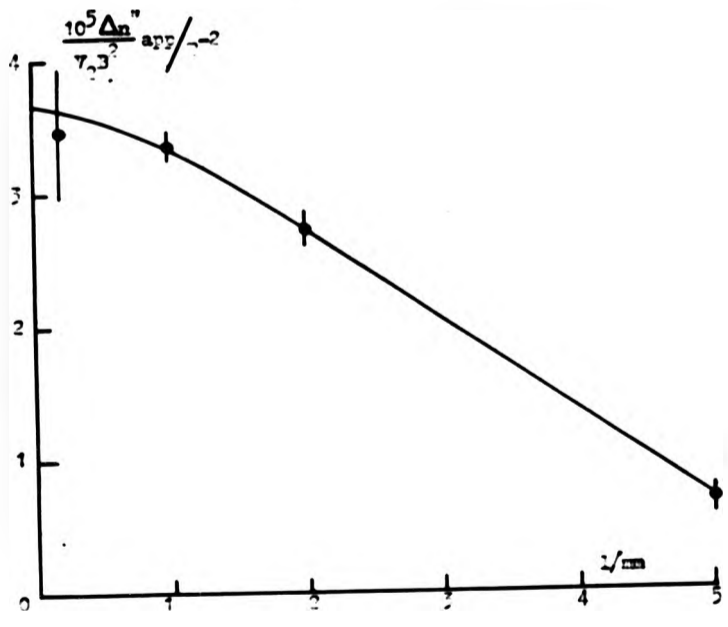


Figure 5.22 $\Delta n'_{app}/\tau_2 J^2$ plotted against pathlength l of concentrated Fluon dispersion ($\tau_2 = 0.116$)



above, even at short pathlengths (<0.5 mm) $\Delta n''$ was about 15% less for the same (high) concentration than $\Delta n''$ measured using the modulator. This was thought to be due to errors arising when using the modulator to measure the magnetic dichroism of a sample with a large magnetic birefringence. These errors which have been discussed earlier are due to small errors in the azimuth setting of the modulator and since $\Delta n'/B^2$ is almost linearly dependent on V_2 , effectively a constant error only is added to the $\Delta n''$ results.

Fluon data analysis

The following is an analysis of the measured Fluon data, comparing it with theoretical predictions. The analysis commences in the dilute region ($V_2 < 10^{-2}$) and enables one to calculate the principal refractive indices of the particles.

Dilute region

Below a volume fraction of 0.01, both $\Delta n'/V_2$ and $\Delta n''/V_2$ are independent of V_2 within experimental error. O'Konski's theory¹⁷⁷ for independent colloidal particles was used to analyse the results. This theory gives (in SI units):

$$\Delta n' = \frac{2\pi V_2}{4\pi\epsilon_0 n'} (g_a - g_b) \phi(\gamma) \quad (5.1)$$

for the birefringence. For the dichroism $\Delta n''$, Stoimenova et al.¹⁸³ give

$$\Delta n'' = \frac{6\pi\epsilon_0 \Delta n'}{k^3 V (g_a + g_b)} \quad (5.2)$$

$$\text{or } \Delta n'' = \frac{2.3}{3^k} \cdot \frac{2\pi V_2}{(4\pi\epsilon_0)^{1/2} n'} V (g_a^2 - g_b^2) \phi(\gamma) \quad (5.3)$$

where V is the volume per Fluon particle

V_2 is the volume fraction of Fluon particles

n' is the refractive index of the dispersion

k is the wave number of the light in the dispersion

= $2\pi/(\text{wavelength in the medium})$

= $2\pi n'/(\text{vacuum wavelength})$

= $2\pi n'/\lambda_0$

$\phi(\gamma)$ is the particle orientation function

= $2\gamma/15$ in the quadratic response region.

$$\text{where } \gamma = \frac{(x_a - x_b)}{\mu_0} \cdot \frac{B^2}{2k_B T} \quad (5.4)$$

where B is the magnetic induction

T is the temperature

x_i is the volume diamagnetic susceptibility along the i axis.

Assume a prolate ellipsoidal particle

with a,b,c axes such that b = c

ϵ_i is the optical susceptibility along the i axis = α_i/V

where α_i is the optical polarizability along the i axis.

α_i may originate from shape or intrinsic anisotropy i.e. particle crystallinity.

Now g can be defined as follows¹⁸⁴:

$$\chi^{\text{opt}} = \chi_1^{\text{opt}} + v_2 g \quad (5.5)$$

where χ^{opt} is the optical susceptibility of the dispersion and χ_1^{opt} is the optical susceptibility of the continuous phase.

Generally $\chi^{\text{opt}} = (\epsilon_r^{\text{opt}} - 1)\epsilon_0 = (n'^2 - 1)\epsilon_0$

$$\text{So (5.5) becomes } n'^2 = n_1^2 + \frac{v_2 g}{\epsilon_0} \quad (5.6)$$

where n_1 is the refractive index of the continuous phase.

And for a randomly aligned set of spheroids

$$n'^2 = n_1^2 + \frac{v_2}{\epsilon_0} \left(\frac{g_a + 2g_b}{3} \right) \quad (5.7)$$

$$\therefore \frac{dn'}{dv_2} = \frac{(g_a + 2g_b)}{6n'\epsilon_0} \quad (5.8)$$

Hence using equations (5.4) and (5.8) measurements of $\frac{\Delta n'}{\Delta \gamma}$, $\frac{dn'}{dv_2}$ and v can in principle give g_a and g_b .

In the dilute dispersions $n' = n_1$ the refractive index of the continuous phase.

Now the volume of an ellipsoid $V = \frac{4\pi A^3}{3P^2}$ (5.9)

where A is the major axis radius
and P is the axis ratio.

Electron micrographs¹⁸² show that $P = 2$ for Fluon therefore $V = \frac{\pi A^3}{3}$.
Also $k = \frac{2m_1}{\lambda_0}$

Substituting for V and k in (5.4) and rearranging gives:

$$g_a + g_b = \frac{9}{4} \epsilon_0 \frac{\Delta n''}{\Delta n'} \left(\frac{\lambda_0}{\pi m_1 A} \right)^3 \quad (5.10)$$

Rearranging (5.8) gives:

$$g_a + 2g_b = 6m_1 \epsilon_0 \frac{dn'}{dV_2} \quad (5.11)$$

Solving (5.10) and (5.11) simultaneously gives:

$$\left. \begin{aligned} g_a &= \epsilon_0 \left[\frac{9}{2} \frac{\Delta n''}{\Delta n'} \left(\frac{\lambda_0}{\pi m_1 A} \right)^3 - 6m_1 \frac{dn'}{dV_2} \right] \\ g_b &= \epsilon_0 \left[6m_1 \frac{dn'}{dV_2} - \frac{9}{4} \frac{\Delta n''}{\Delta n'} \left(\frac{\lambda_0}{\pi m_1 A} \right)^3 \right] \end{aligned} \right\} \quad (5.12)$$

Now $m_1 = 1.333$, $\frac{dn'}{dV_2} = 42.4 \times 10^{-3}$ ¹⁸², $A = 125 \times 10^{-9}$ m¹⁸²

$\lambda_0 = 633 \times 10^{-9}$ m and $\frac{\Delta n''}{\Delta n'} = \frac{1}{14}$ from Figure 5.20

i.e. $\left. \begin{aligned} g_a &= 0.2287\epsilon_0 \\ g_b &= 0.0552\epsilon_0 \end{aligned} \right\} \quad (5.13)$

Now one can compare g_a and g_b with the particle shape and anisotropy.

In liquids the polarisability¹⁸⁴

$$\alpha_i = \frac{\epsilon_1 V}{L_i + \left(\frac{1}{\mu_i - 1} \right)} = \frac{n^2 V}{L_i + \left(\frac{1}{\mu_i - 1} \right)} \quad (5.14)$$

where L_i is a shape factor.

For prolate spheroids:

$$L_a = \frac{1-e^2}{e^2} \left[-1 + \frac{1}{2e} \ln \left(\frac{1+e}{1-e} \right) \right] \quad (5.15)$$

where $e = \frac{(a^2-b^2)^{1/2}}{a}$

and $EL_i = 1$ i.e. $L_a + 2L_b = 1$ (5.16)

And μ_i is the relative refractive index along the i axis

i.e. $\mu_i = \frac{n_i}{n'}$ and $n' = n_1$ in the dilute region.

$$\left. \begin{aligned} \text{Thus } g_a = \frac{\alpha_a}{V} &= n'^2 \epsilon_o \left[L_a + \frac{1}{\mu_a^2 - 1} \right]^{-1} \\ \text{and } g_b &= n'^2 \epsilon_o \left[L_b + \frac{1}{\mu_b^2 - 1} \right]^{-1} \end{aligned} \right\} \quad (5.17)$$

For an axis ratio $P = 2$, $e = 0.866$

Hence from (5.15) and (5.16) $L_a = 0.174$, $L_b = L_c = 0.413$ (5.18)

Rearranging (5.17) gives $\mu_i^2 = 1 + \left[\frac{n'^2 \epsilon_o}{g_i} - L_i \right]^{-1}$ (5.19)

Substituting the values of g_i from (5.13) gives:

$$\mu_a = 1.064, \mu_b = 1.016. \quad (5.20)$$

Thus

$$\left. \begin{aligned} m_a &= n_1 \mu_a = 1.419 \\ \text{and } m_b &= n_1 \mu_b = 1.355 \end{aligned} \right\} \quad (5.21)$$

To be noted is that $\frac{1}{3}(m_a + 2m_b) = 1.376$ which is the value of n' for bulk Fluon¹⁸² ($v_2 = 1$).

Hence a knowledge of three measurable quantities has led to the principal refractive indices of the particle. (5.21) shows the particle refractive index anisotropy ($m_a - m_b$) to be large, 0.064.

From the magnitudes of L_a , L_b , μ_a and μ_b quoted above it can be seen that $L_i \ll (\mu_i^2 - 1)^{-1}$, where $i = a$ or b . Thus the anisotropy of the Fluon particles is predominantly intrinsic, i.e. it arises from their crystallinity and not their shape.

Concentrated region

In the concentrated region ($V_2 > 10^{-2}$) one can see from Figure 5.21 that the ratio $\Delta n''/\Delta n'$ is no longer constant. Also the refractive index of the dispersion, n' cannot be considered as equal to that of the continuous solvent medium, m_1 . Figure 5.21 shows that the value of $\Delta n'/V_2$ rises by ~20% between $V_2 = 0.1$ and 0.446 whilst $\Delta n''/V_2$ falls by ~50% between $V_2 = 0.01$ and 0.446. The theoretical expression derived for the dilute state can be adapted for concentrated dispersions as follows:

Rearranging (5.1) gives

$$\frac{\Delta n'}{V_2} = \frac{\phi(\gamma)}{2\epsilon_0} \frac{(g_a - g_b)}{n'} \quad (5.22)$$

Now if one assumes that the orientation function $\phi(\gamma)$ is independent of concentration, then the ratio of $\Delta n'/V_2$ at a given concentration to $(\Delta n'/V_2)_0$ in the dilute region is given by

$$\frac{(\Delta n'/V_2)}{(\Delta n'/V_2)_0} = \frac{(g_a - g_b) \cdot m_1}{(g_a - g_b)_0 \cdot n'} \quad (5.23)$$

where $(g_a - g_b)_0$ is the value of $(g_a - g_b)$ in the dilute region.

From equation (5.13) $(g_a - g_b)_0 = 0.1735\epsilon_0$ and $m_1 = 1.333$ so (5.23) becomes:

$$\frac{(\Delta n'/V_2)}{(\Delta n'/V_2)_0} = 7.683 \frac{(g_a - g_b)}{\epsilon_0 n'} \quad (5.24)$$

Now g_a and g_b are defined in equation (5.17). To calculate these requires the knowledge of $\frac{dn'}{dV_2} = (42.4 \pm 1) \times 10^{-3}$ obtained from reference 182 and the values of m_a and m_b obtained in (5.21). The theoretical values of $\frac{(\Delta n'/V_2)}{(\Delta n'/V_2)_0}$ for values of V_2 follow in Table 5.15.

Equation (5.2) gives

$$\frac{\Delta n''}{V_2} = \frac{V\theta(\gamma)}{12\pi\epsilon_0^2} \cdot \frac{k^3(g_a^2 - g_b^2)}{n^2} \tag{5.25}$$

Now $k = 2\pi n'/\lambda_0$ where λ_0 is the vacuum wavelength of the incident light.

$$\therefore \frac{\Delta n''}{V_2} = \frac{2\pi^2 V\theta(\gamma)}{3\epsilon_0^2 \lambda_0^3} \cdot n'^2 (g_a^2 - g_b^2) \tag{5.26}$$

If again one assumes that the orientation function $\theta(\gamma)$ is independent of concentration, then the ratio of $\Delta n''/V_2$ at a given concentration to $(\Delta n''/V_2)_0$ in the dilute region ($V_2 < 10^{-2}$) is given by

$$\frac{(\Delta n''/V_2)}{(\Delta n''/V_2)_0} = \frac{n'^2 (g_a^2 - g_b^2)}{n_1^2 (g_a^2 - g_b^2)_0} \tag{5.27}$$

$$= \frac{11.39 n'^2 (g_a^2 - g_b^2)}{\epsilon_0^2} \tag{5.28}$$

Table 5.15 gives calculated theoretical values $\frac{(\Delta n''/V_2)}{(\Delta n''/V_2)_0}$ for values of V_2 in the concentrated region.

Figure 5.23 shows calculated experimental and theoretical values of $\frac{(\Delta n''/V_2)}{(\Delta n''/V_2)_0}$. Experiment shows a rise in this ratio of ~10% at $V_2 = 0.446$ whilst Rayleigh scattering theory yields an actual fall of nearly 3%.

Figure 5.24 shows experimental and theoretical values of $\frac{(\Delta n''/V_2)}{(\Delta n''/V_2)_0}$. Hence experiment shows a fall of ~50% at $V_2 = 0.446$ whilst theory indicates a decrease of only 20% at this concentration.

A possible explanation for the observed concentration dependence of $\Delta n'/V_2$ and $\Delta n''/V_2$ is angular correlations between the non-spherical Fluon particles. One may define a particle angular correlation factor G_2 analogous to that for molecules (g_2) as discussed in earlier sections. Taking the particles to be uncorrelated at high dilution, Figures 5.23 and 5.24 show that $G_2' = 1.1$ as measured by the birefringence and $G_2'' = 0.5$ as measured by the dichroism, both at the maximum volume fraction of $V_2 = 0.446$. These are realistic magnitudes compared to those found for molecular liquids. However, it is difficult to explain why $G_2' > 1$ and $G_2'' < 1$: agreement between the

Figure 3.23 Experimental (continuous line) and theoretical (broken line) values of $\frac{(\Delta n/V_2)}{(\Delta n/V_2)_0}$ vs. the solids volume fraction V_2 of Elton dispersions

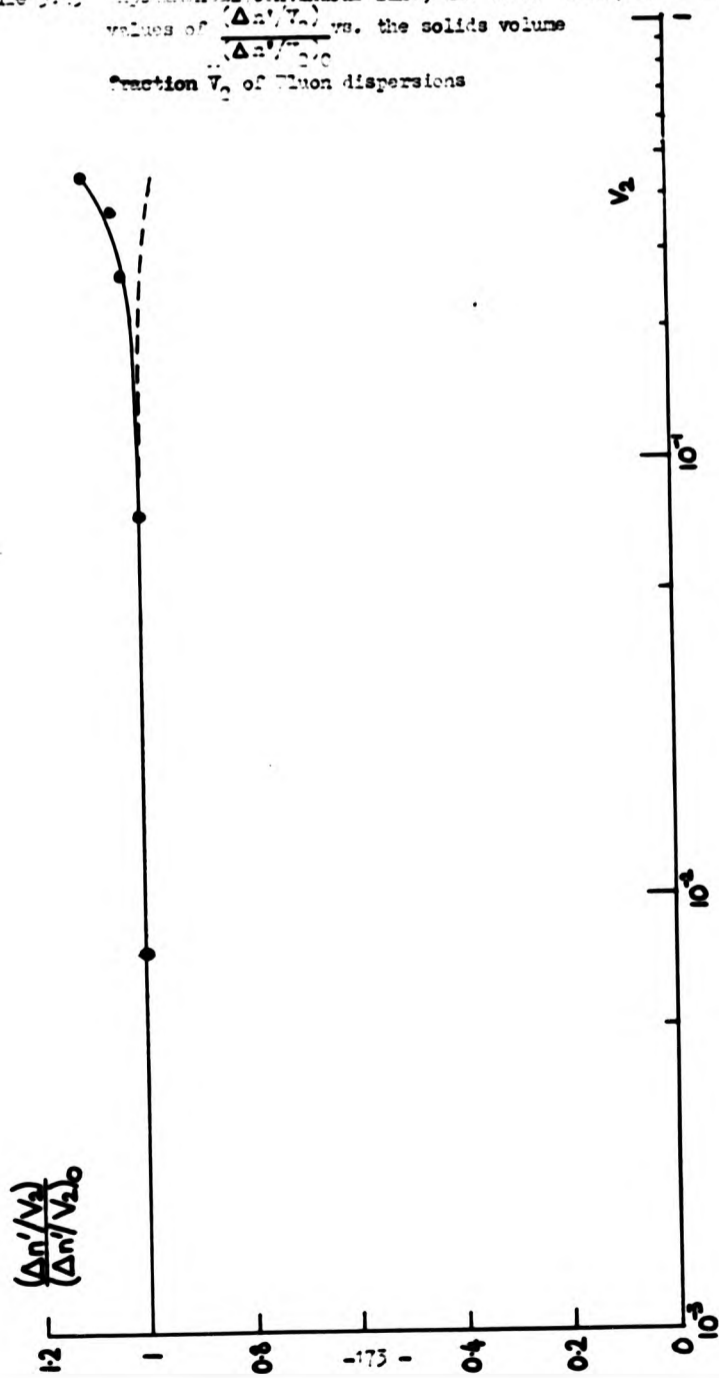


Figure 5.24 Experimental (continuous line) and theoretical (broken line) values of $\frac{(\Delta n^2/V_2)}{(\Delta n^2/V_2)_0}$ vs. the solids volume fraction V_2 of Eblon dispersions

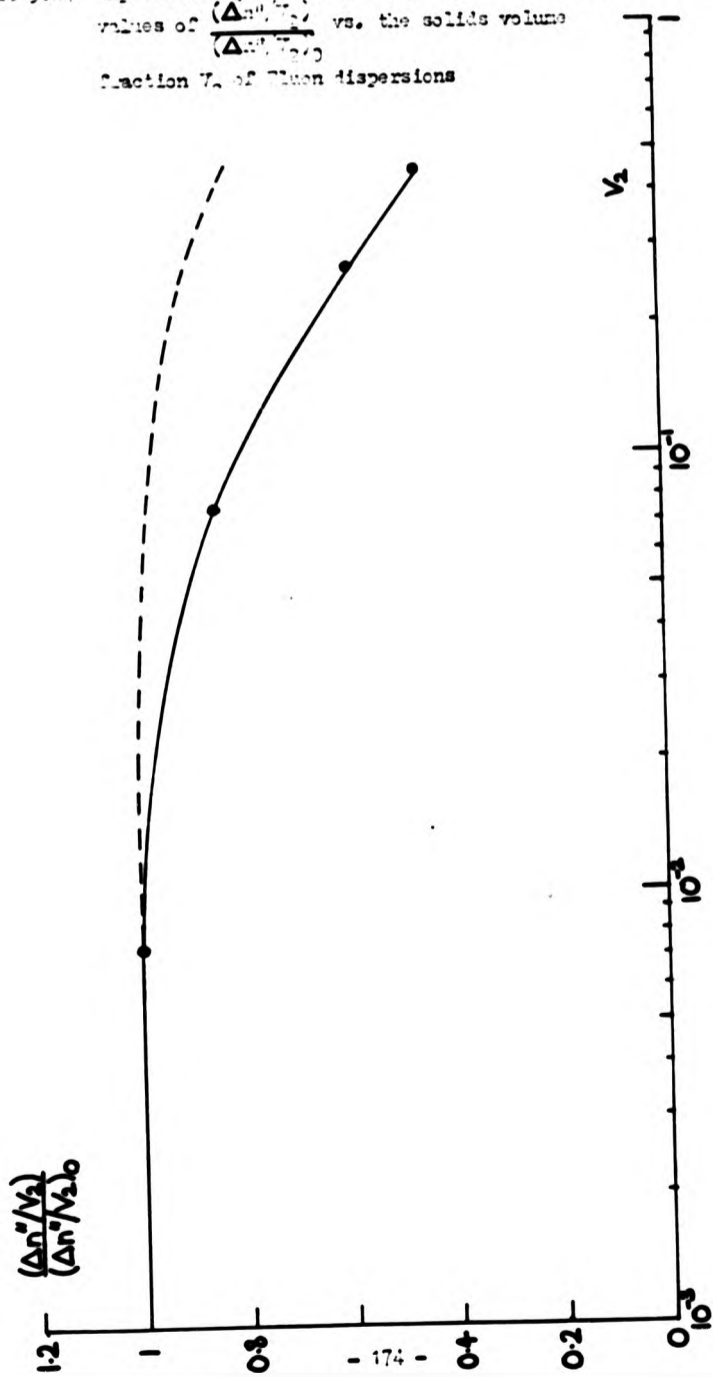


Table 5.15 Theoretical ratios $\frac{(\Delta n'/V_2)}{(\Delta n'/V_2)_0}$ and $\frac{(\Delta n''/V_2)}{(\Delta n''/V_2)_0}$ as a function of V_2 for Fluon, calculated using the Rayleigh approximation

Volume fraction V_2	Dispersion refractive index n'	Optical susceptibilities		$\frac{(\Delta n'/V_2)}{(\Delta n'/V_2)_0}$	$\frac{(\Delta n''/V_2)}{(\Delta n''/V_2)_0}$
		ϵ_a/ϵ_0	ϵ_b/ϵ_0		
7.43×10^{-3}	1.3333	0.2287	0.0552	1.000	1.00
2.29×10^{-2}	1.3340	0.2281	0.0535	1.006	1.00
7.43×10^{-2}	1.3362	0.2247	0.0505	1.002	0.97
0.2675	1.3443	0.2111	0.0384	0.987	0.89
0.3715	1.3488	0.2027	0.0310	0.978	0.83
0.446	1.3519	0.1978	0.0265	0.973	0.80

signs of $G_2' - 1$ and $G_2'' - 1$ would be expected from the physical basis of angular correlation.

Equations (5.1) and (5.3) for $\Delta n'$ and $\Delta n''$ have been derived assuming that the particles interact with the optical field as dipoles. This is the region of the Rayleigh approximation⁵⁷ where the size of the particle should be much less than $\lambda/2\pi$. A size of less than $\lambda/20$ is usually taken as realistic. Particles larger than this experience a specially dependent optical field and an optical dipole interaction becomes an inaccurate description. The major dimension of the Fluon particles was about $8\lambda/20$, well outside the Rayleigh region. Thus it is possible that the concentration dependence of the results is difficult to explain because the wrong initial assumptions have been made in equations (5.1) and (5.3) about the relation of $\Delta n'$ and $\Delta n''$ to the properties and interactions between particles. The few calculations that have been made¹⁸⁵⁻⁶ use more realistic approximations than that of Rayleigh. They show that departures from the Rayleigh approximation for $\Delta n'$ are not great for particles up to $\sim 1 \mu$ m in size, but considerable discrepancies occur for $\Delta n''$ for particles as small as Fluon. These calculations have yet to be extended to concentrated dispersions.

5.6.2 Other Colloidal Dispersions

Two other types of dispersion of different character were examined using the photometric method.

(a) Acrylic co-polymer dispersions

A sample of Ravacryl 344 was obtained from the Harlow Chemical Company Ltd. This aqueous dispersion contained spherical particles of flexible acrylico-polymers having a diameter of $\sim 0.1 \mu\text{m}$.

A sample having a volume fraction of 10^{-3} was examined using a 10 mm pathlength cell. Even at this low concentration the samples was very turbid, so very accurate results were unattainable. A value of $0 \pm 0.2 \times 10^{-3} \text{ T}^2 \text{ m}^{-1}$ was obtained for both $\frac{\Delta n'}{\lambda_0 B^2}$ and $\frac{\Delta n''}{\lambda_0 B^2}$. These null values were expected since the particles have an amorphous structure and spherical shape.

(b) Dispersion of human erythrocyte particles

Particles have recently been made from human erythrocytes that are potentially useful for colloid research¹⁸⁷ since they are nearly monodisperse prolate ellipsoids. They are large particles possessing major and minor dimensions of typically 14 and 3 μm respectively.

A sample was kindly donated by Professor S.P. Suters of Washington University, St. Louis, Missouri. This was a 10% by volume ($V_2 = 0.1$) suspension of erythrocytes in phosphate-buffered saline with a trace of bacterial growth inhibitor. Because the particles scattered and absorbed light a great deal, a short pathlength quartz cell (l = 0.2 mm) was initially used to contain a 0.02 volume fraction sample. A small magnetically induced birefringence was initially noted, but after a short time no birefringence could be measured. This puzzling phenomenon was found to be due to the particles being attracted and adhering to the walls of the quartz cell.

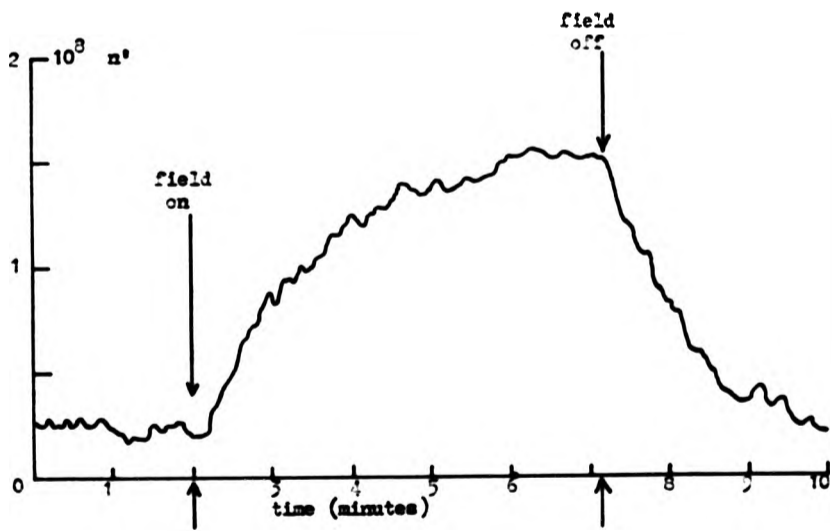
In order to reduce this effect to a minimum, the sample was further diluted, using ethylene glycol to decrease the particle sedimentation rate. A 1 mm pathlength quartz cell was fitted with this sample, of volume fraction 0.005. Now, as the average distance between cell wall and particle is much greater for a 1 mm than a 0.2 mm pathlength cell, the rate of particle adherence to the cell walls was reduced enough to make valid magnetic birefringence measurements.

The magnetic field was raised to a high value (2.2 Teslas) and the resulting birefringence plotted versus time (Figure 5.25). After achieving a steady state value the field was switched off at a point shown on the graph. This was repeated with the apparatus set up for measuring dichroism. Figure 5.25 shows that a maximum birefringence of 1.3×10^{-8} was caused after ~ 300 seconds with a time constant of ~ 150 seconds. This contrasts with the ability of the Fluon particles to preferentially orient along the direction of the magnetic field in a very short time, less than the time constant of the lock-in amplifier (~ 1 second). This is because the erythrocytes are about 50 times the size of the Fluon particles.

Figure 5.25 shows that the birefringence, $\Delta n'$ of the erythrocytes could not be measured nearly as accurately as that of Fluon. This is due partly to their greater scattering power and partly to the relative inhomogeneity of this dispersion, i.e. a small number of large particles leads to a larger variation of particle density for a given volume element through which the light passes. This limited greatly the accuracy of field dependent studies of birefringence although $\Delta n'$ appeared to have a B to B^2 dependence. No magnetically induced dichroism was observed. This is to be expected for very large particles, where theory¹⁸⁵⁻⁶ shows that dichroism is a decreasing function of particle size.

Figure 3.25 Birefringence n' plotted against time for erythrocyte particles dispersed in ethylene glycol/water

volume fraction of particles = 0.005
cell pathlength = 1 μm



CHAPTER 6
CONCLUSIONS

1. An apparatus was developed to measure magnetic birefringence and linear dichroism. This apparatus enabled measurements of the above quantities to be made more accurately than previously reported^{6,8,9,10,16,66}, approximately 10 times for birefringence and over 100 times more accurately for dichroism.
2. Conclusions arising from experimental work have been drawn at the end of each section in Chapter 5. The following paragraphs are a summary of these.

The major part of the experimental measurements was the precise determination of the molar Cotton-Mouton constant, ${}_{\text{m}}C$, of diamagnetic molecular liquids. ${}_{\text{m}}C$ is a function of the intrinsic molecular magneto-optical anisotropy (γ_{mo}^2), the molecular orientational correlation parameter (g_2) and the local electric field (E_1). In addition there are contributions from the magnetic hyperpolarizability (η) and a collision-induced contribution (${}_{\text{m}}C_{\text{CI}}$).

The above are of varying importance depending on the type of liquid. A study of the magnetic birefringence of a variety of homologous and related molecular species has led to a greater understanding of the part played by these parameters in determining ${}_{\text{m}}C$.

3. The first group of molecular liquids studied consisted of benzene derivatives. These had large Cotton-Mouton constants due to their large intrinsic magneto-optical anisotropies (γ_{mo}^2). In comparison, η and ${}_{\text{m}}C_{\text{CI}}$ contributions can be assumed to be small. γ_{mo}^2 is large and positive because the delocalized π molecular orbital causes the diamagnetic susceptibility anisotropy ($\Delta\chi$) to be both large and of the same sign as the polarizability anisotropy ($\Delta\alpha$).

A theoretical value of ${}_{\text{m}}C$ for benzene, derived from gas phase values of $\Delta\chi$ and $\Delta\alpha$ ⁸⁰⁻⁸², was double the experimental value for the liquid. This is probably due to local cavity field effects effectively diminishing $\Delta\alpha$, rather than molecular orientational correlations. Recently^{11,12}, g_2 has been shown to be close to unity for benzene. In combination with depolarized light scattering results^{11,12}, magnetic birefringence

measurements of fluorobenzenes have shown that their higher values of ϵ_C reflect a value of g_2 much greater than unity. Intermolecular forces are much stronger in these liquids and hence g_2 appears to correlate with how closely the molecules are packed.

4. A study was made of liquids of intrinsically isotropic molecules, where γ^2 is zero, so that other effects such as magnetic hyperpolarizability and collision-induced contributions could be studied. ϵ_C was found to be of opposite sign for $\text{Sn}(\text{CH}_3)_4$ than CCl_4 , both being of tetrahedral symmetry. This indicates the operation of two effects and can be explained by paramagnetic and diamagnetic contributions to η of opposite sign. The molar Cotton-Mouton constant of solutions of the two species was measured and did not vary linearly with the concentration of CCl_4 in $\text{Sn}(\text{CH}_3)_4$. Further analysis showed that $\text{Sn}(\text{CH}_3)_4$ behaves as an inert solvent for CCl_4 , but not vice versa. Hence there must be an intermolecular contribution to the magnetic birefringence of neat CCl_4 . This could arise from transient $\text{CCl}_4 \cdot \text{CCl}_4$ dimers or some structure in liquid CCl_4 . Therefore, magnetic birefringence and light scattering studies of weakly anisotropic molecules such as alkanes, using CCl_4 as an assumed isotropic solvent, could be subject to error.
5. The magnetic birefringence of n-alkane liquids was shown to depend quadratically on the number of backbone atoms (n) in the constituent molecules. This is not consistent with theories of molecular anisotropy based on bond polarizability additivity (BPA) and the rotation isomeric model, which predict a linear dependence above a certain chain length. Even allowing for dipole-induced dipole (DID) interactions along the chain, shaped cavity field effects and molecular orientational correlations (MOC), BPA theories appear to be unsatisfactory.

Neither η nor ϵ_C are expected to be quadratically dependent on chain length^{20, 117-8}, therefore for n-alkanes ϵ_C would appear to be determined mainly by the mean magneto-optical anisotropy, $\langle \gamma_{\text{MO}}^2 \rangle$. Depolarized light scattering (DLS) results²⁰ show that the optical anisotropy $\langle \gamma^2 \rangle$ is proportional to n^2 even in the gas phase. Therefore the molecular diamagnetic susceptibility anisotropy ($\Delta\chi$) appears to have the same chain length dependence as the polarizability anisotropy ($\Delta\alpha$), which is surprising since $\Delta\chi$ is unaffected by DID interactions, MOC etc. and therefore should be bond additive. Hence the concept of valence

electrons being localized in bonds may be questioned, even for σ -bonds, and so one of the assumptions on which all EPA theories are based may be incorrect.

Interacting atom theories have been used to explain DLS results of n-alkane gases up to undecane¹⁵², but these theories are as yet insufficiently developed to be compared to experimental DLS and magnetic birefringence studies of n-alkane liquids.

6. For the longer chain n-alkane liquids, $[\mu]_C$ approached the equivalent n-alkane value as the very anisotropic C-C end group was progressively diluted. However for the n-alcohols, whilst $[\mu]_C/n$ is constant above $n=5$, the constant of proportionality was greater than for the n-alkanes such that for $n > 9$, $[\mu]_C^{n\text{-alcohol}} > [\mu]_C^{n\text{-alkane}}$. Once again, this could not be explained in terms of valence-optical theories alone.
7. A study of branched-chain alkanes showed that for monomethylalkane isomers, the nearer the methyl group to the middle of the chain, the lower the value of $[\mu]_C$. This could be explained by conformation changes; at a branch point the bonds in the main chain tend to a gauche rather than trans conformation.

The molar Cotton-Mouton constant is very sensitive to the extent of branching in alkane liquids; two heavily branched alkanes had positive values of $[\mu]_C$. Because positive values are normally associated with delocalized electrons, there is the possibility of accessible excited state molecular orbitals extending over more than one bond for these species.

Because EPA theories appear to be invalid for alkane liquids, a graph theoretical approach was used to determine a scheme of segment additivity. It was shown that for branched chain alkanes, $[\mu]_C$ could be accurately predicted by summing appropriate substructural values. Hence, for alkane liquids $[\mu]_C$ is dependent mainly on the molecular constituents, implying that molecular orientational correlations are relatively unimportant.

8. The study of branched alkanes was extended to tetra-alkyl and tetra-alkoxy compounds. For these, the dependence of $[\mu]_C$ on the number of

backbone atoms per branch was very similar to that of the n-alkanes. The Cotton-Mouton constants observed for these molecules are much larger than predicted by the BPA scheme which, due to the molecular symmetry, allows much cancellation of bond anisotropies. The results show that the arms of these compounds appear to behave optically and magnetically as separate chains, supporting the conclusions reached for branched alkanes. Measurements on a series of tri-n-alkylamines reinforce this view, showing again that molecular orientational correlations appear to have little effect on the magneto-optical anisotropy of alkane liquids.

9. Of the cycloalkane neat liquids studied, cyclopentane and some of its derivatives remarkably yielded significantly positive values of $\Delta\epsilon$. The difference between the molar Cotton-Mouton constant of a linear alkane and its cycloalkane isomer was found to correlate very well with the strain energy per carbon atom of the cycloalkanes. This suggests a relation between the distortion of skeletal bond angles and the extent of electron delocalization. Because the magnitude and sign of $\Delta\epsilon$ are sensitive to delocalization, magnetic birefringence measurements thus provide a very sensitive way of detecting it.
10. Low to medium molecular weight polyisobutenes yielded values of $\Delta\epsilon$ which, when corrected for the unsaturated end groups, indicated that the saturated polymer chains have a very small magneto-optical anisotropy. These heavily branched alkane chains have been shown by depolarized light scattering and electric birefringence^{20,168} to possess optical anisotropies similar to the unbranched alkanes. Therefore a near-zero magnetic anisotropy is implied. This would be predicted from the symmetry of the structure and any bond additive scheme of diamagnetic anisotropy. Hence a bond additive scheme appears to be valid for the diamagnetic anisotropies of these molecules, in contrast with results discussed earlier for the n-alkanes. Unlike their optical counterparts, the effect of interactions between magnetic dipoles should be very small.
11. The magnetic birefringence of high molecular weight PBLG was measured in both rigid rod and flexible coil promoting solvents, DMF and DCA, respectively. For the same concentration, the specific Cotton-Mouton constant (C_{sp}) was many times larger for the rod promoting solvent, reflecting that the magnetic birefringence depends on the conformation

of the macromolecule. C_{sp} changed very slowly over the concentration range 0.1 to 30 kg m^{-3} of PBLG in DMF, giving little indication of polymer-polymer interactions. One would expect these to be evident in this range, although below the critical concentration of liquid crystallinity.

12. An extensive study was made of aqueous dispersions of highly crystalline and roughly ellipsoidal PTFE particles, known commercially as ICI's 'Fluon'. Both real and imaginary birefringences, $\Delta n'$ and $\Delta n''$ respectively, were measured for a very wide range of volume fractions (V_2). $\Delta n'$ could be accurately measured down to $V_2 = 10^{-8}$, and $\Delta n''$ down to $V_2 = 10^{-5}$. The smallest measurable value of $\Delta n'$ was $\sim 10^{-12}$, that of $\Delta n''$ was $\sim 10^{-10}$. $\Delta n'$ and $\Delta n''$ were measured up to a high concentration, $V_2 = 0.45$. Both were observed to depend quadratically on the magnetic induction. This suggested that the particles were diamagnetic, having a fairly small diamagnetic anisotropy.

The range of concentrations measured was very large (~ 8 decades for $\Delta n'$); both $\Delta n'$ and $\Delta n''$ were proportional to V_2 up to $V_2 = 10^{-2}$. Below this concentration, O'Konski's theory¹⁷⁷ was used to analyse the results and obtain the principal refractive indices of the particles. These were found to be 1.419 and 1.355, parallel and perpendicular to the major axis respectively. Hence the refractive index anisotropy of the Fluon particles is very large; 0.064. This was shown to arise predominantly from the crystallinity of the particles and not their shape.

In the concentrated region (V_2 between 0.01 and 0.45), $\Delta n'/V_2$ rose by 10% whilst $\Delta n''/V_2$ fell by 50%. This behaviour was compared with the O'Konski theory¹⁷⁷, which predicted that both fall with increasing concentration. The discrepancy could not be explained in terms of angular correlation between particles, and it was concluded that the assumptions made in the O'Konski theory (i.e. Rayleigh or dipole scatterers) were not valid for particles as large as Fluon.

REFERENCES

1. Kerr Brit. Assoc. Report (1901) 568.
2. A. Cotton, H. Mouton Comptes Rendus (1907) 145 870.
3. Landolt-Bornstein Tables Springer-Verlag, Berlin (1955) 5 827.
4. G.H. Meeten J. Chim. Phys. (1972) 69 1175.
5. R.J.N. Le Fèvre, D.S.N. Murthy, G.L.D. Richie. Austr. J. Chem. (1971) 24 1177.
6. H.G. Corfield PhD Thesis (1969) University of Bristol
7. A.D. Buckingham, W.H. Prichard, D.H. Whiffen J.C.S. Faraday II (1967) 63 1057.
8. M.R. Battaglia, G.L.D. Richie J.C.S. Faraday II (1977) 73 209.
9. M.R. Battaglia Chem. Phys. Lett. (1978) 54 124.
10. M. Stamm PhD Thesis (1979) University of Mainz.
11. P.A. Madden, M.R. Battaglia, T.I. Cox, R.K. Pierens, J.V. Champion Chem. Phys. Lett. (1980) 76 604.
12. T.I. Cox, M.R. Battaglia, P.A. Madden Mol. Phys. (1979) 38 1539.
13. S.P. Stoylov Adv. Colloid. Int. Sci. (1971) 3 45.
14. C. Housier, A. Fredericq 'Electric Dichroism and Electric Birefringence' (1973), Oxford UP, London.
15. W. Heller Rev. Mod. Phys. (1942) 14 390.
16. J.V. Champion, D. Downar, G.H. Meeten, L.F. Gate J. Phys. E. (1977) 10 1137.
17. A. Cotton, H. Mouton J. de Phys. (1911) 1 16.
18. D. Langevin Comptes Rendus (1910) 151 495.
19. M. Born Ann. Phys. (1918) 55 177.
20. J.V. Champion, A. Dandridge, G.H. Meeten Faraday Disc. C.S. (1978) 66 266.
21. G. Otterbein Physikal Z. (1934) 35 249.
22. A.D. Buckingham, J.A. Pople Proc. Roy. Soc. (1956) 69 1133.
23. A.D. Buckingham, B.J. Orr Quart. Rev. (1967) 21 195.
24. J.A. Bucaro, T.A. Litovitz J. Chem. Phys. (1971) 54 3846.
25. G.C. Tabisz Mol. Spec. (1979) 6 137.
26. L. Silberstein Phil. Mag. (1917) 33 92, 521.

27. H.B. Levine, G. Birnbaum J. Chem. Phys. (1971) 55 2914.
28. M. Thiebeau, B. Oksengorn, B. Vodar J. Phys. (1968) 29 287.
29. A.D. Buckingham, M.J. Stephens Trans. Faraday Soc. (1957) 53 884.
30. B.J. Alder, H.L. Strauss, J.J. Weis J. Chem. Phys. (1973) 59 1002.
31. B.J. Alder, J.J. Weis, H.L. Straus Phys. Rev. (1973) A7 281.
32. H.S. Gabelnick, H.L. Strauss J. Chem. Phys. (1968) 49 2334.
33. G.C. Tabisz, W.R. Wall, D.P. Shelton Chem. Phys. Lett. (1972) 15 387.
34. C.W. Carlson, P.J. Flory J.C.S. Faraday II (1977) 73 1505.
35. K. Gans, B. Mrowka Schriften Königsberg gelehrten Ges. Naturwiss K1 (1935) 12 1.
36. R.F. Zürcher J. Chem. Phys. (1962) 37 2421.
37. M.R. Battaglia, T.I. Cox, P.A. Madden Mol. Phys. (1979) 37 1413.
38. L. Onsager J. Am. Chem. Soc. (1936) 58 1486.
39. C.J.F. Böttcher 'Theory of Electric Polarization' (1952), Elsevier, Amsterdam.
40. T.G. Scholte Physica (1949) 15 437, 450.
41. A.K. Burnham, G.R. Alms, W.H. Flygare J. Chem. Phys. (1975) 62 3289.
42. J.P. McTague, P.A. Fleury, D.B. Du Pré Phys. Rev. (1969) 188 303.
43. D. Kivelson, P.A. Madden Ann. Rev. Phys. Chem. (1980) 31 523.
44. R.L. Jernigan, P.J. Flory J. Chem. Phys. (1967) 47 1999.
45. G.D. Patterson, P.J. Flory J.C.S. Faraday II (1972) 68 1098.
46. P. Bothorel, C. Such, C. Clement J. Chim. Phys. (1972) 69 1445.
47. S.N. Wang J. Chem. Phys. (1939) 7 1012.
48. K.G. Denbigh Trans. Faraday Soc. (1940) 36 936.
49. E.V. Chalam Proc. Indian Acad. Sci. (1942) A15 190.
50. Q.D. Chue, V.M. Tatevskiy Dokl. Akad. Nauk. SSSR (1972) 204 371.
51. R.P. Smith, E.M. Mortensen J. Chem. Phys. (1960) 32 502.
52. M.F. Vuks Opt. Spectrosk. (1957) 2 494.
53. R.J. W. Le Fèvre Adv. Phys. Org. Chem. (1965) 3 1.
54. C. Clement, P. Bothorel J. Chim. Phys. (1964) 61 1282.
55. C. Clement, R. Seurin J. Chim. Phys. (1971) 68 22.

56. P. Bothorel J. Chim. Phys. (1974) 71 1133.
57. H.C. Van de Hulst 'Light Scattering by Small Particles' (1957), Wiley, New York.
58. E.J. Burge, O. Snellman Phil. Mag. (1949) 40 993, 1233.
59. J. Badoz J. Phys. Radium (1956) 17 1434.
60. A.D. Buckingham, R.L. Disch Proc. Roy. Soc. (1963) A273 275.
61. J.V. Champion, R.A. Desson, G.H. Meeten Polymer (1974) 15 301.
62. H.G. Jerrard J. Opt. Soc. of Amer. (1954) 44 289.
63. H.G. Jerrard J. Opt. Soc. of Amer. (1948) 38 35.
64. W.A. Shurcliff 'Polarized Light' (1962), Oxford UP, London.
65. V.D. Tronko, G.P. Golovach, E.P. Kolesinkova Opt. Spectrosc. (1978) 44 309.
66. D. Downer PhD Thesis (1978) City of London Polytechnic.
67. G.H. Meeten Unpublished data (1971).
68. A. Goldet Ann. de Phys. (1938) 10 103.
69. J. Dobinson 'Mathematics for Technology 2' (1972), Penguin.
70. B. Koerman, H. Janeschitz-Kriegl J. Phys. E (1979) 12 625.
71. EMI Photomultiplier Catalogue (1979).
72. Optiglass Ltd. Precision Cell Catalogue (1979).
73. Fluka Chemical Catalogues (1978, 1980/81).
74. Aldrich Chemical Catalogues (1977/78, 1979/80).
75. A. Cotton, H. Mouton Comptes Rendus (1910) 151 862.
76. K.H. Grodde Physikal Z. (1938) 39 772.
77. O. Snellman Diss. Uppsala (1944).
78. A. Cotton, H. Mouton Ann. Chim (1913) 28 209.
79. H. KSnig Ann. Phys. (1938) 31 289.
80. G.R. Alms, A.K. Burnham, W.H. Flygare J. Chem. Phys. (1975) 63 3321.
81. W.H. Flygare, R.L.S. Shoemaker J.C.S. Faraday II (1970) 66 119.
82. J. Hoaran, N. Lumbroso, A. Pacault Comptes Rendus (1956) 242 1702.
83. A.K. Burnham, G.R. Alms, W.H. Flygare J. Chem. Phys. (1975) 62 3289.
84. D.R. Bauer, J.I. Brunman, R. Pacora J. Chem. Phys. (1975) 63 53.
85. C. Clement J. Chim. Phys. (1978) 75 747.

86. A.D. Buckingham, P.J. Stiles, G.L.D. Richie *Trans. Faraday Soc.* (1971) 67 577.
87. T.F. Keyes, B.M. Ladanyi *Mol. Phys.* (1977) 33 1063, 1099.
34 765, 1643.
88. See reference No.11.
89. R.J.W. Le Fèvre, D.S.N. Murthy *Austr. J. Chem.* (1966) 19 179, 1315.
90. E. Matull *Ann. Phys.* (1934) 21 345.
91. M.A. Haque *Comptes Rendus* (1930) 190 789.
92. W.H. Moore 'Physical Chemistry' 4th Edition, (1963), Longmans, London, p.119.
93. E.A. Moelwyn-Hughes 'Physical Chemistry', (1957), Pergamon, London, p.779.
94. R.J.W. Le Fèvre, D.S.N. Murthy, P.J. Stiles *Austr. J. Chem.* (1969) 22 1421.
95. E.W. Fischer, G.R. Strobl, M. Dettensmaier, M. Stamm, N. Steidle *Faraday Disc. C.S.* (1979) 68 26.
96. A.T. Frengel, W.S. Cornall *Phys. Rev. A* (1976) 13 253.
97. R.J. Greubel, G.T. Clayton *J. Chem. Phys.* (1967) 46 639.
98. A.H. Marten, M.D. Danford, H.A. Levy *J. Chem. Phys* (1967) 46 4875.
99. G. Reichelt, J.-U. Weidner, H.W. Zimmerman *Ber. Bunsenges. Phys. Chem.* (1974) 78 1050.
100. H.W. Zimmerman 'Organic Liquids', (1978), Wiley, Chichester. (Ed., A.D. Buckingham, E. Lippart, S. Bratos).
101. W.H. Murphy *J. Chem. Phys.* (1977) 67 5877.
102. S.G. Kukolich, W.H. Flygare *Mol. Phys.* (1969) 17 173.
103. S.G. Kukolich *J. Chem. Phys.* (1969) 50 3751.
104. A.A. Bothner-By, J.A. Pople *Ann. Rev. Phys. Chem.* (1965) 16 43.
105. J.R. Lalanne, F.B. Martin, P. Bothorel *J. Colloid Int. Sci.* (1972) 39 601.
106. See reference No. 95.
107. H.A. Boorse *Phys. Rev.* (1934) 46 187.
108. M. Scherer *Comptes Rendus* (1931) 192 1223.
109. G. Fourche, B. Lemaire *J. Chim. Phys.* (1971) 68 117.
110. R.S. Stein *J. Chem. Phys.* (1953) 21 1193.
111. M. Dettensmaier *J. Chem. Phys.* (1978) 68 2319.

112. F.T. Wall, W.A. Seitz *J. Chem. Phys.* (1977) 67 3722.
113. P.E. Schoen, R.G. Priest, J.P. Sheridan, J.M. Schnur *Nature* (1977) 270 412.
114. M.P. Bogaard, A.D. Buckingham, M.G. Corfield, D.A. Dummur, A.H. White *Chem. Phys. Lett.* (1972) 12 558.
115. C.L. Cheng, D.S.M. Murthy, G.L.D. Richie *Mol. Phys.* (1971) 22 1137.
116. M.R. Battaglia, G.L.D. Richie *Mol. Phys.* (1976) 31 1283.
117. G.H. Maeten *J.C.S. Faraday II* (1968) 64 2267.
118. J.P. Hermann, J. Ducuing *J. Appl. Phys.* (1974) 45 5100.
119. S.D. Hong, C. Chang, R.S. Stein. *J. Polymer Sci.* (1975) 13 1447.
120. T. Keyes *J. Chem. Phys.* (1979) 70 5438.
121. M. Pietralla *J. Polymer Sci.* (1980) 18 1717.
122. R.L. Rowell, R.S. Stein *J. Chem. Phys.* (1967) 47 2985.
123. J. Powers, D.A. Kaedy, R.S. Stein *J. Chem. Phys.* (1961) 35 376.
124. P.J. Flory 'Statistical Mechanics of Chain Molecules'. (1969), Wiley, New York.
125. V.A. Kargin *J. Polymer Sci.* (1958) 30 247.
126. P.J. Flory *Trans. Faraday Soc.* (1980) 76 000.
127. E.W. Fischer, J.H. Wendorff, M. Dattenmaier, G. Lieser, I. Voigt-Martin *J. Macromol. B* (1976) 12 41.
128. G. Delmas, S. Turrell *J.C.S. Faraday I* (1974) 70 572.
129. G.W. Longman, G.D. Wignall, R.P. Sheldon *Polymer* (1979) 20 1063.
130. J.T. Bendler *Macromol* (1977) 10 162.
131. A.D. Buckingham *Disc. Faraday Soc.* (1967) 43 205.
132. R.P. Smith, E.M. Mortensen *J. Chem. Phys.* (1960) 32 508.
133. L. Silberstein *Phil. Mag.* (1917) 33 92, 215, 521.
134. K. Pitzer *Adv. Phys. Chem.* (1959) 2 59.
135. R.P. Smith, E.M. Mortensen *J. Chem. Phys.* (1961) 35 714.
136. A.D. Buckingham, H. Sutter *J. Chem. Phys.* (1976) 64 364.
137. C. Clement, P. Bothorel *J. Chim. Phys.* (1964) 61 877.
138. G. Fourche, P. Bothorel *J. Chim. Phys.* (1969) 66 54.
139. K. Nagai *J. Chem. Phys.* (1967) 47 4690.

140. H. Quinones, F. Bothorel *Comptes Rendus* (1973) 277 133.
141. G.D. Patterson, A.P. Kennedy, J.P. Latham *Macromol.* (1977) 10 667.
142. E.M. Mortensen *J. Chem. Phys.* (1968) 49 3732.
143. P. Bothorel, G. Fourche *J.C.S. Faraday II* (1973) 69 441.
144. J.V. Champion, G.H. Meeten, G.W. Southwell *J.C.S. Faraday II* (1975) 71 225.
145. A. Massoulier *Comptes Rendus* (1968) 267 132.
146. C.M. Aval, R.L. Rowell, J.J. Barrett *J. Chem. Phys.* (1972) 57 3104.
147. R. Pasternak, A.Y. Meyer *Theor. Chim. Acta.* (1977) 43 287.
148. Q.D. Trisau, V.M. Tatevsky *Z. Phys. Chemie* (1973) 253 233.
149. J.J.C. Teixeira-Dias, J.N. Murrell *Mol. Phys.* (1970) 19 329.
150. H.J. Bridge, A.D. Buckingham *Proc. Roy. Soc. A* (1966) 295 334.
151. J. Applequist, J.R. Carl, K-K. Fung *J. Chem. Soc.* (1972) 94 2952.
152. B.M. Ladanyi, T. Keyes *Mol. Phys.* (1979) 37 1809.
153. T. Keyes, G.T. Evans, B.M. Ladanyi *J. Chem. Phys.* (1981) 74 3779.
154. T. Ishikawa, K. Nagai *Polymer Journal* (1971) 2 263.
155. G.D. Patterson, P.J. Flory *J.C.S. Faraday II* (1972) 68 1111.
156. J. Timmermans 'Physico-chemical Constants of Pure Organic Compounds' (1965), Elsevier, Amsterdam.
157. J.V. Champion, G.H. Meeten, M.D.R. Tench *J.C.S. Faraday II* (1971) 67 3230.
158. J.V. Champion, G.H. Meeten, M.D.R. Tench *Nature Phys. Sci.* (1971) 233 60.
159. B.H. Zimm, W.H. Stockmayer *J. Chem. Phys.* (1949) 17 1301.
160. M.L. Mattice *J. Am. Chem. Soc.* (1976) 98 3466.
161. M. Camail, A. Proutiera, H. Bodot *J. Phys. Chem.* (1978) 82 2617.
162. L. Kevan *J. Phys. Chem.* (1978) 82 1144.
163. M. Ranclie *Chem. Phys. Lett.* (1978) 53 602.
164. D.C. Bradley 'Advances in Inorganic Chemistry and Radiochemistry' (1972) 15 272. Ed. H.J. Emelius, A.G. Sharpe.
165. J.D. Roberts, M.C. Caserio 'Basic Principles of Organic Chemistry' (1979), Addison-Wesley.
166. M.S. Kosyreva *Opt. Spectrosc.* (1959) 6 303.

167. BP Chemicals Ltd. 'Byvis' Polymer Catalogue (1979).
168. J.V. Champion, A. Dandridge, D. Downer, J.C. McGrath, G.H. Meeten
Polymer (1976) 17 511.
169. M.H. Liberman, L.C. Debolt, P.J. Flory J. Polymer Sci. (1974) 12
187.
170. P. Doty, T.H. Bradbury, A.M. Holtzer J. Am. Chem. Soc. (1956) 78
947.
171. J.O. Ellis PhD Thesis (1977) University of Wales, Bangor.
172. G. Maret, M.V. Schickfus, A. Mayer, K. Dransfield Phys. Rev. Lett.
(1975) 35 397.
173. T. Tohyama, M. Miyata J. Phys. Soc. Japan (1973) 34 1699.
174. H. Block, E.F. Hayes, A.M. North Trans. Faraday Soc. (1970) 66 1095.
175. D.L. Patel, D.B. Du Pré Mol. Cryst. Liq. Cryst. (1979) 53 323.
176. G. Maret, M.V. Schickfus, J.H. Wendorff Colloq. Inst. CNRS (1975)
177. C.T. O'Konski J. Phys. Chem. (1959) 63 1558.
178. G. Maret, J. Torbet, E. Senechal, A. Domard, M. Rimado, H. Milas
Proc. Soc. da Chim. Phys. (1978) 477.
179. P.H. Geil 'Polymer Single Crystals' (1973), Krieger, New York,
2nd Edition.
180. J. Brandrup, E.H. Immergut 'Polymer Handbook' (1975) Wiley,
New York, 2nd Edition.
181. F.H. Billmeyer 'Textbook of Polymer Science' (1962) Wiley, New
York, 2nd Edition.
182. K. Alexander, A. Killey, G.H. Meeten, M. Senior J.C.S. Faraday II
(1981) 77 361.
183. M. Stoimenova, L. Labaki, S. Stoylov J. Colloid Int. Sci. (1980)
77 53.
184. A. Peterlin, H.A. Stuart Z. Phys. (1939) 112 1, 129.
185. G.H. Meeten J. Colloid Int. Sci. (1980) 74 181.
186. G.H. Meeten J. Colloid Int. Sci. (1982) 87 407.
187. S.P. Sutera, C.W. Boylan J. Colloid Int. Sci. (1980) 73 295.

Linear optical birefringence and dichroism measurement in liquids and colloidal dispersions

P Beuteler, J V Chomley and G H Meeson
 Department of Physics, Sir John Cass School of Science and
 Technology, City of London Polytechnic, 31 Jewry Street,
 London EC3N 2EY, UK

Received 17 June 1982, in final form 10 August 1982

Abstract. An apparatus is described for measuring the linear birefringence and linear dichroism induced in liquids or dispersions by an applied magnetic field. The apparatus uses a vibrating beam phase modulator and conventional optical and electro-optical components. It is capable of measuring $\Delta n'$ (the real part of the complex birefringence Δn) down to about 10^{-12} and $\Delta n''$ (the imaginary part of Δn) down to about 10^{-10} . Results are given for liquids of very small Cotton-Moston constant, hitherto unmeasurable, and very dilute colloidal dispersions. Dust removal from sample liquids is shown to be of major importance for weakly birefringent or dichroic samples.

1. Introduction

The application of an external field (e.g. electric, or magnetic) to a fluid containing molecules or particles generally causes the fluid to become optically anisotropic. This may be described by a complex, linear, uniaxial birefringence Δn which can be written $\Delta n' - i\Delta n''$. For weakly scattering molecules or very small colloidal particles the real part of the birefringence $\Delta n'$ is usually dominant and the imaginary part $\Delta n''$ (dichroism) may be safely disregarded when $\Delta n'$ is measured. For turbid dispersions of macromolecules or colloidal-sized particles $\Delta n''$ may not be negligible and it should be allowed for or measured with $\Delta n'$. Recent theory (Meeson 1980a, b) for non-absorbing particles commensurate in size with the optical wavelength shows that $\Delta n'$ and $\Delta n''$ are closely related quantities which both provide information about the particles' size and anisotropy.

An apparatus was previously described (Champion *et al* 1978) for measuring birefringence and dichroism induced by static electric or magnetic fields. These are uniaxial anisotropies, where it may be assumed that the principal axes of $\Delta n'$ and $\Delta n''$ are coincident and have directions which are independent of the magnitude of the applied field, usually being parallel and orthogonal to it. The apparatus we describe below can measure $\Delta n'$ and $\Delta n''$ down to about 10^{-12} and 10^{-10} , respectively. It is about 100 times more sensitive than that previously described, but requires few, relatively inexpensive, extra items.

2. Apparatus description

Figure 1 shows a diagram of the apparatus. Figures 2(a) and (b) show the azimuths of the optical components for measuring birefringence and dichroism, respectively.

The He-Ne laser was a Spectra-Physics 134P model, giving about 2 mW at a wavelength of 633 nm. The initial beam diameter was about 0.5 mm which diverged over a distance of 5 m to about 8 mm diameter at the photocathode of the photomultiplier. Intensity fluctuations of about 1% (ripple and noise) and 5% (long term drift) were present but were allowed for in the operating procedure of the apparatus. The

approximate 200:1 polarisation ratio of the laser light was improved by a high quality Glan-Thompson polariser in the position shown in figure 1.

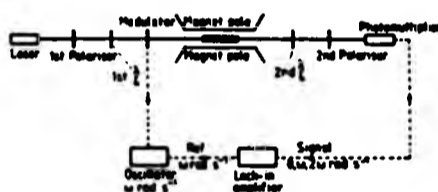


Figure 1. Schematic diagram of apparatus. The 1st $\lambda/4$ plate was removed for measurements of $\Delta n'$. The sample cell lies between the magnet pole pieces.

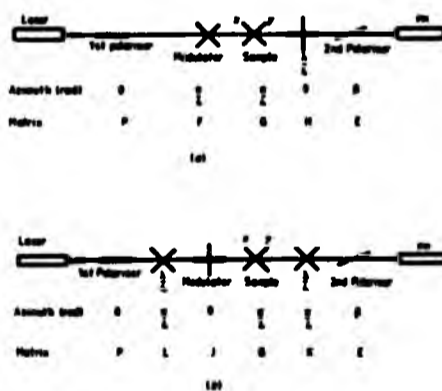


Figure 2. Azimuth diagrams of apparatus in (a) $\Delta n'$ and (b) $\Delta n''$ configurations. The sample axes are those shown in figure 4, with the applied field $(0, B_y, 0)$.

The electromagnet was a Newport type E, providing a uniform magnetic induction B up to 2 T over a light path of about 110 mm. For weakly anisotropic liquids a 200 mm long cell was used and B varied considerably over the cell length (l). For weakly anisotropic liquids both $\Delta n'$ and $\Delta n''$ are usually proportional to B^2 and so the appropriate average value of B^2 was given by

$$\bar{B}^2 = \int_0^l B^2 dl / \int_0^l dl.$$

Shorter path length cells were used for more strongly anisotropic liquids, where B was uniform to within better than 0.1% over the cell.

The photomultiplier tube was a 50 mm EMI type 4658C with an S20 (red sensitive) photocathode. The tube was housed in a magnetic and electrostatic shield. Magnetic focusing was used to reduce the effective cathode area and hence the dark current. Operating potentials were between 500 and 700 V, depending on the attenuation of the sample in the cell. It was

important that the electrical signal was proportional to the optical intensity and the appropriate dynamic chain and tube operating conditions were used.

The signal from the photomultiplier was fed directly into the signal channel of an Ortec-Brookdeal 9501 lock-in amplifier. The reference signal for the amplifier came from the oscillator which energized the optical modulator. The DC output from the amplifier was displayed on a chart recorder.

The optical modulator was similar to that described by Koeman and Janschitz-Kriegl (1979). In both, the principle was that of a composite beam beam, where the central plane of a window of optical glass (or fused quartz) was not coincident with the neutral plane of the composite beam. Hence a net tensile or compressive stress is set up in the glass when the beam bends and a vibrating beam can produce an alternating phase difference in light transmitted through it. Figure 3 shows a diagram of the optical modulator. The mild steel strip *S* and fused quartz window *W* were driven at the fundamental resonant frequency of 190 Hz by a small oscillator via the polarized electromagnet *E*. The depth of phase modulation was about ± 0.6 mrad. The window was chosen for its low strain birefringence before being fixed to the mild steel strip using Araldite. The modulator was housed in a magnetic and draughtproof shield and positioned about 2m from the large electromagnet.

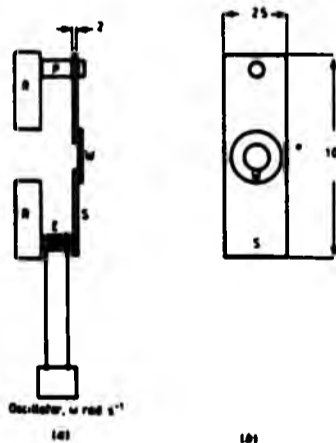


Figure 3. (a) Side view of vibrating strip *S* with window *W* mounted by pillar *P* onto the rotating plate *R* of a divided circle. *E* was a small polarized electromagnet mounted on *R* and energized by the oscillator. (b) Front view of vibrating strip *S* and window *W*. The approximate dimensions are given in mm.

The retarder plates were standard high quality mica quarter wave plates, nominally at 633 nm. The second polarizer was a glass dichroic polarizer with an extinction ratio of about $10^3:1$, mounted in a micrometer-driven divided circle which could be read to $\pm 5 \mu$ rad. Other rotatable components were mounted on divided circles readable to within about 2 mrad.

The apparatus was mounted on a concrete bench in a dark room.

3. Principle of operation

Figure 4 shows schematically the directions of the transmitted light through the sample, the applied field *B*, and the principal refractive index and dichroism axes. The phase differences and amplitudes of light emerging from the sample are also shown for two orthogonal and linearly polarized beams of unit amplitude incident upon the sample.

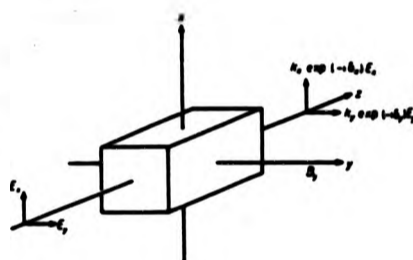


Figure 4. Diagram of a sample in a magnetic field $B = (0, B_y, 0)$ with the light propagating in the *z* direction. (E_x, E_y) represents the incident beam's electric vectors and $(k_x \exp(-i\delta_x)E_x, k_y \exp(-i\delta_y)E_y)$ represents the electric vectors of the emergent beam. The phase difference $\delta_x - \delta_y$, k_x and k_y are the principal transmissions.

For measuring birefringence alone, the modulator was rotated about the light beam direction to make the principal axes of the modulator coincide with those of the sample: *x* and *y* of figure 4, as in figure 2(a). Linearly polarized light emerging from the first polarizer thus became elliptically polarized on leaving the coil. For a purely birefringent sample, the principal axes of the ellipses coincided with those of the quarter-wave plate and light emerged from it linearly polarized but rotated relative to the polarization direction of the light incident on the sample. With the modulator inactive, the linearly polarized light emerging from the quarter-wave plate could be extinguished with the second polarizer rotated by angle β to the first polarizer: the quarter-wave plate and second polarizer used in this way acted as a Sénarmont compensator. With the modulator active, a phase difference was effectively added and subtracted to that of the sample for each period of vibration of the steel strip *S*. Thus the direction of polarization of the light emerging from the quarter-wave plate oscillated symmetrically about the angle β , causing a photomultiplier signal at twice the vibration frequency of the strip *S*.

When used to measure dichroism alone, the apparatus was arranged as in figure 2(b) so that the dichroism caused elliptically polarized light which could be analyzed as described above for the purely birefringent sample. With the modulator inactive, circularly polarized light was incident upon the sample. Because of the differential transmission ratio of a purely dichroic sample, circularly polarized light is rendered elliptical on emerging. The principal axes of this ellipse are rotated by $\pi/4$ rad from their birefringence-measuring positions. With the modulator active, light incident on the sample is slightly and periodically distorted from circular polarization, the principal axes of the near-circular ellipse being coincident with the principal transmission axes of the sample. Thus the effect of the

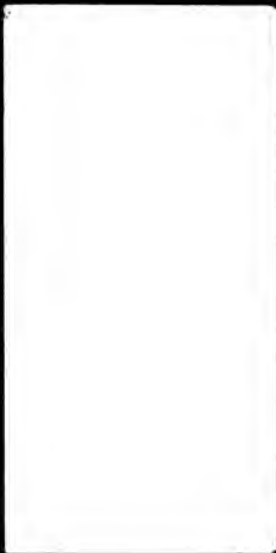


Table 1.

Component	Azimuth	Phase difference	Mueller matrix
Polarizer	β	—	$\frac{1}{2} \begin{bmatrix} 1 & \cos 2\beta & \sin 2\beta & 0 \\ \cos 2\beta & \cos^2 2\beta & \cos 2\beta \sin 2\beta & 0 \\ \sin 2\beta & \cos 2\beta \sin 2\beta & \sin^2 2\beta & 0 \\ 0 & 0 & 0 & 0 \end{bmatrix}$
Quarter-wave plate	ρ	$\frac{\pi}{2}$	$\begin{bmatrix} 1 & 0 & 0 & 0 \\ 0 & \cos^2 2\rho & \cos 2\rho \sin 2\rho & -\sin 2\rho \\ 0 & \cos 2\rho \sin 2\rho & \sin^2 2\rho & \cos 2\rho \\ 0 & \sin 2\rho & -\cos 2\rho & 0 \end{bmatrix}$
Birefringent and dichroic sample	$\frac{\pi}{4}$	δ_1	$M = \begin{bmatrix} 2k_x & 0 & \Delta k & 0 \\ 0 & 2k_x \cos \delta_1 & 0 & -2k_x \sin \delta_1 \\ \Delta k & 0 & 2k_x & 0 \\ 0 & 2k_x \sin \delta_1 & 0 & 2k_x \cos \delta_1 \end{bmatrix}$ <p>where $2k_x = k_y + k_z$, $k_y = (k_x k_z)^{1/2}$, and $\Delta k = k_y - k_z$.</p>
Birefringent and optically active sample of rotation θ	$\frac{\pi}{4}$	δ_1	$\begin{bmatrix} 1 & 0 & 0 & 0 \\ 0 & \cos D & (2\theta/D) \sin D & (-\delta_1/D) \sin D \\ 0 & -2\theta/D \sin D & 1 - 4\theta^2/D^2 \sin^2 D/2 & (4\theta\delta_1/D) \sin^2 D/2 \\ 0 & \delta_1/D \sin D & (4\theta\delta_1/D^2) \sin^2 D/2 & 1 - 2\theta^2/D^2 \sin^2 D/2 \end{bmatrix}$ <p>where $D = (4\theta^2 + \delta_1^2)^{1/2}$</p>

modulator was to alternately add or subtract linear dichroism to that of the sample.

If the sample is both linearly birefringent and linearly dichroic the analysis is more difficult and we resort below to a Mueller matrix method.

3.1. Optical theory

The theory of operation is first outlined for a mixed birefringent and dichroic sample, assuming that all the azimuths are correctly aligned as in figure 2, all the quarter-wave plates are exactly quarter-wave and all the polarizers provide completely linear polarization. The Appendix contains a study of the effects of imperfections in the optical components, including Faraday rotation arising from imperfect alignment of the magnet with the light propagation direction in the sample.

Calculation of the light intensity incident on the photocathode is made using the Mueller calculus described by Sturcliff (1962). Table 1 gives the Mueller matrices relevant to the optical components of the apparatus described.

In the Mueller calculus, a Stokes' column vector $\mathbf{P} = (1, 1, 0, 0)$ represents a beam of linearly polarized light of unit intensity emerging from the first polarizer. If this light is incident on an optical component having a Mueller matrix M , the light emerging from the component has a new Stokes' vector of $M \times \mathbf{P}$. The multiplication sign implies the usual conventions of matrix multiplication.

Thus, in the case of birefringence measurements with the arrangement of figure 2(a), the Stokes' vector of light incident on the photocathode is $\mathbf{E} \times \mathbf{H} \times \mathbf{O} \times \mathbf{P} \times \mathbf{P}$. The relative intensity of a light beam with a Stokes' vector (I, M, C, S) is I . Assuming linearity between I and the photocathode current, the relative

photovoltage response V is given by

$$V = k_x + k_z \cos 2\beta - \delta_1 - \delta_2. \quad (1)$$

For small strains in the optical modulator, the phase difference δ_2 introduced into the light beam by the periodically strained window may be written

$$\delta_2 = \Delta_2 \sin \omega t \quad (2)$$

where ω is the angular frequency of oscillation of the modulator and Δ_2 is the maximum amplitude of δ_2 . If Δ_2 is small (a few mrad in practice), equation (1) to a second-order approximation can be written

$$V = k_x + k_z \{ 1 - (\Delta_2^2/4) + (\Delta_2^2/4) \cos 2\omega t \} \cos(2\beta - \delta_1) + k_z \Delta_2 \sin \omega t \sin(2\beta - \delta_1). \quad (3)$$

From equation (3) the zero-frequency signal is

$$V_0 = k_x + k_z \cos(2\beta - \delta_1). \quad (4)$$

the signal at a frequency ω (fundamental) is

$$V_{\omega} = k_z \Delta_2 \sin \omega t \sin(2\beta - \delta_1) \quad (5)$$

and the double-frequency signal is

$$V_{2\omega} = \frac{1}{2} k_z \Delta_2^2 \cos 2\omega t \cos(2\beta - \delta_1). \quad (6)$$

Equation (5) shows the possibility of linear detection of the phase difference δ_1 induced in the sample, i.e. V_{ω} changes sign when $2\beta - \delta_1 = \pm m\pi$, $m = 0, 1, 2, \dots$ etc. If the first and second polarizers P and E are nearly crossed, then $m=1$ and $\cos(2\beta - \delta_1) = -1$. Thus if $k_x \approx k_z$, and Δ_2 is small, equations (4) and (6) show that $V_{\omega} \approx V_0 - V_{2\omega}$ near the point where V_0

changes sign. This is useful because any light flux extra to that causing V_0 contributes to electrical noise in the photocurrent. The need for an electrical filter to minimise $V_{2\omega}$ relative to V_0 (Champion *et al.* (1978)) is also removed. As V_0 carries the desired information, the reference signal for the phase-sensitive detector was taken from the oscillator which energised the optical modulator.

In the case of dichroism measurements, the arrangement in figure 2(b) was derived from that of figure 2(a) by inserting an extra quarter-wave plate and rotating the existing quarter-wave plate and the optical modulator through an angle of $\pi/4$. Performing the matrix multiplication $\mathbb{E} \times \mathbb{K} \times \mathbb{G} \times \mathbb{J} \times \mathbb{L} \times \mathbb{P}$ and separating the various frequency components of the photovoltage gives

$$V_0 = k_0 - k_2 \cos 2\beta \cos \delta_1 + (\Delta k/2) \sin 2\beta \quad (7)$$

$$V_{2\omega} = k_2 \Delta_2 \left(\frac{\Delta k}{2k_2} + \sin 2\beta \right) \sin \omega t \quad (8)$$

and

$$V_{4\omega} = \frac{-1}{4} k_2 \Delta_2 \cos 2\beta \cos \delta_1 \cos 2\omega t \quad (9)$$

Equation (8) shows that $V_{2\omega}$ carries the dichroism information and that $\Delta k/2k_2$ is measurable by linear detection, as V_0 can be made to change sign by changing the azimuth β of the second polariser. The null condition for $V_{2\omega} = 0$ is $\sin 2\beta = -\Delta k/2k_2$. At this null both V_0 and $V_{4\omega}$ can be shown to be also very small, with the advantages previously mentioned when discussing birefringence. The reference signal for the phase-sensitive detector of the lock-in amplifier was taken directly from the oscillator which energised the optical modulator.

In summary: the nulls of $V_{2\omega}$ for birefringence and dichroism measurements are given by $\beta = \frac{1}{2}(\delta_1 \pm \pi)$ and $\sin 2\beta = -\Delta k/2k_2$. In terms of the change $\Delta\beta$ in the azimuth of the second polariser necessary to recover a $V_{2\omega}$ null after a field has been applied, we have $\Delta\beta = \frac{1}{2}\delta_1$ for birefringence and $\sin 2\Delta\beta = \Delta k/2k_2$ for dichroism.

4. Use of the apparatus

It is necessary that the light beam should pass through the space between the magnet poles at right angles to the field. To achieve this the magnet was rotated in a horizontal plane, about an axis which intersected the light beam, with CCl_4 in the sample cell. CCl_4 has a Verdet constant of about $10 \text{ rad T}^{-1} \text{ m}^{-1}$ but a very small Cotton-Mouton constant. The magnet was thus set at a position which gave a near-zero Faraday rotation. The azimuth zero of the polarisers were then found by using a liquid with a very large Cotton-Mouton constant in the cell (e.g. benzene or nitrobenzene) and rotating both polariser azimuths for zero intensity with a strong field applied. Rotation of the first polariser azimuth by $\pi/4$ rad then sets its azimuth as in figures 2(a) and (b). With the second polariser crossed with the first, the phase modulator was rotated about the light beam axis to obtain a null $V_{2\omega}$ signal. This is the correct azimuth for dichroism measurements (figure 2(b)) and a further rotation of $\pi/4$ rad was made for birefringence measurements. The two quarter wave plates were aligned in a similar way, with the sample cell removed but using the optical modulator in order to find the null in $V_{2\omega}$.

The Appendix shows that large errors can be incurred when measuring dichroism if the azimuths of the principal axes of the optical modulator and the sample in the cell are not set accurately $\pi/4$ apart. To achieve this accurate setting, benzene was used as a sample liquid which had been double filtered to remove any dust which was known to produce dichroism. Using

this dichroism (see but birefringent sample, the azimuth of the modulator was finely adjusted until there was no change in the $V_{2\omega}$ signal on applying and removing the full magnetic field. The apparatus was then set up for measuring dichroism.

The field was measured using a calibrated Hall probe, errors in B being less than 1%. Knowing the length of the sample in a uniform field, an absolute calibration of the apparatus was made.

When measuring large values of $\Delta n'$ or $\Delta n''$, the field was applied and the second polariser rotated to obtain a null $V_{2\omega}$ signal. Hence β was measured and the appropriate relations used to derive $\Delta n'$ or $\Delta n''$. For small values of $\Delta n'$ or $\Delta n''$ two sources of error became important. One was electrical noise on the $V_{2\omega}$ signal, the other was a slow drift of the $V_{2\omega}$ signal with time. The former was reducible only by sacrificing response time. The latter was due to small thermally-induced drifts in the optical components, particularly in the fused quartz windows of the cell. Both sources of error were satisfactorily treated by displaying the $V_{2\omega}$ signal on a Y-t recorder trace, B being increased in steps by returning to zero between each step. The rate of drift of the $V_{2\omega}$ signal was much slower than the response time of the apparatus, so that changes in $V_{2\omega}$ caused by changes in B could be measured. The noise shown on the trace was visually averaged. The Y-t recorder signal was calibrated by rotating the second polariser through a known angle. Although the above procedure proved satisfactory for nominally transparent samples it could not be used if the turbidity of the sample was also field-dependent because $V_{2\omega}$ was proportional to the transmitted intensity. Hence its use was confined to weakly scattering materials as colloidal dispersions usually exhibit both field-dependent turbidity and dichroism.

The real part $\Delta n'$ of the complex birefringence Δn is related to the measured phase difference δ_1 by

$$\Delta n' = (\lambda/2\pi) \delta_1 \quad (10)$$

where λ is the free space wavelength. The imaginary part $\Delta n''$ is related to the measured value of $\Delta k/2k_2$ by

$$\Delta k/2k_2 = -\tanh(2\pi/\lambda \Delta n'') \quad (11)$$

Table 2 compares our $\Delta n'$ results for benzene and carbon tetrachloride with those given by other workers. Except for the value of Stamm (1979) our benzene result agrees well with the others given. For carbon tetrachloride there is a wide disagreement between results and only Curiale's (1969) value is close to ours.

Figure 5 shows $\Delta n'$ results for two very weakly birefringent liquids, water and 2,2,3-trimethylbutane. These liquids had been filtered five times using $0.05 \mu\text{m}$ pore size Millipore filters, and there was no change in $\Delta n'/B^2$. The change on repeated filtration was assumed to arise from the removal of fine dust particles. Large dust particles were also found to cause a nonquadratic dependence of $\Delta n'$ on B . Dichroism in pure liquids was measurable until the dust had been removed, and formed a useful check for its presence. Dependence of $\Delta n'$ on small quantities of fine dust is clearly important in the case of weakly birefringent liquids, and may account for differences in the carbon tetrachloride results of table 2, and in the water results previously compared (Bachelder *et al.* 1981). The theory (Merton 1980a, b) of $\Delta n'$ and $\Delta n''$ for colloidal particles shows that $\Delta n'$ is most sensitive to the presence of very fine dust, whereas $\Delta n''$ is most sensitive to dust with a particle size commensurate with the optical wavelength. The data in figure 5 shows that the Cotton-Mouton constant ($\Delta n'/B^2$) of water is measurable to an accuracy of a few percent. That of 2,2,3-trimethylbutane is shown by the scatter of experimental results to be measurable to within about $\pm 10\%$. To the authors' knowledge it is the smallest

Table 2. Molar Cotton-Mouton constants at 633 nm
 $10^5 \text{Cm}^2 \text{A}^{-2} \text{mol}^{-1}$

	This work	Literature	
Benzene	24.9 ± 1	24.6 ± 1.0	Corfield (1969)
		24.8 ± 0.8	Butaglia and Ritchie (1977)
		29.1	Stamm (1979)
CCl_4	-0.165 ± 0.003	-0.166 ± 0.006	Corfield (1969)
		-0.30 ± 0.07	Butaglia and Ritchie (1977)
		-0.23	Stamm (1979)

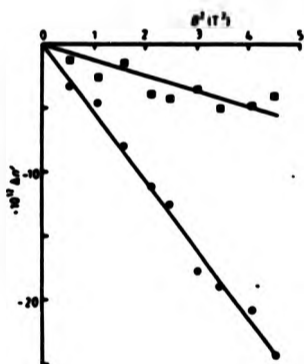


Figure 5. Graph of the real part of the complex birefringence, $\Delta n'$, plotted with the square of the magnetic field, B^2 . Key: \circ , water; \square , 2,2,3-trimethylbutane.

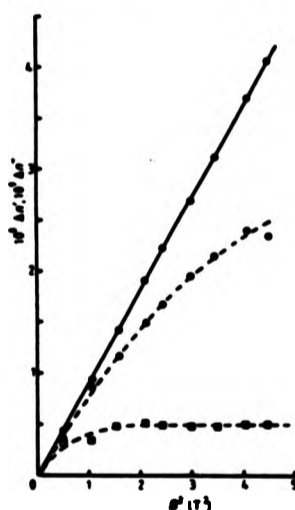


Figure 6. Graph of the real (continuous line, $\Delta n'$) and imaginary (broken line, $\Delta n''$) parts of the complex birefringence of Flouon dispersions. Key: \circ , solid volume fraction = 7.43×10^{-2} ; \square , solid volume fraction = 7.43×10^{-1} . A 10 mm path cell was used for both volume fractions.

Cotton-Mouton constant reported for a pure liquid $(-2 \pm 0.3) \times 10^{-5} \text{T}^{-2} \text{m}^{-1}$.

Figure 6 shows $\Delta n'$ and $\Delta n''$ measured for dilute aqueous dispersions of highly crystalline polytetrafluoroethylene (ICI 'Flouon' GP1). $\Delta n'$ is seen to behave quadratically with B but $\Delta n''$ does not. Flouon particles are small particles ($\sim 0.2 \mu\text{m}$) with a weak diamagnetic anisotropy and both $\Delta n'$ and $\Delta n''$ are thought to originate from the preferential orientation of the particles by the field. Hence it is unlikely that $\Delta n'$ and $\Delta n''$ depend differently on B and an explanation for the nonquadratic $\Delta n''$ behaviour is the presence of dust, or colloidal particles bigger than Flouon in the dispersion. As with dust in pure liquids these larger particles would contribute negligibly to $\Delta n'$ but significantly to $\Delta n''$. Figure 6 also demonstrates the ability of the apparatus to measure values of $\Delta n''$ lower than 10^{-10} .

Appendix. Error analysis

Errors in the measurement of $\Delta n'$ or $\Delta n''$ arise from imperfections in the optical components and their settings. A complete error analysis examines the effects of e.g. coll window strain, modulator azimuth error, etc on the measured values of $\Delta n'$ and $\Delta n''$.

Many tedious matrix multiplications are required to do this in full and here we quote only the most important sources of error. In the following we assume that both $\Delta n'$ and $\Delta n''$ are

small, so that all compensatory rotations of the second polariser are a few mrad, and second-order approximations are sufficient.

Birefringence ($\Delta n'$)

The effect of imperfections and azimuth errors in the optical components was found to decrease the sensitivity of the apparatus, but did not otherwise introduce error.

The effect of Faraday rotation in the sample was studied. This could arise from a slight misalignment of the magnetic field with a direction at right angles to the path of the light in the cell. In conjunction with the strain birefringence of the end windows of the cell, Faraday rotation was found by Corfield (1969) to cause large errors in the measured birefringence.

Neglecting dichroism, so that $k_x = k_y = 1$, and using the birefringence-rotation matrix in table 1 with the sample phase

difference assumed to be small, gives

$$V_{\theta} = \Delta_1 \sin \omega t \left\{ -\delta_1 \frac{\sin D}{D} (\cos 2\beta + \delta_1 \sin 2\rho_1 \sin 2\beta) \right. \\ \left. + \left(1 - \frac{2}{D} \delta_1^2 \sin^2 \frac{D}{2} \right) (\sin 2\beta - \delta_1 \sin 2\rho_1 \cos 2\beta) \right. \\ \left. + \frac{4\theta}{D} \delta_1 \delta_2 \sin^2 \frac{D}{2} \cos 2\rho_1 \sin 2\beta \right\}. \quad (\text{A.1})$$

Here, θ is the Faraday rotation caused by the component of B along the light propagation direction, $D = (4\theta^2 + \delta_1^2)^{1/2}$, δ_1 is the magnitude of the window strain birefringence and ρ_1 is its azimuth. For typical values of θ , δ_1 , and δ_2 of a few mrad, equation (A.1) reduces in the second order of approximation to

$$V_{\theta} = \Delta_1 \sin \omega t [\sin 2\beta - (\delta_1 + \delta_2 \sin 2\rho_1) \cos 2\beta]$$

and the null condition $V_{\theta} = 0$ is when $\tan 2\beta = \delta_1 + \delta_2 \sin 2\rho_1$, or for small β , $\beta = \frac{1}{2} (\delta_1 + \delta_2 \sin 2\rho_1)$. Thus the effects on β of Faraday rotation θ together with window strain δ_1 are not θ dependent or B dependent. The effect of δ_2 is to shift the zero of the null, so that the change $\Delta\beta$ necessary to recover a V_{θ} null after a field has been applied remains $\Delta\beta = \frac{1}{2} \delta_1$, as derived previously. In this regard the phase modulation system we have described is superior to the system of Corfield (1969), who used a Faraday modulator to effect azimuth modulation.

Dichroism ($\Delta\sigma'$)

The calculation of the effect of Faraday rotation in the sample on measured values of linear dichroism is difficult to carry out analytically, as no suitable Mueller matrix appears to be available. Experiments showed that field direction reversal had no measurable effect on obtained dichroism values and this was taken as proof that any optical rotation present was either very small or that it combined additively with $\Delta\sigma'$.

As pointed out in the text above, large errors can be caused when measuring dichroism if the azimuths of the principal axes of the optical phase modulator and the sample in the cell were not set accurately $\pi/4$ apart. Multiplication of the appropriate matrices from table 1 gives a dichroism signal of

$$v_{\theta} = k_2 \Delta_1 \sin \omega t \left(\frac{\Delta k}{2k_2} + \frac{2\Delta'\delta_1}{k_1} + \sin 2\beta \right) \quad (\text{A.2})$$

where Δ' is setting error in the azimuth angle of the modulator, i.e. the angle by which the azimuth angle differs from $\pi/4$. Compared with equation (8), equation (A.2) shows that V_{θ} is a null when

$$\sin 2\beta = - \left(\frac{\Delta k}{2k_2} + \frac{2\Delta'\delta_1}{k_1} \right).$$

Hence there is an error in the dichroism ratio $\Delta k/k_2$ of $4\Delta'\delta_1/k_1$. This can be large for strongly birefringent liquids with a weak dichroism, e.g. taking $\delta_1 = 1$ mrad, $\Delta' = 10 \mu$ rad and $k_2 \approx 1$ gives an error of $\sim 4 \times 10^{-5}$ in $\Delta k/k_2$. Hence great care was taken in modulator azimuth setting and a high quality divided circle was required. It should be noted that the existence of dichroism when measuring birefringence does not cause errors in the way described above: the existence of dichroism changes the intensity null to an intensity minimum and the effect is to decrease the signal/noise ratio.

References

- Battaglia M R and Ritchie G L D 1977
J. Chem. Soc. Faraday Trans. II 73 209-21
 Batchelor P J, Champion J V and Meeten G H 1981
J. Chem. Soc. Faraday Trans. II 76 1610-7

Champion J V, Downer D, Meeten G H and Gale L F 1978
 Measurement of magnetically induced linear optical
 birefringence and dichroism in colloidal dispersions
J. Phys. E: Sci. Instrum. 10 1137-41

Corfield M G 1969 Thesis University of Bristol

Kueman B and Janeschitz-Kriegl H 1979 Analysis of slightly
 elliptically polarised light
J. Phys. E: Sci. Instrum. 12 625-8

Meeten G H 1980a

J. Colloid. Interface Sci. 73 38-44

Meeten G H 1980b

J. Colloid. Interface Sci. 74 181-5

Stamm M 1979 Thesis University of Mainz

Shurcliff W A 1962 *Polarized Light* (Harvard: University Press)

Magnetic Birefringence in Liquids of Near-isotropic Molecules

BY PETER J. BATCHELOR, JOHN V. CHAMPION AND GERALD H. MEETEN*
Department of Physics, Sir John Cass School of Science and Technology,
City of London Polytechnic, 31 Jewry Street, London EC3N 2EY

Received 11th June, 1980

The magnetic field-induced birefringence and dichroism of several weakly birefringent liquids has been measured, both neat and in solution. Some liquids had not been measured before and others have been remeasured with a precision considerably greater than previously reported. Linear dichroism measurements yielded the expected null result for all liquids if dust had been removed. The birefringence also was found to be sensitive to the presence of dust. Care was taken to eliminate the effect of Faraday rotation on the birefringence measurements.

Field-induced molecular re-orientation and magnetic hyperpolarizability were sufficient to explain the results, except for solutions of CCl_4 and $\text{Sn(CH}_3)_4$, where the partial molar Cotton-Mouton constant of both components was found to be strongly composition dependent at mole fractions of CCl_4 > 0.5 . An intramolecular contribution to the magnetic birefringence of CCl_4 has been proposed to explain this. It is concluded that CCl_4 should not be regarded as an inert solvent for infinite dilution studies of molecular anisotropy in weakly anisotropic solute molecules.

The Cotton-Mouton effect (birefringence induced by a transverse magnetic field) has generally been assumed to arise from two basic mechanisms. (1) The partial orientation of magnetically and optically anisotropic molecules into the applied field direction against the disorienting effect of rotary Brownian motion. (2) The creation of optical anisotropy in molecules by the applied field, through their magnetic hyperpolarizability.

Very few estimates of the magnetic hyperpolarizability have been made: such measurements depend on extrapolation of gas-phase results to 0 K and are subject to large errors.^{1,2} Calculations of magnetic hyperpolarizability are much more difficult than the electrical analogue.

Several workers have used magnetic birefringence data to estimate the diamagnetic anisotropy of molecules in liquids or solutions,^{3,4} assuming the magnetic hyperpolarizability to be negligible. Fair agreements have been obtained between diamagnetic anisotropies thus measured and values derived from crystalline magnetic susceptibilities particularly for the strongly diamagnetically anisotropic compounds.⁵ There are, however, significant differences for the same solute when using different solvents which are not removed by extrapolation to infinite dilution.⁵

Recently, temperature-dependent Cotton-Mouton measurements have been made on liquid *n*-alkanes and polyethylene.^{6,7} The results were interpreted in terms of local order and orientational or angular correlations between neighbouring molecules. In these studies magnetic hyperpolarizability was neglected. The angular correlations deduced were in fair agreement with those derived from depolarized Rayleigh light scattering on the same liquids. However the interpretation of Rayleigh scattering data remains uncertain, particularly for polymer chain molecule liquids which at present show very large discrepancies between molecular-optical anisotropies in liquid solution and gaseous states.⁸

One apparent advantage of magnetic birefringence measurements over electric birefringence or depolarized Rayleigh scattering to determine intermolecular orientational correlations is that there is a negligible magnetic dipole-induced dipole interaction between molecules. However, other short-range intermolecular mechanisms exist which could lead to a collisional or intermolecular contribution to the magnetic birefringence. For example, the valence electrons of a molecule make the dominant contribution to both molecular electric polarisability α and magnetic susceptibility χ . Hence molecular interactions which modify α may also modify χ . We present experimental evidence for this below.

EXPERIMENTAL

Measurements of magnetic birefringence were made with a previously described apparatus with modifications to increase its sensitivity.⁹ The two main changes were the substitution of a 2 mW He-Ne laser for the tungsten filament source and a piezo-optic modulator for the rotating phase plate. The apparatus could then measure phase differences within an error of ca. $\pm 1 \mu\text{rad}$. This gave the lower limits of measurable birefringence and linear dichroism as $n_{\parallel} - n_{\perp} = 10^{-12}$ and $2\Delta k_{\parallel} - k_{\parallel}(k_{\parallel} + k_{\perp}) = 10^{-5}$, respectively. Here n is the refractive index, k the transmission ratio and l and r refer to light polarized parallel and transverse to the direction of the applied magnetic induction B . Contrary to the experience of Fischer *et al.*⁷ small amounts of dust became apparent by producing mostly a non-quadratic dependence of Δn on B . Any measurable linear dichroism was always attributable to colloidal-sized dust particles in the liquids and could be reduced to very low values by liquid filtration using 50 mm Millipore filters. The ability to measure linear dichroism was a useful check for the presence of dust in liquids used for birefringence measurements, in particular as the birefringence caused by the smallest dust particles had a quadratic dependence on the field and so was indistinguishable from that of the liquid.

A calibration of the apparatus gave absolute Cotton-Mouton constants within ca. $\pm 2\%$ of the literature values for liquids such as benzene, nitrobenzene and chloroform.

The liquids measured were as pure as could be obtained commercially, spectroscopic or 99% grades being used wherever these were available. Apart from dust removal by filtration they were used as received.

All measurements were made at a wavelength of 632.8 nm and a temperature of $20 \pm 1^{\circ}\text{C}$. Great care was taken to align the magnetic field at right-angles to the light beam to avoid Faraday rotation, which in small Cotton-Mouton constant liquids is not commensurately small. The criterion used was that the Cotton-Mouton constant of the liquid should not change on reversing the exciting current of the electromagnet. Table 1 shows the experimental results

TABLE 1.—BULK AND MOLAR COTTON-MOUTON CONSTANTS OF NEAT LIQUIDS AT $20 \pm 1^{\circ}\text{C}$ AND $\lambda = 633 \text{ nm}$ UNLESS NOTED

Liquid	This paper		Literature	
	$C/10^{10} \text{ T}^2 \text{ m}^{-1}$	$\Delta C/10^{-10} \text{ m}^3 \text{ A}^{-2} \text{ mol}^{-1}$	$C/10^{10} \text{ T}^2 \text{ m}^{-1}$	$\Delta C/10^{-10} \text{ m}^3 \text{ A}^{-2} \text{ mol}^{-1}$
CCl ₄	-30 ± 6.5	-165 ± 3	-51 ± 12^a	-300 ± 70^b
Bz	119 ± 0.7	95 ± 6	—	0 ± 200^c
Ph	26 ± 1	—	0 ± 20^d	—
Ph	-74 ± 1	-520 ± 10	-63^e	—
C ₆ H ₆	—	—	-107^f	—
H ₂ O	-9 ± 0.6	-16.1 ± 0.7	-69^g	—

^a Ref. (5); ^b ref. (6); ^c ref. (13); ^d ref. (12); ^e ref. (8); ^f ref. (10); ^g measured at a wavelength of 546 nm.

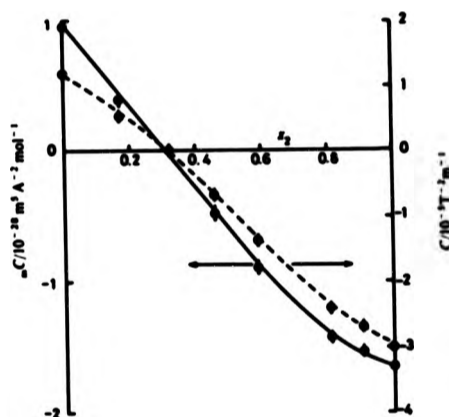


FIG. 1.—Bulk (C) and molar (L_C) Cotton-Mouton constants of CCl_4 and $\text{Sn}(\text{CH}_3)_4$ solutions plotted against the mole fraction x_2 of CCl_4 .

together with literature values of bulk (C) and molar (L_C) Cotton-Mouton constants. The birefringence of $\text{CCl}_4 + \text{Sn}(\text{CH}_3)_4$ mixtures was measured over the whole concentration range. Measured densities of these solutions showed a linear dependence of density on concentration within a density error of $\pm 0.1\%$. Within this error, volumes were additive. Fig. 1 shows the Cotton-Mouton and molar Cotton-Mouton constant plotted with molar fraction.

DISCUSSION

THEORY

The Cotton-Mouton constant C of a pure liquid or a solution is here defined in the usual way for light of wavelength λ ,

$$C = \frac{n_{\parallel} - n_{\perp}}{\lambda B^2} \quad (1)$$

A magnetic induction B causes uniaxial birefringence in the liquid, n_{\parallel} and n_{\perp} being the principal refractive indices parallel and perpendicular to B , respectively.

The molar Cotton-Mouton constant¹⁰ of a liquid can be written as¹¹

$$L_C = \frac{2nV(n_{\parallel} - n_{\perp})\mu_0^2}{27L_{\infty}M_0^2B^2} \quad (2)$$

where L_{∞} and M_0 are the local field factors for the optical field and static magnetic field, respectively. B is the magnetic induction in the liquid and V is the molar volume. For diamagnetic liquids $\mu \approx 1$ and $M_0 \approx 1$ to an error $< 10^{-3}\%$, μ being the permeability of the liquid. Here and in common with most authors we assume a Lorentz local optical field and put $L_{\infty} = \frac{1}{3}(n^2 + 2)$, n being the mean refractive index of the liquid. μ_0 is the permeability of free space.

Hence

$${}_m C^* = \frac{2nV\mu_0^2 \lambda C}{3(n^2 + 2)^3} \quad (3)$$

The molar Cotton-Mouton constant ${}_m C$ of a binary solution is also given by eqn (2) with V replaced by the molar volume of the solution, C being the Cotton-Mouton constant of the solution. As with other molar quantities, the molar Cotton-Mouton constant of a binary solution containing components 1 and 2 can be written in terms of partial molar Cotton-Mouton constants ${}_m C_1$ and ${}_m C_2$ of the components,

$${}_m C = x_1 {}_m C_1 + x_2 {}_m C_2 \quad (4)$$

where x_1 and x_2 are the mole fractions of the components. The molecular theory of the Cotton-Mouton effect for any single component shows that¹⁰

$${}_m C = \frac{N\mu_0^2}{270\epsilon_0} \left(\eta + \frac{2\gamma_{ms}^2}{3kT} \right) \quad (5)$$

where N , k , T and ϵ_0 are Avogadro's number, Boltzmann's constant, the Kelvin temperature and the permittivity of free space, respectively. η is the mean value of the magneto-optic hyperpolarizability, γ_{ms}^2 is the magneto-optical anisotropy parameter defined for an isolated molecule by

$$\gamma_{ms}^2 = \frac{1}{2}[(\alpha_1 - \alpha_2)(\chi_1 - \chi_2) + (\alpha_2 - \alpha_3)(\chi_2 - \chi_3) + (\alpha_3 - \alpha_1)(\chi_3 - \chi_1)] \quad (6)$$

The 1, 2, 3 axes of the molecule are those in which the magnetic susceptibility tensor χ is diagonal; α_i is the optical polarizability along these axes.

If both η and γ_{ms}^2 are unchanged by the process of dilution then ${}_m C_1^* = {}_m C_1$, ${}_m C_2^* = {}_m C_2$ and eqn (4) shows that the measured value of ${}_m C$ varies linearly with mole fraction. It is possible that partial molar Cotton-Mouton constants are changed on dilution because of the effect of angular or radial near-neighbour molecular correlations on γ_{ms}^2 . In this case the infinite-dilution value of a partial molar quantity is often taken as representing the intrinsic molecular value.⁵ The molar Cotton-Mouton constant at infinite dilution is then ${}_m C_1^*$ and is given by

$${}_m C_1^* = {}_m C_1 + \left(\frac{d {}_m C}{d x_1} \right)_{x_1 \rightarrow 0} \quad (7)$$

${}_m C_1^*$ is the quantity called ${}_m({}_m C_1)$ by Battaglia and Ritchie⁵ in their Cotton-Mouton study of magnetic susceptibility anisotropy of several solute molecules. If there is no dilution effect on η or γ_{ms}^2 then the infinite dilution and pure liquid Cotton-Mouton constants are identical, i.e., ${}_m C^* = {}_m C$.

In this work we have obtained ${}_m C^*$ and ${}_m C^*$ for several molecules of tetrahedral and near-tetrahedral symmetry.

NEAT LIQUIDS

Table 1 shows considerable differences between experimental Cotton-Mouton constants for the same liquids. Where results are compared at different wavelengths, dispersion of the birefringence accounts partly for the differences, C generally decreasing with increasing wavelength. Colloidal-sized dust was found by us to contribute to the measured birefringence and may also account for some of the differences. Single, isolated, CCl_4 molecules have tetrahedral symmetry producing op-

tical and magnetic isotropy so the $\gamma_{\text{m}}^2 = 0$. $\text{Sn}(\text{CH}_3)_4$ and $\text{Si}(\text{CH}_3)_4$ do not generally possess tetrahedral symmetry if their CH_3 groups undergo internal rotation. However, the trigonal symmetry of each group produces optical and magnetic isotropy in the plane to which the trigonal axis is normal. If interactions between the CH_3 groups are assumed to be negligible then the tetrahedral orientations of the trigonal axes within a molecule lead to molecular isotropy so that $\gamma_{\text{m}}^2 = 0$. Any radial correlations which may exist in the liquid state do not contribute to γ_{m}^2 because of the negligible intermolecular MDID interactions. The molar Cotton-Mouton constant becomes ${}_mC = N\mu_0^2\eta/270$ and values of η have been so derived¹¹ on the assumption that no other mechanism in liquids contributes to ${}_mC$. This assumption is discussed below when applied to liquid mixtures.

For water, our value of C is much lower than the available literature values, which agree closely with each other.¹² However, these values are about 50 years old and likely to be of low accuracy.

Polyisobutene has been re-measured with the higher sensitivity apparatus. Previous work¹² gave a zero Cotton-Mouton constant within experimental error; $(0 \pm 20) \times 10^{-6} \text{ T}^{-2} \text{ m}^{-1}$.

SOLUTIONS

A series of $\text{CCl}_4 + \text{Sn}(\text{CH}_3)_4$ solutions were measured covering the entire concentration range. Fig. 1 shows the molar and bulk Cotton-Mouton constants of these mixtures.

If magnetic hyperpolarizability is the only contribution to the magnetic birefringence in CCl_4 and $\text{Sn}(\text{CH}_3)_4$, then we may write, from eqn (5), for the neat liquids

$${}_mC_1 = \frac{N\mu_0^2\eta_1}{270\alpha_0} \quad (8)$$

and

$${}_mC_2 = \frac{N\mu_0^2\eta_2}{270\alpha_0} \quad (9)$$

where subscripts 1 and 2 refer to $\text{Sn}(\text{CH}_3)_4$ and CCl_4 , respectively. Since each molecule is isotropic orientational correlations are absent. Since the magnetic dipole-individual dipole is negligible, 1-1, 2-2 and 1-2 type radial correlations in solution or the neat liquid provide no contribution to the magnetic birefringence. Hence we may put

$${}_mC_1 = {}_mC_1 = {}_mC_1 \quad (10)$$

and

$${}_mC_2 = {}_mC_2 = {}_mC_2 \quad (11)$$

where ${}_mC_1$ and ${}_mC_2$ are partial molar Cotton-Mouton constants at arbitrary dilutions. Hence eqn (4) becomes

$${}_mC = x_1 {}_mC_1 + x_2 {}_mC_2 \quad (12)$$

so that the measured molar Cotton-Mouton constant should vary linearly from one neat liquid to the other. Fig. 1 shows that this is not the case.

The molar Cotton-Mouton constant ${}_mC$ of the solution is dependent on the

solution composition. If there are n_1 moles of $\text{Sn}(\text{CH}_3)_4$ and n_2 moles of CCl_4 then the partial molar quantities ${}_mC_1$ and ${}_mC_2$ may be generally defined¹⁴ by

$${}_mC_1 = \left(\frac{\partial {}_mC}{\partial n_1} \right)_{n_2} \quad \text{and} \quad {}_mC_2 = \left(\frac{\partial {}_mC}{\partial n_2} \right)_{n_1}$$

Both are intensive quantities and as such may be derived by the method of intercepts^{14,15} applied to fig. 1. In this method, a tangent to the curve in fig. 1 intersects the $x_2 = 0$ axis at ${}_mC_1$ and the $x_2 = 1$ axis at ${}_mC_2$. Hence ${}_mC_1$ and ${}_mC_2$ are generally composition-dependent variables, being ${}_mC_1^0$ and ${}_mC_2^0$ at $x_2 = 1$ and 0, respectively. This approach contrasts with the usual Le Fèvre method³ of obtaining an infinite-dilution molar Cotton-Mouton (or Kerr) constant, where the Cotton-Mouton constant of the solvent is assumed to be independent of its concentration in the solution.

Fig. 2 and 3 show that both ${}_mC_1$ and ${}_mC_2$ deviated markedly from constants beyond ca. 50 mole %. This implies that both CCl_4 and $\text{Sn}(\text{CH}_3)_4$ molecules contribute anomalously, extra to their hyperpolarizability, when they are surrounded with CCl_4 molecules. $\text{Sn}(\text{CH}_3)_4$ thus behaves as an inert solvent for CCl_4 but the reverse is not the case. CCl_4 as a neat liquid appears to behave anomalously, having a mechanism other than magnetic hyperpolarizability which contributes to the magnetic birefringence. This mechanism is intermolecular, as it ceases when the CCl_4 molecules are widely separated in dilute solution with $\text{Sn}(\text{CH}_3)_4$.

Because of its intermolecular contribution to the birefringence which changes rapidly as it is diluted with a solute, CCl_4 would not seem to be an entirely inert solvent suitable for infinite-dilution molar Cotton-Mouton constant studies. Magnetic birefringence studies of solute intermolecular orientational correlation using CCl_4 as a solvent must be regarded with caution particularly when the solute species is a weakly anisotropic *n*-alkane molecule.^{6,7} The use of CCl_4 as a solvent changes the molar Cotton-Mouton constant of $\text{Sn}(\text{CH}_3)_4$ from a positive value in the neat liquid to a negative value at infinite dilution, as fig. 3 shows. Molecular magnetic hyperpolarizability cannot be derived from Cotton-Mouton measurements on neat liquids of isotropic molecules unless it is known that there is no other contribution to the magnetic birefringence.

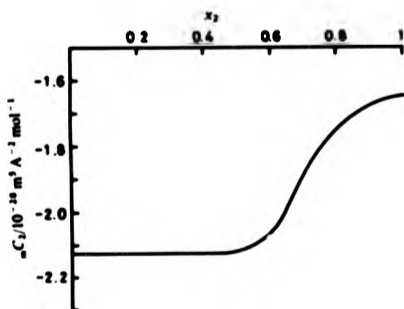


FIG. 2.—Partial molar Cotton-Mouton constant ${}_mC_2$ of CCl_4 plotted against the mole fraction x_2 of CCl_4 .

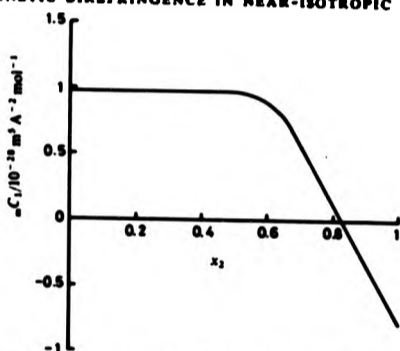


Fig. 3.—Partial molar Cotton-Mouton constant mC_2 of $\text{Sn}(\text{CH}_3)_4$, plotted against the mole fraction x_2 of CCl_4 .

Origins of the intermolecular contribution to the magnetic birefringence in CCl_4 are suggested below. It is not because of the distortion of the radial distribution function $g(r)$ by intermolecular forces between induced molecular magnetic dipoles; these forces (unlike their Kerr effect analogue) are too weak as the magnetic dipole-induced dipole is negligibly small. A collisional contribution to magnetic birefringence has been suggested, where intermolecular collisions in a liquid deviate both the molecular optical polarizability and the magnetic susceptibility from isotropy.³ These correlated transient anisotropies then provide an orientational contribution to the birefringence. Another possibility is that the magnetic hyperpolarizabilities of molecules are influenced by intermolecular interactions.

Specific orientational correlations between CCl_4 molecules have been deduced from X-ray studies on liquid CCl_4 .¹⁶⁻¹⁸ Here there is found a tendency for CCl_4 molecules to align so that a Cl atom of one molecule fits into the depression of a neighbouring molecule formed by three of the Cl atoms. The isotropy of an isolated CCl_4 molecule originates from the tetrahedral symmetry of position and interaction between its Cl atoms or C—Cl bonds. If the intermolecular environment or interactions in any way affect the properties of one Cl atom or C—Cl bond differently than others in the same molecule, this molecular symmetry and hence the isotropy is destroyed. This is likely to be the case for the short-range oriented structure described above. Clearly such a structure would be changed or lost as solute molecules of a different kind were added.

The above suggestions must remain speculative until their contribution to the magnetic birefringence can be calculated.

CONCLUSION

We have shown that there appears to be a contribution to the magnetic birefringence of CCl_4 other than magnetic hyperpolarizability. This contribution decreases as CCl_4 is diluted with a solute and so appears to have an intermolecular origin. The magnetic hyperpolarizability coefficient η of CCl_4 cannot therefore be measured from the neat liquid magnetic birefringence. CCl_4 should not be regarded as an inert solvent for infinite-dilution studies of molecular anisotropy, particularly for weakly anisotropic molecules.

We are grateful to the referees for their valuable comments.

- ¹A. D. Buckingham, W. H. Prichard and D. H. Whiffen, *Chem. Commun.*, 1965, 51.
²A. D. Buckingham, W. H. Prichard and D. H. Whiffen, *Trans. Faraday Soc.*, 1967, 63, 1057.
³R. J. W. Le Fèvre, P. H. Williams and J. M. Echert, *Aust. J. Chem.*, 1965, 18, 1133.
⁴C. L. Cheng, D. S. N. Murthy and G. D. L. Ritchie, *Mol. Phys.*, 1971, 22, 1137.
⁵M. R. Battaglia and G. D. L. Ritchie, *J. Chem. Soc., Faraday Trans. 2*, 1977, 73, 209.
⁶M. Stamm, *Untersuchung der Konformation von Polymermolekülen mittels Neutronenstreuung und magnetischer Doppelbrechung (Thesis)* (University of Mainz, 1979).
⁷E. W. Fischer, G. R. Strobl, M. Dornseifer, M. Stamm and N. Seidler, *Faraday Discuss. Chem. Soc.*, 1979, 68, 26.
⁸J. V. Champion, A. Dandridge and G. H. Meesten, *Faraday Discuss. Chem. Soc.*, 1978, 66, 266.
⁹J. V. Champion, D. Downer, G. H. Meesten and L. F. Gale, *J. Phys. E.*, 1977, 10, 137.
¹⁰M. R. Battaglia, *Chem. Phys. Lett.*, 1978, 54, 124.
¹¹A. D. Buckingham and J. A. Popple, *Proc. Phys. Soc. London, Ser. A*, 1955, 68, 905; *Proc. Phys. Soc. London, Ser. B*, 1956, 69, 1133.
¹²*Landolt-Börnstein Tables*, vol. 5, 827.
¹³J. V. Champion, A. Dandridge, D. Downer, J. C. McGrath and G. H. Meesten, *Polymer*, 1976, 17, 511.
¹⁴W. J. Moore, *Physical Chemistry* (Longmans, London, 4th edn, 1963), p. 119.
¹⁵E. A. Moolenaar-Hughes, *Physical Chemistry* (Pergamon, London, 1957), p. 779.
¹⁶R. W. Grubel and G. T. Clayton, *J. Chem. Phys.*, 1967, 46, 639.
¹⁷A. H. Norton, M. D. Dandford and H. A. Levy, *J. Chem. Phys.*, 1967, 46, 4875.
¹⁸H. W. Zimmermann, *Organic Liquids*, ed. A. D. Buckingham, E. Lippert and S. Bratos (Wiley, Chichester, 1978).

THE BRITISH LIBRARY DOCUMENT SUPPLY CENTRE

TITLE An Experimental Study of the Magnetic
..... linear Birefringence and Dichroism of
..... Liquids, solutions and Dispersions

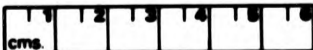
AUTHOR P. J. Batchelor

INSTITUTION
and DATE City of London Polytechnic
..... 1982

Attention is drawn to the fact that the copyright of this thesis rests with its author.

This copy of the thesis has been supplied on condition that anyone who consults it is understood to recognise that its copyright rests with its author and that no information derived from it may be published without the author's prior written consent.

THE BRITISH LIBRARY
DOCUMENT SUPPLY CENTRE
Boston Spa, Wetherby
West Yorkshire
United Kingdom



REDUCTION X

21



DX



8	4	3	9	2	
----------	----------	----------	----------	----------	--

